THE MORPHOLOGICAL, FLOW AND FAILURE CHARACTERISTICS OF FRACTIONATED NATURAL BULK MATERIAL

Evaluation of flowability of fractionated powdered liquorice using a specially designed flowmeter. The particle morphology was assessed by computer image analysis and the failure properties by shear cell testing.

by

Mohammad Esmail ZOLFAGHARI
B.Sc.
MS
MS (Pharmacy)

Submitted for the degree of
Doctor of Philosophy

University of Bradford

Postgraduate School of Studies in Powder Technology

Department of Chemical Engineering

1986

ACKNOWLEDGEMENTS

My sincere and grateful thanks to Dr N.G. Stanley-Wood for his supervision and continued helpful guidance during the regular meetings at all stages of this thesis, and his encouragement and personal support during the course of this work.

I should also like to express my thanks to Dr J.C. Williams for the helpful discussions and interest he has shown.

My thanks are also extended to Mr R. Wilks and to the Chemical Engineering drawing office and workshop staff for their technical assistance and preparation and construction of equipment used in this work.

My grateful thanks to my family and parents for their moral support and encouragement, and my employer Darou-Pakhsh Pharmaceutical Company for the generous trusts and support.

My sincere thanks are also due to Mrs Deborah Collard of the Computer Centre who elegantly typed this thesis.

ABSTRACT

With the technological development in biologically orientated industries more and more natural products in powdered form are being handled and processed.

Three differently comminuted liquorice rhizome products were classified into 23 narrow size fractions to investigate the particle and bulk characteristics of the material, and to study the influence of particle shape on powder flowability.

The morphology of the fibrous particulate was investigated by using a Quantimet 720 Image Analyser. The perimeter (P), projected area (A), breadth (B), length (L), horizontal and vertical projected lengths (P_V and P_H) and the horizontal and vertical Feret diameters (F_V, F_H) were measured from which four dimensionless shape factors were evaluated, [$P^2/4\pi A$, $P_H x P_V/A$, L/B, F_V/F_H]. The surface texture of the particles was measured by fractal analysis.

The influence of particle shape and size on the mean flow rate, coefficient of flow variation and flow uniformity were measured using a specially designed inclined tube flowmeter.

The failure properties of powdered liquorice when sheared under known normal compressive stresses were measured and from a series of yield loci the unconfined yield strength, major consolidation stress and effective angle of internal friction were obtained. The effects of particle shape and size on the angle of internal friction, wall friction, bulk and packed densities were investigated and the experimental correlations expressed in terms of mathematical equations. These relationships, together with the failure function plots, indicate that comminuted liquorice powder behaves as a "simple" powder.

CONTENTS

CONTENTS (continued) **Page No.**

CONTENTS (continued) Page No.

C H A P T E R O N E

INTRODUCTION

and

LITERATURE SURVEY

1. INTRODUCTION

1.1 General Introduction

In many chemical and pharmaceutical industrial processes the handling of powders to fabricate a product is one of many operational stages and is therefore an important unit of operation.

In developing countries, which have a rich supply of flora containing potential therapeutical effects and biologically active substances, there is a strong desire to promote, develop and produce pharmaceuticals from medicinal plants. A large section of the population in developing countries still depend on such traditional pharmacognistical systems of medicine (191), because of the relatively low cost of herbal medicine.

It is therefore essential that the handling, storage, processing, physical and chemical characterisations of natural products and powdered medicinal plants be investigated. The handling of bulk powdered materials requires storage in hoppers, silos, bins or bunkers for certain periods of time and ultimately powders are discharged at known rates of flow. For economical reasons this is usually achieved by gravity.

In all cases of conveying, whether for packaging, dispensing, tableting, filling or any transportation, knowledge of the flow properties and characterisation of materials is essential to predict the particle behaviour and understand the mixing, segregation, product uniformity or weight variation. Free flowing materials have the tendency to segregate (80, 205), while materials which are cohesive produce a non-uniform flow pattern, and mixing occurs with difficulty (146).

By studying the flow behaviour of powdered material information may be obtained which could lead to natural materials being directly

compacted. This is at times, preferred to wet granulation and subsequent compaction of granules, because of the simplicity of the direct process, the need to protect the active ingredient within the natural products, and to achieve **optimal bioavailability** at much **lower costs.**

Relevant information on the **flowability of powders** in terms of particle size, particle shape and powder cohesiveness together with measurement of the uniformity of flow rate is advantageous to ensure quality assurance. For instance, in the case of a **shape characteristic** where a powder consists of relatively elongated particles there is a great possibility of non-uniform flow. This occurs as a consequence of the interlocking of particles into a rigid three dimensional structure.

In an attempt to investigate some of the problems associated with size, shape and flow, this thesis extends the research of other workers into the area of natural fibrous plant material. The effect of shear, shape and size on the bulk properties of particulates as; **direct flow rate, flow uniformity** and **failure properties** of natural plant material, which has had little scientific attention, is investigated.

The material selected was milled **LIQUORICE ROOT** with a size range from 38 to 315 micrometre which,depending upon the size chosen,is either a **cohesive** or a **free flowing** material.

From the present work a **new powder flowmeter** has been designed to measure the flow rate and the flow uniformity of fibrous or similar types of material. With the information from the thesis, it should be possible to **design a uniform and high quality product.**

1.2 Flow Rate of Solids

1.2.1 Flow properties

Industry requires powder flow to be consistent and regular in order to obtain high quality products. The quantity of powder handled can be of a kilogram size for processes such as tableting or the flow of catalysts from a hopper to a reactor, while for materials such as iron ore, calcium carbonate, coal or cement the quantity flow from storage bins could be thousands of tons. In all cases of handling and processing however it is essential that the rate of flow should have a minimum probability of interruption and have good uniformity of flow.

The flow of a powder can be defined as : **"a state of continuous deformation or relative displacement of its mass points with time which involves movement of the centre of gravity and in which the continuity of the displaced body is understood to be preserved".**

The fundamental difficulty of discussing powders in rheological terms is due to the fact that a powder mass consists of discrete particles and there is an absence of the continuity found in liquids. The factors which influence powder behaviour are size, shape and size and shape distributions which are capable of great variation. Jenike (96) compared solids and liquids and classified the differences as:

I) Solids can transfer a shearing stress under static conditions. They have a static angle of friction which is greater than zero, while liquids do not have a static angle of friction. The static angle of friction is the reason why solids form heaps while liquids form level surfaces.

II) Many solids, when consolidated - that is after force has been applied - possess cohesive strength and retain a shape under load. Solids also can form a stable dome or a stable well on

discharge from a hopper while liquids do not possess this property.

III) The shearing stresses which occur in a slowly deforming (flowing) bulk solid are usually considered to be independent of the rate of shear but dependent upon the mean pressure acting within the solid. In a liquid, the situation is reversed, shearing stresses are dependent on the rate of shear and independent of the mean pressure.

It can be seen from the above differences that it is not easy, with any degree of certainty, to predict the flow properties of powders from their dynamic or static conditions.

Behaviour of a mass formed by a large number of particles depends strongly on different forces. These forces are affected by the characteristics of both individual and bulk particle properties.

The important individual particle properties are:

particle size

particle shape

particle density

surface texture

chemical constitution

atomic structure

surface chemical composition

surface atomic structure

particle elastic-plastic behaviour

It is not however possible to obtain realistic values for these properties except as average values.

In order to characterise the properties of an assembly of particles or a bulk mass of particles, a distribution of the collected particle properties is required. Although distribution of particle

size and most recently particle shape can be obtained, the distribution of other properties is at times difficult to achieve and analyse.

The properties and phenomena associated with an assembly of particles are:

particle size distribution and specific surface area

particle shape distribution

packing property (bulk density, porosity)

rate of packing

compressibility of packing

internal friction

wall friction

cohesion and adhesion on to various surfaces

flowability and failure properties

segregation

angle of repose

It is a combination of the above properties that determine the behaviour of bulk solid materials.

Some powdered materials flow easily under gravity and the flow properties of this type of cohesion-free particles is well-documented (20, 22, 23, 41, 135,145). The flow behaviour of powders which are termed sticky or cohesive has been less well researched. **"cohesiveness" for powders can be defined as the tendency of individual particles to agglomerate or stick together.** This cohesiveness can be attributed to one or more of the following factors:

I) Surface forces:

Van der Waals, electrostatic, ionic, valency forces exist between the particles (73). There are also capillary or pendular

forces which arise from the presence of adsorbed films of vapours or liquids on the surfaces of the particles (162). These forces can also cause the particles to adhere to a non-powder surface such as container walls.

These forces arise because the structure of the solid surface is different in many ways from that of the body of the particle or crystal. Broken chemical bonds on the surfaces of crystals create strained lattice layers and a force field around the particles. As a consequence, physically and often chemically adsorbed substances are deposited as layers almost instantaneously on any newly created surface. These layers may extend to only a thickness of a few molecules (approximately 0.01th micrometre), but their influence is immense (69). Without adsorbed surface layers the solid surface energy would be greater and the cohesion and frictional affects would increase to cause strong particle agglomeration and attraction. In addition to solid surface energies the chemical composition and atomic structure of a solid particle effects the rheological or flow behaviour of powders as well as the deformation, strength and electrical properties of individual particles (113).

II) Inter particulate friction may be appreciable especially if the particles surfaces are rough and pitted.

III) Particles may mechanically interlock causing 'bridging' or 'arching', especially if the particles are irregularly shaped. Therefore the failure to flow is a consequence of all forces of attraction such as long-range Van der Waal's and electrostatic forces or short range valency, ionic, electrical or frictional forces.

Cohesion in materials usually occurs when the median particle size is in the range 50 - 100 μm but can also be present with a lower particle size range of 20 - 50 μm for inorganic slightly irregularly shaped particles and with material in the size range 100 - 200 μm for highly irregularly shaped organic material (111). There is a high tendency for very fine particles (< 5 μm) to form agglomerates when shaken, and to block orifices (130, 139).

Damp powders are also more cohesive than dry powders. In 1958 the significance of moisture on the agglomeration of powder was shown by Newitt and Conway-Jones (131). According to these workers liquid could be distributed in three different ways:

I) At low moisture contents liquid is present as a torus shaped bridge between particles, this is called the pendular state.

II) At a higher moisture content the rings join and make a continuous network of liquid, interspersed with air which is called the funicular state.

III) Increase in the moisture content results in the formation of a capillary state in which all pore spaces are filled with liquid.

The funicular and capillary states occur only when the amount of moisture is greater than 5% W/W while the pendular state can occur by the adsorption of moisture onto dry particles from the atmosphere. The effect of pendular state, on the forces of attraction betweeen particles have been examined by several workers. Newitt and Conway-Jones (131) showed that the cohesive stress arising from the presence of moisture between dry spheres by using the Fisher method (50), who concluded that the cohesive stress arises steadily as the moisture content is reduced to reach the pendular state. Derjaguin (42), Princen (143) and Pickness (137) all predicted an increase in tensile

strength between particles as the amount of moisture adsorbed on solid surfaces increased. Derjaguin (43) concluded that, below the moisture level at which pendular bounds form, adhesion between particles sharply decreases.

These physical and chemical forces between powder particulates can explain the flow behaviour of different size fractions of a powder.

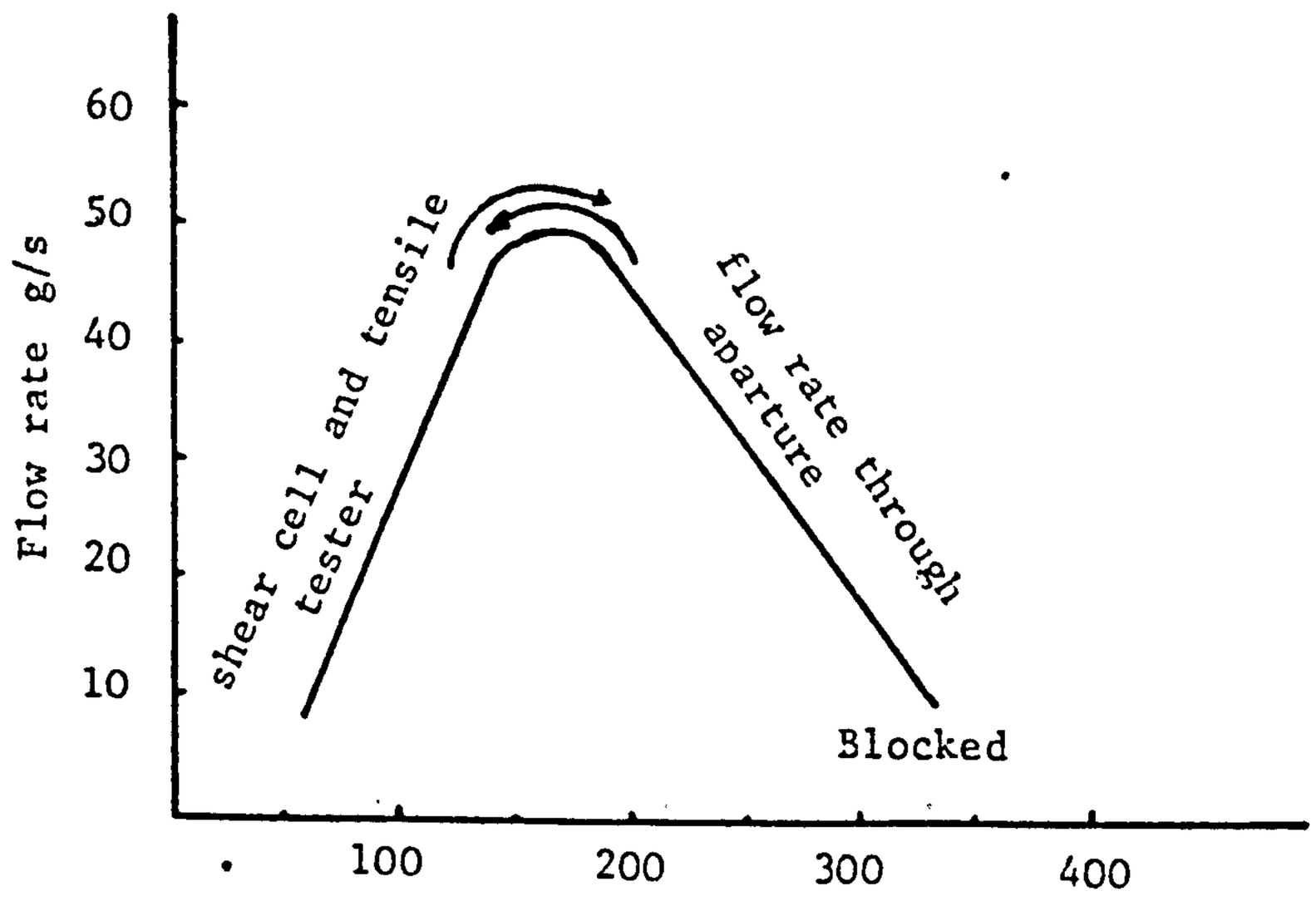

Figure 1.1 The flow rate of a powder or granular mass through an orifice in respect to particle size

A characteristic curve for virtually all materials is similar to that in Figure 1.1. The position and height of the maximum, and the position where blocking occurs, however vary from material to material. Also Figure 1.1 shows the approximate particle size ranges given by Harwood and Pilpel (74) in which the different flow testing techniques can be applied.

1.2.2 Terminology and factors defining flow and failure in the present work

I Flow patterns

There are two common types of flow pattern:

a - Core Flow

Core flow occurs when a channel is formed within the solid toward the outlet, therefore walls of the container has no influence on either the shape of the channel or the velocity profile of the solid within the channel.

b - Mass Flow

Mass flow occurs when all particles are in motion with fully mobilised friction at the wall with a constant coefficient of wall friction. Many industries require mass flow discharge because of the following advantages:

Relatively uniform flow rate, first in - first out discharge sequence, complete emptying of contents and the minimum segregation.

II Powder packings (Bulk density, packed density, porosity)

A packed powder can be defined as a system of particles in which each individual particle is supported by being in direct contact with another particle or with the wall of a container.

In general, when a powder rests as a heap, gravity is the only force acting on it. A powder bed in a container however may be in a state of opened or closed packing with an external compression force acting upon it. To find the most favourable or closest packing the powder may be vibrated or "tapped" to facilitate particle re-arrangement. Values of bulk density depend upon the filling method and particle size (130) and shape. Bulk density (ρ_B) and bed porosity (ϵ_B) are commonly used to

describe the state of packing of a powder bed. Porosity can be defined as the ratio of inter-particle void space to the total volume of the packing per unit mass of material:

$$\text{Bed porosity } \varepsilon_B = 1 - \frac{\rho_B}{\rho_p} \qquad 1.1$$

where ρ_p is particle density.

Brown (21) showed, excluding small voidages, that there was no significant effect of voidage on flow rate. Other workers (16, 76, 173) have indicated that the greater the bulk density the easier materials will flow.

III Compressibility

Compressibility can be defined as the change of volume caused by application of a compressive force acting on the surface of an assembly of particles, this thus includes compressibility achieved by vibration or tapping. The vertical force on a bed is not readily transmitted to deeper particle layers but is transmitted throughout the bed in a zig-zag manner between the particles and the force tends to decrease as it approaches the surrounding wall.

IV Strength of materials

a - Elastic strain

A perfectly elastic body is one which when a load is applied can be recovered by unloading the material.

The dimensional extension, usually length, is due to the stretching of the atomic bonds and changes in the internal energy of the loaded and unloaded specimen.

b - Plastic strain

When a load is applied to some material there is no recovery of the strain on unloading, in this case the material has been

beyond the elastic limit. This occurs by slippage of atomic planes over one another and is probably the most important phenomenon in the understanding of the behaviour of solids when subjected to stress.

c - Fracture

In engineering terminology depending on the amount of plastic flow present, fracture can either be Ductile or Brittle. Ductile fracture occurs when there is a slow breakage or a separation of crystal planes under an external load.

Brittle fracture occurs when there is a separation which spreads rapidly throughout the material, gaining energy for further breakage from the elastic energy of the surrounding material.

d - Stress

The engineering definition of stress is the applied force divided by the original cross section area before application of the force. When a force is normal to a plane over which it is acting then a normal stress is produced. If the force is parallel to the plane a shear stress is generated. A force acting at an arbitary angle can be resolved into normal and shear components of stress.

V Flow-factor (ff)

Jenike and co-workers (71) have calculated the stress distribution of slowly moving powders, where acceleration can be neglected, in various shaped hoppers. They concluded that a solid will flow if a dome of powdered particles does not develop across the outlet of the hopper. For this obstruction to occur the solid has to be consolidated to a degree to develop a dome of sufficient strength to support the weight of material above the

dome. The flow factor can be expressed as:

$$ff = \frac{\text{consolidating stress}}{\text{stress acting on an obstruction}} = \frac{\sigma_1}{f_c}$$

The smaller the value of ff, the less likelihood of dome formation.

VI Failure Function(FF)

The failure function as well as many other flow and failure parameters can be obtained from a yield locus (Section 1.3.1). Jenike (96) who originally defined the term "flow function" stated that this function is dependent upon the unconfined yield strength of materials, f_c, (stress acting on the free surface of failure), and major principal stress, σ_1, both of which can be found from a Mohr's circle drawn tangential to the yield locus, one passing through the origin of graph τ versus σ (Figure 1.9) and another circle tangent to the end point. The intercept with the σ axis indicates both values for f_c and σ_1. From a family of loci a number of σ_1 and f_c values can be obtained and then a graph of σ_1 versus f_c can be plotted which represents the "failure function" of material under certain conditions and it is a measure of the flowability of a material.

VII Unconfined yield strength (f_c)

Unconfined yield strength of material is defined as the stress which is acting tangential to a stress free surface of failure.

1.2.3 Theory of flowability of solid particulates

Many theoretical and experimental works have been conducted to study the flow of material through an opening. Brown and Hawksley in 1947 (20) studied the velocity patterns of granules being discharged from a container, and characterised the regions within a bed where the particles had different velocities. Novosad in 1968 (135) studied the steady-state flow of sand in a flat-bottomed cylindrical vessel, and subdivided flow material into four regions. Van Denburg and Bauer (193) studied the flow pattern developed when a powder has a wide range of particle sizes. According to these workers some segregation takes place, since the largest particles, those with the highest energy, roll down the side of the vessel during filling, and consequently they come to rest and occupy a lower stationary proportion of the hopper. Thus, if the filling of the container is not done correctly, at the end of the discharge the coarse particles are the last to be discharged. This phenomenon is also explained by Jenike (96):

"particles dropping through an orifice are dependent upon their size, size distribution and shape and will segregate and form different angles of inclination".

Many other workers including Franklin and Johanson (53), Deming and Mehring (41), Rausch (145), Bingham and Wikoff (14), Ketchum (108), Brown and Richards (21) have studied the relationship between the flow rate and orifice diameter and obtained different equations. The work of McDougall and Evans (123) which took into account the pressure inside a vessel, gave the following equation and values for the constants.

$$W = K D_o^n \qquad 1.2$$

$$W = 0.59 D_o^n$$

where K = constant equivalent to 0.59

W = Mass flow through a circular orifice into open air (lb/sec)

D_o = orifice diameter (inch)

n = a constant with values between 2.5 - 3 which in case of McDougall is 2.5.

Many other factors, such as wall friction (16), direction of forces inside the vessel (23, 37) and the effective angle of internal friction of the material (164, 206) need to be measured. Rose (157) in a comprehensive study of the relationship between many different parameters affecting the flowability of materials concluded that the following factors made a contribution to flow.

I) the diameter of the particle (d)

II) the diameter of the orifice (D_o)

III) the density of the material involved (ρ_B)

IV) coefficient of friction (μ)

V) cohesive forces operative between the particles (C)

VI) the shape factor (Z)

VII) acceleration due to gravity (g)

VIII) the height of the material above the orifice (H)

IX) the inlet diameter of the container (Δ)

X) the cone angle of the base (θ)

These relationships can be written symbolically as:

$$\text{Flow rate } (W) = \phi [D_o, d, \Delta, H, C, \rho_B, g, \theta, Z,]$$

where ϕ denotes a function of each of the variables, and the relationships found by Rose between these factors were :

a - Δ/D_o parameter

When $\Delta / D_o > 2.6$, then the rate of discharge in cylinders fitted with conical bases is independent of the value

of Δ/D_o. Other workers (108, 23) have proposed a value of $\Delta/D_o > 2.5$.

b - H/D_o parameter

When $H/D_o > 2.5$, then the flow rate is independent of the head (H). Other workers (21, 157, 75) have however reported that the flow is independent of head of material unless the vessel be nearly empty or when the head is approximately twice the diameter for cylindrical hopper, and three times the diameter for a conical hopper. However, all studies are approximately in accord with the results of Newton (132) who stated that the flow rate is proportional to $H^{0.04}$. It is agreed for cohesive material, even though the effect is small but is greater than free flowing materials which is nearly none.

c - D_o/d parameter

Rose indicated that the influence of the ratio of the orifice diameter over particle diameter (D_o/d) on flow is not simple and can be complicated by a number of extraneous variables such as cohesion and particle friction. The rate of flow decreases when the diameter of particulate system is less than approximately 100 μm (111, 62, 180). This size is only an approximation because flow is also material dependent. The effects of cohesion and friction then become significant (130, 139, 21); therefore Rose considered the groups: D_o/d, $C/D_o^3\rho_B g$ and μ together. He found the following relationship :

$$(W/D_o^{2.5}\rho_B{}^{0.5}g^{0.5}) = K\,(D_o/d - 3)^n \qquad 1.3$$

where the term $(D_o/d-3)$ has been included to represent zero flow. $D_o/d \leqslant 3$ indicates no flow through orifice. According to Langmaid (116) the bridging of an outlet occurs when the diameter

of the outlet is about 2.5 x d. It is strongly recommended instead finding the coefficient of friction (μ) by using an angle of repose, as applied by Rose, that the Jenike shear cell or similar method for angle of internal friction be used as this is more successful (7).

d - <u>The shape factor (Z)</u>

The effect of particle shape has not been as widely investigated as other factors. Rose used the ratio (f/K) where f and K have been defined by Heywood (82) (Section 1.4.1).

Rose and Tanaka (157) adopted this ratio as a shape factor $Z = f/K$, when Z is equal to 6 the shape of the particles are spherical. From the flow of steel balls, silica sand, powdered glass and steel discs the following relationship (Figure 1.2) between flow and shape was obtained, which could be mathematically expressed as:

$$\phi(Z) = 0.16/(Z - 5)^{0.5}$$

and for practical purpose:

$$\phi(Z) = K/(Z - 5)^{0.5} \qquad 1.4$$

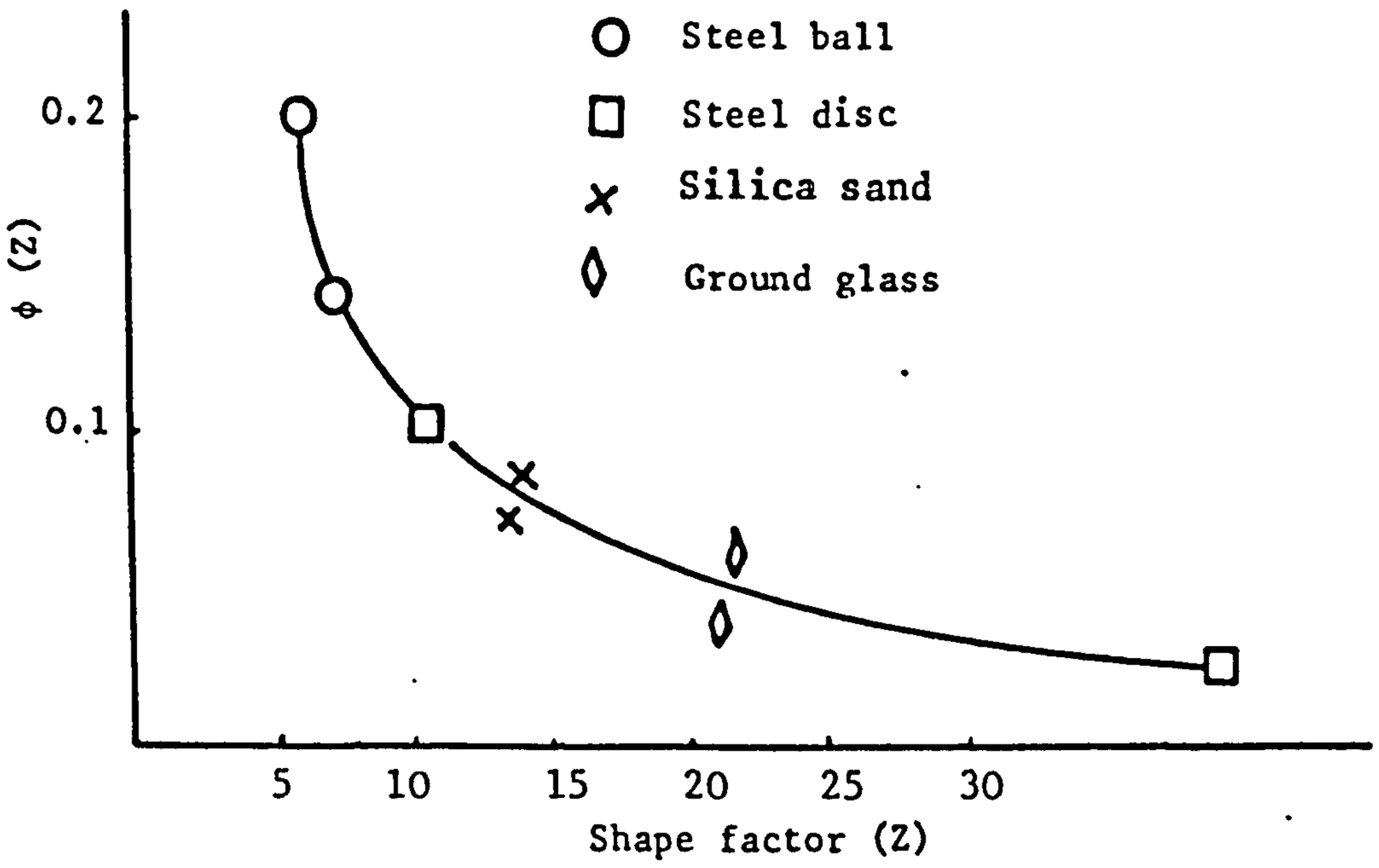

Figure 1.2 Flow rate and shape interrelationship

From Figure 1.2 it can be observed that the flow rate from an orifice is extremely sensitive to any variation in the particle shape especially when particles are nearly spherical. The sensitivity decreases as the sphericity of the particles decreases.

1.2.4 Flow rates of dry powders in inclined tubes

There have been some attempts to measure the flow rate of materials along an inclined tube. The initial difficulty in such study is the need to maintain a steady flow rate from a container which feeds the inclined tube. To ensure steady flow rates a known uniform material in terms of size, size distribution, density and morphology was used by Austin and co-worker in 1978 (8) to investigate the axial flow of 250 to 400 μ m silicon carbide.

Campbell et al (27) also tried the axial flow along a non-rotating 2.4 metre inclined channel by using glass beads.

It is common practice in industry when seeking information on the flowability of powders to measure the flowrate through an orifice. The different types of equipment used for these purposes have been reviewed for various industries (40) and by different workers (102, 63) to obtain some indications of material flowability.

1.3 Strength and Failure Properties

In order to study the flowability of cohesive material which does not readily flow through any aperture, there is a need to relate the flow properties of such materials to the internal particle deformation in terms of stress-strain behaviour of the materials as well as to the friction between particle-particle and particle-wall.

Discussions on powder behaviour in terms of stress-strain deformation and failure have been fully documented elsewhere (6, 7, 22, 92, 94, 95, 97, 170, 181, 207). Reiner (147) defined deformation as:

"a movement of points or particles of a material body relatively to one another such that the continuity of the body is not destroyed".

This definition however implies that the powder bed is a continuum body. The alternative approach is to calculate the physical and mechanical properties of a particle assembly from knowledge of the properties of the individual particles. Allowance has to be made for the orientation and packing arrangement of particles and also for the various forces which operate between them. Rowe (160) and Horne (89) explained the physical and mechanical properties of particulate materials in terms of an atomic model. Because of the complexity of a particle system these explanations have not been entirely successful. There is a need to combine both the continuum model and atomic model to account for both bulk properties of powders and the forces between individual particles at the points of contact.

The study of the behaviour of powders under applied stresses had its origin in soil mechanics. Jenike et al (94, 95) have shown that the particulate solids handled in soil mechanics are however different from the bulk solids used in the process industries. Soils are usually clay-like material with a degree of water present. The

strength of moist compacted materials therefore is usually of a higher order of magnitude than of a dry bulk material. In soil mechanics the failure of a material is of interest while in the process industries both failure and beyond failure are of concern. Despite these differences the principles involved in determining the strength of both soils and powders are similar.

The peak shear stress at failure (τ) for remoulded saturated cohesive soils is a function of both the effective normal stress (σ) and the void ratio (ε) at the failure plane. These parameters can be expressed as:

$$\tau = \mu\sigma + \lambda\, e^{-(\beta\varepsilon)} \qquad 1.5$$

where:

μ interparticle coefficient of friction (constant for particular material)

λ angle of shear plane to incline plane (constant for particular material)

β angle of shear plane to horizontal (constant for particular material)

There are generally three types of material which can be used to describe a model for the rheological or flow behaviour of materials.

I) an elastic

II) an elastic/plastic

III) a rigid/plastic

If a small element of one of the above materials is subjected to a constant and uniform normal stress (σ), and available shear stress (τ).

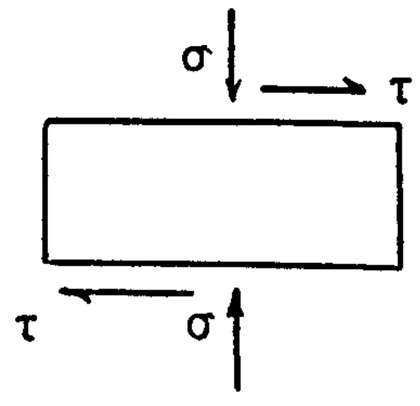

The following typical relationship between shear stress and shear strain of material can occur (Figure 1.5).

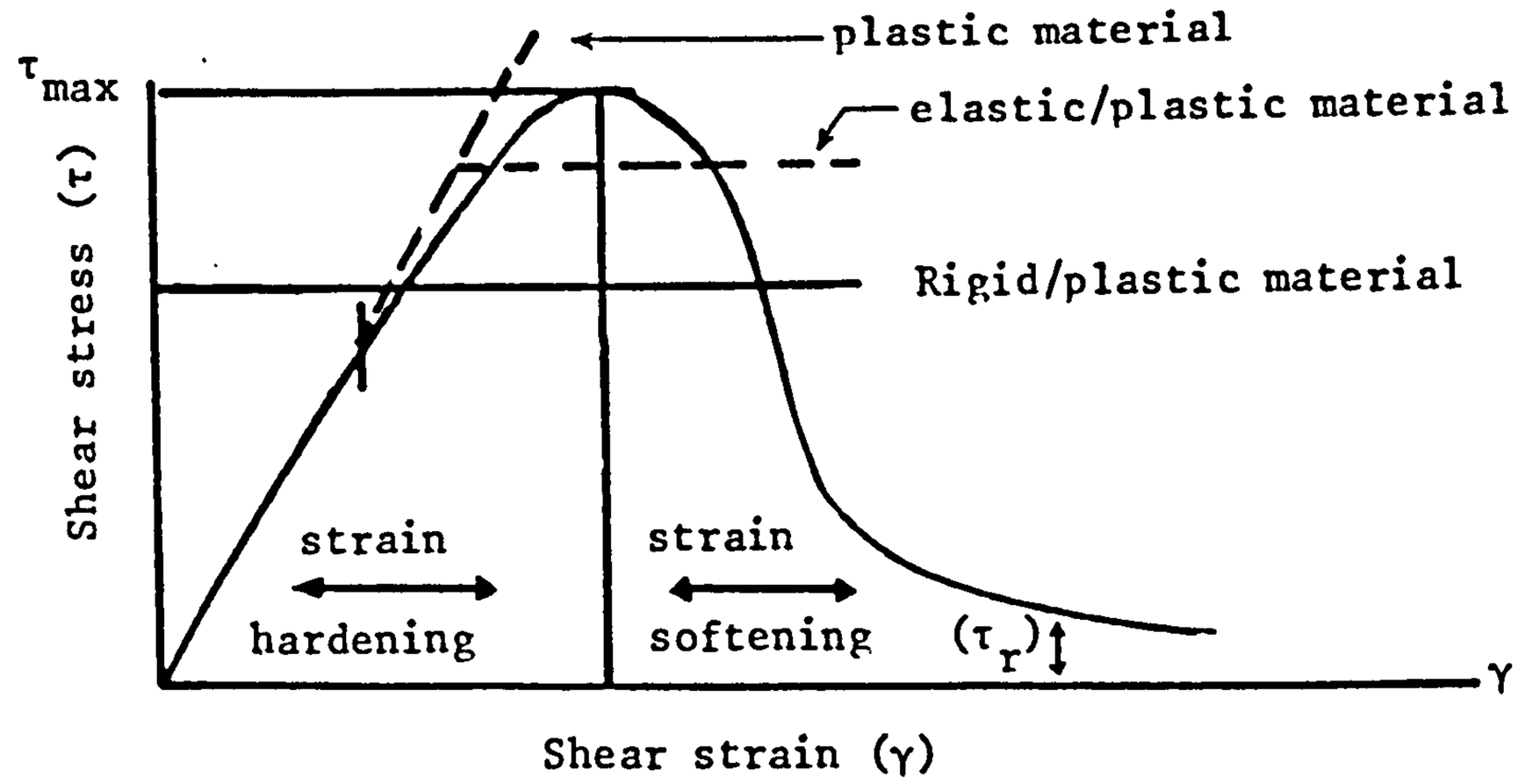

Figure 1.5 Stress and strain relationship of material

For very small values of shear stress, the corresponding strains is nearly linear and elastic. As the shear stress increases a point is reached where significant plastic shear strains begin to develop. At this point, the material is said to undergo yield. The resistance of the material to increasing plastic shear strains is called the shear strength. Initially, the plastic strains are strictly limited, because the material shows an increase in resistance to further deformation. The material is said to be "strain harden". Strain hardening can only increase the resistance to shear stress to a strictly limited extent. When the applied stress exceeds a limiting value (τ_{max}), the material becomes unstable and material is said to fail. After failure the material can undergo a phenonmenon described as "strain softening" or "work softening". Eventually after quite large strains have taken place a residual strength (τ_r) can be developed which is nearly independent of further strains.

None of these models however completely simulate the behaviour of moist soils. The more realistic model, according to Jenike and Shield

(93) is the rigid/plastic body or Coulomb solid. Jenike (95) studied a number of dry powders and concluded from the yield loci as in Figure 1.6 that even the Coulomb rigid/plastic model required modification to describe completely the behaviour of the powders.

The reasons given were:

I) The yield loci of dry powders deviates significantly from linearity at low normal stresses.

II) The yield locus does not extend indefinitely but terminats at a specific point termed the "Endpoint", (σ_E or τ_E), beyond which consolidation takes place.

III) The value of the yield locus is not constant but is a function of either the sample preparation, the extent to which the powders have been consolidated or the packing density.

IV) The intersection of the yield locus with the shear (τ) axis is termed the cohesion of the powder (C).

V) The negative intersection of the yield locus with the normal stress axis (σ) represents a point of failure of the sample in tension which is termed the tensile strength (T).

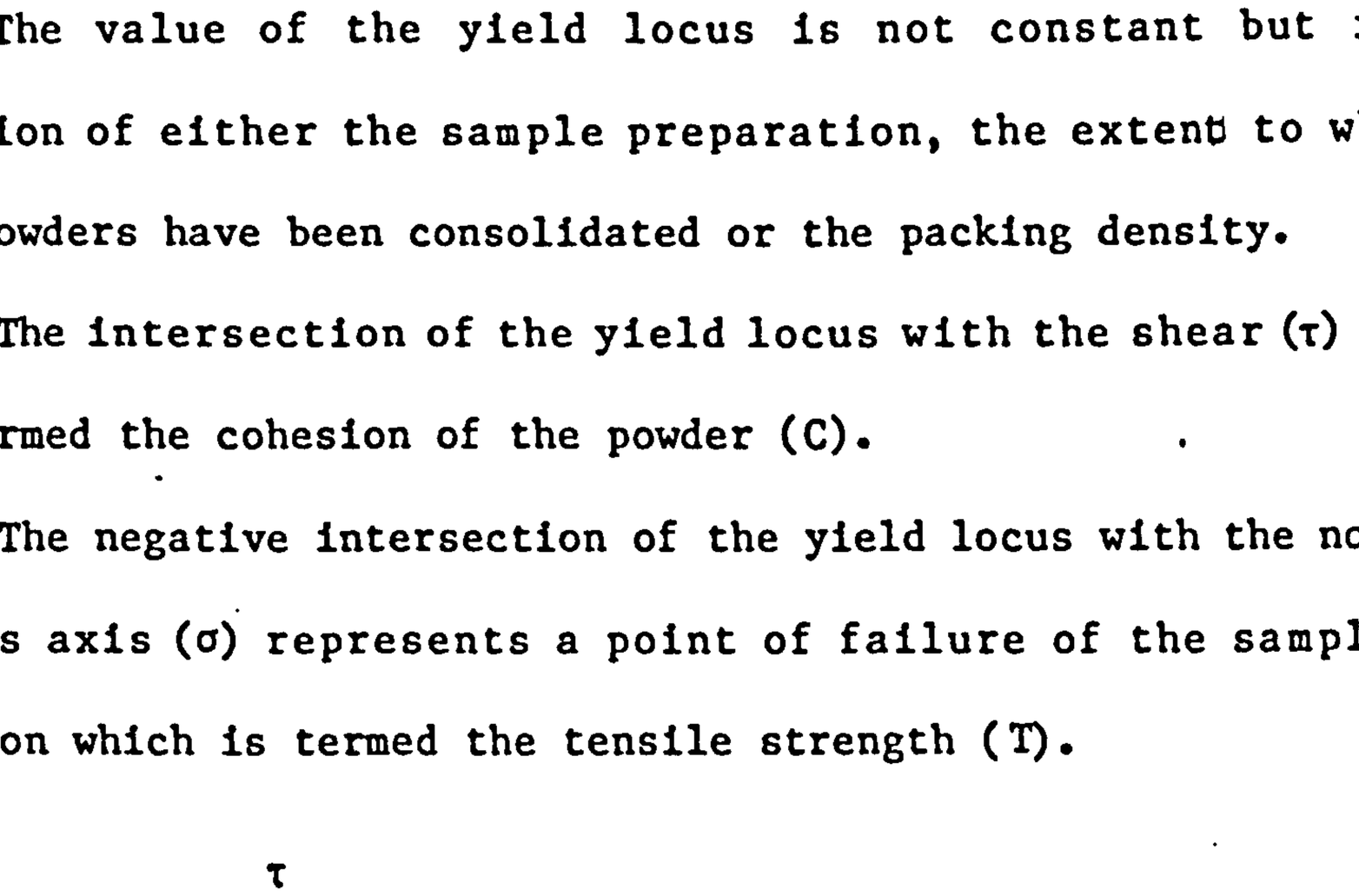

Figure 1.6 Yield locus, cohesion (C) and tensile strength (T) of powder

Jenike extended this work to measure the shear strength of powders in a specially designed shear cell. From the stresses arising from gravity, Jenike developed a theory of arch stability which can obstruct powder flow from hoppers. The design of mass flow hoppers is based on the measurement of a family of yield loci using a Jenike shear cell.

Roscoe et al (155) using a three dimensional space concept (τ,σ , ε,Figure 1.7) showed that equation 1.5 could generate failure surfaces in space. Since Hvorslev was first to deduce the relationship between τ, σ , ε , to give the condition of failure surface in three dimensional system the surface is known as the "Hvorslev surface".

Values above either the Roscoe or Hvorslev surface represent the stress conditions which cannot be experienced without material failure.

Projection of the surface outline onto the $\sigma : \tau$ plane, at constant voidage ($\varepsilon = 0$), show lines inclined at an angle $\phi = \mathrm{Tan}^{-1}\mu$ to the $\tau = 0$ plane. These are termed the yield loci of the material and can be expressed as:

$$\tau = \mu\sigma + \Sigma \qquad 1.6$$

where: Σ is equivalent to $\lambda\ \rho^{-\beta\varepsilon}$ and remains a constant dependent only on ε and μ.

Roscoe and co-workers extending the work of Hvorslev and others (156) led to the deduction that the conditions under which material fails without change in volume, can be called the critical state line (C.S.L.) or critical void ratio (C.V.R.). Any stress pathway of sufficient magnitude will ultimately terminate on the failure surface when this point is reached.

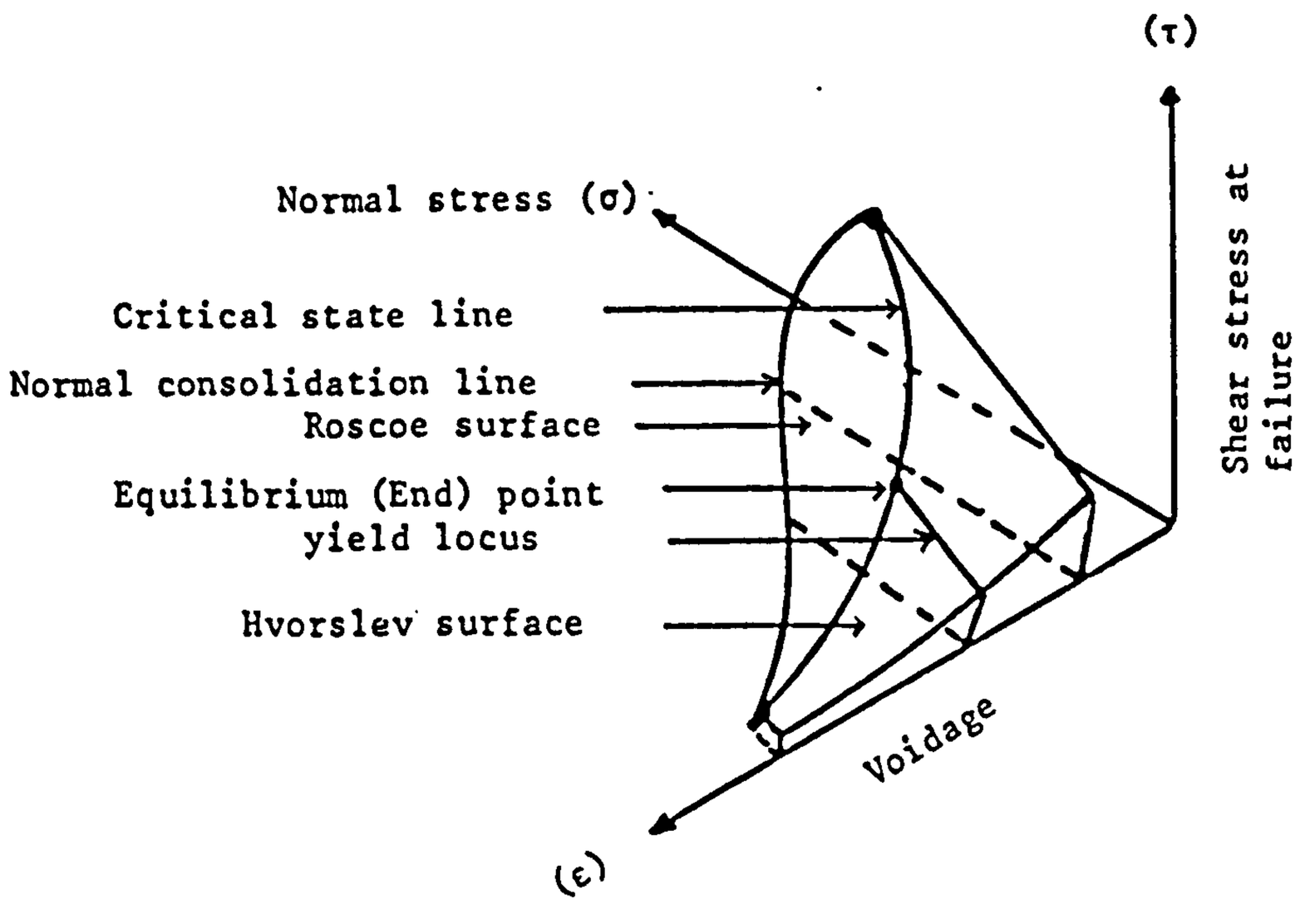

Figure 1.7 The yield surface in three dimensional space

1.3.1 Yield Locus of a powder

An unconsolidated powder has no yield strength, in fact, an aerated solid may behave like a fluid. When a solid is consolidated stresses arise under the weight of the powder which force air out and particles are brought closer together. Thus molecular forces can begin to develop, and as a result of this consolidation process the particle assembly gains strength. The higher the applied stress usually the greater the degree of consolidation and the greater the "strength" of the final powder state.

Not all solids however gain strength under a consolidation stress. Dry sand which is known to be cohesionless, gains practically no strength within the range of stresses normally seen in storage plants. In order to cause such solids to flow, it is sufficient to overcome only the true angle of internal friction (Δ) which is usually above a value of 45^{o}. If dry sand is sheared with a shearing force (S) under a normal force (N), no continuous deformation occurs as long as the expression $S < N \tan\Delta$ remains but when slip occurs then $S = N \tan\Delta$. This expression can be regarded as Coulomb friction (96). For values of N, S laying below the line (Figure 1.8), the solid can be considered to have rigidity. For values laying on the line

($S = N \tan \Delta$) slip or yield occurs, and the line is then the locus of the yield values of the normal and shearing stresses. This locus can be termed either the yield locus (YL) or the Jenike yield locus (JYL).

For free-flowing material, like sand, the yield locus coincides with the effective yield locus (EYL) which is also the Mohr stress envelope and passes through the origin. The effective yield locus has an angle (δ) to the normalstress (N) axis and is termed **"the (Jenike) effective angle of internal friction".** If however the test solid is cohesive, then usually "powder strength" is gained as stress is applied. In N, S coordinates such a solid can be represented by a family of yield loci (Figure 1.9), where each locus corresponds to a different sample consolidation. The slip occurs when

$$S = N \tan \delta + C \qquad 1.7$$

where δ and C (material cohesion) are approximately constant for any particular material. This expression is called the Coulcomb equation.

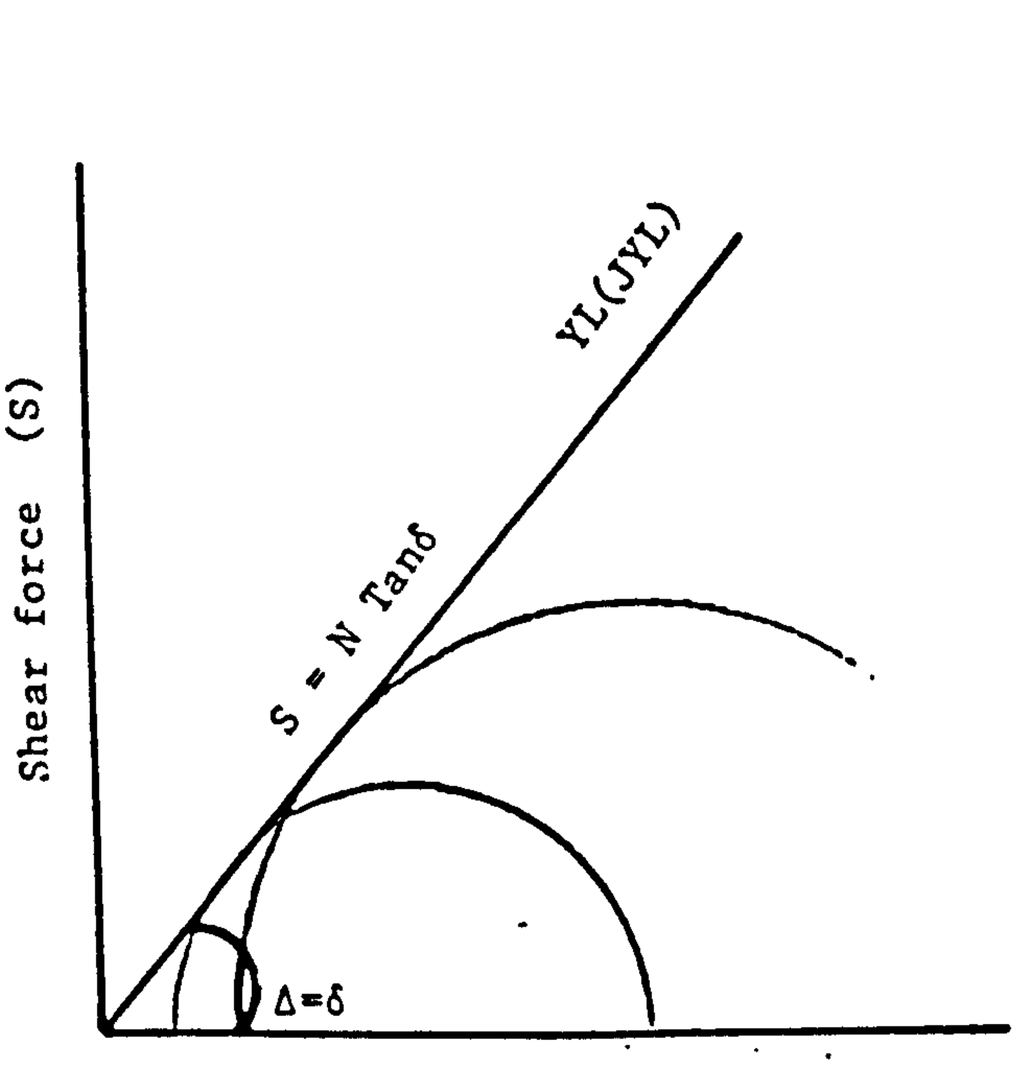

Figure 1.8 Free flowing material yield locus

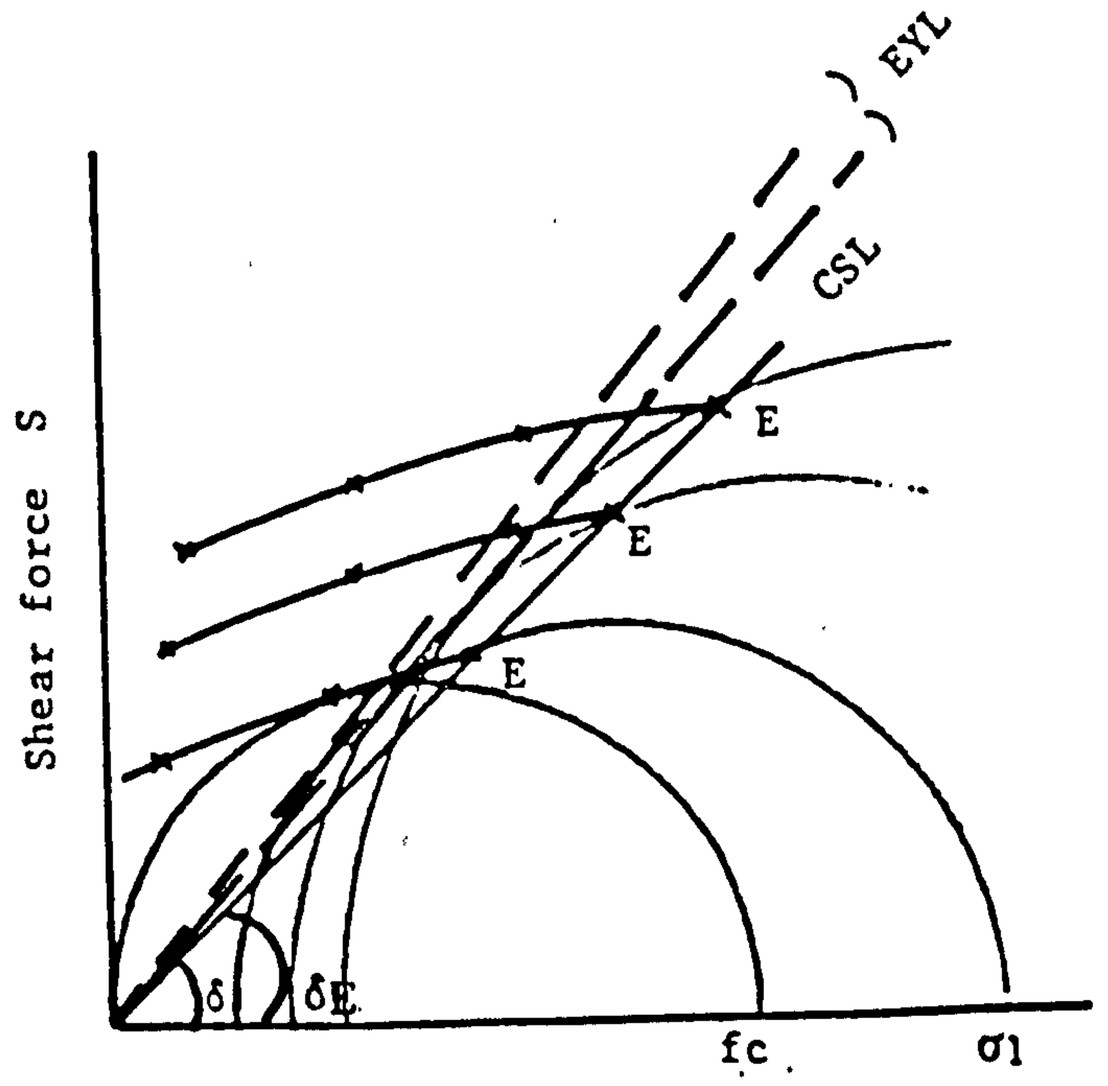

Figure 1.9 Cohesive material, a family of yield loci

1.3.2 Critical State Line (C.S.L.)

Jenike and others (30, 95, 96, 208) found that the end points (E) of the yield loci lie on a straight line which passes through the origin of a "S : N" axis. The critical state line is the line which joins all the values of these shear stress and normal stresses when there is no change in volume. These end points are unique because at all other positions on the yield locus shear produces an expansion of the powder bed, with work being done against both internal and external forces. The slope of this critical state line is the angle of internal friction (δ_E) of the powder. An alternative and possibly more accurate assessment of the angle of internal friction for cohesive materials can be obtained when shear stress is plotted versus the applied compound normal stress and termend Tan Δ_c . Compound normal stress is calculated from the addition of the normal stress (σ) to the tensile stress (T) (208).

1.3.3 Wall yield locus (W.Y.L)

When a solid slides along a hopper wall the stress conditions along the wall produce a wall yield locus.

The wall yield locus can be obtained with the same apparatus as used for powder failure measurements but with a modified procedure, to give the angle of wall friction (ϕ_w).

Wall friction is an important parameter which is used in the design of solids handling equipment, hoppers, conveyors and mixers. Strijbos (185) investigated the frictional behaviour of a metal wall over a layer of ferric oxide powder, he concluded that the behaviour is dependent upon two ratios, the particle diameter d_p to wall roughness, R_w- (d_p/R_w), and the particle hardness, H_p, to the wall hardness, H_w-(H_p / H_w). He found that for $d_p/R_w < 1$ a cohesive layer of material formed at the wall, which is independent of ratio H_p / H_w.

Therefore the friction measured was due to a powder on powder friction which gave a high dynamic wall friction coefficient. When the ratio $d_p/R_w > 1$ and the ratio $H_p/W_w < 1$ conditions are different because as the d_p/R_w ratio increases the number of contacts between the wall and particle become less. No adhering particles layer forms on the wall and a pure powder and wall friction occurs. The wall friction may be affected either by the presence of very fine particles near the wall or by a change in the average size of the particles in this wall layer. Investigations (53, 192) also have indicated that the angle of wall friction is affected by a combination of **migration of fines adjacent to the wall, scratching of the wall, consolidation of powder sample** and **breakage of particles.** The angle of wall friction is assumed to have a direct correlation with particle size in immediate contact with the wall.

1.3.4 Classification of flowability of solids and effect of some parameters on it

Jenike (96) by using the method of failure function (FF) classified the flowability of solids as following:

FF < 2	Very cohesive and non-flowing
2 < FF < 4	cohesive
4 < FF < 10	easy-flowing
FF > 10	free-flowing

Table 1.1 Flowability of solids based on failure function

Harwood (75) has obtained the following FF values and classifications for some pharmaceutical materials.

Material	FF	Qualitative description
Agglomerated anhydrous		
Cephaloridine (batch 1)	10.6	free flowing
" (batch 2)	12.3	free flowing
Finely powdered cephaloridine	4.7	cohesive
Anhydrous Griseofulvin "12 μm"	2.4	cohesive
Micronised Paracetamol "nominal 2 μm"	1.6	very cohesive

From the analysis of the yield loci of a large number of powders including: Buckland sands, fine dust, fine silica, limestone dust, cement, soya flour, icing sugar, dried egg powder, titanium dioxide, sodium bicarbonate and antibiotic, etc., where the last two are hygroscopic and on exposure to atmosphere became more cohesive, Ashton, Cheng, Farley and Valentin (7) deduced equation 1.8 to mathematically express the yield loci of these materials.

$$\left(\frac{\tau}{C}\right)^{n} = \frac{\sigma + T}{T} \qquad 1.8$$

where the exponent 'n' is termed the shear index of the material. Equation 1.8 is generally termed the Warren Spring Equation. Pilpel (140) proposed the total amount of work done at failure by the shearing stress could be divided into three parts:

1. work done at constant volume against the internal friction plus;
2. work done against the external force due to volume change plus;
3. work done against the internal forces due to the volume

change,

and later was suggested (208) that the shear stress at failure could be expressed as:

$$\tau = (\sigma + T)\ (\mathrm{Tan}\Delta_c + \frac{d\varepsilon}{d\gamma}) \qquad 1.9$$

where: $\mathrm{Tan}\ \Delta_c$ is angle of internal friction (see Section 1.3.2)

ε is the normal strain

γ is the shear strain

In practice, the value of $\mathrm{Tan}\ \Delta_c$ is similar to $\mathrm{Tan}\delta_E$. Application of equation 1.9 is difficult because of the measurement of the normal strain should occur at the zone of bed failure. An advantage of using the angle of internal friction rather than the cohesion "C" or the tensile stress "T" values to assess the flowability and general mechanical properties of a powder is that the angle of internal friction is independent of the bulk density of the sample.

Some workers have proposed (48) the direct correlation between C (cohesion under zero applied stress) and T (Tensile strength at the particular packing density) at which the yield locus was determined as $C \simeq 2\ T$. Later investigators (30, 75) have shown that the ratio C/T can vary from 0.3 to 9.0 dependent upon the packing and density of the sample. The shear index, n, like the failure function (FF) can also be employed as a quantative measurement of the flowability of powders. The shear index is seen to vary from a value of 1, for free flowing, to 2, for very cohesive powder. When, n, is unity the Warren Spring Equation becomes:

$$\tau = \mu\sigma + C$$

which is similar to the Coulomb equation (equation 1.7).

Ashton, Cheng, Farley and Valentin further concluded that: the tensile strength and the cohesion were found to be a similar power law function of the bulk density. The power index in Warren Spring equation "n" for powders at relatively constant humidity was found to be independent of the bulk density. Therefore the yield locus of a powder, at any values of bulk density can be evaluated from the yield locus for the same powder at another bulk density by measuring just the tensile strength and shear values. The effects of particle size and size distribution on the shear properties of powder were also studied by Ashton et al (7). Harwood (76) investigated the effect of bulk density on the shear index obtained with griseofulvin and lactose and described as the bulk density increased the shear index value decreased. This indicated that the powders became more free-flowing and supported the work of Williams and Birks (208). However it was not suggested that a powder will be more free flowing if compacted much higher than when it is at its normal bulk density.

The published works before 1970 (Fowler and Chodziesner (54) and Ridgway, Rupp (150)) on the effect of the shape of particles on the mechanical properties of powders was attempted with either the coarse powders or granules which are generally always free flowing. Walton and Pilpel (199, 200) however studied the effects of particle size, shape and moisture on the tensile properties of procaine penicillin powder and concluded that the tensile strength of the powder was strongly dependent upon the interparticle separation.

A similar investigation was conducted by Farley and Valentin (48) using fine griseofulvin and iron oxide to find the effect of particle shape and size on the shear index. The shear index could be related to particle shape and size by the following expression:

$$\text{Shear index} \quad n = 1 + \frac{B}{d} K \qquad 1.9$$

where: B is constant depend on shape which has a value of 0.7 for spherical and 0.4 for elongated particles

K is constant (0.6 - 0.7)

d is particle volume/surface diameter

Nikolakakis and Pilpel (133) concluded that the overall range of forces of interparticle attraction, decrease with increase in the particle shape coefficients. They also described the difficulty of sorting fine powders (< 100 μm) into different shape fractions. Little quantative work has been done on the specific effects of particle shape. The strength of powders however is affected by the number of contacts in an assembly of particles, the amount of contacts being dependent more and more upon the particle shape as the particle size is reduced (31).

Gerritsen and Dekker (58) studied the unconfined yield strength of potato starch and showed that the behaviour of small particles in bulk is different from that seen with large particles. The yield strength of the sample < 25 μm is only slightly dependent upon the time of consolidation, while the sample > 60 μ m is highly dependent upon the time of consolidation. The difference in this time dependency may be due to the large difference in the area of surface contact or in the number of contact points per unit of volume. They also concluded that the yield strength of the potato starch is strongly dependent on the water content of the material from an initial 11% w/w moisture content an increase of strength occured with increase in moisture. For more than 19% w/w moisture content a decrease of strength however was observed.

1.4 Morphology

In the production, handling and interaction of materials where particles are generated, reacted, stored, packaged and transported, particle behaviour can be described as a function of particle size, shape, density and surface forces. Each of these factors contribute a variable degree of influence upon the total particle behavioural pattern. Many investigations (21, 22, 41, 98, 130, 131) have been conducted on the behaviour of bulk powders but the effect of particle shape in most cases has been neglected. The morphological characteristics of particles have however an important influence in the behaviour of powder. In particular, in the paint, ink and cosmetic industries powder products are influenced by the particle shape because of the orientation and packing of particles in formation of films which change the optical properties of surfaces (87). For particles of the same volume, round particles require a thicker surface layer than thin flakey particles in order to produce the same hiding power. In the rubber industry, in which high tensile strength products are required, elongated particles are undesirable because during the formulation process such particles can be orientated to produce a grain interface which could facilitate tear in a preferential direction. Spherical particles such as carbon blacks therefore are better rubber reinforcers. In contrast elongated particles such as wool, asbestos and textile fibres make better reinforcers for plastics(171) because plastics require a high impact strength rather than high tensile strength, while the abrasive industry require sharp edged irregular particles for the products. In the handling of materials smoother and more spherical particles are preferred to give better product uniformity, higher degrees of predictability, higher flow rates and more constant bulk volumes (65,

180).

It is very difficult to produce a powder with identical particle shapes even at very highly controlled conditions, particularly when the particles are below 200 μm in diameter (150). It is therefore only possible to observe the average shape in an assembly of particles. A common method of producing various shaped particles with different sizes is by comminution (13). The shape of comminuted particulate materials has not however received enough attention mainly because of difficulies in accurate shape determination. Gaudin (57), Giles (61), Twenhufel and Tyler (190) and Alling (4) studied the shapes of various minerals including Quartz, Microcline, Tourmaline and Garnet by crushing them with different equipment , found that the shapes of the grains were dependent upon the size of the grains and after a known grinding time the type of mill used affected the particle shapes. Giles stated that for minerals such as sandstone, the angularity of these particles showed a constant increase with increasing fineness of grains, the finer grains being more acircular than the larger grains. Gaudin observed for minerals such as quartz that the actions of a jaw crusher, a roll mill, a ball mill, on the shape of particles are basically the same.

Yigit et al (212) did not agree with this concept and demonstrated that an electrohydraulic crusher produced more cubic shapes than elongated particles in comparison to jaw crusher. Whittemore (204) also observed that with kaolin a roll crusher produced more uniform angular particles than a dry-panning method which produced more compact coarse particles. It is generally agreed that roll crushers produce angular particles while ball mills generally produce equidimensional and rounded particles (88).

Tsubaki and Jimbo (188) examined the size and shape relationships

of limestone and glass powders and concluded, that:

"particle shape varies not only with the constituent of the material but also with particle size".

Bond (15) mentioned that:

"the character of the material has more influence on the shape than the type of equipment used for size reduction".

In contrast, Rose (158) stated that the properties of a material have some effect, but the type of equipment has certainly a marked effect upon the particle shape. Heywood (85) suggested that the shape obtained from the initial fracture of material is solely dependent upon the material itself, but in contrast, Charles (29) stated that the shape of glass particles from an initial fracture was dependent upon the rate of stress applied. Bond (15) confirmed that high speed impacts produced cubical-shaped, whereas low speed impacts did not. Pilpel studied the shape of pigments (138) and stated that the different sized particles often have different shapes. In micronised pigments the fine particles were often less irregular and more spherical in shape than coarser ones. The relationships between the shape of comminuted particles and their size specially for size under 1 mm (114) is still unclear. Shape analysis may help therefore to improve not only comminution to obtain a desirable particle shape but also many other processing in industrial systems.

Several workers (1, 2, 151, 152, 153) have been able to correlate the Heywood shape factor (Section 1.4.1) with flow rate, die filling and sieving properties. The Heywood shape coefficient does not however provide a complete picture of shapes and the effects of particle elongation and flatness are not distinguished, unless they are combined with additional shape information.

Shotton and Obiorah (173) studied the effect of shape on bulk density and other physical properties of sodium chloride. They observed that cubic sodium chloride had a smaller shape factor than dendritic salt crystals and thus gave a higher bulk density and higher tap density. Beddow (10) used the ratio of apparent density (AD) to tap density (TD) as a shape parameter for metal powder particles. This technique relies upon the rapid establishment of a limiting value of tap density from a tap density tester.

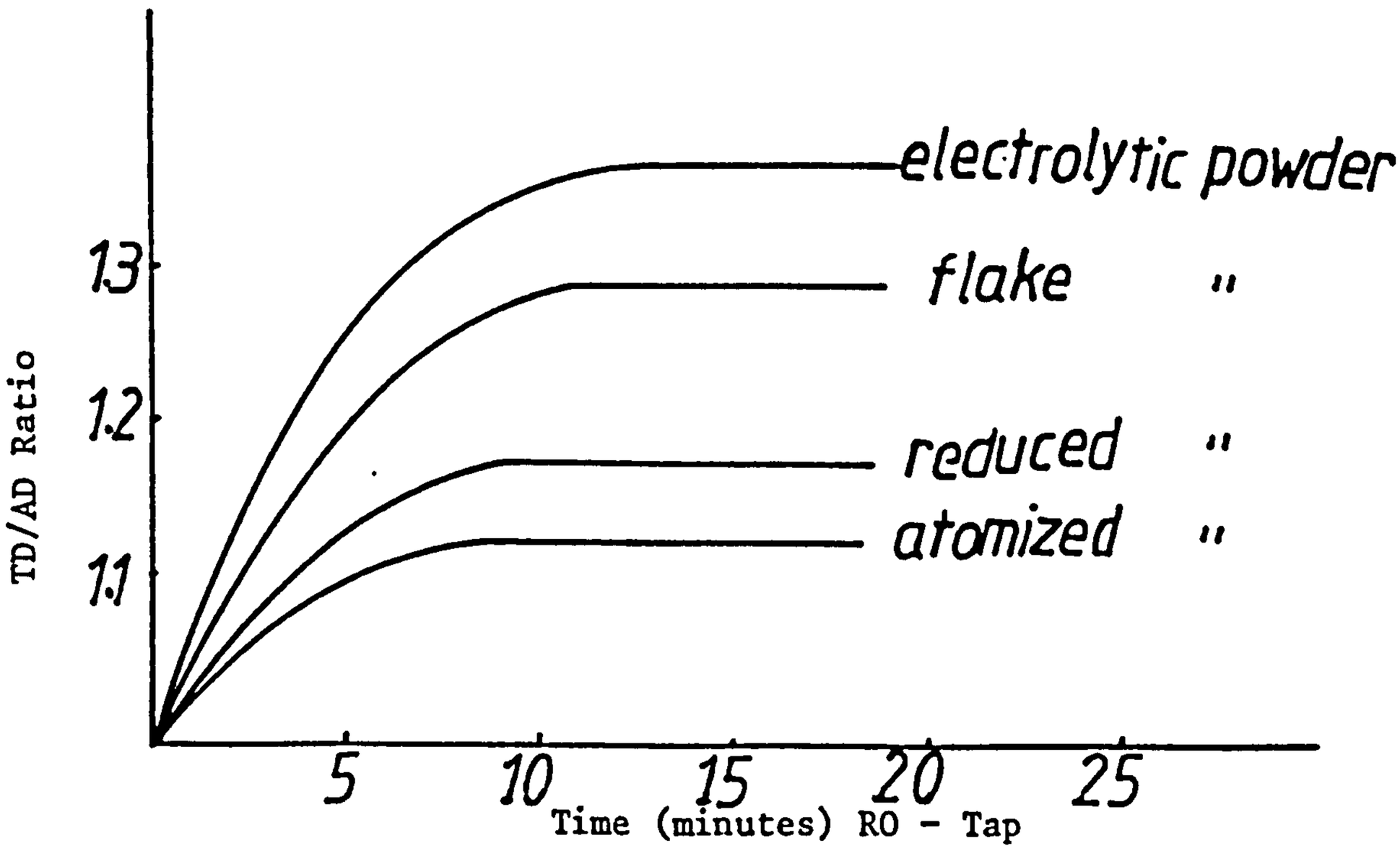

Figure 1.10 **Inter-relationship between different shaped metal powder and change of tap density/apparent density with respect to tapping time**

Figure 1.10 shows that this density ratio is dependent upon the morphological characteristics of the powders. Guo and Beddow (71) studied the effects between particle shape and the bulk properties, "density, flow rate and ratio of tapped density to apparent density", and expressed their observations as follows:

$$P\ (\text{bulk property}) = P\ (\text{ideal}) + kP\ (\text{deviation})$$

where: P (bulk property) is a bulk property of the solids

P (ideal) is the ideal state of the property (for perfect spheres)

P (deviation) is the deviation from the ideal state, and k is a proportionality constant.

Other workers (174, 184) using the same ratio relationship studied the effects between shape and compacted powder mass at different degrees of compaction and permeability and powder flow rate (180).

The main problem in any morphological study is to ascertain a comprehensive technique to measure particle shape. Many attempts have been tried, but as Orr has stated (201):

"shape is rarely satisfactorily measured, not because of shortage of shape factor definition but because no one has yet found a completely satisfactory means of measurement".

It is generally agreed that for irregular particles, shape is not independent of size. The size of a spherical homogeneous particle can be uniquely defined by its diameter. While for a cube, the length and one edge are characteristic parameters. For other regular particles it may be necessary to specify more than one dimension but for irregular particles, the assigned size usually depends upon the method of measurement. The particle sizing technique therefore becomes dependent upon the final product requirement. Thus analysis of a paint pigment is best achieved by measurement of the projected area diameter, while for particles combined in chemical reactors it is more advantageous to measure the surface area by permeametry, gas adsorption or any suitable surface area measurement technique. Particles having the same diameter can however have completely different shapes, therefore one dimensional parameter should not be

considered in isolation. There are many differently defined diameters (3) and the particle dimensions related to the present work are defined in Section 2.3.5.

Particle shape has been defined in descriptive or literal qualitive terms in the British Standard 2955 (1958) as:

Irregular	lacking any symmetry
Spherical	global shape
Acicular	needle-shaped
Fibrous	regularly or irregularly thread-like
Angular	sharp-edged or roughly polyhedral shaped
Flakey	plate-like
Granular	having approximately an equidimensional irregular shape
Modular	having a branched crystalline shape
Crystalline	freely developed with geometric shape

However the literal terms are inadequate for the determination of shape factors.

1.4.1 Particle shape measurement

Methods for particle shape measurement can be summarised in Figure 1.11.

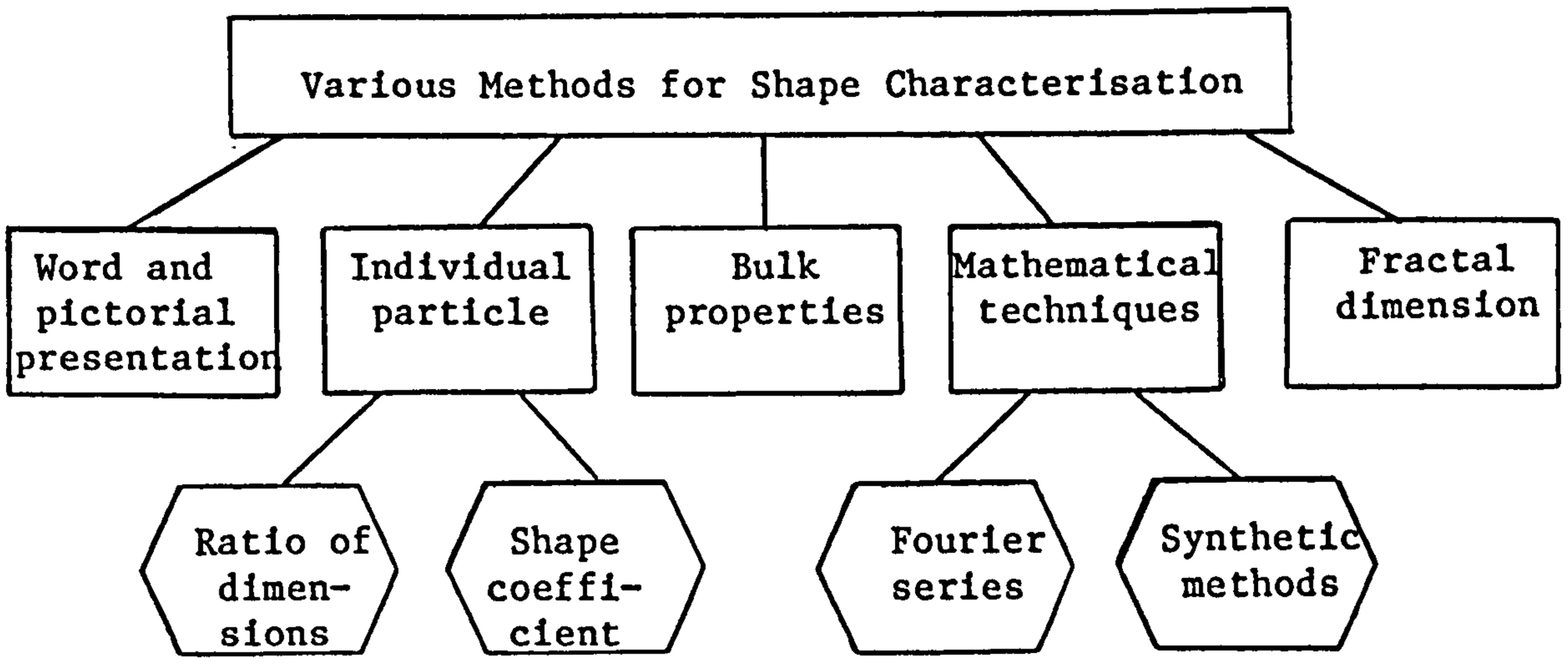

Figure 1.11 Various morphological studies of individual and bulk particulate material

For the method of characterisation of shape by **pictorial presentations** various authors (77, 86, 159) have chosen arbitrary ratios of B/L and T/B to designate a word to describe the shape of a particle.

Sneed and Folk (176) deduced a factor termed the maximum projection sphericity (ψ_M). This value was then correlated with the ratios c/a and (a-b)/(a-c) where a, b, c, are respectively length, breadth and thickness.

$$\psi_w = 3\sqrt{\frac{c^2}{ab}} \qquad 1.10$$

When these three parameters (ψ_M, c/a, (a-b)/(a-c)) were plotted on triangular co-ordinates , particle shape can be shown pictorially. This method called the triaxial ratio of particle shape, was extended by Davies (39) to a quadraxial system which included the particle roundness.

Mathematical shape characterisation began to develop with the advent of automated microscope systems linked to micro computers which then specified the shape of a profile digitally using complex mathematical functions such as Walsh functions and Fourier Transform series (11, 107, 126, 127, 128, 168, 214).

Some other worker used mathematics in a new concept called syntatic methods (56, 186). Thelanguage consists of strings of characters called terminal symbols.

A technique which has been used by many investigators in the last two decades and has gained well acceptance is the method of **individual particle shapes characterisation,** in which particle shapes are either compared with the characteristics of an equivalent sphere (179) or various dimensions of particle profile are measured.

When defining particle shape by comparison method the volume coefficient k and surface coefficient f of the particle need to be known:

$$\text{Volume of particle } (V) = k\ da^3$$

$$\text{Surface of particle } (S) = f\ da^2$$

The ratio f/k is then a measure of particle shape in form of surface area as described by Heywood (83, 86). The value (f/k) for a sphere is equal to 6 and may exceed double this value for particles of irregular shape. Wadell (195, 196) proposed the following definition for sphericity and roundness.

$$\text{sphericity } (\psi_w) = \frac{\text{surface area of sphere having same volume as particle}}{\text{surface area of the particle}}$$

$$\text{roundness} = \text{mean of } \frac{\text{radius of inscribed circle}}{\text{radii of all corners and edges}}$$

Shape factors of this type do not however distinguish between the elongation and flatness of particles (187).

As mentioned above, individual particle shapes measurement can also be found by measurement of the distance between parallel tangents and other dimensions outlining the irregular particle profiles. Shape factors derived from the **primeter, area, Feret's diameter, projected length** can achieve a more accurate estimate of particle shape rather than only the overall shape information.

Hausner was one of the first to deal in a more descriptive way, the form of particle shape and texture (77, 78). Hausner accurately assessed particle shape by assuming the particle had an enveloping rectangle of minimum area with length of L and breadth of B surrounding the particle profile. Three shape characteristics could then be defined:

The elongation factor	X	=	L/B
The bulkiness factor	Y	=	A/L.B
The surface factor	Z	=	$P^2/A \times 4\pi$

where: A is projected area of the particle

P is circumference of the particle

Other workers followed the same approach although with some modifications (99). Medalia (124, 125) adopted Hausner's methodology to study the shapes of carbon black aggregates, while Hess (81) used different dimensional ratios to study different grades of carbon black, and indicated that the most meaningful morphological characterisation should be based on both the primary unit size and the shape parameter. Hess used the ratio $P^2/A \times 12.57$ and $P_H \times P_V/A$ where P_H and P_y are horizontal and vertical projection length of particle respectively to measure the surface irregularity and particle branching seen in carbon blacks.

White and Batsone (202) for crystal sugar, Ghosh (65) in the food industry, Stein and Corn (178) in the coal industry, Butters (24) in

the study of polymers, Scoth (172) in the assessment of the morphology of soot particles and many other workers (35) have used one or more shape factors obtained from dimensional ratios and correlated these shape factors with processes variables. In the present work four shape factors are employed based on Hausner and Hess definitions (Secton 2.3.5).

1.4.2 Fractal Dimensions

A different approach for quantitative description of corrugated particles and surface texture named "FRACTAL" introduced by Mandelbrot (121). He found that the perimeter of a coastline estimated by L. F. Richardson tended to increase without limit as the step size taken to measure the perimeter decreases (Figure 1.12)

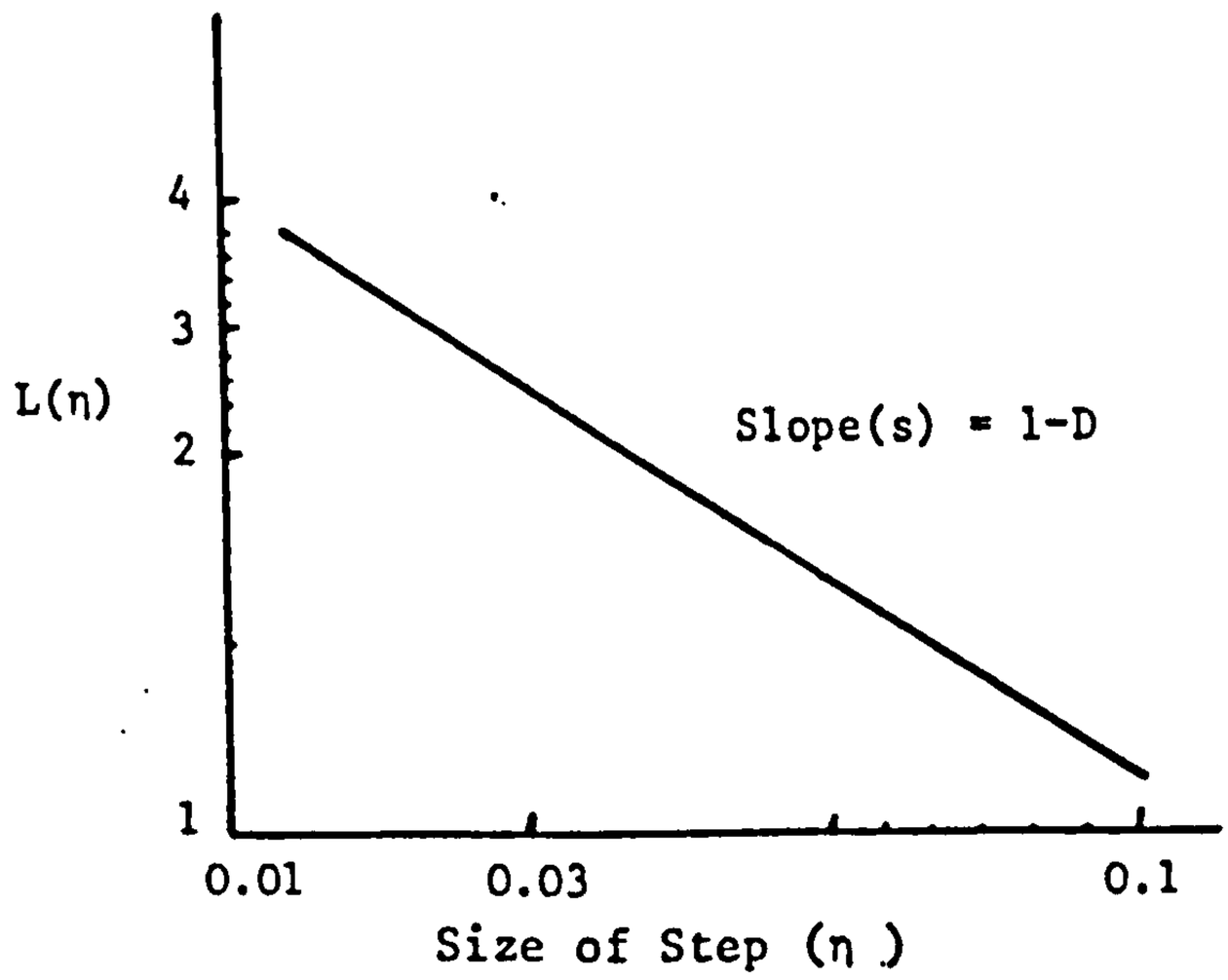

Figure 1.12 **The log of the length (L) against the log of the size of step (η) has a slope of (1-D), where D is the fractal dimension of the curve**

A fractal dimension D can be defined as:

$$D = 1 - S$$

where: S is equal to slope of the curve.

For a two-dimensional curve D has values in the range of 1 to 2. Unity indicates a straight line, while a highly rugged particle has a

value of two (34). In practice edges of a particle silhouettes can have fractal dimensions between 1.05 and 1.36 (142).

The fractal dimension has some limitations, the method is dependent upon the type of materials analysed. Some particles do not show a fractal structure (104, 9). Irregular polyethylene particulate solids did not offer a promising approach compared to other methods of shape analysis (24).

Aluminium particles obtained by an atomisation process showed a non-fractal surface structure at high optical resolution, while in the same cases the fractal behaviour for some particles did not change with decrease in stride length (47).

The ideal fractal curve has to have two important properties (9):

I) It must possess an indeterminate boundary tending to infinity

II) It must be mathematically self-similar at two scales of scrutiny.

This means that the boundary remains independent of the scale or magnifications of scrutiny.

Fractals often do not give a straight line. Orford (136) has shown plots which are curved over the whole stride length chosen indicating a continuous variation in ruggedness with change of scale. The fractal analysis technique is more suited for jagged or highly re-entrant particle silhouettes (51 - 106) than using Fourier Image Anlysis (126 - 214).

C H A P T E R T W O

EXPERIMENTAL

2. EXPERIMENTAL

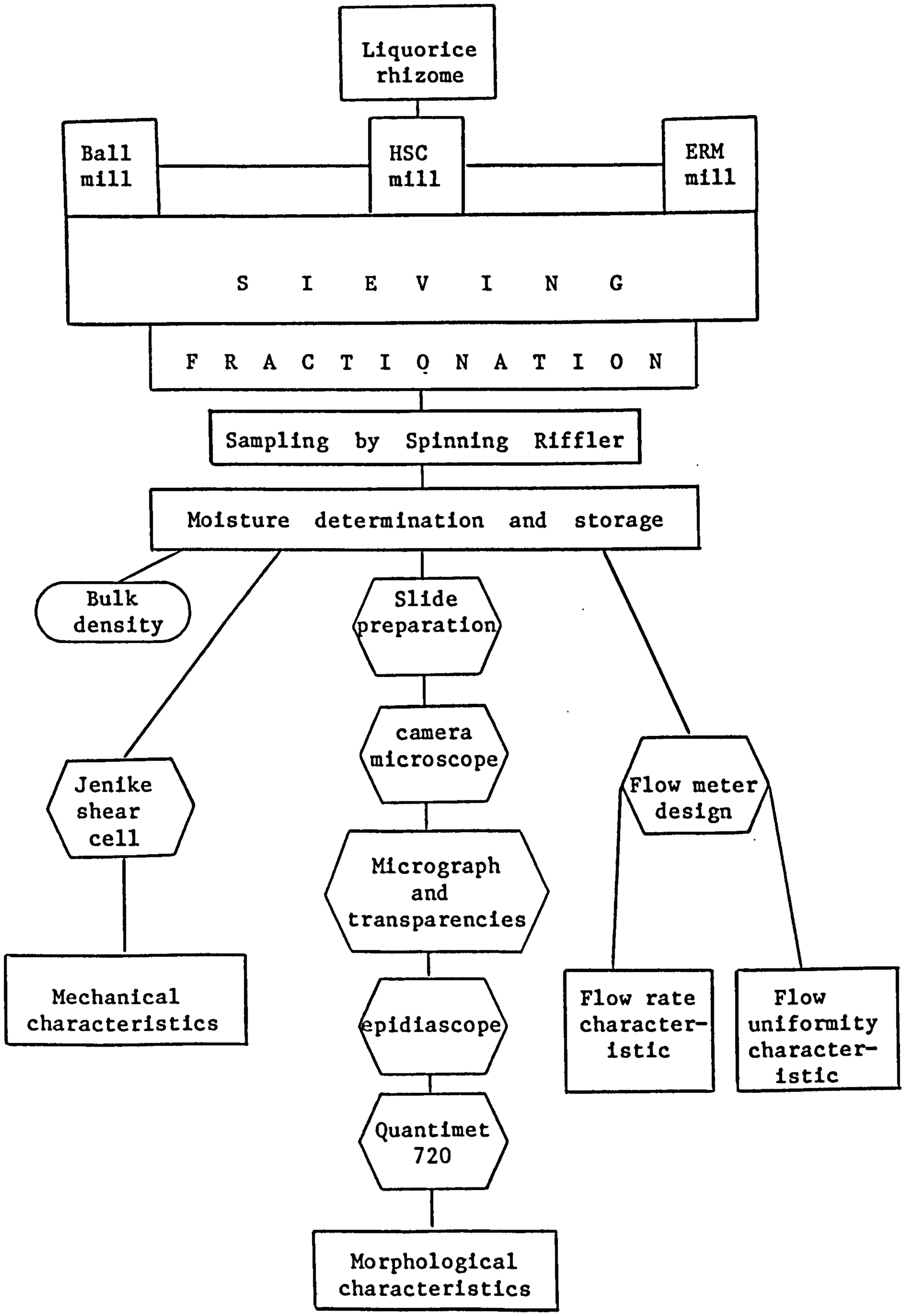

Figure 2 **Flow diagram of Experimental Program**

2.1 Materials

The material chosen for this investigation was the milled product of naturally grown liquorice rhizome or glycyrrhiza collected from the southern province of Iran called "Farss". This, which is used in considerable quantities in the pharmaceutical and other industries was selected as a typical plant for this study.

Figure 2.1 (46) shows the micro-structure of the powdered glycyrrhiza which is seen to contain many different fibrous components.

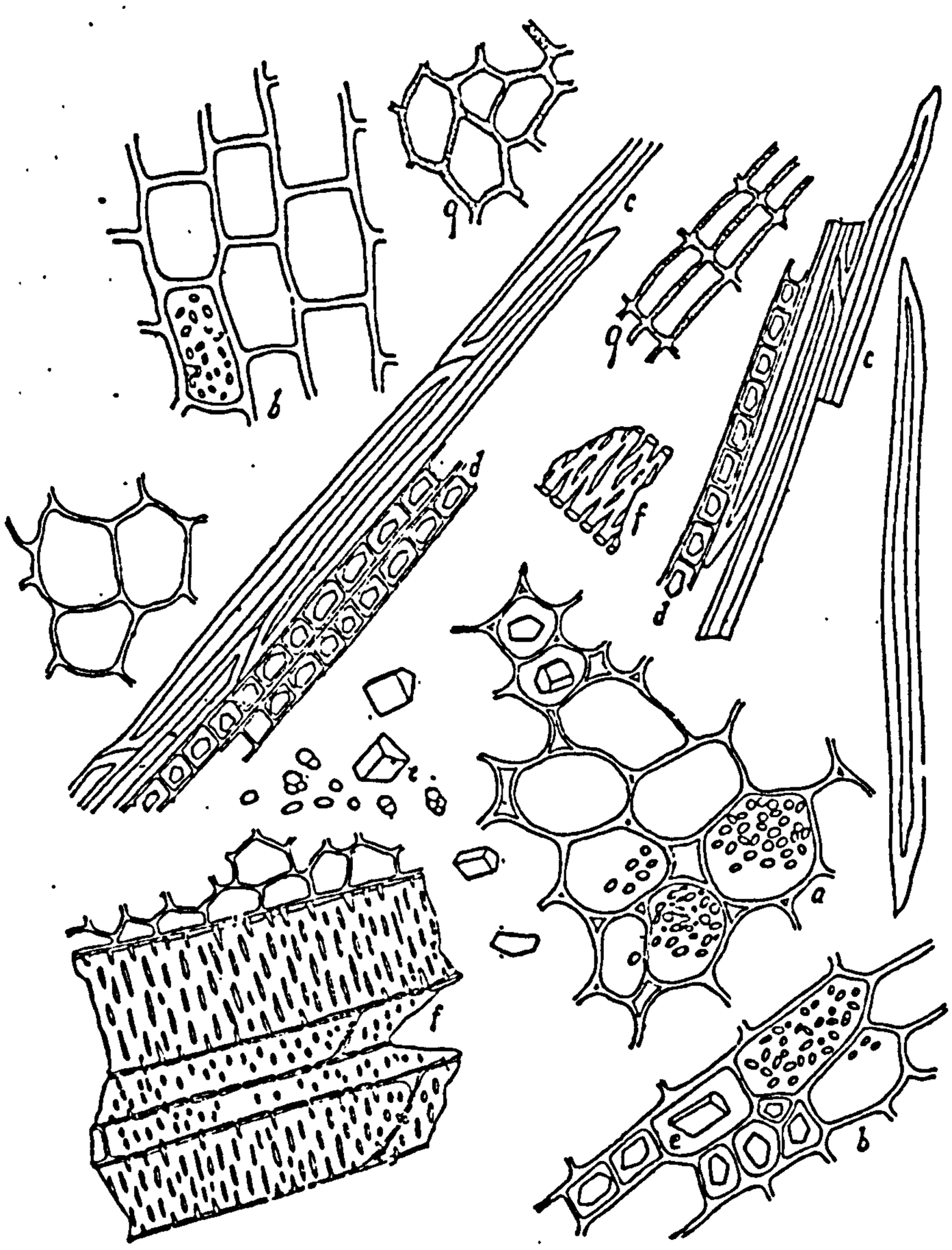

Figure 2.1 - Powdered Glycyrrhiza. (a) Parenchyma; (b) parenchyma with crystals and starch; (c) bast; (d) crystal bearing fibres; (e) crystals; (f) ducts and tracheids; (g) cork tissue. (Schneider)

2.2 Sample Preparation

2.2.1 Comminution

The liquorice rhizome was milled in three different types of equipment:

a) High speed cutter mill (HSCM)

This mill was a continuous EXTECK model manufactured by Loher Gmbh, West Germany.

b) Ball Mill (BM)

This was a 22 centimetre diameter porcelain drum with a length of 25 centimetre containing a 50% load of mild steel balls of 25 mm and 9 mm diameter manufactured by PASCALL ENGINEERING Company Ltd, West Sussex, England. The drum rotated at a speed of 35 rpm for either 45 minutes (BMa) or 75 minutes (BMb).

c) End Runner Mill (ERM)

This mill was manufactured by CROFTS (Engineers) Ltd, Bradford England and consisted of a 25 cm diameter mild steel revolving bowl with an 11 cm diameter vertically moveable cylinder. The time of milling was either 10 minutes (ERMa) or 20 minutes (ERMb).

The aim of using different mills and different milling times was to produce different and various shape particles.

2.2.2 Size Fractionation

The five different products from the above three mills were sieved using ENDECOTT test sieves and the methodology of The British Standard BS410 specification on an automatic "FRETSCH" vibrator manufactured by "FRETSCH GMBH", Laborgeraetebau, Fed. Rep. of Germany", into 23 size fractions.

A weight of 50 grams of milled powder was fractionated at a speed of vibration, setting of 80 for 12 minutes for all fragmentations.

Subsequent to each sieving the sieves were air and brush cleaned. The weights per sieve size are shown in Figure 2.2.

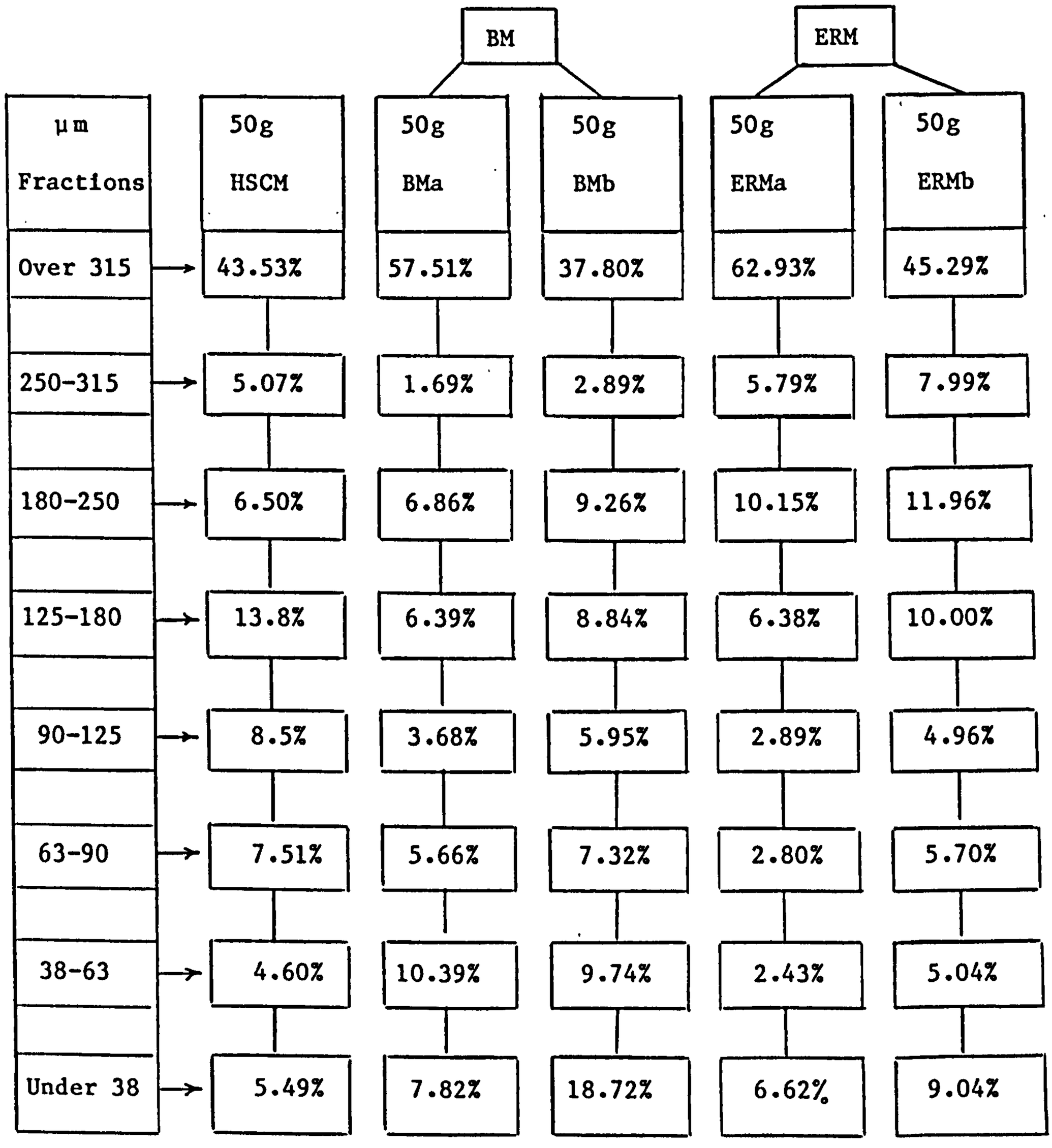

Figure 2.2 Average weight percent of fractions in each size range for different milled products

2.2.3 Moisture Content

After comminution and sieving of the milled liquorice rhizome all fractions were stored in air tight glass jars and placed in a desicator for later use. The amount of moisture presented in the

samples was determined by drying 5 grams of sample in a hot air oven (Vindon Scientific Ltd , Oldham, Lancs) for 24 hours at 110°C. The average loss on drying, from at least 3 determinations, is shown in Table 2.1.

Size Fraction (μm)	% Moisture content (W/W)
Over 315	6.8
250-315	6.7
180-250	6.6
125-180	6.5
90-125	6.5
63-90	6.5
38-63	6.6
Under 38	6.4

Table 2.1 Moisture content of different size fractions

The average moisture for all liquorice size fractions is 6.57% (W/W). The moisture differences within fractions is not significant because the coefficient of variation was found to be 1.9 which was regarded as being within experimental error.

2.2.4 Microscopic slide preparation prior to shape measurement

A Spinning Riffler at a standard speed of 15 rpm was used to sub-divided the fractionated samples and to minimise the sampling errors. From the riffled samples one gram was ultrasonically dispersed in acetone (Ultrasonic Ltd., Shipley, W. Yorks) at 50 watts for 2 minutes. Approximately 1 millilitre of dispersed suspension was then taken and fixed onto a microscope slide with the particles in a stable position. For each fraction at least four slides were prepared and kept in a vacuumed desicator before microscopical examination.

2.3 Equipment for morphological observation and analysis

2.3.1 Microscope

An OLYMPUS photomicrographic system camera (Model PM-10-A) made by "Olympus Optical Co. Ltd., Tokyo, Japan" was used to observe and photograph the particle images from the prepared slides at magnifications between 10X to 40X depending on the size range of the powdered fractions under observation. To calibrate the image analysis apparatus, "Quantimet 720", a calibrated graticule was photographed at each magnification. For optimum results the total area of the particles should not cover more than 10 percent of the picture area. To reduce the non-uniformity of microscope focusing which affects the shape measurement, a standardised method was used. Figure 2.3-a shows photomicrographs of some BMa and Figure 2.3-b HSCM particles before transparency preparation in their random orientations.

2.3.2 The Quantimet "Image Analyser"

The QUANTIMET 720 (Cambridge Scientific Instruments Ltd., U.K.) is an image analyser designed for a wide range of research applications in different sciences (Figure 2.4). In this system the resolution and accuracy of measurements has been enhanced by the adoption of a 720-line slow scanning camera. This gives higher resolution, less noise and less shading (variation of sensitivity in different parts of the image) than a normal television camera used in earlier equipment. In addition, the 720 scan camera can process low-contrast features which could not previously be observed from the background. These 720 line camera scanners use either plumbicon or vidicon tubes. The most important improvements of the 720 model from previous models is the reduction of shading by a new automatic shading correction, higher resolution power and speed of feature measurement (44, 49, 60).

Figure 2•3-a BMa Particles viewed under microscope

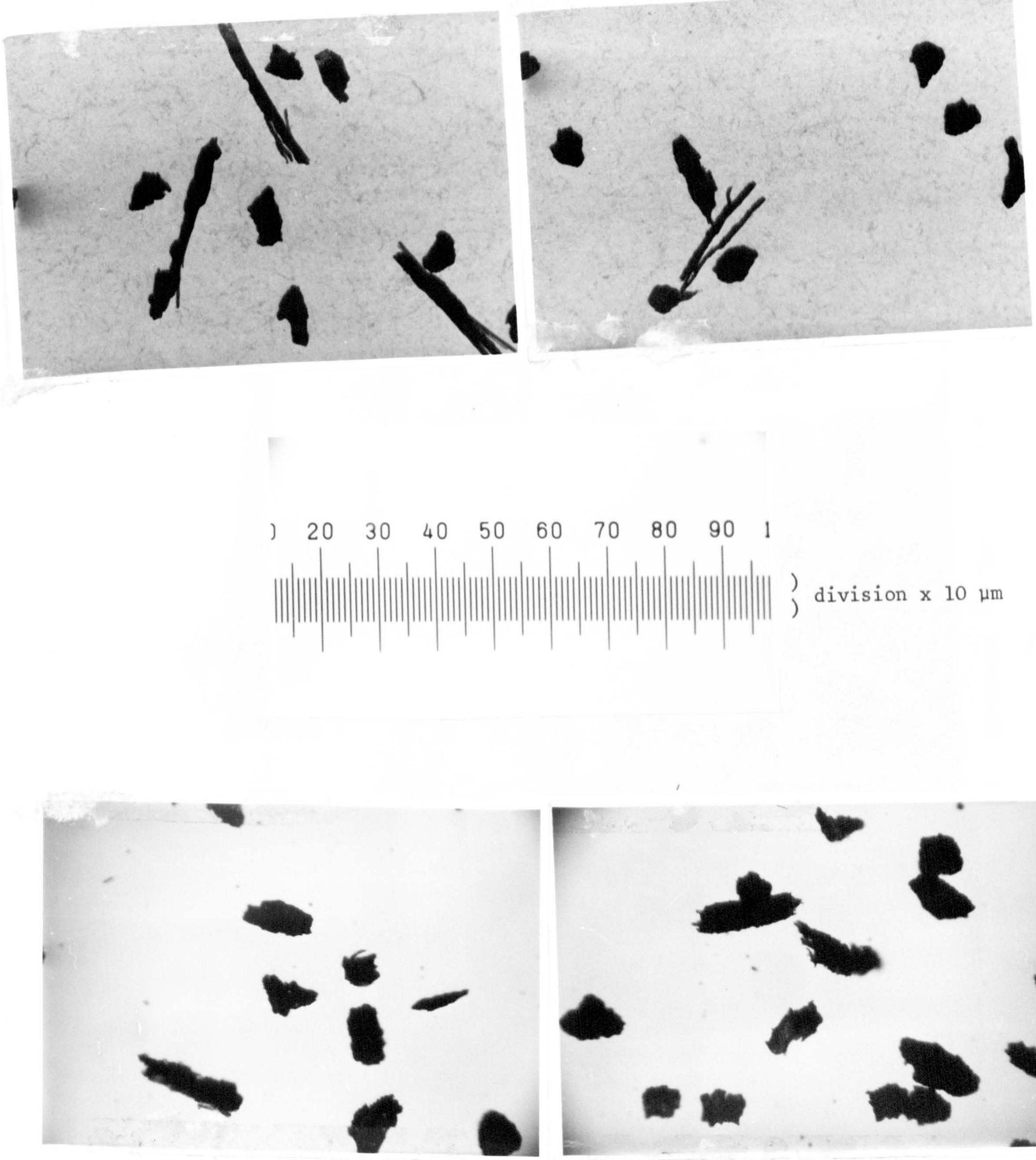

Figure 2.3-b HSCM Particles viewed under microscope

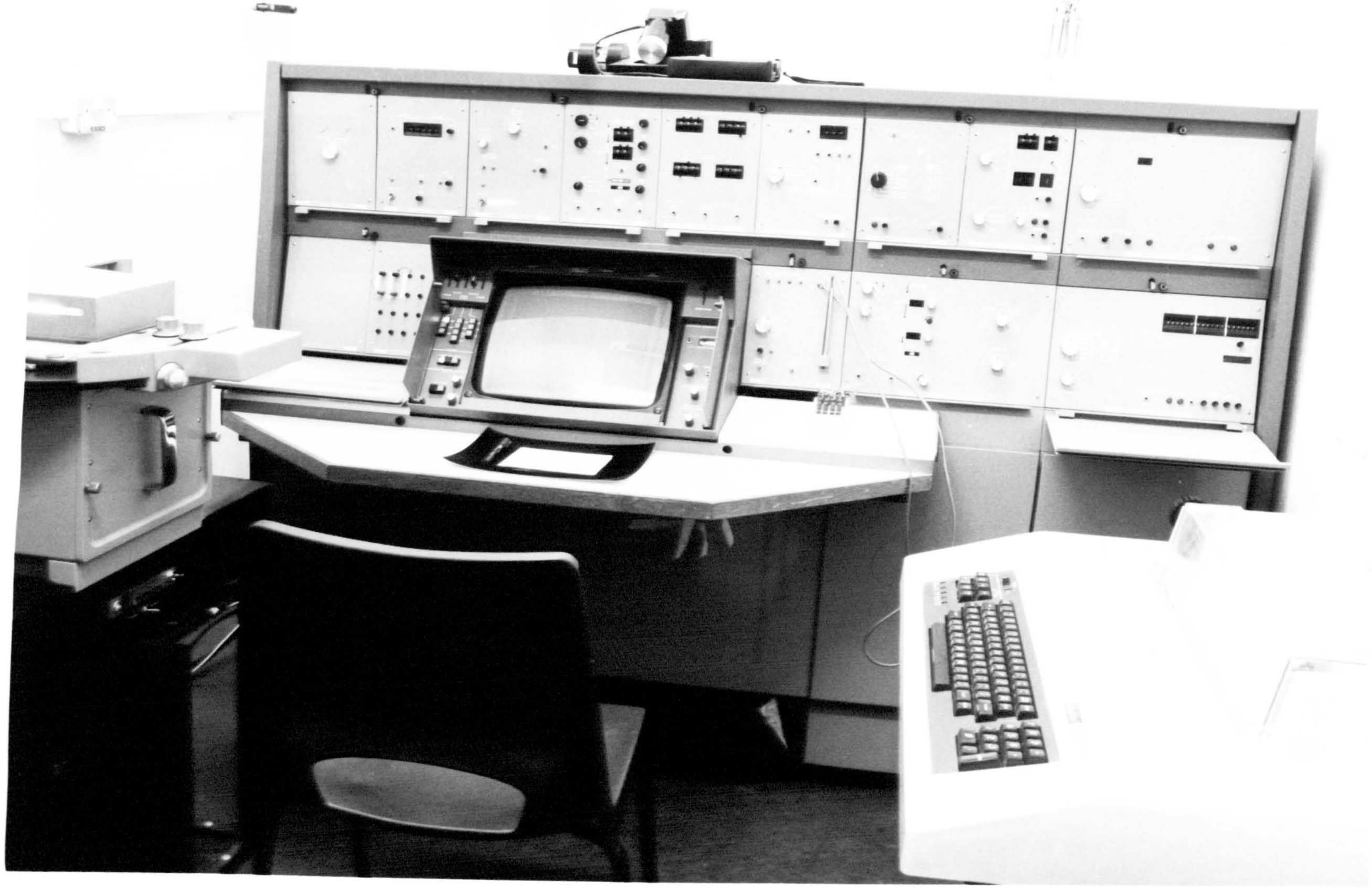

Figure 2.4 Quantimet 720 Image Analyser

Brief description of hardware and software

The Quantimet 720 system consists of:

I. An input and output peripheral,

II. A central processor unit,

III. A computer system,

IV. and software.

I. A number of options exist for items I to III. In the case of the input peripheral, the following hardwares can be used:

a. Epidiascope - this consists of transmitted and incident optics, phase contrast and polarised fluorescent.

b. Optical microscope - a Reicher Zetopan microscope filled with an automatic stage and autofocus system or any other suitable microscope.

c. Scanning or Transmission electron microscope.

II. The Central Processor

The central processor is a collection of different electronic items of hardware such as the image anlaysis, the computer interface and the monitor. Figure 2.5 shows the main functions of the central unit.

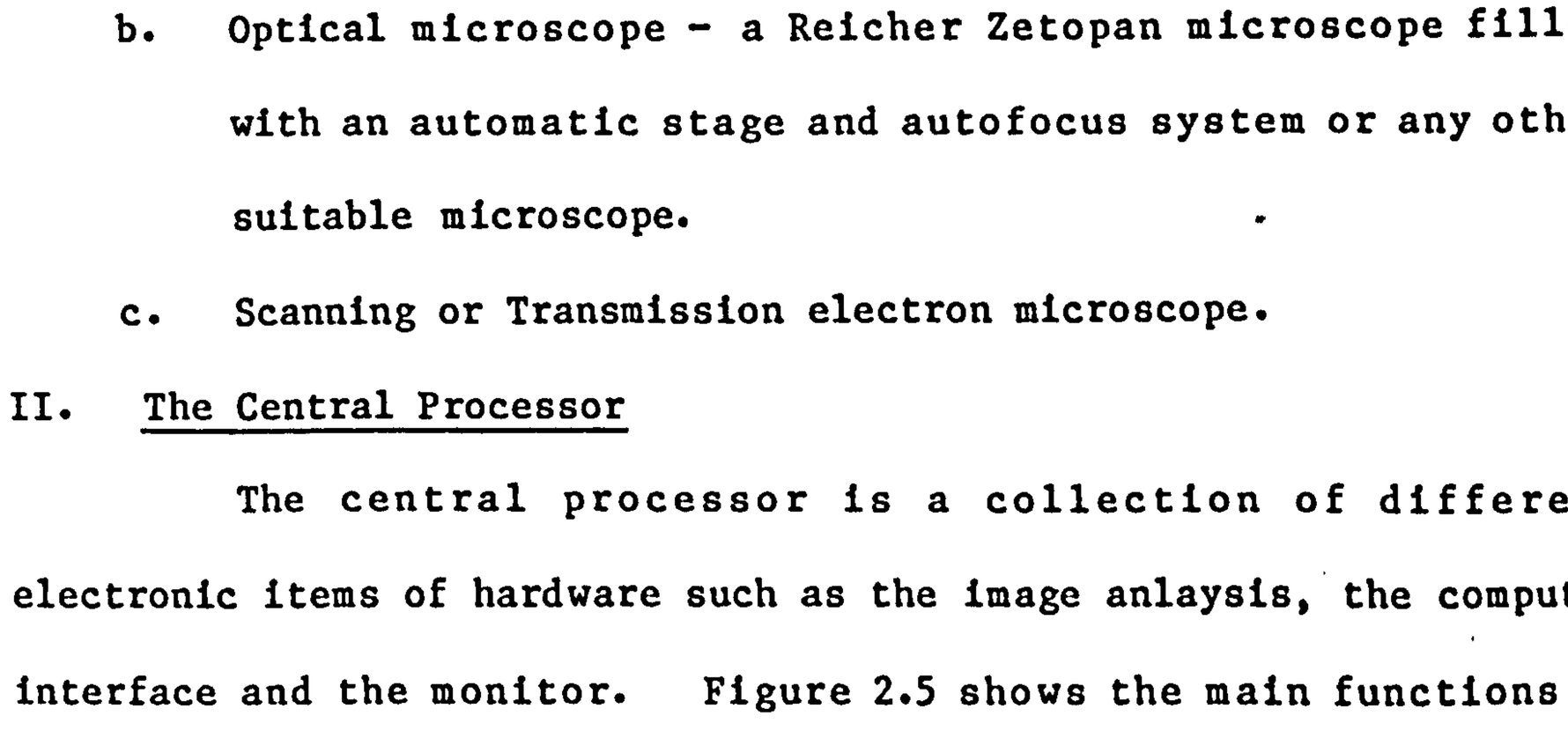

Figure 2.5 The block diagram of central unit

The Shade Corrector

Even with excellent optical images shade correction is necessary and must be used before the optical image can be detected and digitised.

The Detector

The automatic detector has an autodelineation algorithm which employs a two-dimensional look-round pattern. This improves the image measurement accuracy and can almost eliminate image thresholding and halo errors. The mechanism of detection is a function of the plumbicon camera which observes the particle images and displays them on a monitor. The electronic signals then pass to a detection circuit where a particle or particles are detected. The processed data can be displayed in numeric characters along the top of the monitor image or the signals can be directed to different modules as required.

The Amender

The amending facility provides a systematic erosion and dilation of the detected image. Features of an image which are touching can either be separated or separate grouping of images can be joined.

The Editor

The image editor allows the operator to modify existing detected images or draw new ones with the aid of a light pen.

The Analysers

The analysers make field and feature specific measurement, such as the parameters of: number count, area, perimeter, projection, length and feret diameter.

The Frame

The field of measurement can be restricted by applying a live frame.

The Monitor

The monitor displays the images which are being analysed. The correct setting of the high resolution monitor allow both the text and the graphic markers to be accurately positioned on the video monitor.

III. The computer system and software

The standard computer system (23), used in the Quantimet 720 which is a PDP 11-03 and has 28K of memory and dual R x 11 floppy discs. In the present work a RT-H system PDP 11 was used which has a larger memory (International Ltd., Galway, Ireland). The software systems were magnetic discs written in macro assembly language by Plessey Peripheral Systems, U.S.A.•

Output Peripheral

The output terminal is a digital keyboard decwriter II which was specially programmed with image analysis instructions to provide a hard copy print out of the results and routines.

2.3.3 Particle detection

In Quantimet Image analysis detection is the process of extracting particulate features from an optical image. This is often complicated because there are unwanted regions which are indistinguishable at certain grey levels (59). This can be overcome by manual selection of features by a light-pen. This however relies upon the eye to achieve the correct pattern recognition and is also a slow and laborious process. An alternative solution is to select "wanted" features from "unwanted" extraneous matter. With this machine pattern recognition system each feature or particle has an associated store, and the descriptions of the feature are accumulated as the feature is scanned line by line. At the end of the feature (the Anti co-incidence point or A.C.P.) a complete description can then be fed out. Because all processing is carried out in real time

the stored information registers are emptied and available to store another particle description.

Problems arise however due to difference in light intensity between the particles and the particle background. A black particle against a white background (or vice versa) is the most advantageous condition of the detection of a particle border (44). At fixed threshold settings system the features may either be over detected (over sized) or underdetected (under sized), depending upon the position of the fixed threshold. In the present automatic setting these errors are eliminated by the introduction of the autodelineation programme, which determines precisely the edges of features and the image thus corresponds to the real size.

2.3.4 Recommendations for accurate image analysis using the Quantimet 720

I) There must be a significant difference in the grey scale contrast between the wanted and unwanted feature areas.

II) The inability to produce adequate grey level separation is due either to noise or shading. The equipment should therefore be set at steady state and the lowest possible noise level. Before each measurement the shade should be adjusted by means of the shade correction switch.

III) High particle image magnifications and correct threshold setting procedures cure problems of resolution.

IV) The errors of particle overlap and difficult image boundry detection can be minimised by allowing a total area of picture in which less than 10% is covered by the particles.

V) Before each image analysis measurement, when the Quantimet 720 has reached steady state, calibration with known characteristic sets of particles must be performed.

2.3.5 Quantimet 720 Functions

There are several different functions which can be measured by the Quantimet 720 (35, 59, 197) and many others which can be measured by other methods (3). In the present work the following functions have been used to evaluate particle shape factors (Figure 2.6):

I) Projected Area (A)

This is the surface of the particle profile when viewed in a direction perpendicular to the dimensions of breadth and length.

II) Perimeter (P)

This is the length of the boundary around a detected region.

III) Feret's diameter (F_V and F_H)

These are sometimes known as the Tangent diameters. The Feret diameter is the perpendicular distance between two parallel lines in any directions drawn tangential to the feature. The most commonly used orientations are the vertical Feret (F_V) at 45° and Horizontal Feret (F_H) at 135° degree to the particle image orientation.

IV) Projected Length (P_H and P_V)

This is the cumulative length of lines with the trialing edges of a projected feature. The Horizontal projection (P_H) is effectively a vertical measurement of all vertical edges while the vertical projection (P_V) measures the horizontal edges.

V) Length (L)

This is the distance between two parallel planes which are perpendicular to the planes defining thickness and breadth and which are tangential to the opposite sides of the particle or feature. The longest dimension (L') is equal to maximum Feret's diameter.

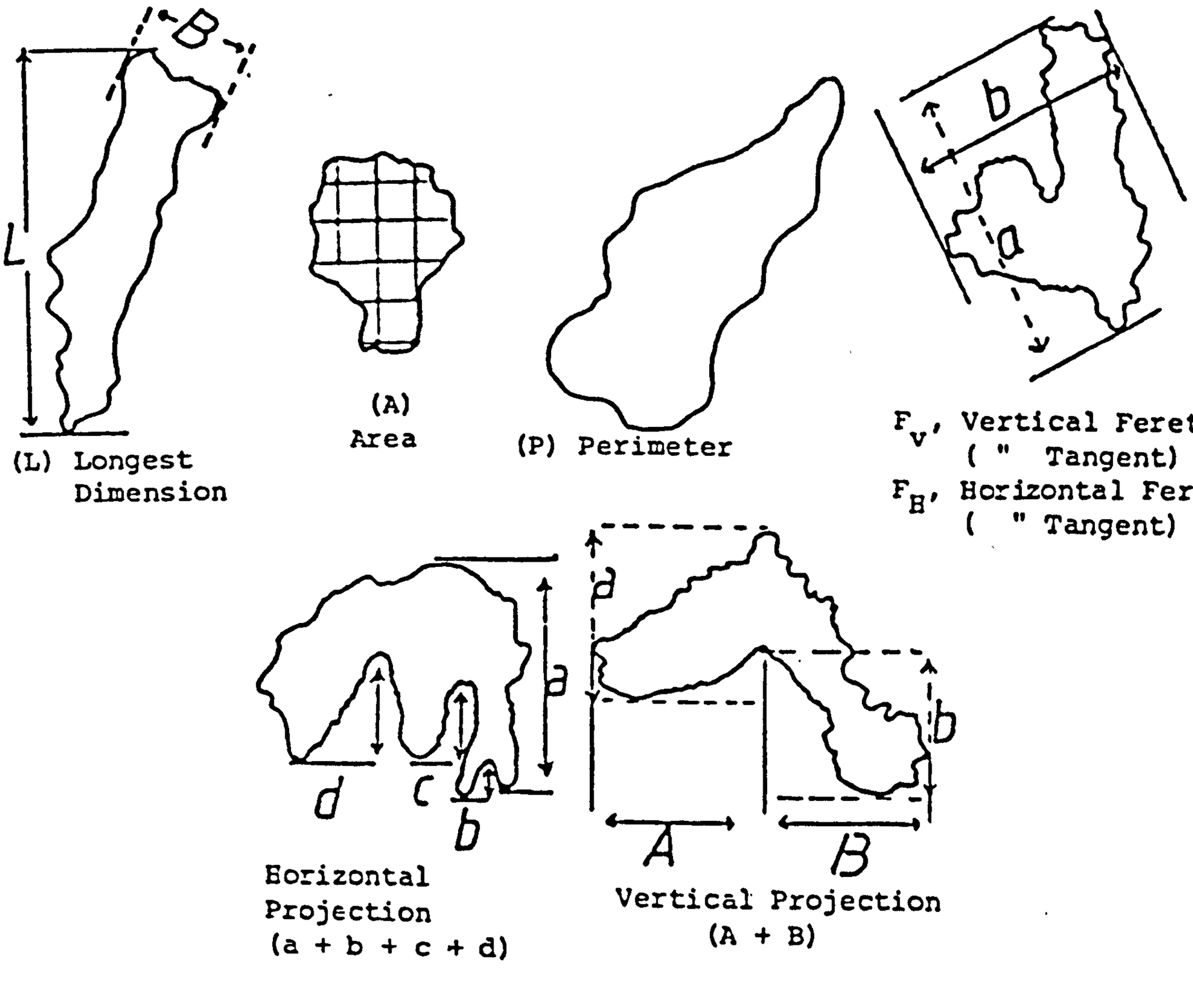

Figure 2.6 Plane of maximum stability viewed by microscope

VI) Breadth (B)

This is the minimum distance between two parallel planes which are perpendicular to the planes defining the thickness and are tangential to opposite sides of the particle or feature.

The thickness is defined as the minimum distance between two parallel planes which are tangential to opposite surfaces of the particle, one plane being the plane of maximum stability. The Feret diameters and projected lengths are sensitive to image orientation and therefore prior to shape analysis or measurement these two particle parameters should be orientated along the longest dimension.

Orientation independent functions such as area and perimeter can be directly observed and calculated from prepared Image Transparencies.

In the case of orientation dependent functions, particles were drawn in an ordered orientation on Transparent paper, using an illumination box, from the transparent photograph with randomly orientated particles. The ordering and colouring of particles onto transparent paper also provided the best image contrast between the grey level of the image and media necessary for accurate particle detection. Figure 2.7 shows the reduced form of orientated particles for few samples from different mills. The Quantimet can measure the various shape factors according to the relationship:

$$\frac{A \times B}{C^n}$$

where A, B, C are any of different functions available from the function computers and n is the power relationship with values of 1, 2, 3 .... to obtain non-dimensional shape quotients.

To prevent incomplete shape measurement and mis-interpretation of particle morphological evaluation, it is desirable to measure a minimum of two particle shape factors, one being a surface and the other being a form image descriptor. In the present work the following four shape factors have been investigated:

1. $\frac{P^2}{A4\pi}$ surface descriptor (sphericitiy)

2. $\frac{F_V}{F_H}$ form descriptor (elongation)

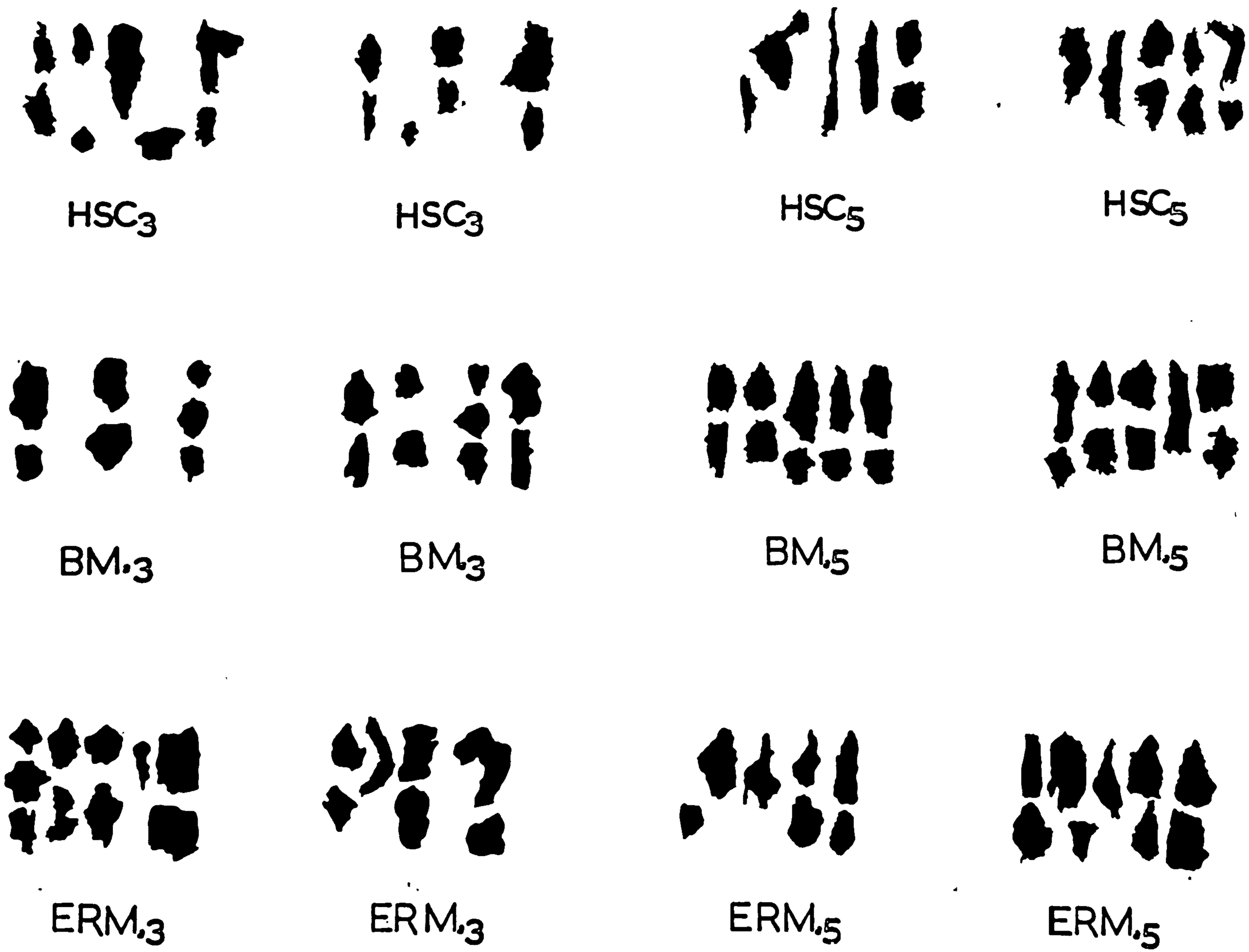

Figure 2.7 Orientated particles arrangement for various fractions

3. $\frac{P_H \times P_V}{A}$ **surface descriptor (roughness by projections and irregularities)**

4. L/B **form descriptor (elongation)**

(See also Section 1.4.1)

2.4 Inclined Tube Flowmeter

This section of the thesis deals with the measurement of the flow rate and the flow uniformity of particulate liquorice material in terms of the shape and size of different fractions of the comminuted powder. The investigations were performed with 23 size fractions of liquorice powder (Sec. 2.2). The flowmeter was designed to measure the flow rate and flow uniformity over a wide range of size fractions (30 -400 μ m,) a range of mildly cohesive to free flowing materials and also for low and high density materials. The flow meter (Figure 2.8) consists of a 33^{o} semi-angle conically shape mild steel hopper of 15 cm diameter, 15 cm height and 2 cm circular orifice diameter, above a vibrating feeder (Sinex Minor Feeder).

The vibrating feeder fed the milled material into a 40 mm diameter perspex tube of length 500 mm supported on mild steel rollers of approximately 6 cm diameter driven by a 1/4 h.p. electric motor with variable speed control (Rotary Regavolt British Electric Resistance Co. Ltd). The degree of inclination of the revolving perspex tube can be adjusted by two screws under the main mild steel base plate. Dry powder flowed from the hopper onto the vibrating feeder, and then into a revolving perspex tube. The clearance from the hopper to the feeder being adjustable. The material moved along the conveying cylinder until discharged onto a horizontal revolving collection tray containing eight sample containers (Figure 2.9). The speed of the sample collector could be varied from one revolution per minute to one revolution for every 120 minutes. The wide variation in revolution speed and time allowed a variety of material from easy flowing to very poorly flowing material to be distributed evenly between the eight collection containers. The inclination and revolving speed of the perspex tube was found by trial and error to ensure a

uniform delivery from feeder to collector. The optimum angle was a tube inclined at 10^{o} to horizontal and revolving at 10 rpm.

2.4.1 Uniformity of flow and flow rate measurement

The designed flowmeter represents a common system of dispensing powdered material into unit dose containers or packing of a finished form of solid materials when flow uniformity is an important factor. The failure properties of a material will affect the flow uniformity and flow rate of material passing through an orifice. Any external forces such as a vibrator attached to hopper wall, or an auger or stirrer installed inside a hopper used to break powder archs in hoppers will affect the arrangement and orientation of the particles, their packing conditions, the powder strength and consequently the failure properties of the material.

In the present flowmeter, gravity is the only driving force on the material in the hopper. For each experiment approximately 200 grams of a known size fraction of liquorice was introduced into the hopper. To ensure flow remained contstant with differently milled products throughout the experiments the following parameters were adjusted to set conditions.

		Range
Hopper clearance	6 mm	0-15 mm
Feeder reading (vibration amplitude)	1.3	0-8
Perspex tube revolving speed	12 rpm	0-100
Tube angle of inclination	10 degree	0-45
Collection tray speed (depend on particle size)	896, 448, 224 sec/round	

The underlined values are those values chosen for all size functions of liquorice milled by HSCM, BM or ERM mills.

To eliminate the possible effect of non-steady state flow due to the variation of the material head within the hopper, the contents of the first container after weighing was recycled.

From the weight collected in each container at known times the average flow rate (gram/second) and standard deviation around the mean values to study the flow uniformity were calculated. Measurements of the flow rate were repeated twice to give an overall mean flow rate of three runs.

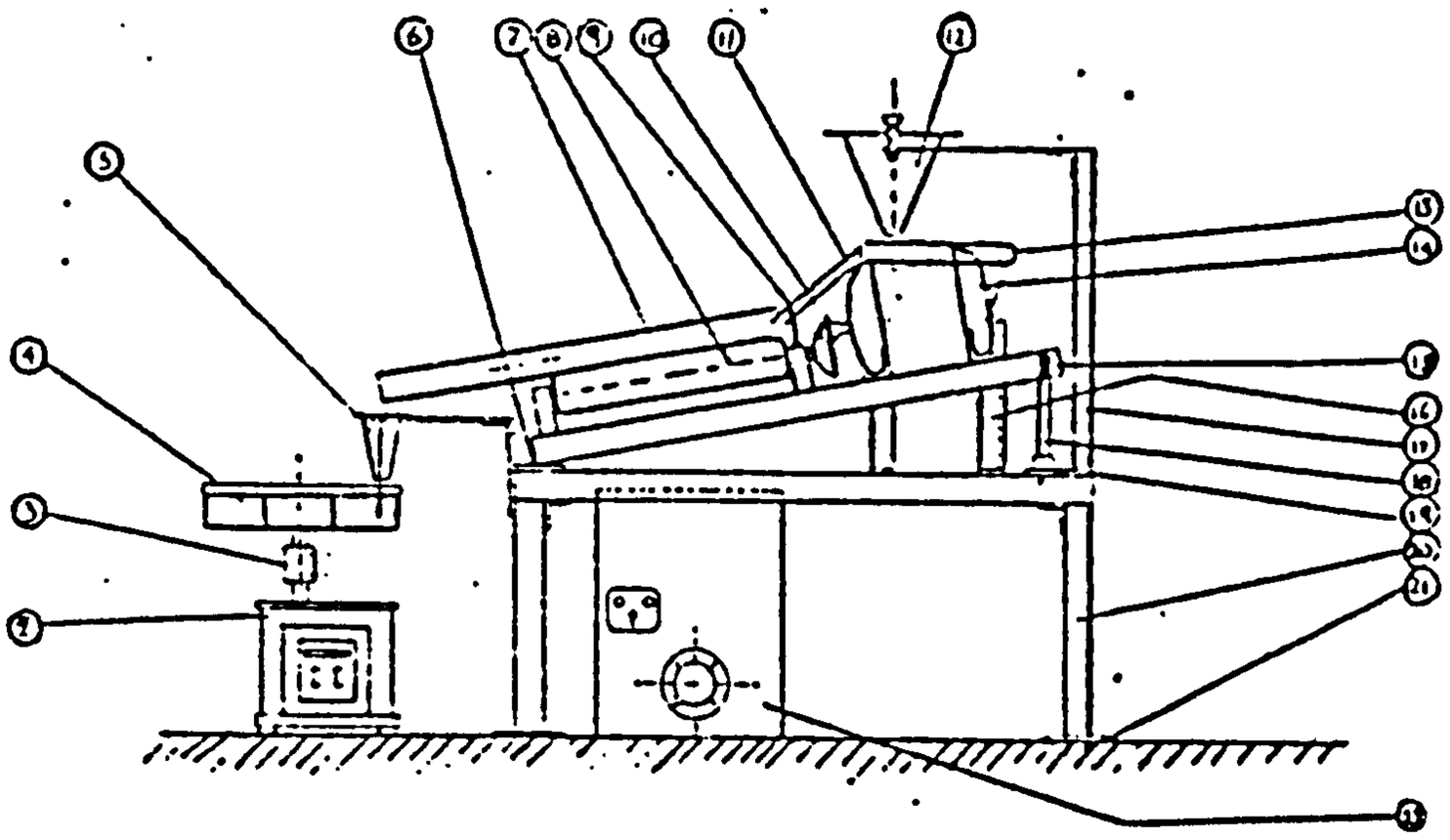

1 - sample container
2 - speed controller
3 - coupling
4 - collecting tray
5 - conical shute
6 - stops
7 - revolving tube
8 - rollers
9 - pillar blocks
10 - pulleys & belt
11 - adjustable feeder
12 - storage hopper
13 - vibrating feeder
14 - motor ¼ HP
15 - base plate
16 - feeder platform
17 - hopper framework
18 - adjustable screw
19 - horizontal plate
20 - main framework
21 - feet
22 - tube speed controller

Figure 2.8 Inclined Rotating Tube Flow Meter

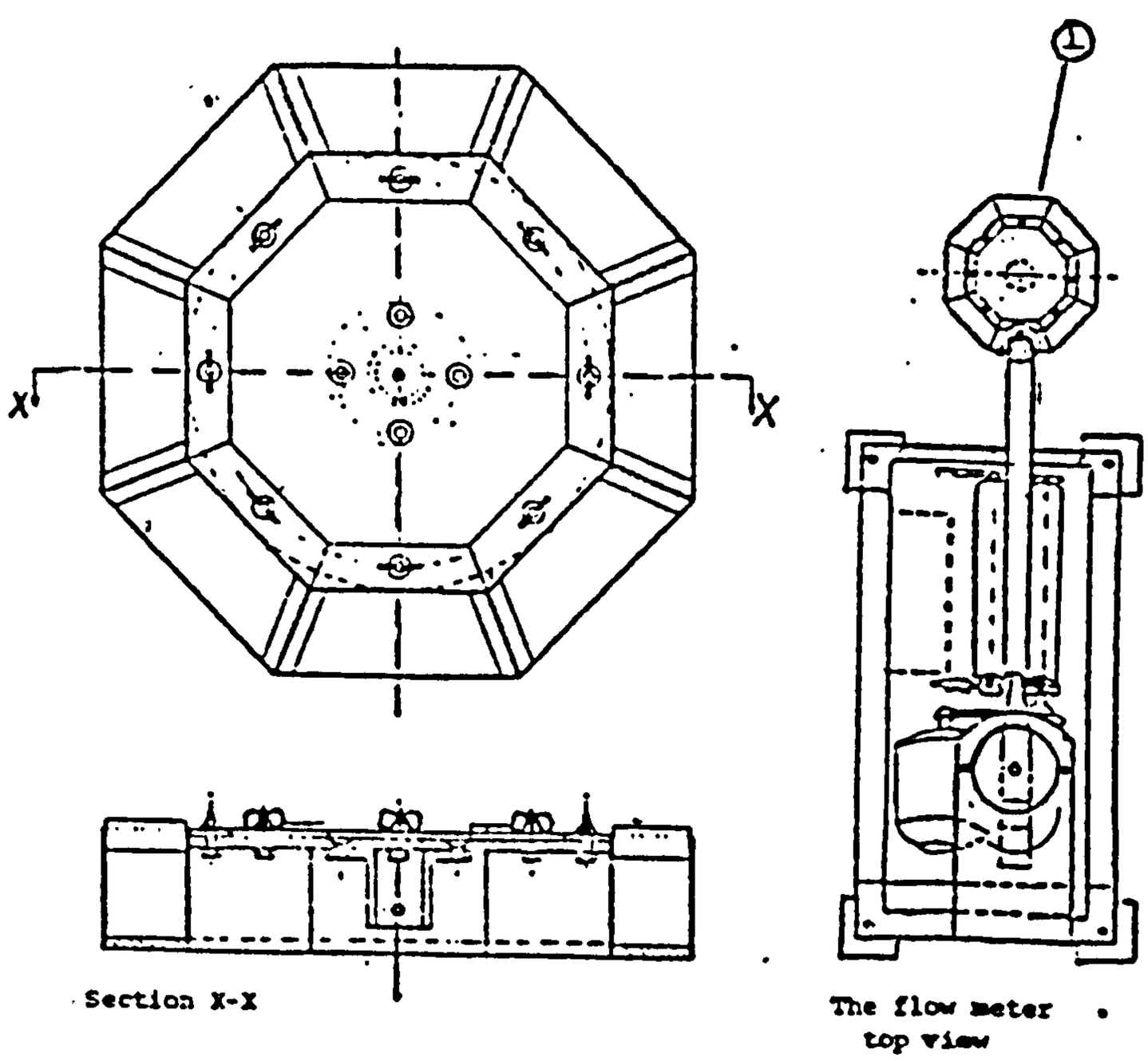

Figure 2.9 Collection Unit, top and side view

2.5 Shear stresses at failure

2.5.1 Jenike shear cell

The Jenike shear cell consists of a circular cell split horizontally. The volume of the top half is approximately 55.55% and the bottom half is 45.45% of the total cell volume when covered with a shearing lid. The ring and the base have equal diameters of 95.25 mm with the heights of each unit being 16.00 mm and 12.70 mm respectively. The internal cross-section area and the internal volume of the ring and base being 7.12557×10^{-3} m^2 and 2.045×10^{-4} m^3 respectively. The floor of the base and bottom side of shearing lid were grooved to prevent slippage of particles. The shearing lid carried a bracket onto which a shearing force could be applied via a loading pin (Figure 2.10 b). A vertical normal stress was applied to the twisting lid via yoke and hanger which carried out known weights. The horizontal shear force was applied to the bracket on the lid at a constant strain rate (0.93 mm/min). A calibrated load cell produced a record of the stress-strain relationship. Before the sample was sheared the powder specimen had to be specially prepared using a moulding ring (Figure 2.10 a) and a known number of twists (see Section 2.5.2).

Although the Jenike shear cell is believed to be superior to the original shear box (64, 95, 96,207) and has become the standard method for studying the mechanical properties of powders, it requires a large quantity of powder for failure or yield determinations. At least four or five separate shear cell measurements are necessary to obtain one yield locus. Such large quantities in the case of pharmaceuticals are difficult and expensive to obtain.

In the present work a smaller modified shear cell using less material than that required by a standard Jenike shear cell was used.

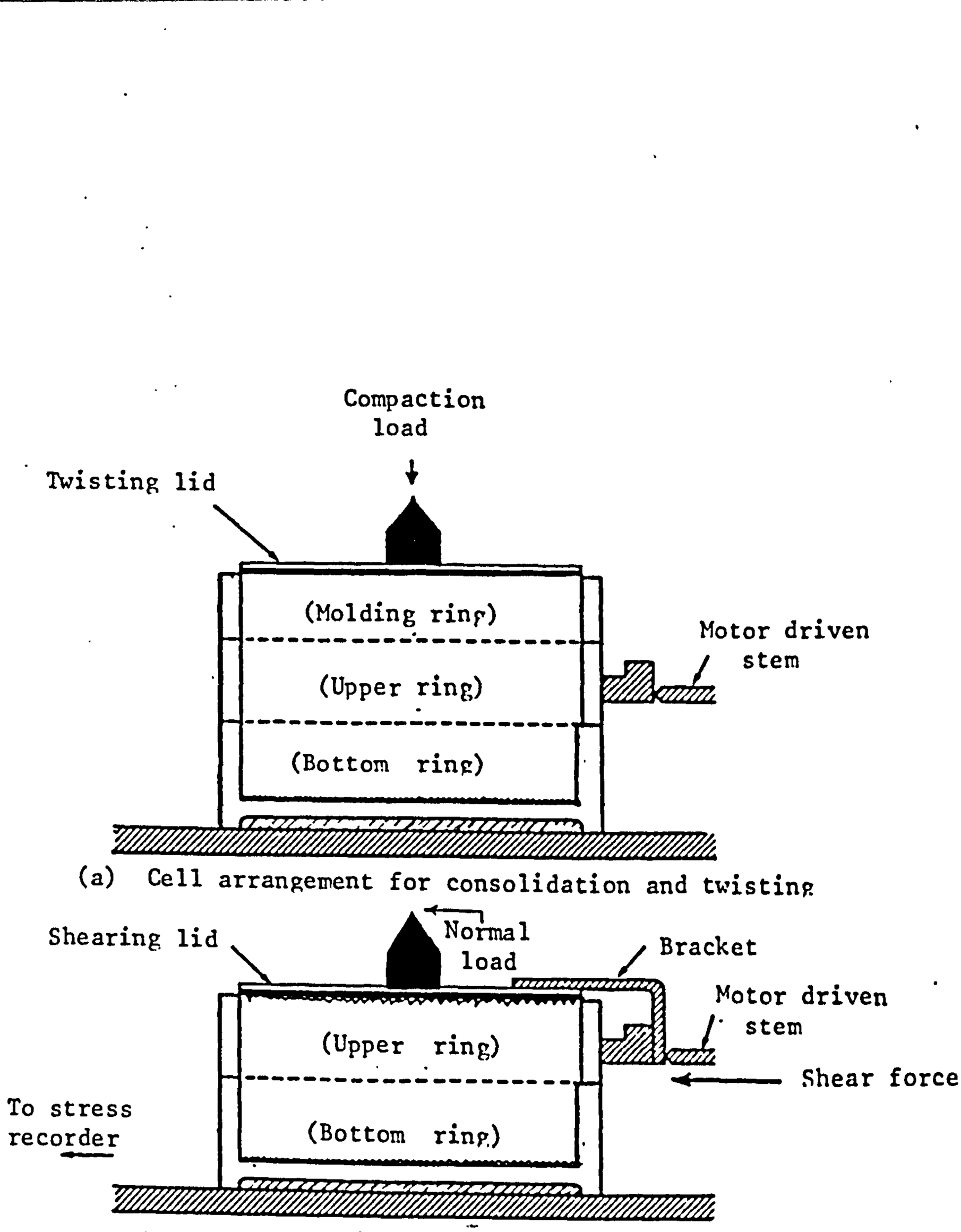

(a) Cell arrangement for consolidation and twisting

(b) Jenike shear cell

Figure 2.10 (b) Jenike shear cell

Modified shear cell specifications:

This shear cell having a smaller cross-sectional area (1.963495 x 10^{-3} m^2 could undergo higher compaction stresses.

The bottom ring bored into the base plate had a diameter of 50 mm and a depth of 7.3 mm. The upper ring and molding ring also of internal diameter 50 mm both had a height of 8.0 mm. The shearing lid had grooves on the bottom surface, the lid with shearing bracket had a

diameter of 49 mm. The compaction lid with the same diameter as the shearing lid had a smooth bottom surface in contact with the powder.

2.5.2 Method of sample preparation

The aim of sample preparation is to critically compact a specimen so that when a known normal load is applied and subsequently sheared, failure at this known load can occur without change in volume. The sample preparation procedure and the criterion for critical consolidation is fully described by Jenike (96). Williams and Birks (207) discussed the process and pointed out that for some materials it was not possible to achieve critical consolidation by the Jenike method, because the process of twisting the powder may introduce some unreliability in to the state of the compacted powder. They showed that it was possible to achieve critical consolidation without applications of any twists.

In the present work with a fibrous powder a twisting procedure using 3 to 10 cycles was essential to produce a uniform compaction to a critical value, using a compaction load alone could not produce sufficient alignment of the particles to reach a steady state consolidation.

Steps in the procedure

I) The base ring was firmly placed on a base plate and the upper ring of the shear cell attached to the molding ring located in a slightly off-set position on the base cell.

II) The powder (Section 2.2) was built up in layers of approximately 2 mm, each layer being lightly pressed down until the cell was full. The excess powder was then delicately leveled to the top of moulding ring with a sharp edged scraper.

III) The sample was critically consolidated by applying known normal load.

IV) The twisting lid on the powder bed was twisted through an angle of approximately 30°. The number of twists is dependent upon the size fractions under investigation but ranged from 3 to 10 twists.

V) The compaction load, twisting lid and moulding ring were removed and the excess powder delicately scraped level with the upper ring of the shear cell.

VI) The roughened shearing lid was then placed in position on the compacted powder. A normal load was applied using the yoke and hanger.

VII) When the powder is subjected to shear the upper half of the shear ring moves forward at a constant rate and the stress-strain curve is recorded .

The shape of the stress-strain curve is characteristic and is dependent upon applied compaction load and the number of twists used in the sample preparation. If the curve is of type B (Figure 2.11) the specimen has been critically consolidated to give a relationship with no change in volume which is termed an equilibrium point (τ_E). Specimens which have been over-consolidated produce a stress-strain curve of type A. To achieve critical consolidation either the value of normal stress (σ) or the number of the twists or both must be reduced. For an under-consolidated powder type C curve is produced.

Therefore by trial and error the number of twists, the consolidation load and the value of shear load is found to give a type B stress-strain relationship and the equilibrium point (τ_E).

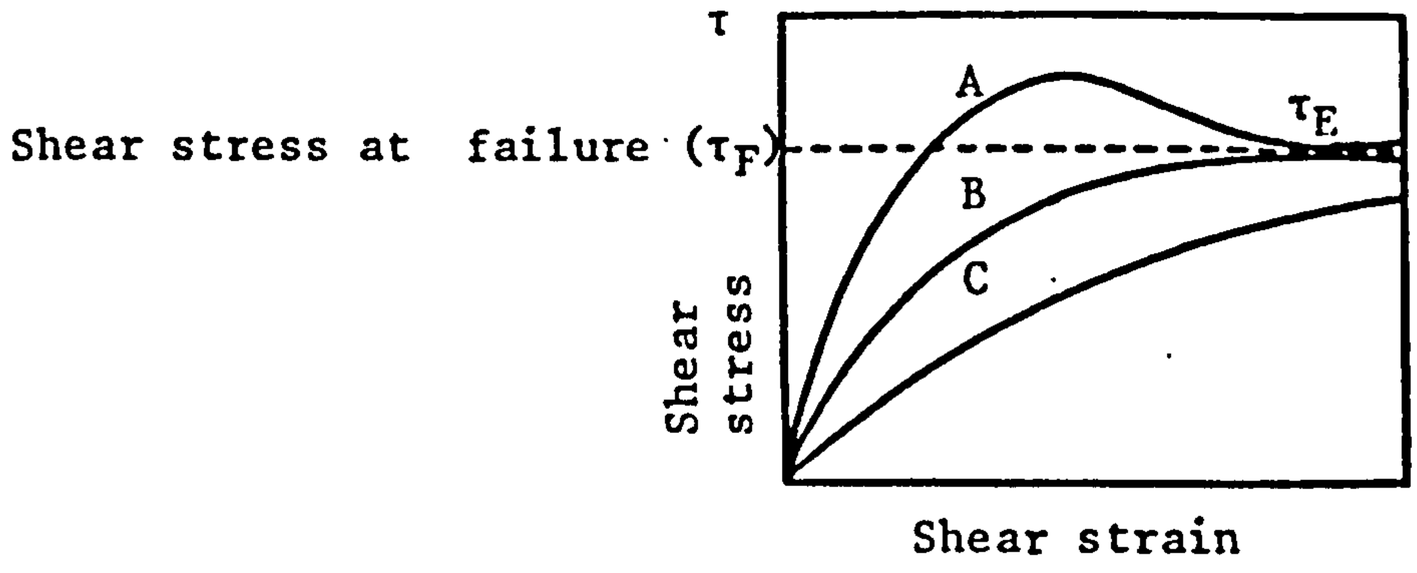

Figure 2.11 Typical stress-strain curves for powders

The original normal load is then replaced by a smaller load to locate one point on the yield locus. The shear force is applied until a failure plane or failure has been developed which is indicated by the shear stress recording reaching a maximum value (Figure 2.12). The evaluation of one yield locus requires the determination of at least four shear tests (Figure 2.13). For each shear test a powder specimen has to be newly prepared and critically consolidated.

The major principal consolidated stress (σ_1) and the unconfined yeild stress (f_c) can be evaluated by constructing two Mohrs circles. One Mohrs circle must pass through the end point (σ_E) and tangential to the yield locus and the other must pass through the origin and also be tangential to the yield locus. In the present work to construct the Mohr circles, and to compute the values of f_c,σ_1 and the Jenike effective angle of internal friction (δ), a BBC microcomputer program which first plots the values of shear over normal stresses and then calculates the best fit line to parabolic equation (210).

2.5.3 Shear Stress calibration

Using a Jenike shear test calibration device attached horizontally to the driving stem of the shear cell the load transducers of the shear tester was calibrated. A series of known

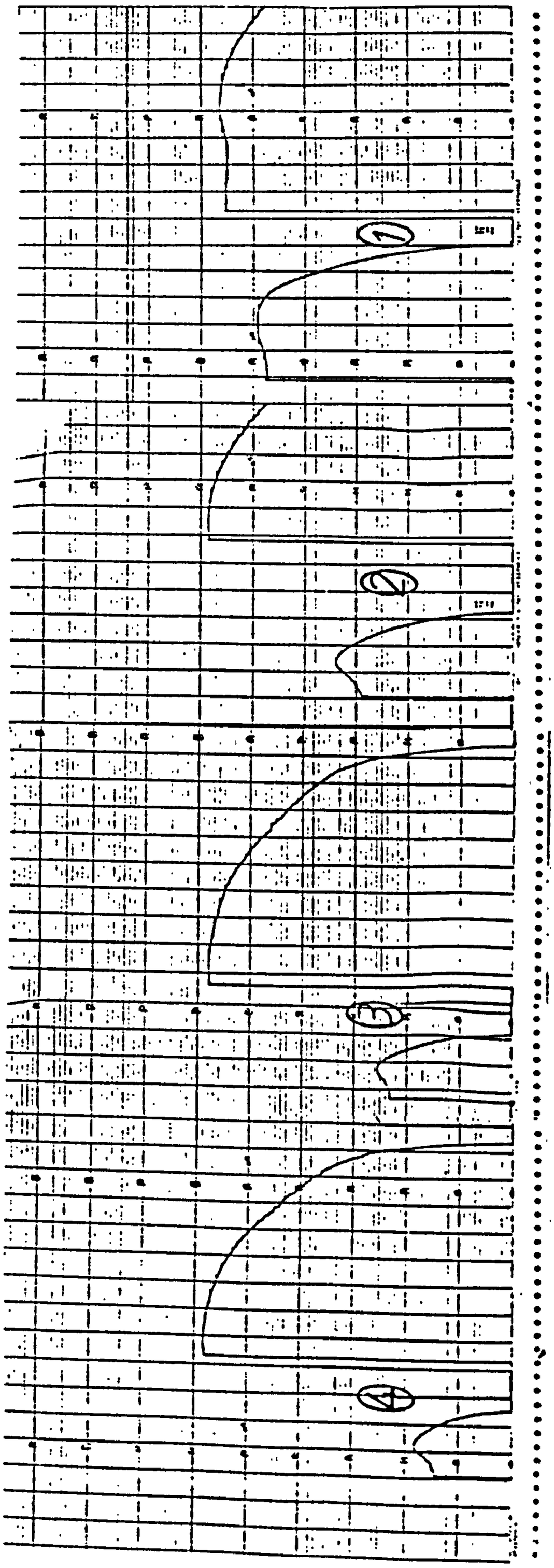

Figure 2.12 Strain-stress relationship at failure for BMa3

weights were attached to yoke and hanger suspended from the nipple of the calibrating device. When the load transducer stem was driven forward, a pen recorded (Kelvin Electronics Co. of Smiths Industries Ltd., England) measured the deflection trace from different suspended loads. Figure 2.14 shows a typical calibration graph of the Jenike shear cell which was obtained by plotting the chart displacement against the applied loads. The slope of this graph is the calibration coefficient used for the calculation of shear stress from the stress-strain charts.

2.5.4 Wall friction measurement

The same equipment used for the shear test (Section 2.5.1) was used to measure the angle of friction between the liquorice powders and a solid mild steel plate. For a wall friction test only the bottom shear cell (standard) and shear lid are needed (Figure 2.15). The following procedure was used for the wall friction measurements.

I) The mild steel base plate under test was located on the fixed base of the Jenike shear tester.

II) The shear ring was located on the mild steel surface filled with the liquorice powder of a known sized fraction and scraped level then the shearing lid was placed in position the specimen was ready for shearing.

III) A normal load using the yoke and hanger was placed in position and the samples were sheared until the shear force reached a constant value.

IV) The normal load was increased in known steps up to a maximum value and for each step the steady state shear force was read from chart recorder.

Sensitivity setting 5

Wt. (g)	Chart Reading
316	2.5
1320	10.0
1820	13.9
2320	17.4
2820	21.2
3820	28.9
4820	36.4
6820	51.8

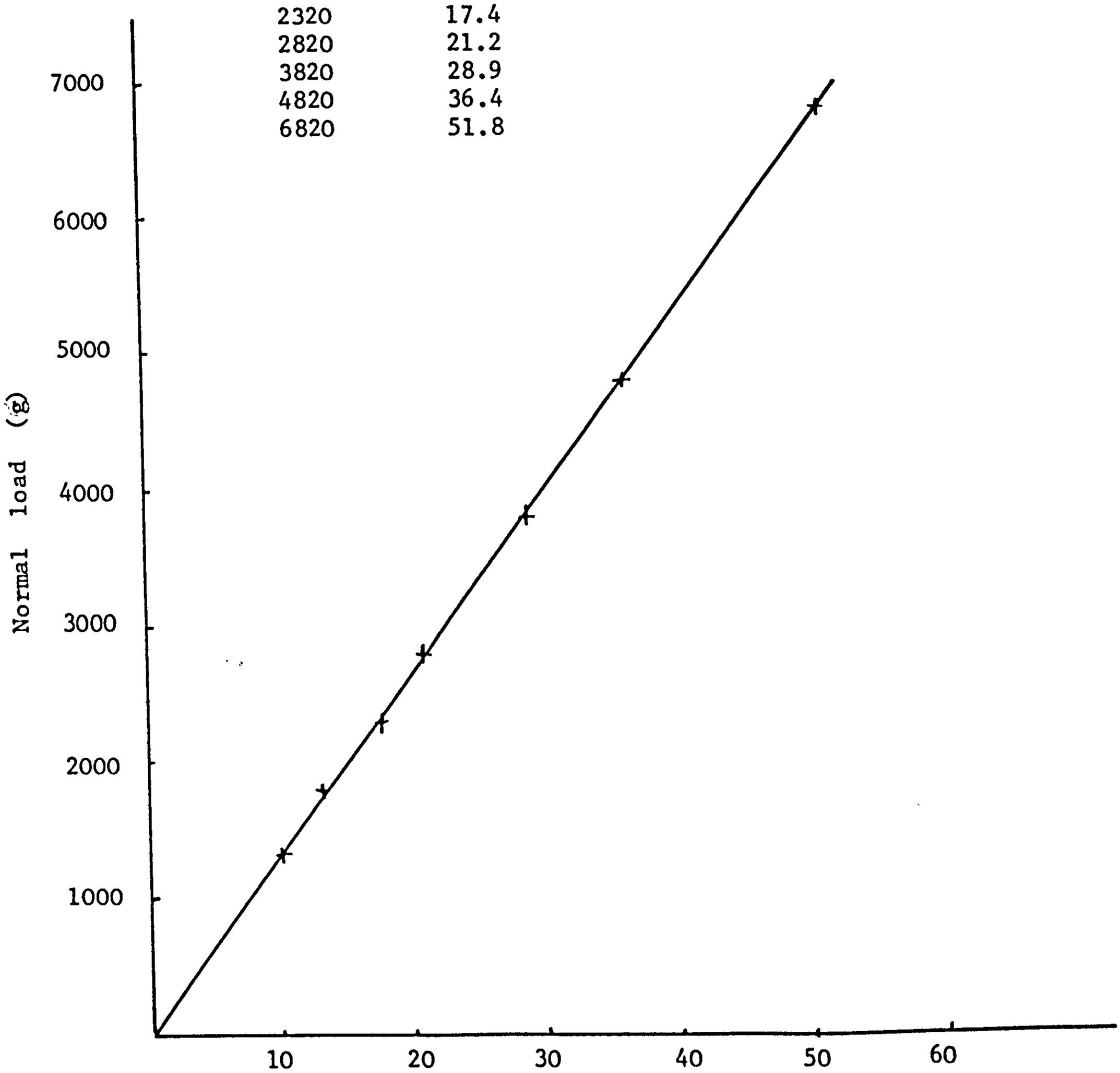

Figure 2.14 Calibration of Jenike shear cell

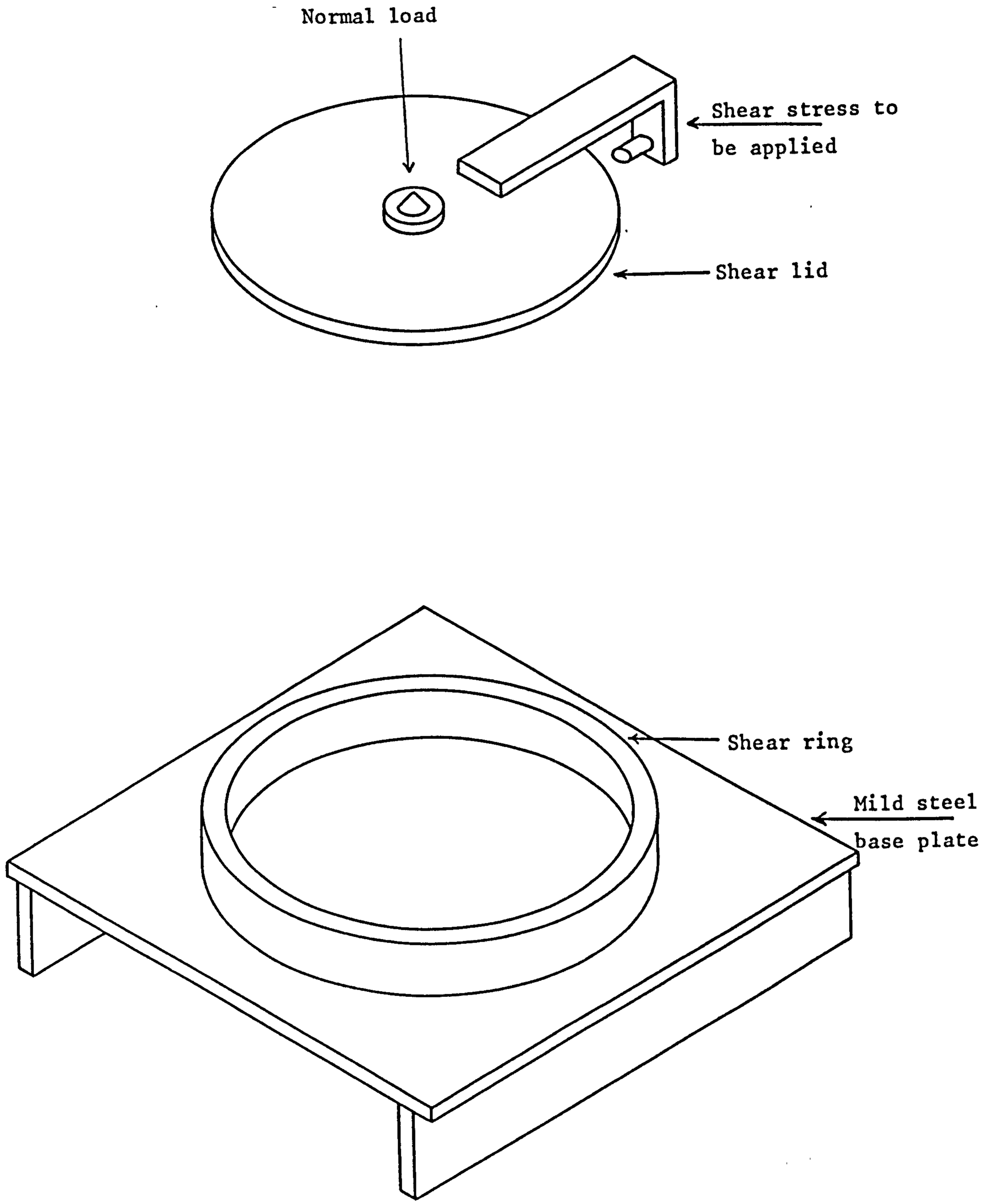

Figure 2.15 Shear cell, shear lid and base plate for wall friction measurement

V) The normal load was reduced in known steps in the same order (as number IV), for each load the steady state shear force was determined.

VI) The shear stress was then plotted against the normal stress (the weight of the sample, ring and lid have also to be included) to give the wall failure locus (Figure 2.16). The slope of this graph is the angle of wall friction. For granular or similar materials the locus is usually a straight line through the origin.

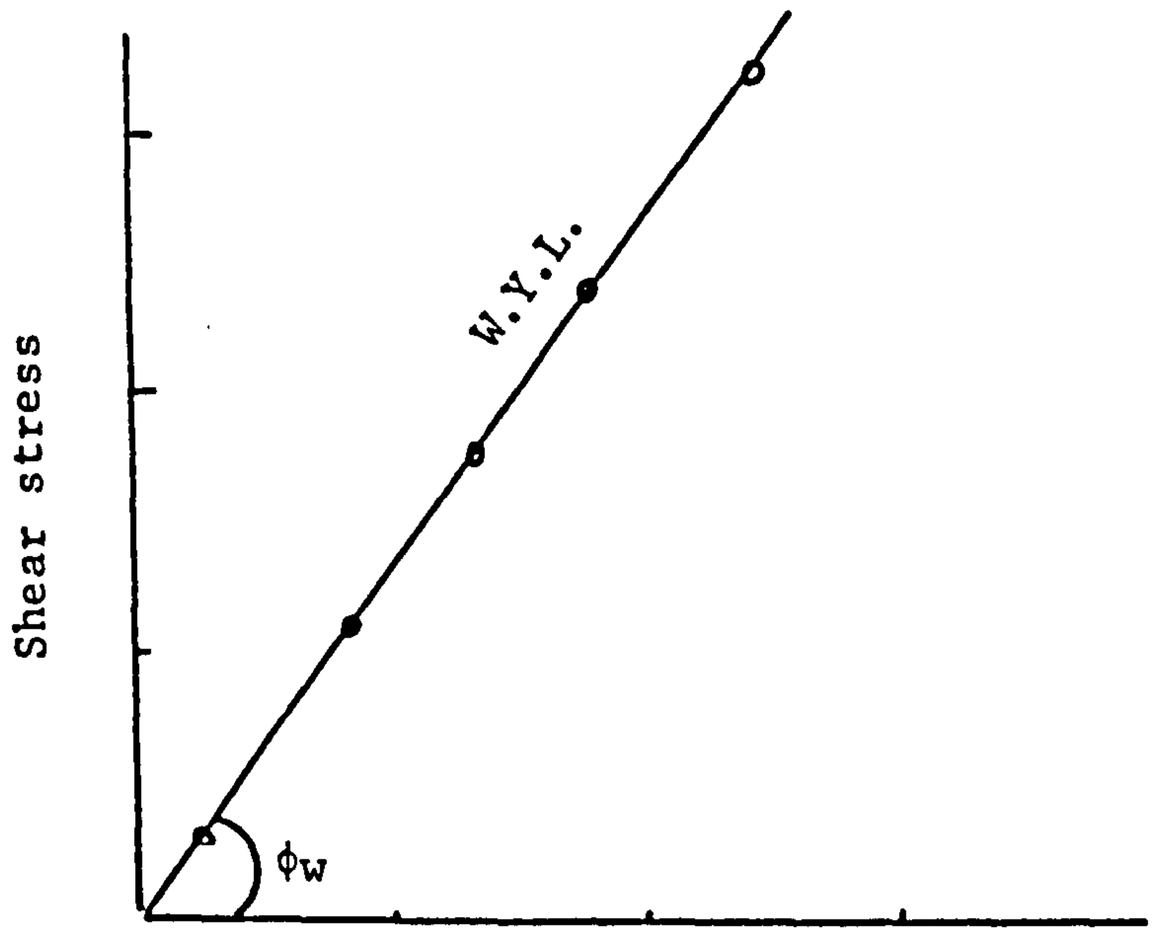

Figure 2.16 Wall yield locus

2.5.5 Bulk density and rate of packing

The measurement of bulk and pack densities are dependent upon the feed rate and the impact pressure of powders into a known volume. To achieve any reproducibility in the measurement of the bulk densities the uniformity of filling the bulk density cup must be ascertained and maintained. A "powder characteristic tester" manufactured by Hosokawa Iron Works Ltd, Osaka, Japan, was used to measure the bulk density and rate of packing of the comminuted liquorice powders.

CHAPTER THREE

RESULTS

3. RESULTS

3.1 Summary of Contents and Flow Properties

The results of the present work including Bulk and particle characterisation are arranged in the following order:

Section 3.1.1 Flow rate and flow uniformity of fractionated liquorice.

Section 3.1.2 A summary of the statistics of the flow rate and flow uniformity.

Section 3.2 Mechanical properties of various sized fractions using a Jenike shear cell.

Section 3.2.1 Wall friction of various sized fractions.

Section 3.3 Bulk density and rate of packing.

Section 3.4 Shape analysis.

Section 3.4.1 Shape factor distribution.

Section 3.4.2 Fractal measurement

3.1.1 Flow rate and flow uniformity of fractionated liquorice

Size fractions in the particle size range 38 to 315 micrometre of powdered liquorice were obtained from:

I A High Speed Cutter Mill.

II A Ball Mill with comminution times of either 45 (BMa) or 75 (BMb) minutes.

III An End Runner Mill with comminution times of 10 (ERMa) and 20 (ERMb) minutes.

The milled product of the High Speed Cutter was then divided into 8 size fractions (Section 2.2) of which fractions no. 2 to 7 were selected for further investigation (Table 3.1).

Fraction Number	Sieve Size range (μm)
1	< 38
2	38-63
3	63-90
4	90-125
5	125-180
6	180-250
7	250-315
8	> 315

Table 3.1 Size fractions produced by HSCM

From the product of the Ball Mill, which was comminuted for 45 minutes (BMa), the 5 size fractions (2 - 6) were selected, whilst the product comminuted for 75 minutes (BMb) together with the End-Runner Mill, comminuted for 10 (ERMa) and 20 (ERMb) minutes respectively, the 4 size fractions selected were from fractions 3 - 6. The total number of size fractions investigated were therefore 23 samples.

Measurement of the flow rate of these size fractions (Section 2.4) along an inclined tube flowmeter was obtained by weighing the liquorice collected in eight identical sample containers of the rotating collector (Figure 2.9).

Tables 3.2 to 3.24 show the weights of the collected samples in a known time and the calculated mean flow rates. The average flow rate (Q_r) was evaluated from the mean flow rates into each container of three experimental runs. A statistical standard deviation (σ_{Q_r}) of the flow rate for each size fraction could subsequently be calculated. To prevent the possible effect due to material head variation in the hopper above the inclined tube, the weight of material in last sample

container (number 8) was discarded from the analysis.

Tables 3.2 to 3.24 also show the statistical analysis of column parameters in terms of **standard deviation (S), variance** (S^2), average weight ($\bar{X}$) collected over the 7 containers of the collector, and **column mean flow rate of each experiment (W).**

Statistical analysis of the rows are also shown, where (μr) is **the mean of the collected sample weights in each container from 3 experiments.** The parameter (σ_{Qr}) is the standard deviation of the experimental flow rate means which ultimately gives the **coefficient of variation (CV) of the flow rates** when divided by (Q_r). σ_r^2 is the variance of the weights of the rows, while S_p^2 is the pooled variance of the 3 columns. σ_{ave} **is the average of the 3 column standard deviations and is regarded as a measure of weight uniformity.**

The F-ratio, which is equivalent to the ratio of between-groups variance/within groups variance, indicates whether the mean weight of 3 experimental runs significantly different. The test sample taken from a population must be representative and this can be judged from the F-ratio. The F-ratio is acceptable when between groups variance (σ_r^2) is smaller than the within groups variance (S_p^2) or the F-ratio value is thus smaller than 1.

COMMINUTED PRODUCT: HSCM				**SIZE FRACTION:** 38 - 63 μm	
Container No.	RUN 1 [g]	RUN 2 [g]	RUN3 [g]	Mean of Runs [g]	Mean flow rate [g/s]
1	23.25	25.99	22.13	23.79	0.212
2	21.35	24.64	17.87	21.28	0.190
3	19.46	22.18	17.30	19.64	0.175
4	18.21	24.39	15.00	19.20	0.171
5	20.14	21.55	15.76	19.15	0.170
6	19.47	19.01	14.90	17.79	0.158
7	16.78	17.10	14.10	15.99	0.142
8	14.60	12.22	13.83		
S	2.09	3.2	2.73		
S^2	4.38	10.2	7.49		
$\bar{X}$[g]	19.8	22.22	16.72		
W[g/s]	0.176	0.197	0.174		
μ_r[g]				19.54	
σ_r^2[g]				6.17	
Q_r[g/s]					0.174
σ_{Qr}[g/s]					0.0223

OVERALL STATISTICS

σ_{ave} = 2.71 g

S^2_P = 7.35 g

CV_Q = 12.8 %

$F_{ratio} = \frac{6.17}{7.35} < 1$

Table 3.2 Weights and statistics of HSCM2 sample collected over 112 seconds

COMMINUTED PRODUCT: HSCM				SIZE FRACTION: 63 - 90 μm	
Container No.	RUN 1 [g]	RUN 2 [g]	RUN3 [g]	Mean of Runs [g]	Mean flow rate [g/s]
1	17.09	17.46	17.23	17.26	0.308
2	18.15	17.19	17.40	17.58	0.313
3	16.08	18.23	18.08	17.46	0.311
4	16.12	15.77	15.36	15.75	0.281
5	15.26	16.82	15.93	16.00	0.285
6	15.16	16.51	15.33	15.66	0.279
7	15.92	15.98	15.13	15.67	0.279
8	14.60	14.20	14.40		
S	1.04	0.85	1.19		
S^2	1.09	0.73	1.42		
$\bar{X}$[g]	16.25	16.85	16.35		
W[g/s]	0.29	0.30	0.29		
μ_r[g]				16.48	
σ_r^2[g]				0.81	
Q_r[g/s]					0.29
σ_{Qr}[g/s]					0.016

OVERALL STATISTICS

σ_{ave} = 1.03 g

S^2_p = 1.08 g

CV_Q = 5.47 %

$F_{ratio} = \frac{0.81}{1.08} < 1$

Table 3.3 Weights and statistics of HSCM3 sample collected over 56 seconds

COMMINUTED PRODUCT: HSCM				SIZE FRACTION: 90 - 125 μm	
Container No.	RUN 1 [g]	RUN 2 [g]	RUN3 [g]	Mean of Runs [g]	Mean flow rate [g/s]
1	21.73	17.73	23.74	21.06	0.37
2	20.76	19.03	24.09	21.29	0.38
3	21.74	19.16	23.34	21.41	0.38
4	19.56	18.46	19.91	19.31	0.34
5	18.36	20.00	19.89	19.41	0.34
6	18.71	18.72	19.52	18.98	0.33
7	20.03	17.23	18.95	18.73	0.33
8	18.81	18.36	18.45		
S	1.35	0.85	2.25		
S^2	1.83	0.92	5.08		
$\bar{X}$[g]	20.10	18.61	21.34		
W[g/s]	0.35	0.33	0.38		
μ_r[g]				20.02	
σ_r^2[g]				1.37	
Q_r[g/s]					0.35
σ_{Qr}[g/s]					0.0228

OVERALL STATISTICS

σ_{ave} = 1.60 g $\quad CV_Q$ = 6.5 %

S^2_p = 2.58 g $\quad F_{ratio} = \frac{1.37}{2.58} < 1$

Table 3.4 Weights and statistics of HSCM4 sample collected over 56 seconds

COMMINUTED PRODUCT: HSCM				SIZE FRACTION: 125-180 μm	
Container No.	RUN 1 [g]	RUN 2 [g]	RUN3 [g]	Mean of Runs [g]	Mean flow rate [g/s]
1	22.37	26.14	19.99	22.83	0.40
2	24.93	26.17	22.45	24.51	0.437
3	22.51	24.79	19.49	22.26	0.397
4	22.74	24.54	19.07	22.11	0.394
5	22.58	25.54	18.97	22.30	0.398
6	22.43	25.21	18.14	21.92	0.391
7	21.56	23.92	16.52	20.66	0.368
8	20.74	21.94	16.16		
S	1.04	0.83	1.81		
S^2	1.08	0.69	3.29		
$\bar{X}$[g]	22.73	25.18	19.20		
W[g/s]	0.40	0.44	0.34		
μ_r[g]				22.37	
σ_r^2[g]				1.15	
Q_r[g/s]					0.40
σ_{Qr}[g/s]					0.02

OVERALL STATISTICS

σ_{ave} = 1.30 g $\quad$ CV_Q = 5 %

S^2_p = 1.68 g $\quad$ $F_{ratio} = \frac{1.15}{1.68} < 1$

Table 3.5 Weights and statistics of HSCM5 sample collected over 56 seconds

COMMINUTED PRODUCT: HSCM6				SIZE FRACTION: 180-250 μm	
Container No.	RUN 1 [g]	RUN 2 [g]	RUN3 [g]	Mean of Runs [g]	Mean flow rate [g/s]
1	30.21	27.59	24.85	27.55	0.49
2	27.51	25.34	28.32	27.05	0.48
3	22.66	26.56	21.41	23.54	0.42
4	28.66	26.16	26.56	27.12	0.48
5	26.10	24.70	23.81	24.87	0.44
6	24.95	22.38	20.33	22.55	0.40
7	23.04	22.21	19.63	21.62	0.39
8	25.34	21.15	18.88		
S	2.82	2.05	3.26		
S^2	7.98	4.22	10.64		
$\bar{X}$[g]	26.16	24.99	23.55		
W[g/s]	0.46	0.44	0.42		
μ_r[g]				24.9	
σ_r^2[g]				5.7	
Q_r[g/s]					0.44
σ_{Qr}[g/s]					0.041

OVERALL STATISTICS

σ_{ave} = 2.75 g

S^2_P = 7.61 g

CV_Q = 9.3 %

$F_{ratio} = \frac{5.7}{7.61} < 1$

Table 3.6 Weights and statistics of HSCM6 sample collected over 56 seconds

COMMINUTED PRODUCT: HSCM				SIZE FRACTION: 250-315 μm	
Container No.	RUN 1 [g]	RUN 2 [g]	RUN3 [g]	Mean of Runs [g]	Mean flow rate [g/s]
1	24.77	22.21	22.23	23.10	0.41
2	22.66	23.09	19.96	21.90	0.39
3	22.44	25.26	27.77	25.15	0.44
4	24.69	19.77	18.35	20.93	0.37
5	22.17	19.52	16.60	19.43	0.34
6	19.38	19.00	15.22	17.86	0.31
7	19.01	18.73	18.37	18.70	0.33
8	16.24	15.34	17.17		
S	2.28	2.47	4.18		
S^2	5.19	6.13	17.55		
$\bar{X}$[g]	22.16	21.08	19.80		
W[g/s]	0.39	0.37	0.35		
μ_r[g]				21.01	
σ_r^2[g]				6.67	
Q_r[g/s]					0.37
σ_{Qr}[g/s]					0.046

OVERALL STATISTICS

σ_{ave} = 3.1 g

S^2_P = 9.62 g

CV_Q = 12.4 %

$F_{ratio} = \frac{6.67}{9.62} < 1$

Table 3.7 Weights and statistics of HSCM7 sample collected over 56 seconds

COMMINUTED PRODUCT: BMa				SIZE FRACTION: 38 - 63μm	
Container No.	RUN 1 [g]	RUN 2 [g]	RUN3 [g]	Mean of Runs [g]	Mean flow rate [g/s]
1	22.59	21.78	17.43	20.60	0.183
2	21.95	19.23	15.02	18.73	0.167
3	19.15	19.33	19.23	19.23	0.171
4	17.34	17.48	13.59	16.13	0.144
5	15.60	16.41	13.27	15.09	0.134
6	20.11	14.77	16.90	17.26	0.154
7	16.59	15.04	12.94	14.85	0.132
8	16.13	14.57	13.00		
S	2.67	2.54	2.41		
S^2	6.13	5.57	5.00		
$\bar{X}$[g]	19.04	17.72	15.48		
W[g/s]	0.17	0.158	0.138		
μ_r[g]				17.41	
σ_r^2[g]				4.11	
Q_r[g/s]					0.155
σ_{Qr}[g/s]					0.019

OVERALL STATISTICS

σ_{ave} = 2.54 g $\quad$ CV_Q = 12.5 %

S^2_P = 5.56 g $\quad$ $F_{ratio} = \frac{4.11}{5.56} < 1$

Table 3.8 Weights and statistics of BMa2 sample collected over 112 seconds

COMMINUTED PRODUCT: BMa				SIZE FRACTION: 63 - 90 μm	
Container No.	RUN 1 [g]	RUN 2 [g]	RUN3 [g]	Mean of Runs [g]	Mean flow rate [g/s]
1	21.05	18.05	20.03	19.71	0.351
2	22.57	18.10	19.32	19.99	0.357
3	21.54	17.02	19.40	19.32	0.345
4	21.09	18.12	17.32	18.84	0.336
5	19.22	16.78	16.68	17.56	0.313
6	18.80	15.78	18.53	17.70	0.316
7	18.29	17.29	17.52	17.70	0.316
8	19.91	18.30	18.22		
S	1.59	0.87	1.26		
S^2	2.55	0.76	1.56		
$\bar{X}$[g]	20	17.31	18.40		
W[g/s]	0.36	0.31	0.32		
μ_r[g]				18.58	
σ_r^2[g]				1.06	
Q_r[g/s]					0.33
σ_{Qr}[g/s]					0.018

OVERALL STATISTICS

σ_{ave} = 1.27 g

S^2_P = 1.62 g

CV_Q = 5.5 %

$F_{ratio} = \frac{1.06}{1.62} < 1$

Table 3.9 Weights and statistics of BMa3 sample collected over 56 seconds

COMMINUTED PRODUCT: BMa				SIZE FRACTION: 90-125 μm	
Container No.	RUN 1 [g]	RUN 2 [g]	RUN3 [g]	Mean of Runs [g]	Mean flow rate [g/s]
1	18.09	15.40	18.00	17.16	0.600
2	16.35	16.18	17.10	16.54	0.590
3	16.48	14.56	16.46	15.84	0.565
4	16.91	14.02	15.95	15.62	0.557
5	17.84	14.64	16.11	16.13	0.576
6	19.64	15.50	17.26	17.46	0.623
7	18.22	14.68	17.25	16.72	0.597
8	18.24	15.21	16.91		
S	1.16	0.72	0.73		
S^2	1.34	0.53	0.53		
$\bar{X}$[g]	17.6	14.99	16.87		
W[g/s]	0.63	0.53	0.60		
μ_r[g]				16.49	
σ_r^2[g]				0.45	
Q_r[g/s]					0.58
σ_{Qr}[g/s]					0.022

OVERALL STATISTICS

σ_{ave} = 0.90 g

S^2_P = 0.80 g

CV_Q = 3.9 %

$F_{ratio} = \frac{0.45}{0.80} < 1$

Table 3.10 Weights and statistics of BMa4 sample collected over 28 seconds

COMMINUTED PRODUCT: BMa				SIZE FRACTION: 125-180 μm	
Container No.	RUN 1 [g]	RUN 2 [g]	RUN3 [g]	Mean of Runs [g]	Mean flow rate [g/s]
1	22.35	18.00	18.37	19.57	0.699
2	19.51	16.70	19.87	18.69	0.667
3	19.83	18.92	17.53	18.76	0.670
4	19.00	14.80	17.13	16.97	0.606
5	19.95	15.22	18.33	17.83	0.636
6	21.15	16.36	17.85	18.45	0.659
7	19.71	16.04	17.90	17.88	0.638
8	—	—	—		
S	1.14	1.46	0.87		
S^2	1.31	2.14	0.76		
$\bar{X}$[g]	20.20	16.57	18.14		
W[g/s]	0.72	0.59	0.64		
μ_r[g]				18.30	
σ_r^2[g]				0.69	
Q_r[g/s]					0.650
σ_{Qr}[g/s]					0.029

OVERALL STATISTICS

σ_{ave} = 1.18 g $\quad CV_Q$ = 4.5 %

S^2_p = 1.40 g $\quad F_{ratio} = \frac{0.69}{1.40} < 1$

Table 3.11 Weights and statistics of BMa5 sample collected over 28 seconds

COMMINUTED PRODUCT: BMa				**SIZE FRACTION:** 180-250 μm	
Container No.	RUN 1 [g]	RUN 2 [g]	RUN3 [g]	Mean of Runs [g]	Mean flow rate [g/s]
1	20.83	20.54	21.63	21.00	0.75
2	19.83	20.40	22.35	20.86	0.74
3	18.87	20.45	19.90	19.74	0.70
4	18.91	19.60	20.32	19.61	0.70
5	18.79	17.95	19.59	18.77	0.67
6	18.23	18.98	20.78	19.33	0.69
7	19.04	17.57	18.59	18.40	0.66
8	–	–	–		
S	0.85	1.22	1.26		
S^2	0.72	1.50	1.60		
$\bar{X}$[g]	19.21	19.35	20.45		
W[g/s]	0.68	0.69	0.73		
μ_r[g]				19.60	
σ_r^2[g]				0.95	
Q_r[g/s]					0.70
σ_{Qr}[g/s]					0.033

OVERALL STATISTICS

σ_{ave} = 1.12 g $\quad CV_Q$ = 4.7 %

S^2_p = 1.27 g $\quad F_{ratio} = \frac{0.95}{1.27} < 1$

Table 3.12 Weights and statistics of BMa6 sample collected over 28 seconds

COMMINUTED PRODUCT: BMb3				SIZE FRACTION: 63 - 90μm	
Container No.	RUN 1 [g]	RUN 2 [g]	RUN3 [g]	Mean of Runs [g]	Mean flow rate [g/s]
1	20.60	19.25	19.63	19.82	0.350
2	19.48	18.31	19.47	19.08	0.340
3	20.74	19.03	18.34	19.37	0.350
4	21.11	21.70	19.90	20.90	0.370
5	19.80	19.82	18.49	19.37	0.350
6	18.85	17.50	19.50	18.61	0.330
7	17.90	18.90	19.20		
8	18.51	18.50	18.92		
S	1.14	1.13	0.58		
S^2	1.30	1.73	0.34		
$\bar{X}$[g]	19.70	19.20	19.20		
W[g/s]	0.35	0.34	0.34		
μ_r[g]				19.2	
σ_r^2[g]				0.61	
Q_r[g/s]					0.350
σ_{Qr}[g/s]					0.0139

OVERALL STATISTICS

σ_{ave} = 1.05 g

S^2_p = 1.12 g

CV_Q = 3.9 %

$F_{ratio} = \frac{0.61}{1.12} < 1$

Table 3.13 Weights and statistics of BMb3 sample collected over 56 seconds

COMMINUTED PRODUCT: BMb				SIZE FRACTION: 90-125 μm	
Container No.	RUN 1 [g]	RUN 2 [g]	RUN3 [g]	Mean of Runs [g]	Mean flow rate [g/s]
1	16.80	18.33	20.87	18.66	0.660
2	15.54	18.13	20.35	18.00	0.640
3	15.48	18.07	19.28	17.61	0.620
4	16.23	18.15	19.28	17.88	0.630
5	16.24	18.46	19.20	17.96	0.640
6	17.38	16.50	18.37	17.41	0.620
7	15.91	17.40	19.10	17.47	0.620
8	16.09	16.85	19.22		
S	0.68	0.71	0.83		
S^2	0.46	0.51	0.70		
$\bar{X}$[g]	16.22	17.88	19.49		
W[g/s]	0.580	0.640	0.690		
μ_r[g]				17.85	
σ_r^2[g]				0.18	
Q_r[g/s]					0.630
σ_{Qr}[g/s]					0.015

OVERALL STATISTICS

σ_{ave} = 0.74 g

S^2_P = 0.55 g

CV_Q = 2.3 %

$F_{ratio} = \frac{0.18}{0.55} < 1$

Table 3.14 Weights and statistics of BMb4 sample collected over 28 seconds

COMMINUTED PRODUCT: BMb				SIZE FRACTION: 125-180 μm	
Container No.	RUN 1 [g]	RUN 2 [g]	RUN3 [g]	Mean of Runs [g]	Mean flow rate [g/s]
1	21.09	19.97	19.51	20.19	0.720
2	19.83	19.98	19.96	19.92	0.170
3	18.35	19.99	19.69	19.34	0.690
4	18.24	19.48	18.48	18.48	0.660
5	19.54	19.56	19.17	19.42	0.690
6	20.19	18.94	19.44	19.52	0.690
7	20.23	18.55	18.11	18.96	0.680
8	—	—	—		
S	1.14	1.31	0.58		
S^2	1.30	1.73	0.34		
$\bar{X}$[g]	19.7	19.2	19.2		
W[g/s]	0.35	0.34	0.34		
μ_r[g]				19.40	
σ_r^2[g]				0.32	
Q_r[g/s]					0.690
σ_{Qr}[g/s]					0.019

OVERALL STATISTICS

σ_{ave} = 1.05 g

S^2_P = 1.12 g

CV_Q = 2.8 %

$F_{ratio} = \frac{0.32}{1.12} < 1$

Table 3.15 Weights and statistics of BMb5 sample collected over 28 seconds

COMMINUTED PRODUCT: BMb				SIZE FRACTION: 180-250 μm	
Container No.	RUN 1 [g]	RUN 2 [g]	RUN3 [g]	Mean of Runs [g]	Mean flow rate [g/s]
1	23.75	23.64	24.21	23.87	0.850
2	23.88	24.00	23.39	23.75	0.840
3	22.64	22.88	22.16	22.56	0.800
4	22.63	23.62	22.74	22.99	0.820
5	22.42	22.22	24.97	23.20	0.820
6	23.71	23.12	24.68	23.83	0.850
7	21.04	22.05	24.00	24.36	0.800
8	22.80	21.20	23.12		
S	1.01	0.74	0.99		
S^2	1.02	0.54	0.98		
$\bar{X}$[g]	22.86	23.07	23.71		
W[g/s]	0.81	0.82	0.84		
μ_r[g]				23.22	
σ_r^2[g]				0.38	
Q_r[g/s]					0.820
σ_{Qr}[g/s]					0.021

OVERALL STATISTICS

σ_{ave} = 0.92 g

S^2_P = 0.84 g

CV_Q = 2.6 %

$F_{ratio} = \frac{0.38}{0.84} < 1$

Table 3.16 Weights and statistics of BMb6 sample collected over 28 seconds

COMMINUTED PRODUCT: ERMa				SIZE FRACTION: 38 - 63 μm	
Container No.	RUN 1 [g]	RUN 2 [g]	RUN3 [g]	Mean of Runs [g]	Mean flow rate [g/s]
1	16.45	18.91	17.98	17.78	0.31
2	16.05	19.15	19.92	18.37	0.33
3	17.21	15.94	16.80	16.65	0.29
4	16.12	16.95	16.28	16.45	0.29
5	16.90	18.72	17.75	17.79	0.31
6	18.68	20.62	19.28	19.52	0.35
7	17.40	17.48	17.90	17.59	0.31
8	15.75	17.03	18.08		
S	0.91	1.56	1.27		
S^2	0.83	2.45	1.63		
$\bar{X}$[g]	16.97	18.25	17.93		
W[g/s]	0.30	0.32	0.32		
μ_r[g]				17.7	
σ_r^2[g]				1.07	
Q_r[g/s]					0.31
σ_{Qr}[g/s]					0.021

OVERALL STATISTICS

σ_{ave} = 1.27 g CV_Q = 6.8 %

S^2_P = 1.63 g $F_{ratio} = \frac{1.07}{1.63} < 1$

Table 3.17 Weights and statistics of ERMa3 sample collected over 56 seconds

COMMINUTED PRODUCT: ERMa				SIZE FRACTION: 90-125 μm	
Container No.	RUN 1 [g]	RUN 2 [g]	RUN3 [g]	Mean of Runs [g]	Mean flow rate [g/s]
1	20.98	23.08	22.82	22.29	0.398
2	19.39	22.76	23.90	22.01	0.390
3	20.56	20.11	20.91	20.52	0.360
4	19.67	23.56	20.01	21.08	0.370
5	21.35	24.05	21.99	22.46	0.400
6	20.31	24.30	22.62	22.41	0.400
7	19.91	23.11	22.12	21.71	0.380
8	18.80	22.40	20.16		
S	0.71	1.36	1.27		
S^2	0.50	1.92	1.63		
$\bar{X}$[g]	20.34	22.99	22.05		
W[g/s]	0.36	0.41	0.390		
μ_r[g]				21.78	
σ_r^2[g]				0.54	
Q_r[g/s]					0.380
σ_{Qr}[g/s]					0.016

OVERALL STATISTICS

σ_{ave} = 1.16 g

S^2_p = 1.35 g

CV_Q = 4.2 %

$F_{ratio} = \frac{0.54}{1.35} < 1$

Table 3.18 Weights and statistics of ERMa4 sample collected over 56 seconds

COMMINUTED PRODUCT: ERMa				SIZE FRACTION:125-180 μm	
Container No.	RUN 1 [g]	RUN 2 [g]	RUN3 [g]	Mean of Runs [g]	Mean flow rate [g/s]
1	28.68	29.16	23.90	27.24	0.48
2	28.57	26.60	26.85	27.34	0.49
3	28.96	25.08	23.40	25.81	0.46
4	25.28	26.48	23.09	24.95	0.44
5	28.87	24.61	23.80	25.76	0.46
6	28.93	27.55	22.90	26.46	0.47
7	26.63	25.66	22.18	24.82	0.44
8	25.89	26.23	21.80		
S	1.44	1.55	1.49		
S^2	2.1	2.41	2.23		
$\bar{X}$[g]	27.98	26.40	23.73		
W[g/s]	0.50	0.47	0.41		
μ_r[g]				26.05	
σ_r^2[g]				1.00	
Q_r[g/s]					0.46
σ_{Qr}[g/s]					0.0189

OVERALL STATISTICS

σ_{ave} = 1.50 g $\quad CV_Q$ = 4.1 %

S^2_P = 2.24 g $\quad F_{ratio} = \frac{1}{2.24} < 1$

Table 3.19 Weights and statistics of ERMa5 sample collected over 56 seconds

COMMINUTED PRODUCT: ERMa				SIZE FRACTION: 180-250 μm	
Container No.	RUN 1 [g]	RUN 2 [g]	RUN3 [g]	Mean of Runs [g]	Mean flow rate [g/s]
1	30.03	31.80	32.22	31.35	0.56
2	29.12	32.72	30.80	31.35	0.56
3	25.84	34.14	28.12	29.36	0.52
4	27.12	30.01	28.82	28.65	0.51
5	24.99	28.72	26.18	26.63	0.47
6	26.16	30.70	27.70	28.18	0.50
7	26.56	30.92	28.25	28.57	0.51
8	27.01	29.20	29.00		
S	1.82	1.78	2.02		
S^2	3.31	3.19	4.08		
$\bar{X}$[g]	27.1	31.28	28.87		
W[g/s]	0.48	0.55	0.51		
μ_r[g]				29.1	
σ_r^2[g]				2.93	
Q_r[g/s]					0.520
σ_{Qr}[g/s]					0.032

OVERALL STATISTICS

σ_{ave} = 1.87 g $\quad CV_Q$ = 6.2 %

S^2_p = 3.52 g $\quad F_{ratio} = \frac{2.93}{3.52} < 1$

Table 3.20 Weights and statistics of ERMa6 sample collected over 56 seconds

COMMINUTED PRODUCT: ERMb				SIZE FRACTION: 63 - 90 μm	
Container No.	RUN 1 [g]	RUN 2 [g]	RUN3 [g]	Mean of Runs [g]	Mean flow rate [g/s]
1	19.30	20.11	18.88	19.43	0.35
2	17.99	18.85	19.72	18.85	0.34
3	16.68	18.12	18.78	17.86	0.32
4	16.03	17.00	18.25	17.09	0.30
5	18.92	18.15	18.55	18.54	0.33
6	20.21	20.15	16.98	19.11	0.34
7	18.52	16.90	17.70	17.70	0.32
8	17.85	17.20	17.02		
S	1.4	1.32	0.88		
S^2	2.1	1.75	0.77		
$\bar{X}$[g]	18.23	18.46	18.40		
W[g/s]	0.32	0.33	0.33		
μ_r[g]				18.37	
σ_r^2[g]				0.71	
Q_r[g/s]					0.33
σ_{Qr}[g/s]					0.016

OVERALL STATISTICS

σ_{ave} = 1.24 g $\quad CV_Q$ = 5.0 %

S^2_p = 1.54 g $\quad F_{ratio} = \frac{0.71}{1.54} < 1$

Table 3.21 Weights and statistics of ERMb3 sample collected over 56 seconds

COMMINUTED PRODUCT: ERMb				**SIZE FRACTION:** 90-125 μm	
Container No.	RUN 1 [g]	RUN 2 [g]	RUN3 [g]	Mean of Runs [g]	Mean flow rate [g/s]
1	22.37	23.99	24.12	23.49	0.42
2	22.05	25.01	24.40	23.82	0.42
3	19.99	24.77	25.18	23.31	0.41
4	20.95	25.60	21.98	22.84	0.40
5	21.14	23.12	23.82	22.69	0.40
6	21.01	23.01	23.71	22.57	0.40
7	20.15	22.11	22.29	21.51	0.38
8	20.72	22.08	22.12		
S	0.88	1.3	1.3		
S^2	0.78	1.7	1.29		
$\bar{X}$[g]	21.09	23.8	23.8		
W[g/s]	0.37	0.42	0.42		
μ_r[g]				22.83	
σ_r^2[g]				0.57	
Q_r[g/s]					0.40
σ_{Qr}[g/s]					0.014

OVERALL STATISTICS

σ_{ave} = 1.12 g $\quad$ CV_Q = 3.5 %

S^2_P = 1.25 g $\quad$ $F_{ratio} = \frac{0.57}{1.25} < 1$

Table 3.22 Weights and statistics of ERMb4 sample collected over 56 seconds

COMMINUTED PRODUCT: ERMb				SIZE FRACTION: 125-180 μm	
Container No.	RUN 1 [g]	RUN 2 [g]	RUN3 [g]	Mean of Runs [g]	Mean flow rate [g/s]
1	29.22	25.40	27.18	27.26	0.48
2	30.20	26.12	28.81	28.37	0.50
3	31.80	27.80	28.91	29.47	0.52
4	32.22	28.22	28.20	29.54	0.52
5	30.80	26.40	27.70	28.30	0.50
6	29.70	25.62	26.95	27.42	0.49
7	29.13	26.14	27.20	27.49	0.49
8	30.14	26.52	25.14		
S	1.22	1.07	0.80		
S^2	1.49	1.15	0.64		
$\bar{X}$[g]	30.43	26.50	27.85		
W[g/s]	0.54	0.47	0.49		
μ_r[g]				28.26	
σ_r^2[g]				0.90	
Q_r[g/s]					0.50
σ_{Qr}[g/s]					0.015

OVERALL STATISTICS

σ_{ave} = 1.04 g $\quad CV_Q$ = 3.0 %

S^2_p = 1.09 g $\quad F_{ratio} = \frac{0.90}{1.09} < 1$

Table 3.23 Weights and statistics of ERMb5 sample collected over 56 seconds

COMMINUTED PRODUCT: ERMb				SIZE FRACTION: 180-250 μm	
Container No.	RUN 1 [g]	RUN 2 [g]	RUN3 [g]	Mean of Runs [g]	Mean flow rate [g/s]
1	31.82	34.72	33.71	33.41	0.59
2	33.22	30.12	34.93	32.75	0.58
3	30.29	31.06	34.11	31.82	0.57
4	30.81	31.20	30.81	30.94	0.55
5	29.22	33.12	32.14	31.49	0.56
6	31.80	30.84	33.16	31.93	0.57
7	30.22	30.27	32.73	31.07	0.55
8	28.77	31.11	31.22		
S	1.32	1.68	1.36		
S^2	1.75	2.83	1.85		
$\bar{X}$[g]	31.05	31.61	33.08		
W[g/s]	0.55	0.56	0.59		
μ_r[g]				31.91	
σ_r^2[g]				0.80	
Q_r[g/s]					0.57
σ_{Qr}[g/s]					0.015

OVERALL STATISTICS

σ_{ave} = 1.46 g

S^2_P = 2.14 g

CV_Q = 2.6 %

$F_{ratio} = \frac{0.80}{2.14} < 1$

Table 3.24 Weights and statistics of ERMb6 sample collected over 56 seconds

3.1.2 A summary of the statistics of the flow rate and weight and flow uniformity from the Tables 3.2 to 3.24

Table 3.25 shows a summary of the results obtained when the liquorice was comminuted by a HSC Mill and fractionated into the size fractions flowing along an inclined tube. Table 3.26 shows a similar summary table for liquorice Ball Milled for 45 and 75 minutes respectively while Table 3.27 shows the results from the End Runner fractions milled at 10 and 20 minutes.

The overall flow rate (Qr), the standard deviation of the flow rate (σ_{Qr}) and the coefficient of variation of the flow rates (CV_Q) with respect to the sieve mean size together with the standard deviation of the collected weight (σ_{ave}) are tabulated to evaluate the flow rate and flow uniformity of different sized fractions and different milled products.

Figure 3.1 shows the flowability of all 23 fractions against the mean particle size of the milled products from the various mills while Figure 3.2 represents the weight uniformity versus mean particle size for all the fractions of the milled products.

Mill type and fractions	Size range μm	Mean size μm	Q_r g/s	σ_{Ave} g	σ_{Q_r} g/s	C.V. %
HSCM2	38-63	50	0.174	2.71	0.0223	12.80
HSCM3	63-90	76	0.29	1.03	0.016	5.47
HSCM4	90-125	106	0.35	1.60	0.0228	6.50
HSCM5	125-180	152	0.40	1.30	0.020	5.00
HSCM6	180-250	215	0.44	2.75	0.041	9.3
HSCM7	250-315	275	0.37	3.10	0.046	12.4

Table 3.25 Summary table for High Speed Cutter milled liquorice of different sized fractions

Mill type and fractions	Size range μm	Mean size μm	Q_r g/s	σ_{Ave} g	σ_{Q_r} g/s	C.V. %
BMa2	38-63	51	0.155	2.54	0.0194	12.5
BMa3	63-90	76	0.33	1.27	0.018	5.5
BMa4	90-125	105	0.58	0.90	0.022	3.9
BMa5	125-180	152	0.65	1.18	0.029	4.5
BMa6	180-250	215	0.70	1.120	0.033	4.7
BMb3	63-90	76	0.35	1.05	0.0139	3.9
BMb4	90-125	106	0.63	0.74	0.015	2.3
BMb5	125-180	152	0.69	1.05	0.019	2.8
BMb6	180-250	215	0.82	0.92	0.021	2.6

Table 3.26 Summary Table for Ball Milled liquorice of different sized fractions

Mill type and fractions	Size range μm	Mean size μm	Q_r g/s	σ Ave g	σ_{Q_r} g/s	C.V. %
ERMa3	63-90	76	0.31	1.27	0.021	6.8
ERMa4	90-125	106	0.38	1.16	0.016	4.2
ERMa5	125-180	152	0.46	1.50	0.0189	4.1
ERMa6	180-250	215	0.52	1.87	0.032	6.2
ERMb3	63-90	76	0.33	1.24	0.016	5.0
ERMb4	90-125	106	0.40	1.12	0.014	3.5
ERMb5	125-180	152	0.50	1.04	0.015	3.0
ERMb6	180-250	215	0.57	1.46	0.015	2.6

Table 3.27 Summary Table for End Runner Milled liquorice of different size fractions

● *High speed cutter mill (HSCM)*

★ *Ball mill (BMa) time 45 mins*

■ " " (BMb) " 75 "

▲ *End runner mill (ERMa) time 10 mins*

♦ " " " (ERMb) " 20 "

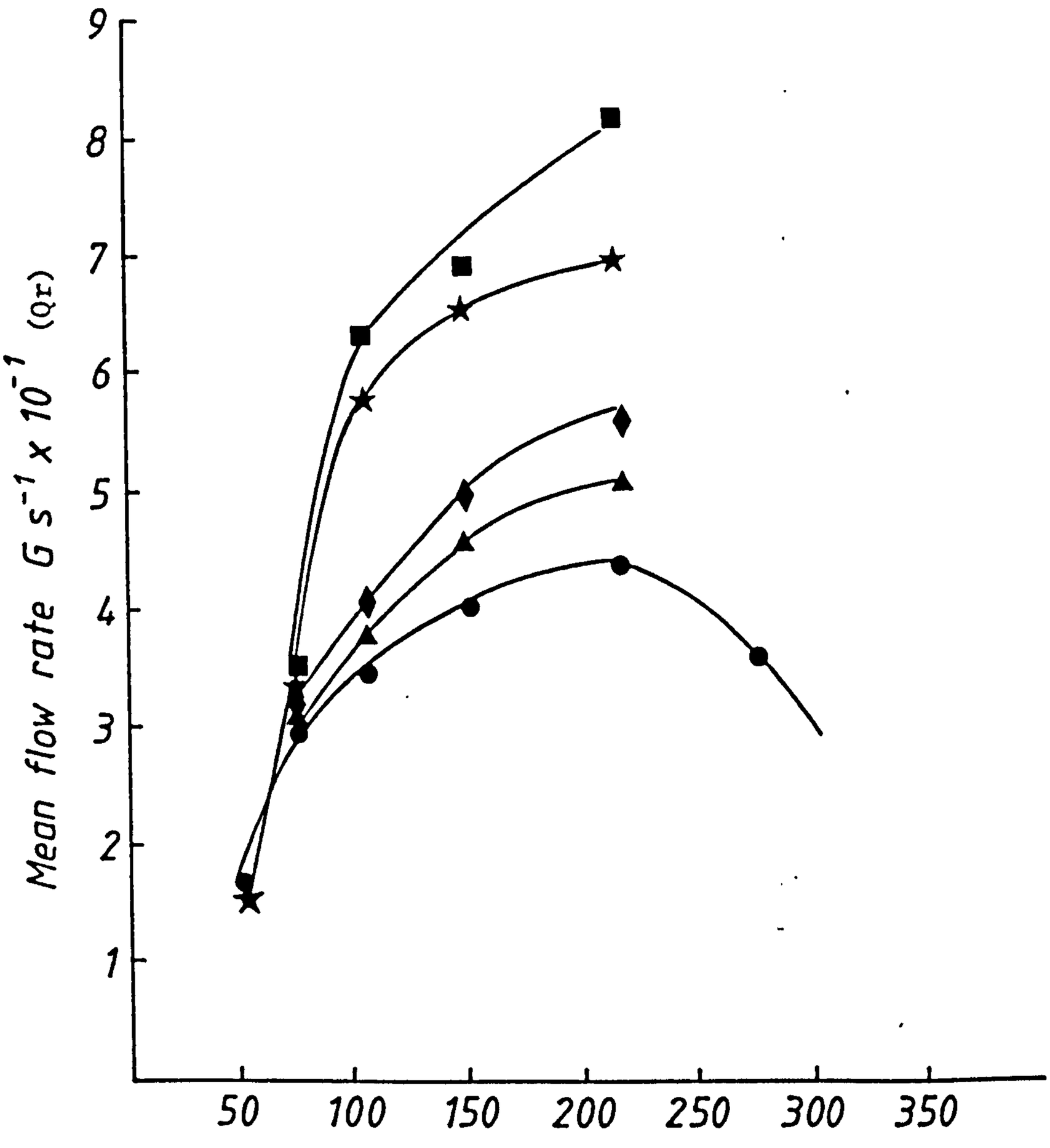

Fig.3.1 *Mean rate of flow versus mean particle size for various milled products*

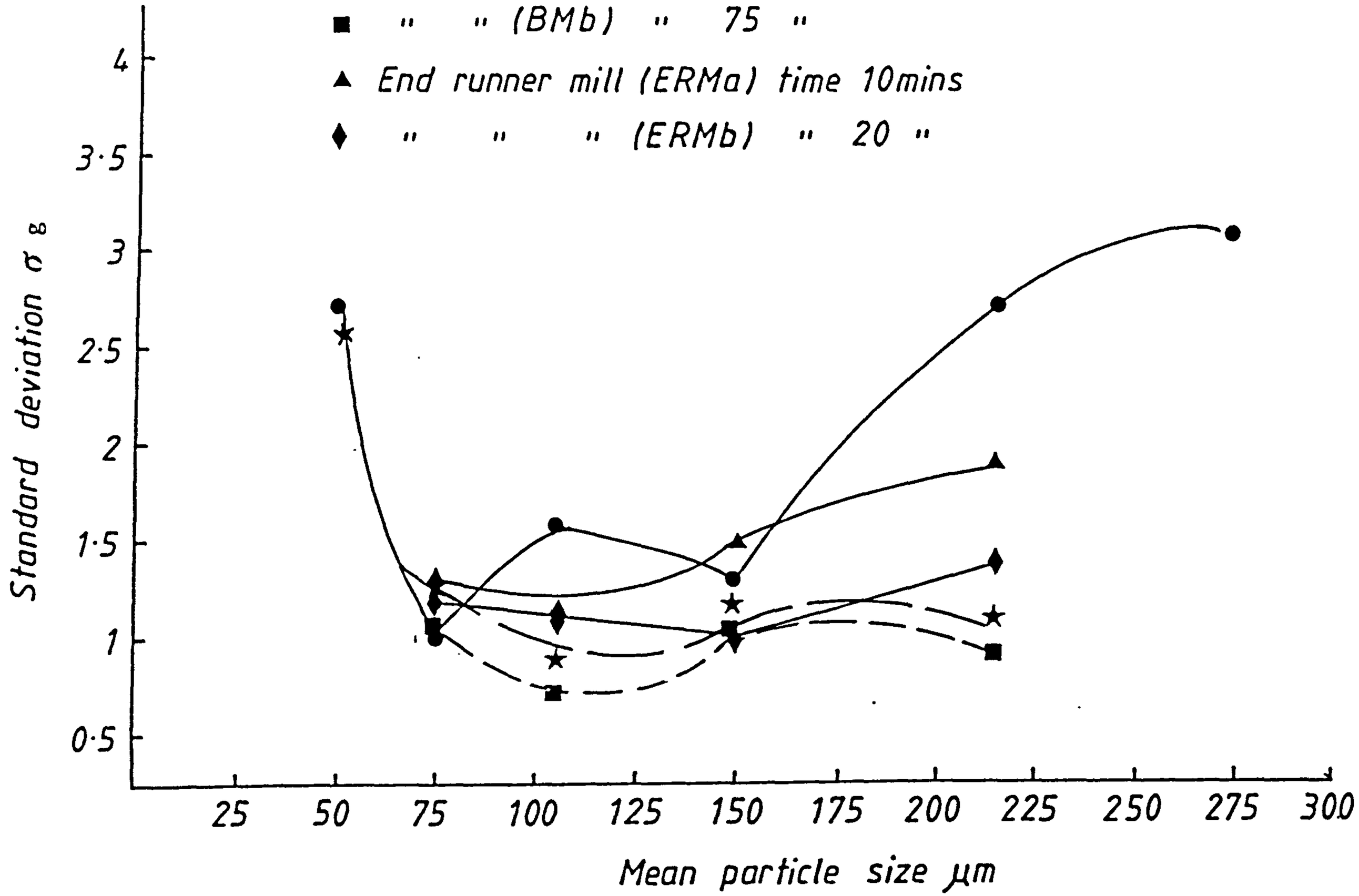

Fig. 3.2 std. of collected weight versus mean particle size by different mills and times

3.2 Mechanical properties of the fractionated material using a Jenike shear cell method

The mechanical properties of the various sized fractions of liquorice investigated to determine the effect of both particle size and shape on flow parameters were:

1. Jenike effective angle of internal friction (δ)
2. Angle of internal friction, using CSL (δ_E)
3. Major principal consolidating stress (σ_1)
4. Unconfined yield stress (f_c)
5. and Failure Functions (FF)

From the liquorice powder used to measure the flow rate and flow uniformity (Section 3.1.1) six size fractions and one HSCM fraction mixture were selected.

Fraction No.	Size range (μm)
HSCM2	38 - 63
HSCM3	63 - 90
HSCM5	125 - 180
BMa2	38 - 63
BMa3	63 - 90
BMa5	125 - 180
and HSCM mixture	Combination of the four fraction 2, 3, 4, 5

The HSCM mixture of the four size fractions 2, 3, 4, and 5 was prepared with a similar weight proportionality to that of the initial product obtained from the high speed cutter mill (Section 2.2).

The shear properties of these size fractions were measured at various compaction loads with different normal stresses using modified Jenike shear cell (Section 2.5.1).

The shear stresses at failure are shown in Tables 3.28 to 3.34. Each table presents data obtained for 3 experimental yield loci, which together form a family of loci.

Figures 3.4 to 3.24 of shear stress versus normal applied stress show the Jenike yield locus together with the tangent to the Mohr circles one passing through the origin for evaluating the unconfined yield stress(f_c)and the other end point (σ_E) for evaluating the major consolidation stress (σ_1) are also noted in each figure.

Table 3.35 summarises the parameters of f_c, σ_1, and σ for each family of yield loci, obtained from figures 3.4 to 3.24.

The notations on figures 3.4 to 3.24 are equivalent to the following shear parameters and symbols.

FC	=	f_c	unconfined yield stress
SIGMA1	=	σ_1	major consolidation stress
DELTA	=	δ	Jenike effective angle of internal friction.

1ST LOCUS		2ND LOCUS		3RD LOCUS	
Compaction Load (CL) 9 kg No. of Twist (T) 5 Normal Load (NL) 1.722 kg		CL 14 kg T 5 NL 2.623 kg		CL 20 kg T 3 NL 3.623 kg	
Normal stress [σ] kPa	**Shear stress** [τ] kPa	**Normal stress** [σ] kPa	**Shear stress** [τ] kPa	**Normal stress** [σ] kPa	**Shear stress** [τ] kPa
8.603	7.554	13.105	11.670	18.100	16.030
7.104	6.601	10.606	9.622	14.603	13.725
5.106	4.971	8.109	7.981	10.606	10.185
2.608	3.040	5.610	6.048	5.610	6.100
		3.112	3.709	3.112	4.227

Table 3.28 Jenike shear test on HSCM size fraction 2

1ST LOCUS		2ND LOCUS		3RD LOCUS	
Compaction Load (CL) 8.5 kg No. of Twist (T) 10 Normal Load (NL) 1.318 kg		CL 13.4 kg T 8 NL 2.619 kg		CL 18 kg T 6 NL 4.019 kg	
Normal stress [σ] kPa	**Shear stress** [τ] kPa	**Normal stress** [σ] kPa	**Shear stress** [τ] kPa	**Normal stress** [σ] kPa	**Shear stress** [τ] kPa
6.589	5.471	13.085	11.182	20.079	16.640
5.094	4.320	10.090	8.870	15.078	13.506
3.591	3.353	6.590	6.237	10.081	9.635
2.593	2.680	3.093	3.628	6.589	6.623
				4.091	4.612

Table 3.29 Jenike shear test on HSCM size fraction 3

1ST LOCUS		2ND LOCUS		3RD LOCUS	
Compaction Load (CL) 22 kg No. of Twist (T) 10 Normal Load (NL) 4.90 kg		CL 25 kg T 8 NL 5.4 kg		CL 28 kg T 6 NL 5.90 kg	
Normal stress [σ] kPa	**Shear stress** [τ] kPa	**Normal stress** [σ] kPa	**Shear stress** [τ] kPa	**Normal stress** [σ] kPa	**Shear stress** [τ] kPa
24.481	24.993	26.979	27.282	29.470	29.892
19.485	21.999	19.485	22.428	21.983	24.484
14.488	16.401	14.489	16.855	16.987	20.350
9.992	11.599	10.741	13.280	11.990	15.137
2.198	3.467	3.677	4.960	4.056	5.795

Table 3.31 Jenike shear test on HSCM size fraction 5

1ST LOCUS		2ND LOCUS		3RD LOCUS	
Compaction Load (CL) 10 kg No. of Twist (T) 10 Normal Load (NL) 3.02 kg		CL 16 kg T 8 NL 3.82 kg		CL 20 kg T 6 NL 4.72 kg	
Normal stress [σ] kPa	**Shear stress** [τ] kPa	**Normal stress** [σ] kPa	**Shear stress** [τ] kPa	**Normal stress** [σ] kPa	**Shear stress** [τ] kPa
15.088	14.568	19.085	18.435	23.581	23.044
11.091	11.173	16.087	16.100	19.585	20.409
		11.591	11.983	13.090	14.090
7.094	7.240	6.095	6.992	7.094	8.318
2.598	3.777	2.598	4.181	2.598	4.271

Table 3.31 Jenike shear test on HSCM size fraction mixture (2,3,4, and 5)

1ST LOCUS		2ND LOCUS		3RD LOCUS	
Compaction Load (CL) 9 kg No. of Twist (T) 5 Normal Load (NL) 1.924 kg		CL 14 kg T 5 NL 2.925 kg		CL 20 kg T 3 NL 3.924 kg	
Normal stress [σ] kPa	**Shear stress** [τ] kPa	**Normal stress** [σ] kPa	**Shear stress** [τ] kPa	**Normal stress** [σ] kPa	**Shear stress** [τ] kPa
9.612	8.392	14.610	12.702	19.605	16.880
7.114	6.787	9.617	8.813	14.608	13.219
4.616	4.901	7.119	7.014	9.612	9.105
		4.621	5.171	6.115	6.565
2.617	3.102	2.623	3.462	3.117	4.136

Table 3.32 Jenike shear test on BMa size fraction 2

1ST LOCUS		2ND LOCUS		3RD LOCUS	
Compaction Load (CL) 8 kg No. of Twist (T) 10 Normal Load (NL) 1.419 kg		CL 13 kg T 8 NL 2.519 kg		CL 18 kg T 6 NL 3.919 kg	
Normal stress [σ] kPa	**Shear stress** [τ] kPa	**Normal stress** [σ] kPa	**Shear stress** [τ] kPa	**Normal stress** [σ] kPa	**Shear stress** [τ] kPa
7.073	5.382	12.585	9.958	19.584	15.457
5.094	4.044	10.087	8.279	15.087	12.625
		6.592	5.934	10.087	9.260
3.594	3.077	4.595	4.413	6.595	6.325
2.593	2.450	3.096	3.250	4.095	4.425

Table 3.33 Jenike shear test on BMa size fraction 3

1ST LOCUS		2ND LOCUS		3RD LOCUS	
Compaction Load (CL) 21 kg No. of Twist (T) 10 Normal Load (NL) 4.9 kg		CL 25 kg T 8 NL 5.4 kg		CL 28 kg T 6 NL 5.9 kg	
Normal stress [σ] kPa	**Shear stress** [τ] kPa	**Normal stress** [σ] kPa	**Shear stress** [τ] kPa	**Normal stress** [σ] kPa	**Shear stress** [τ] kPa
24.481	21.407	26.979	24.275	29.477	26.252
18.485	17.450	19.485	18.950	21.983	22.018
13.489	13.179	14.488	14.003	16.987	16.987
9.490	8.804	10.741	11.238	11.990	12.494
2.198	2.604	3.672	4.364	3.672	4.524

Table 3.34 Jenike shear test on BMa size fraction 5

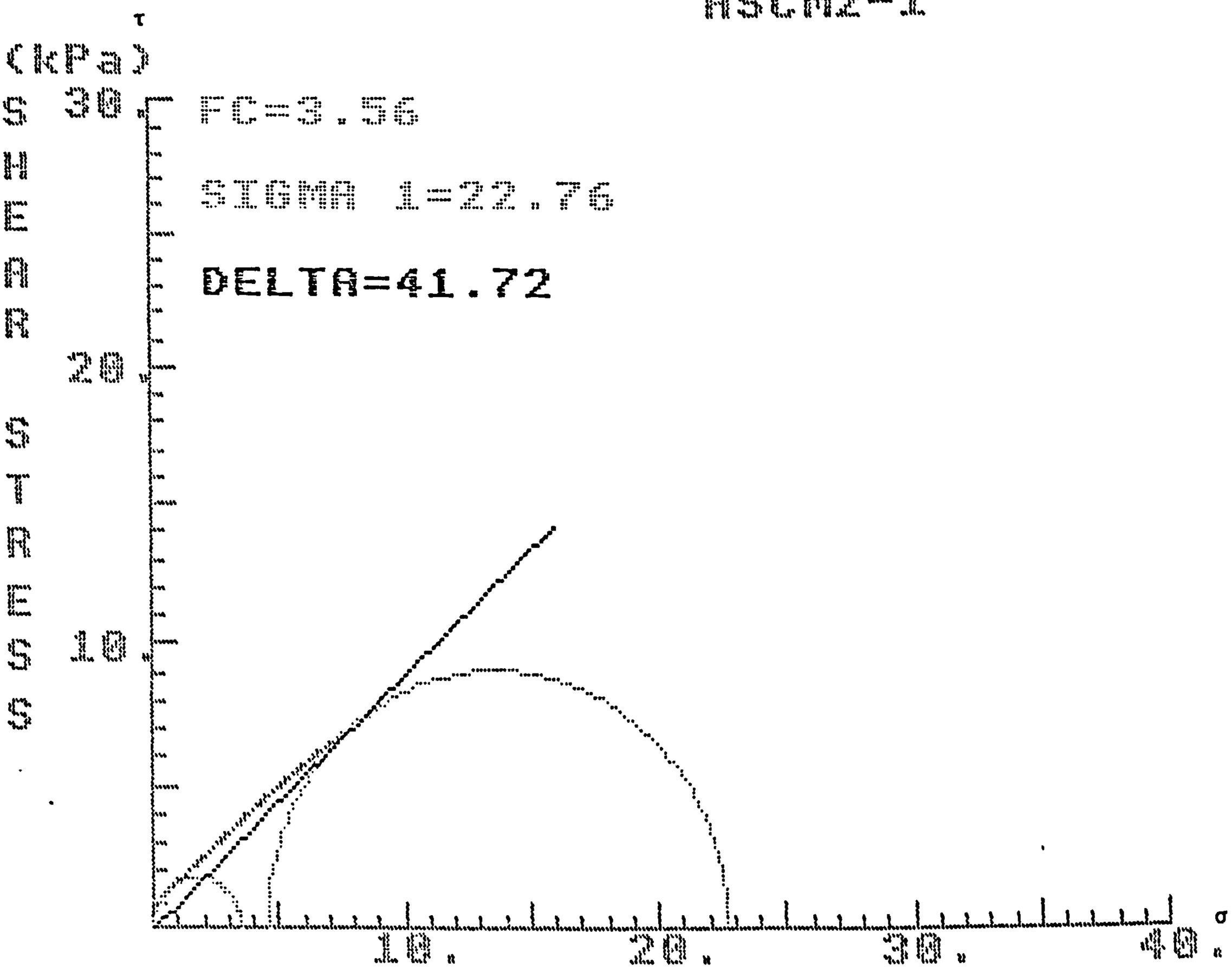

Figure 3.4 First failure yield locus for HSCM2 Fraction

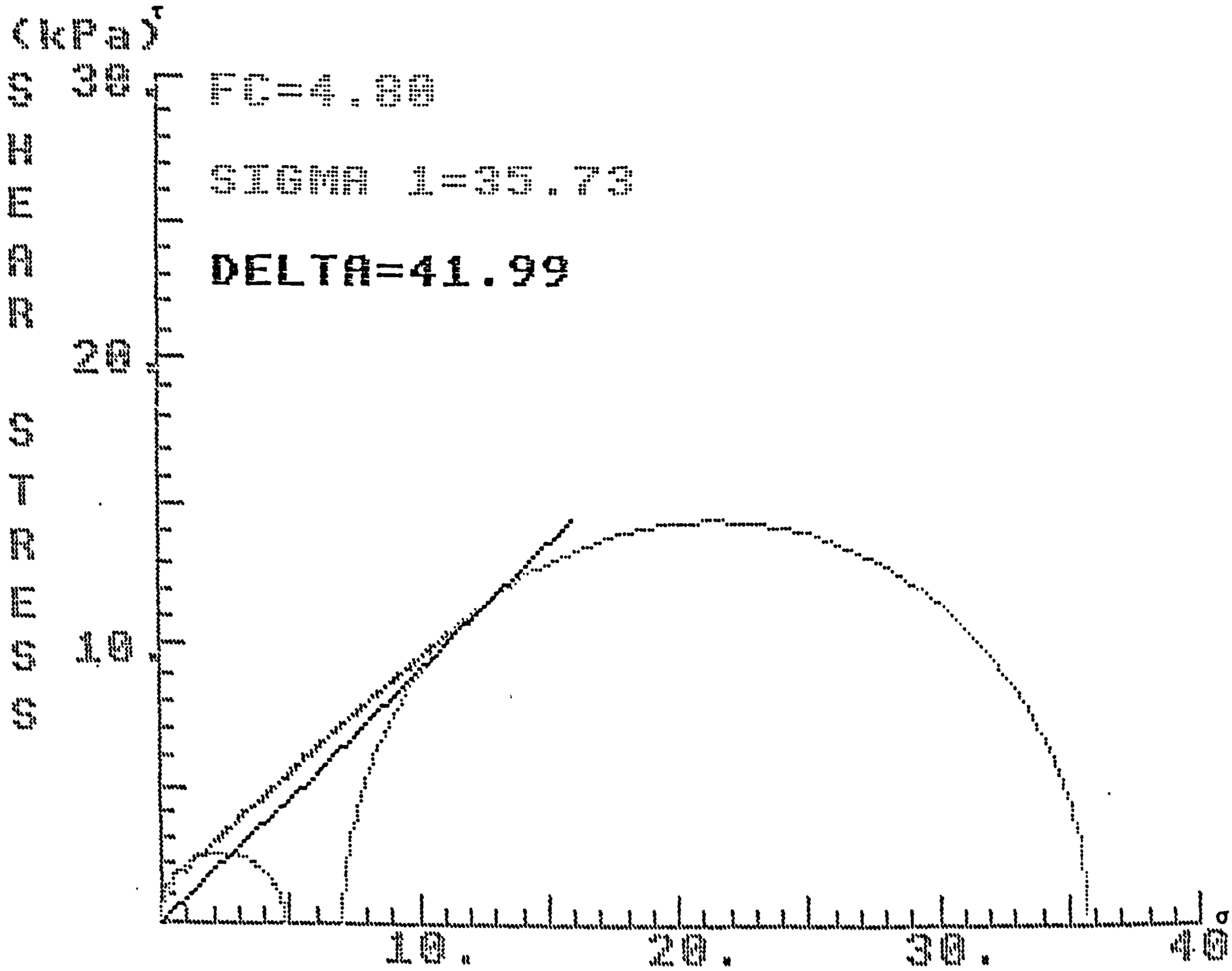

Figure 3.5 Second failure yield locus for HSCM2 Fraction

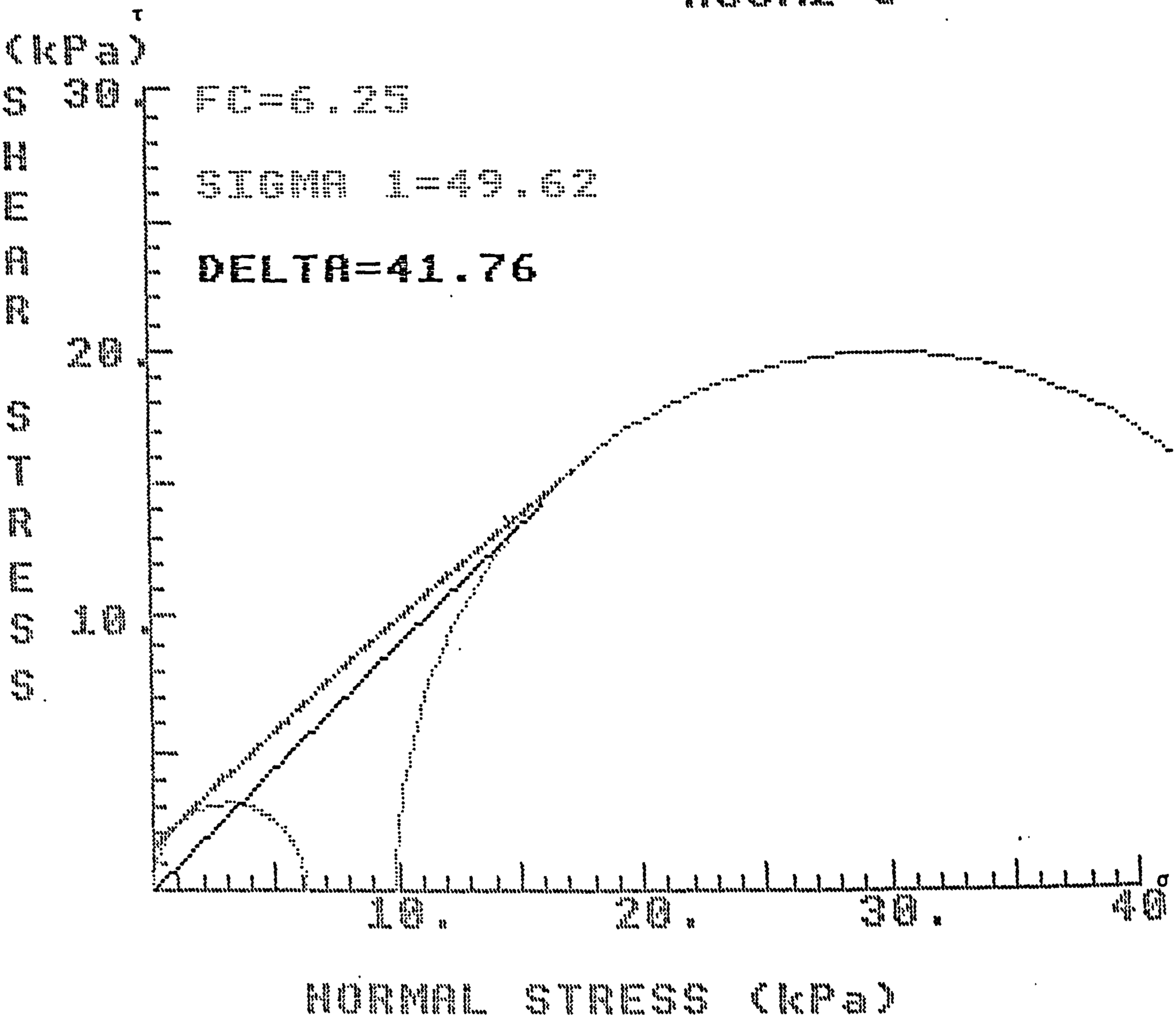

Figure 3.6 Third failure yield locus for HSCM2 Fraction

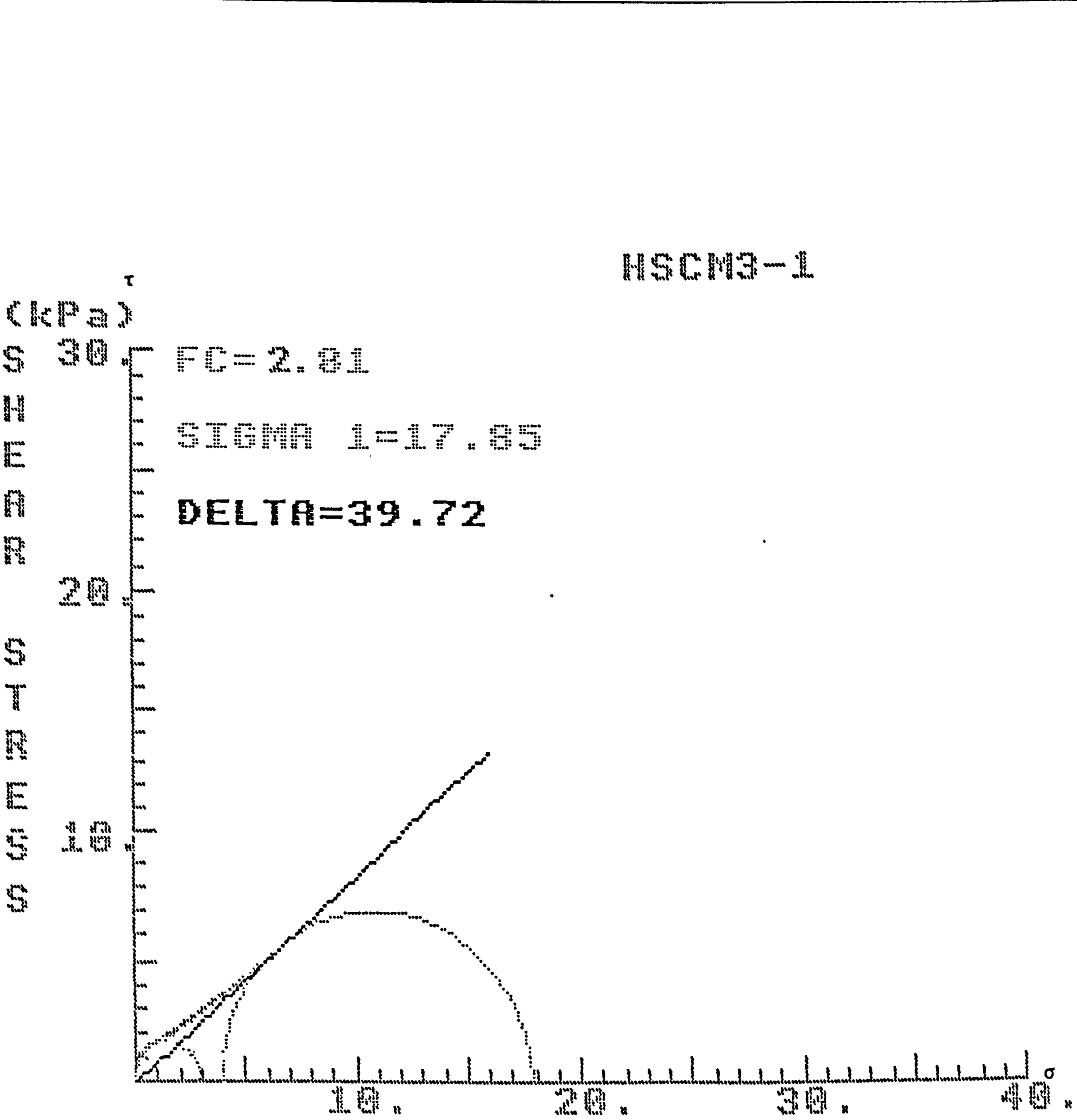

Figure 3.7 First failure yield locus for HSCM3 Fraction

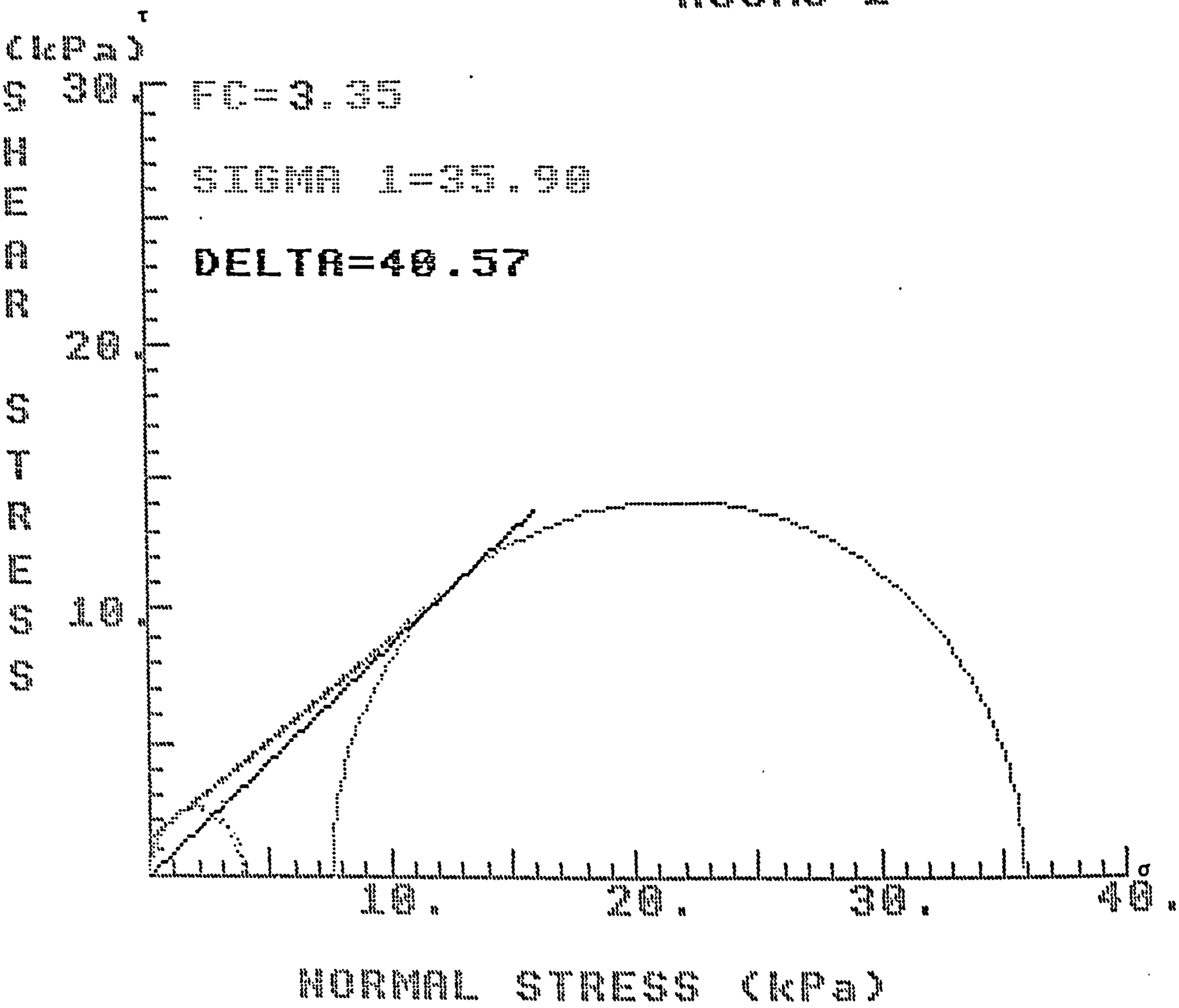

Figure 3.8 Second failure yield locus for HSCM3 Fraction

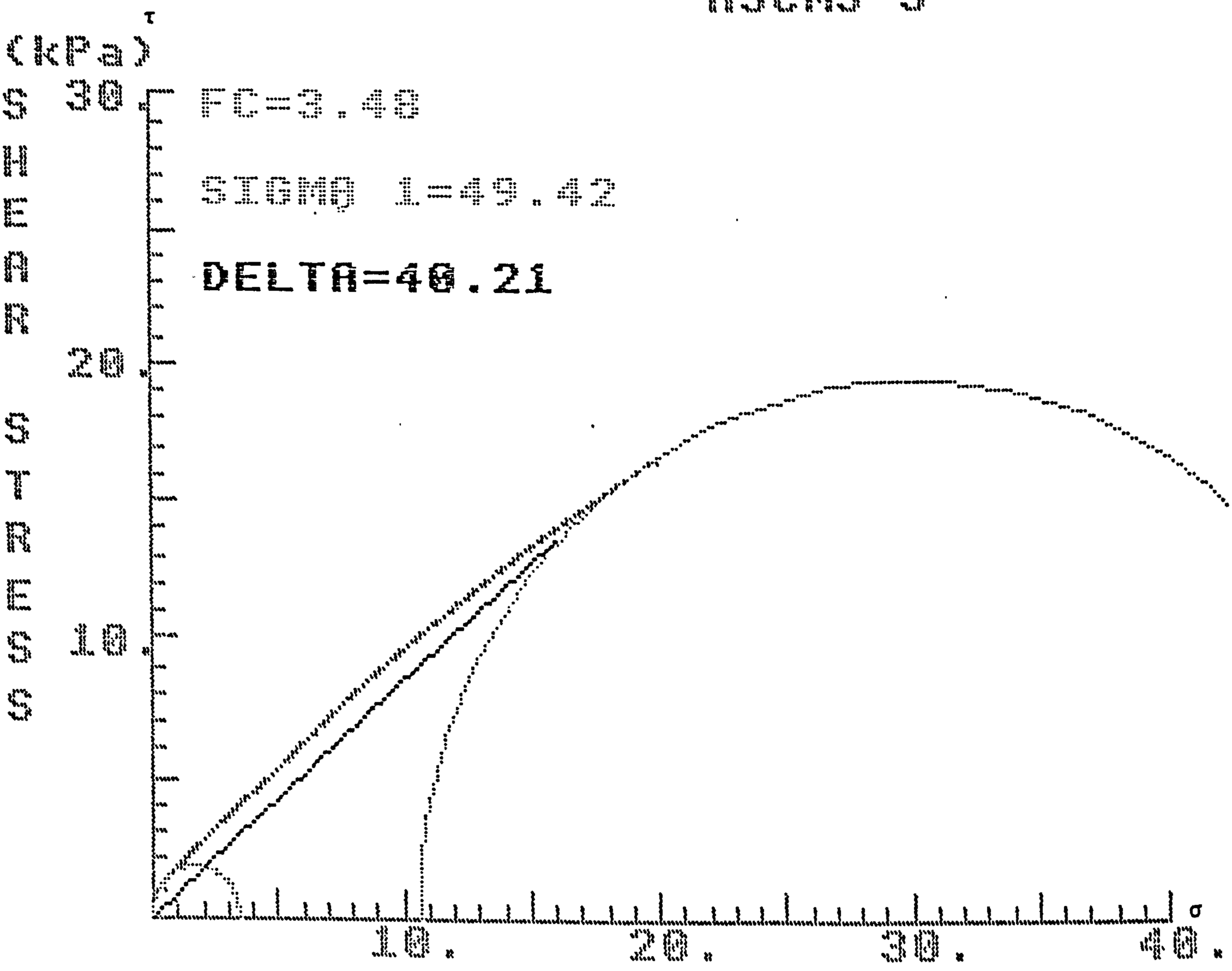

Figure 3.9 Third failure yield locus for HSCM3 Fraction

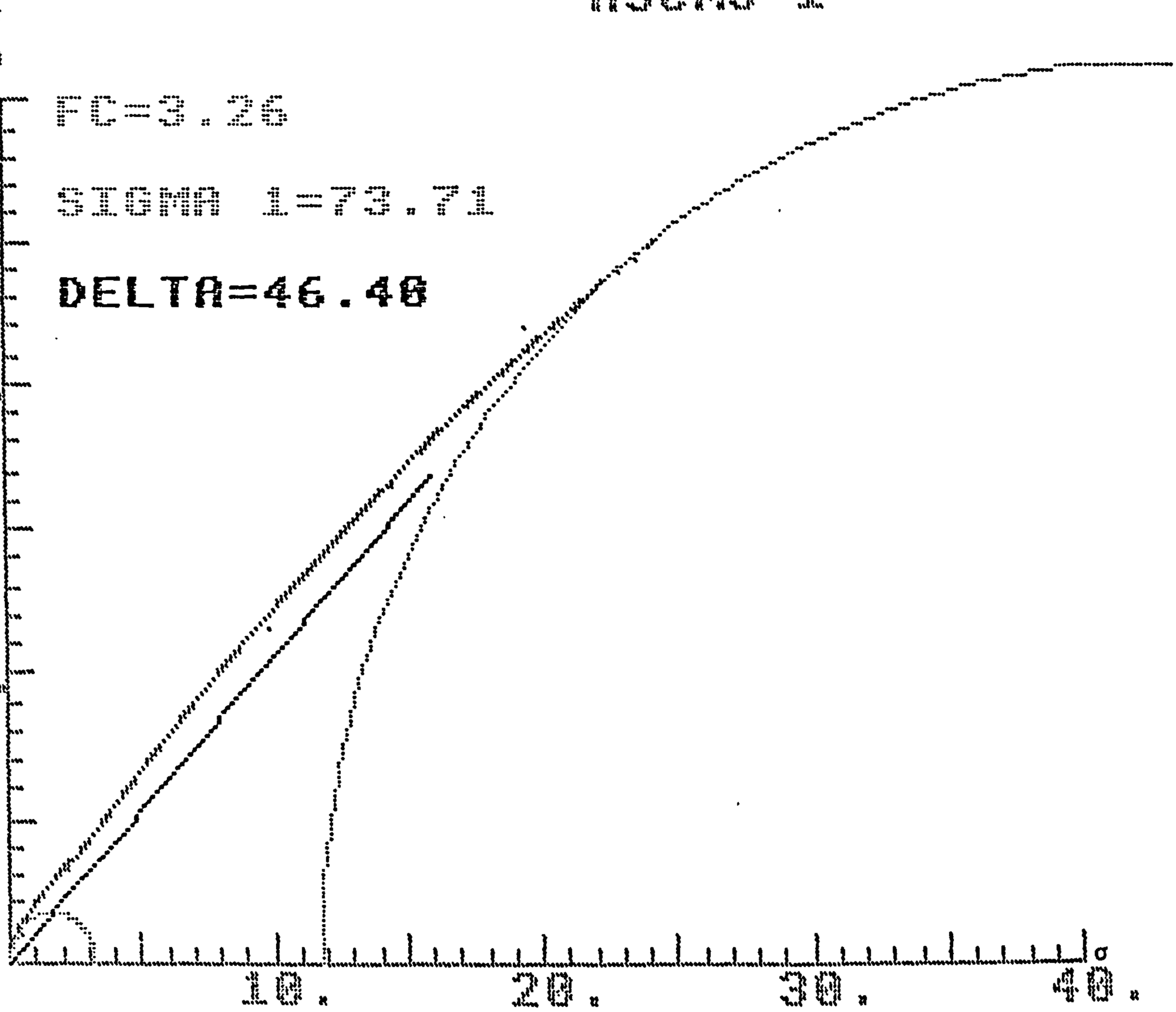

Figure 3.10 First failure yield locus for HSCMS Fraction

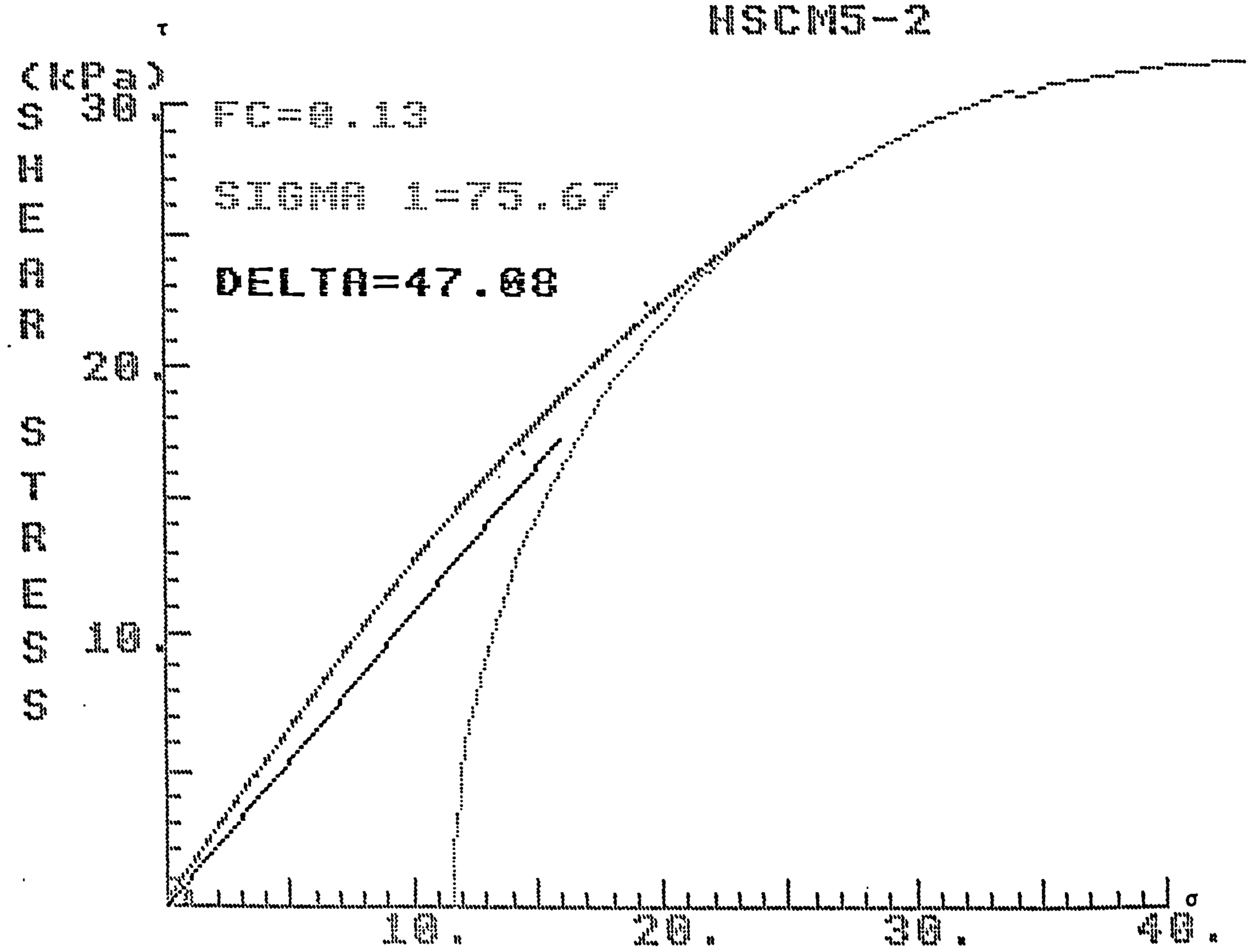

Figure 3.11 Second failure yield locus for HSCM5 Fraction

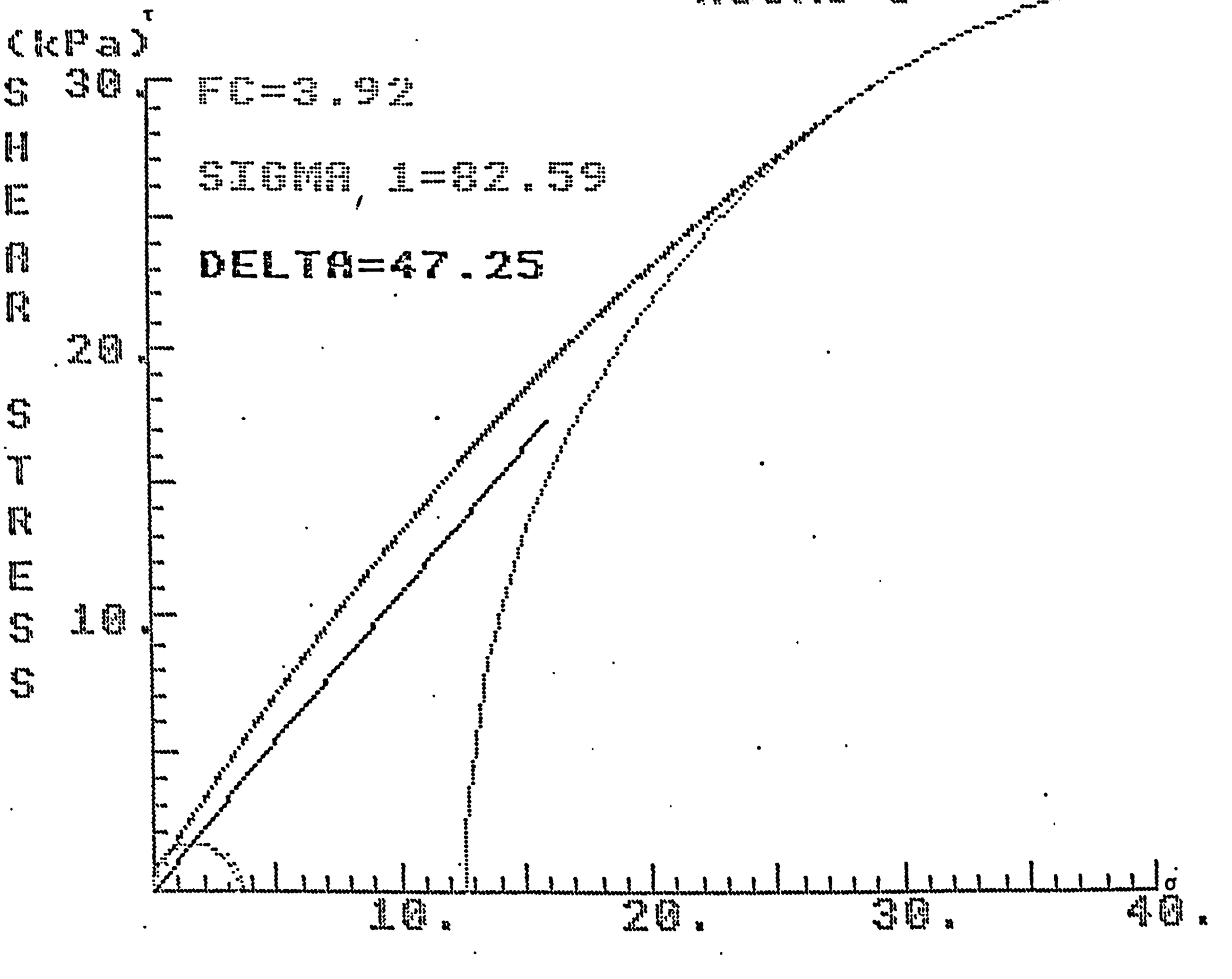

Figure 3.12 Third failure yield locus for HSCM5 Fraction

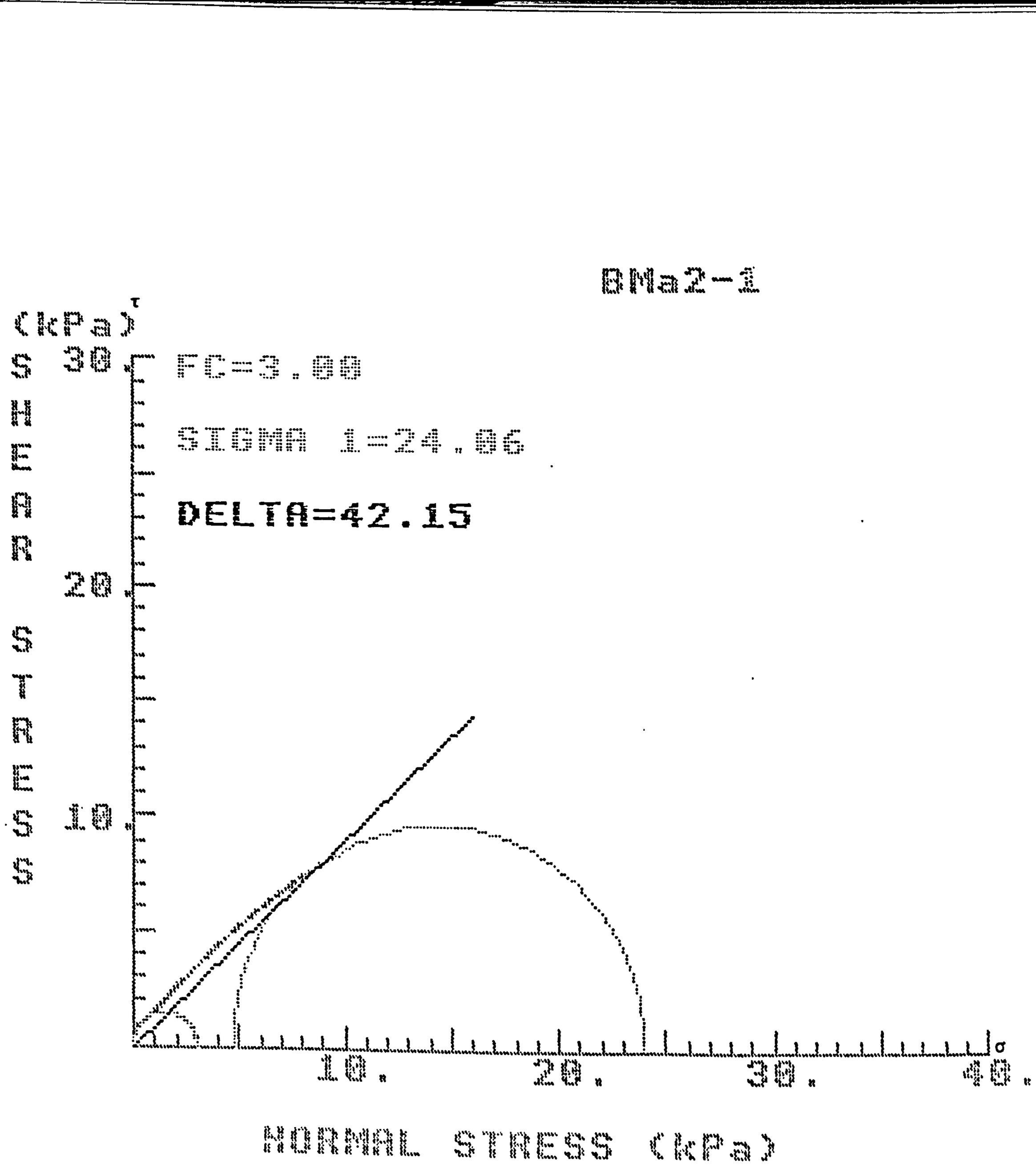

Figure 3.13 First failure yield locus for BMa2 Fraction

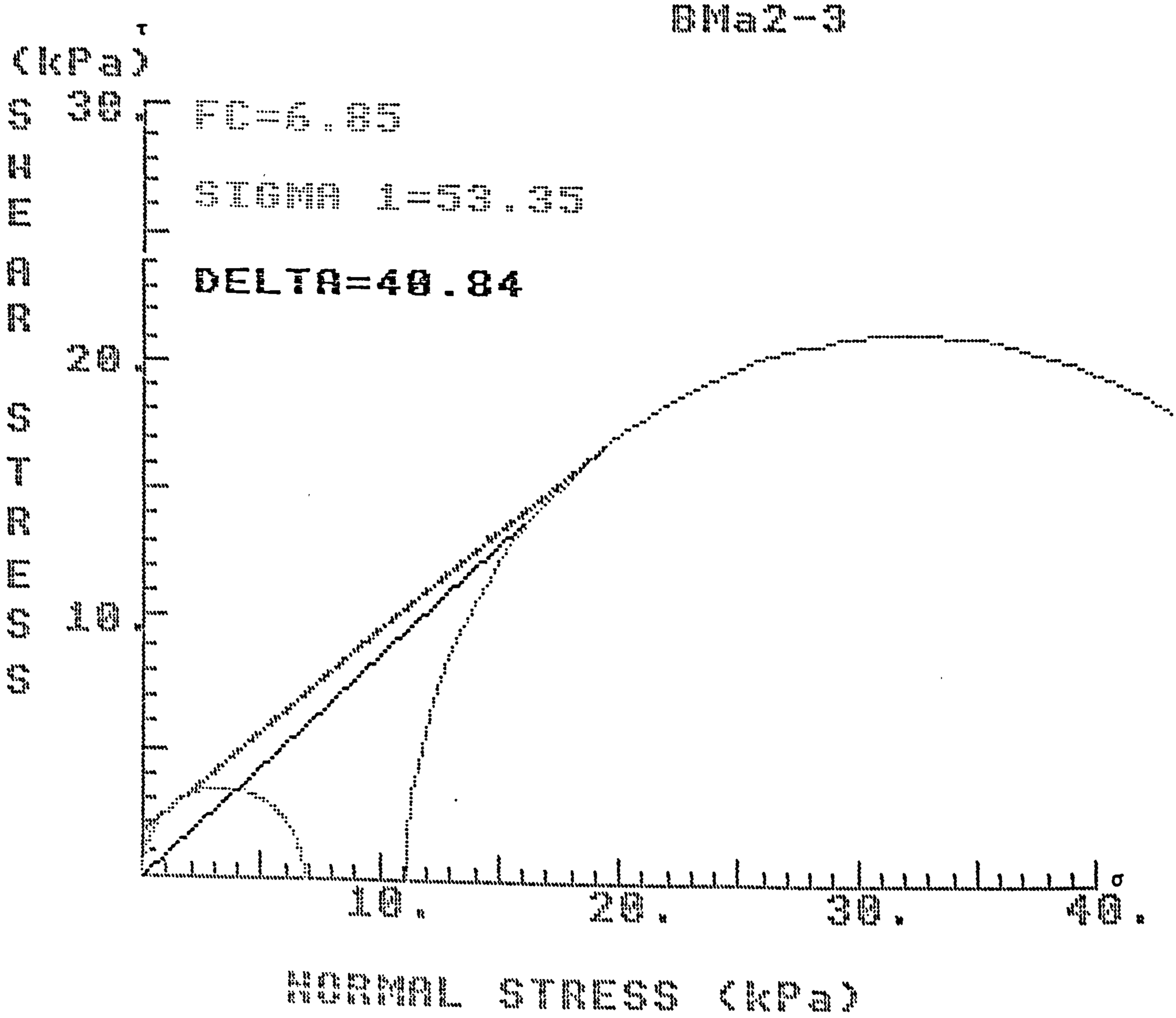

Figure 3.15 Third failure yield locus for BMa2 Fraction

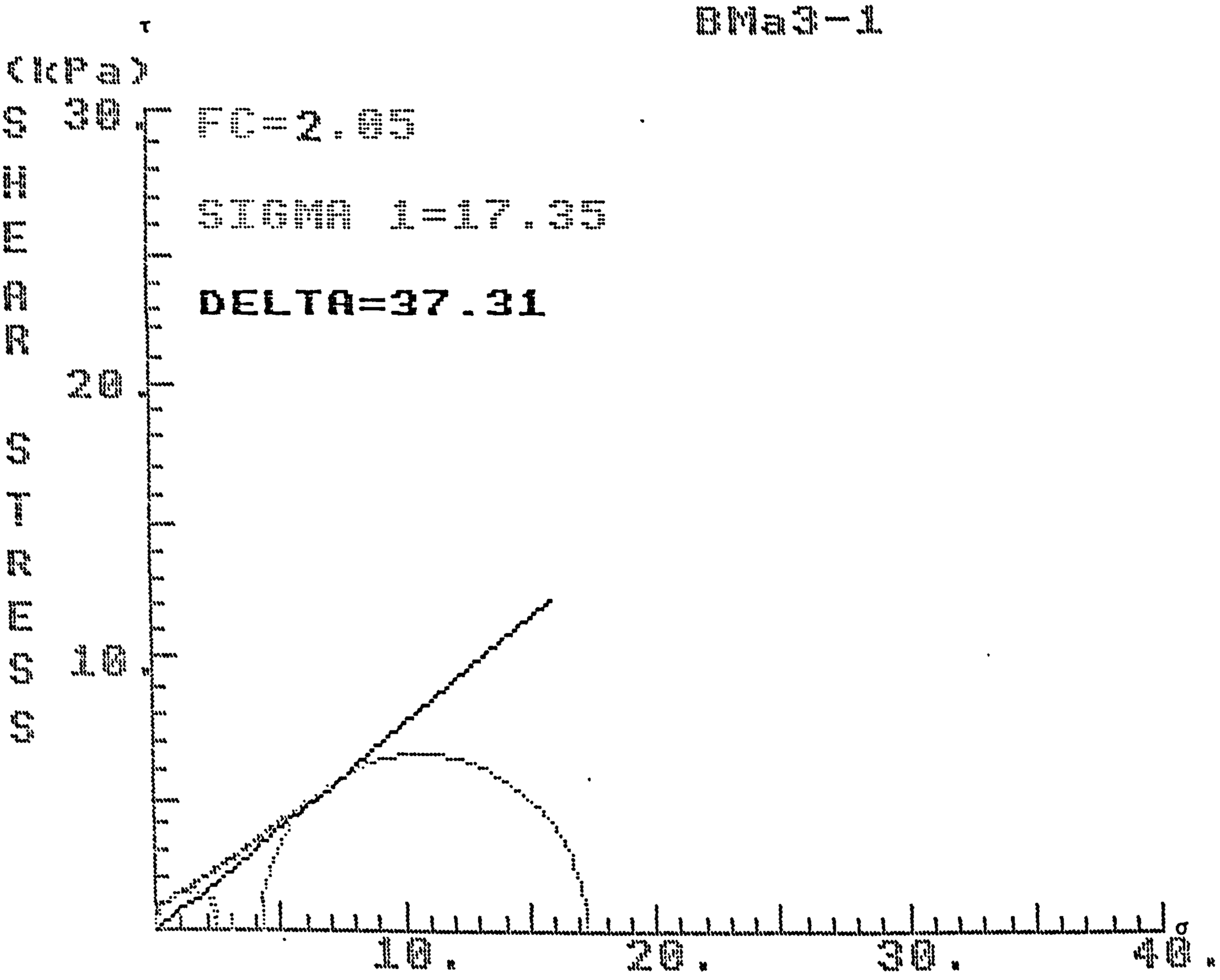

Figure 3.16 First failure yield locus for BMa3 Fraction

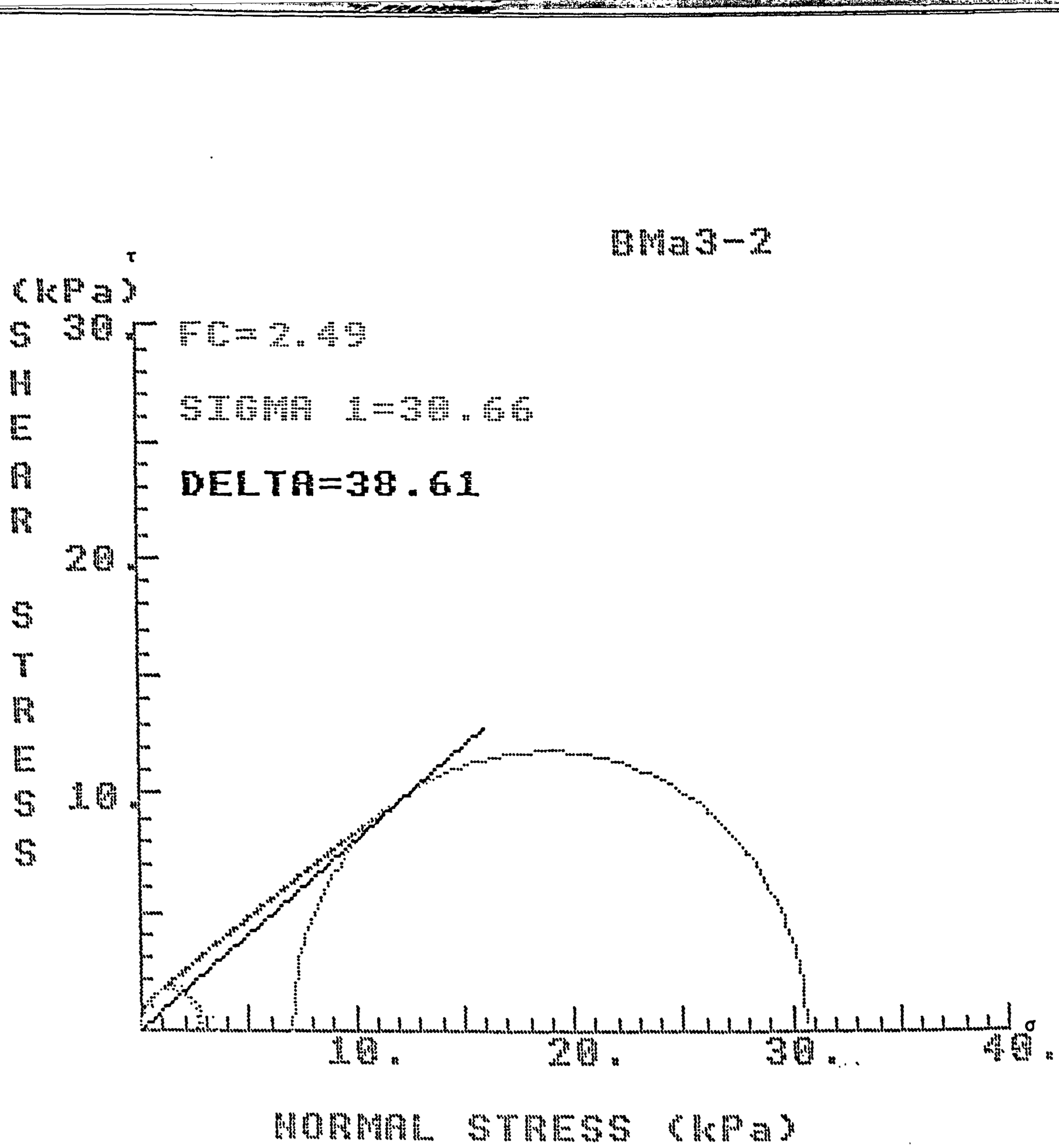

Figure 3.17 Second failure yield locus for BMa3 Fraction

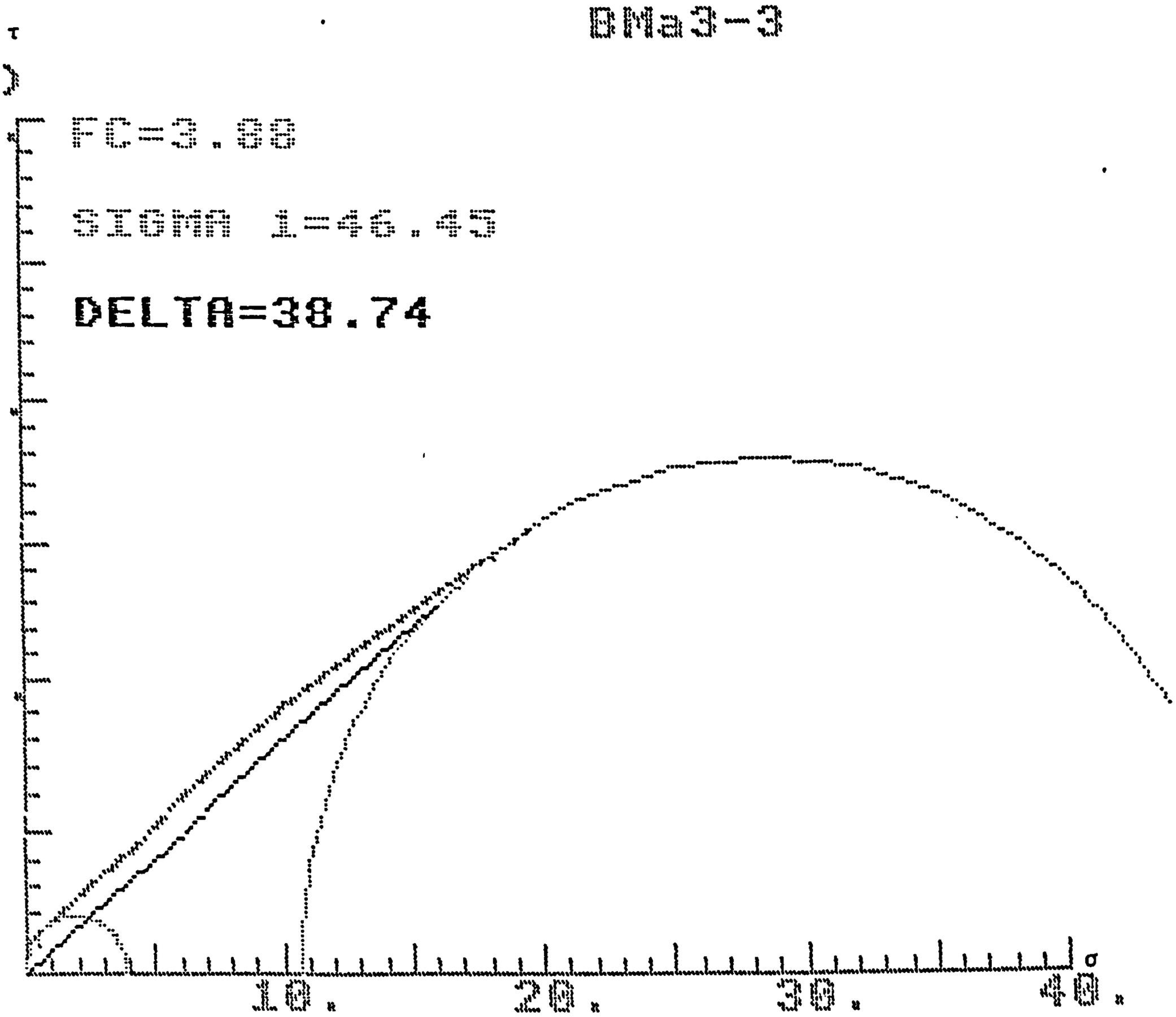

Figure 3.18 Third failure yield locus for BMa3 Fraction

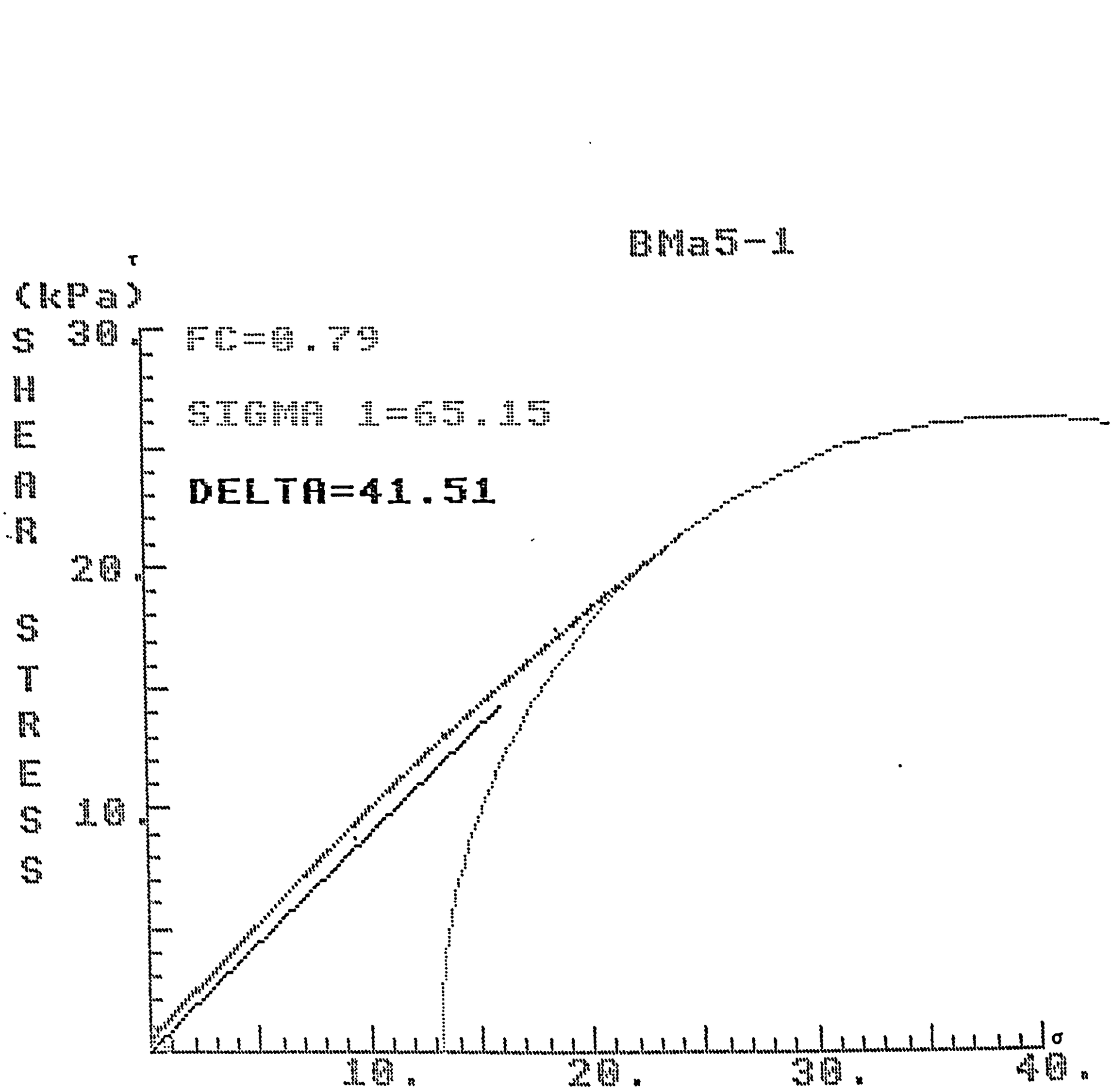

Figure 3.19 First failure yield locus for BMa5 Fraction

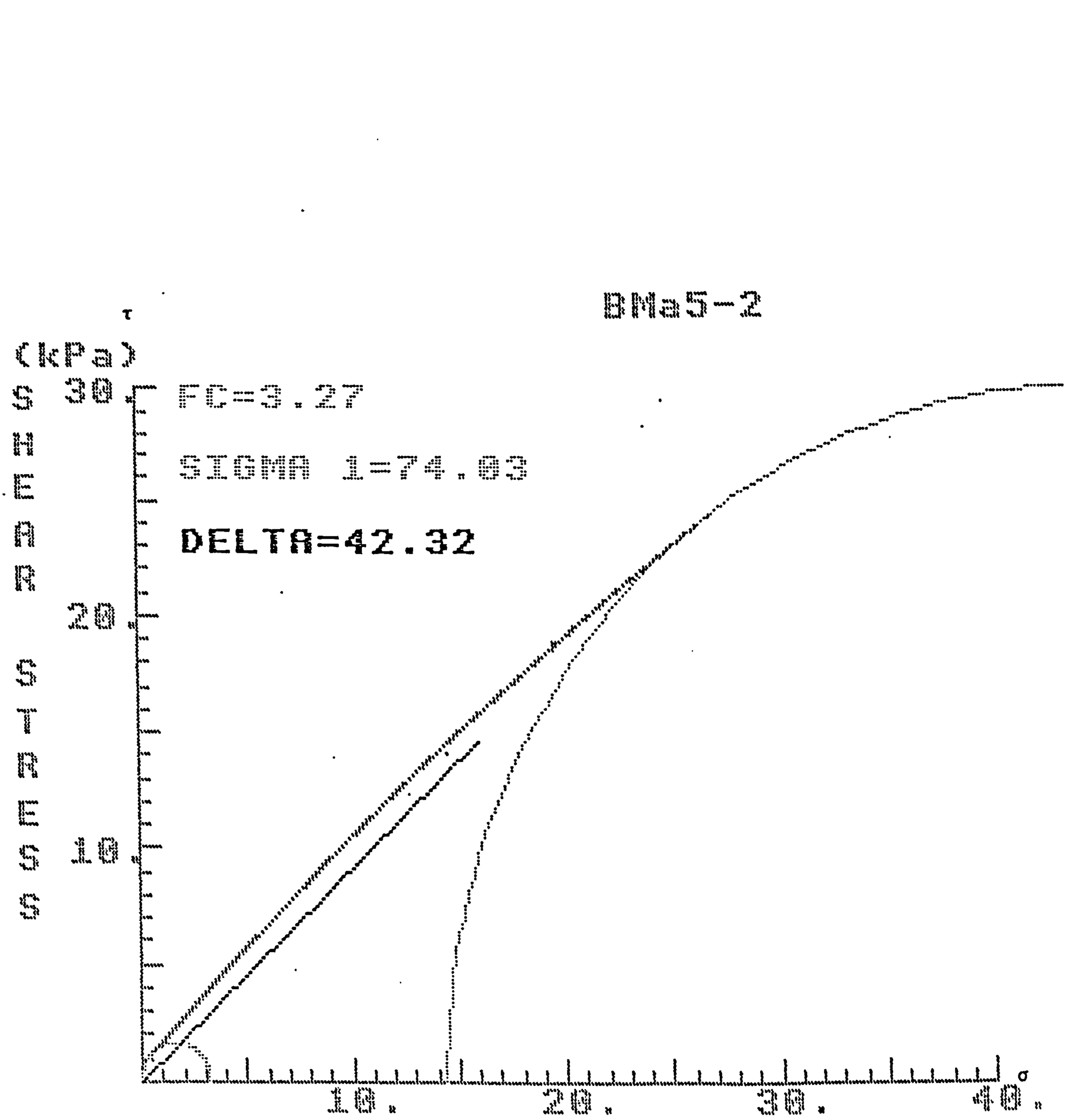

Figure 3.26 Second failure yield locus for BMa5 Fraction

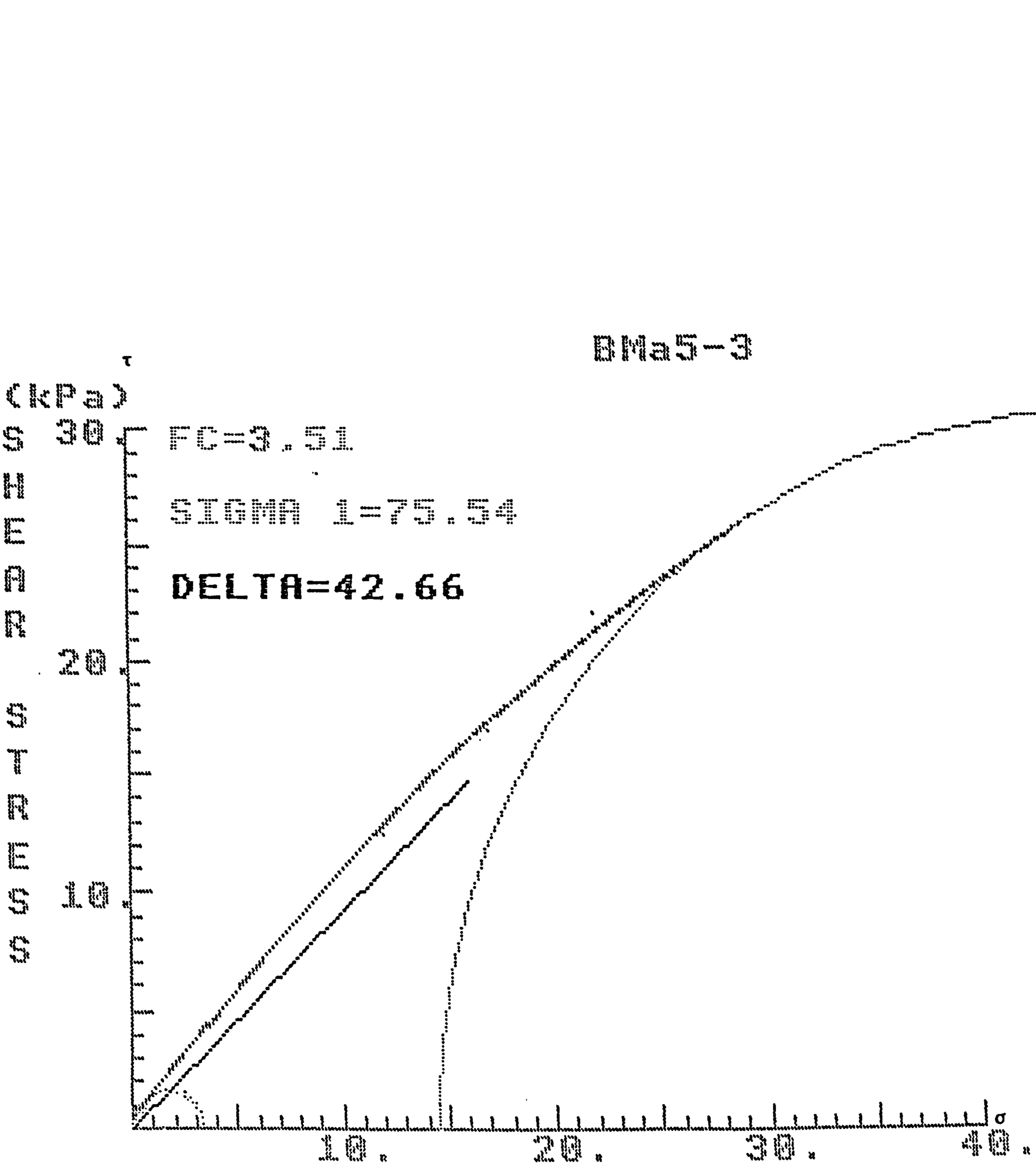

Figure 3.21 Third failure yield locus for BMa5 Fraction

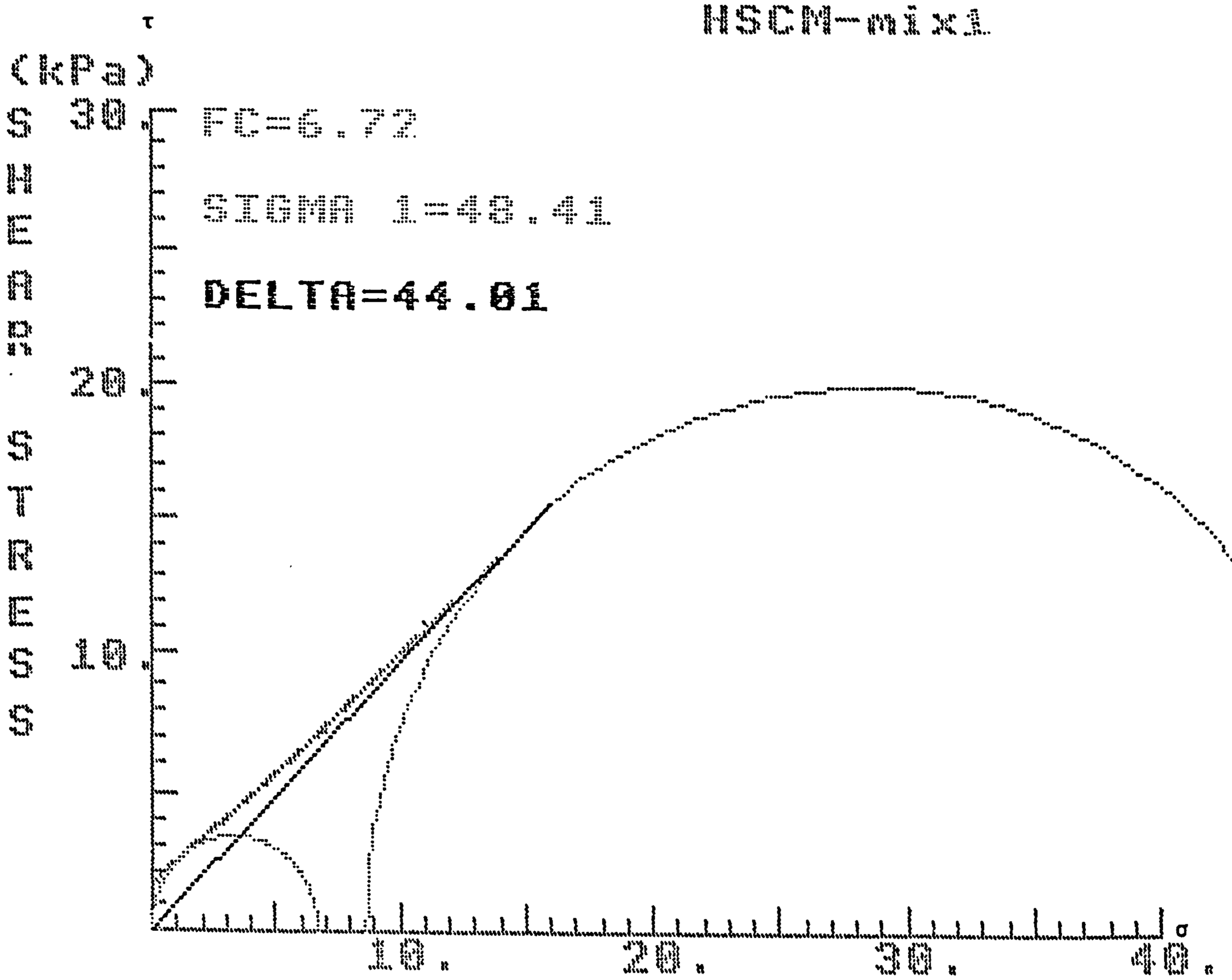

Figure 3.22 First failure yield locus for HSCM - mix fraction

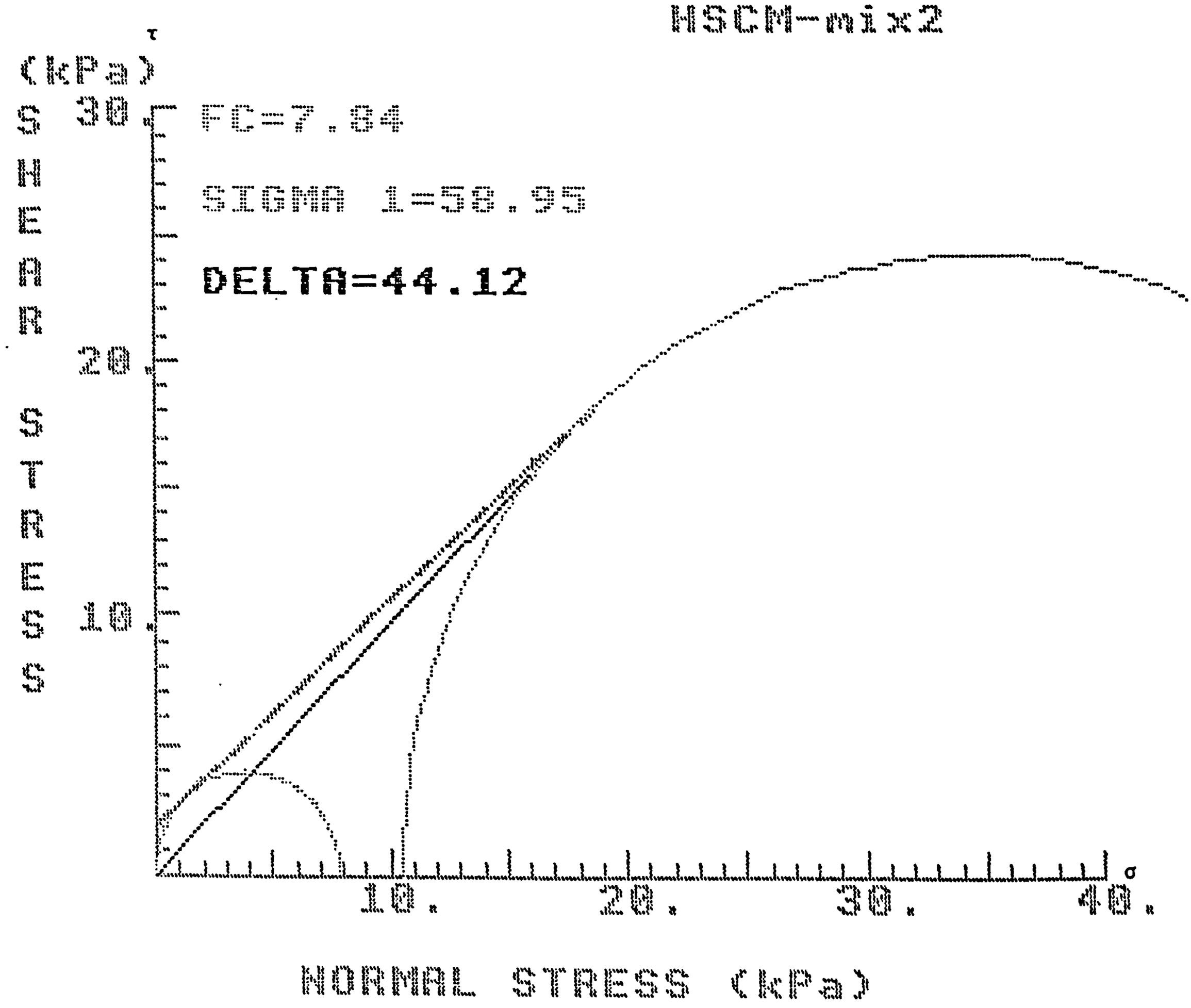

Figure 3.23 Second failure yield locus for HSCM-mix Fraction

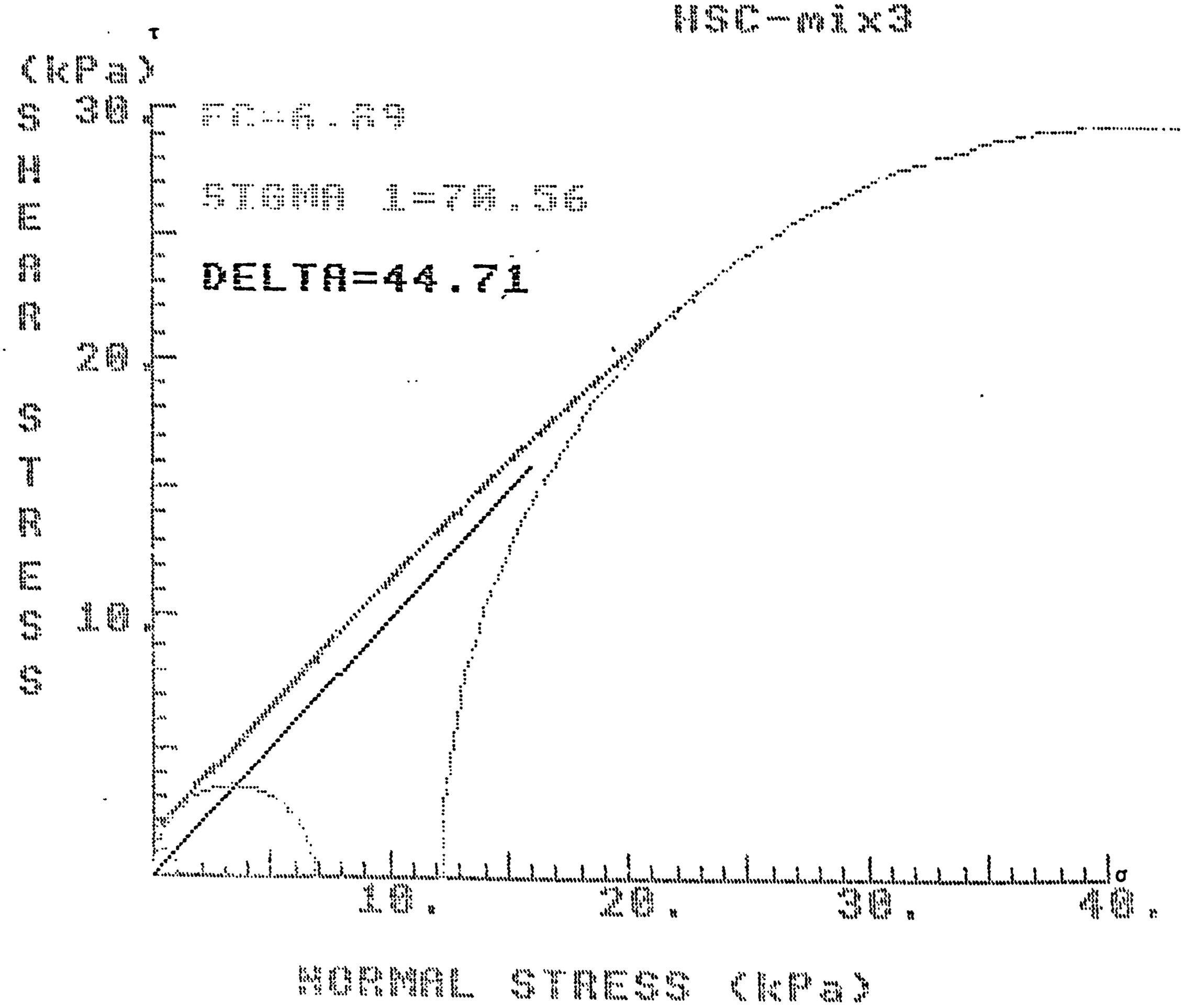

Figure 3.24 Third failure yield locus for HSCM - mix Fraction

Size fraction from various mills		f_c kpa	σ_1 kpa	δ degree	Mean δ degree
HSCM2	1	3.56	22.76	41.72	41.82
	2	4.80	35.73	41.99	
	3	6.25	49.62	41.76	
HSCM3	1	2.81	17.85	39.72	40.166
	2	3.35	35.90	40.57	
	3	3.98	49.42	40.21	
HSCM5	1	3.26	73.71	46.40	44.91
	2	0.13	75.67	47.08	
	3	3.32	82.59	41.25	
*HSCM (Mix)	1	6.72	48.41	44.01	44.28
	2	7.84	58.95	44.12	
	3	6.89	70.56	44.71	
BMa2	1	3.00	24.06	42.15	41.36
	2	6.13	40.20	41.11	
	3	6.85	53.35	40.84	
BMa3	1	2.05	17.35	37.31	38.22
	2	2.49	30.66	38.61	
	3	3.88	46.45	38.74	
BMa5	1	0.79	65.15	41.51	42.16
	2	3.27	74.03	42.32	
	3	3.51	75.54	42.66	

* HSCM (Mix) is a mixture of 4 fractions (HSCM2, HSCM3, HSCM4, HSCM5) with the same proportion as in the initial product obtained from the HSCM.

Table 3.35 Summary Table from Jenike shear tests, extracted from Figures 3.4 to 3.24

3.2.1 Wall friction

Jenike shear cell was used to measure the wall friction of liquorice powder and to investigate the angle of wall friction (ϕ_w) of liquorice powder against a steel plate. For this investigation 11 size fractions were selected:-

Fraction No.	Size Range (μm)
HSCM2	38 - 63
HSCM3	63 - 90
HSCM4	90 - 125
HSCM5	125 - 180
HSCM6	180 - 250
HSCM7	250 - 315
BMa2	38 - 63
BMa3	63 - 90
BMa4	90 - 125
BMa5	125 - 180
BMa6	180 - 250

. Table 3.36 and 3.37 show the values of shear stresses obtained when different normal stresses were applied on to different size fractions of liquorice comminuted either by a high speed cutter or ball mill.

Figures 3.25 and 3.26 show the correlation between the shear stress and normal stress. A Curve fit computer program to draw the best line through the points is used for the construction of these figures (Appendix 2.1).

The angle of wall friction, as calculated from the slope of various curves (Figure 3.25 and 3.26) for all 11 size fractions are tabulated in Table 3.38.

Normal stress σ kPa	Shear stress τ kPa	Normal stress σ kPa	Shear stress τ kPa	Normal stress σ kPa	Shear stress τ kPa
HSCM	Size Fraction 2	HSCM	Size Fraction 3	HSCM	Size Fraction 4
6.018	4.025	6.015	3.957	6.018	3.704
4.582	3.068	4.579	3.024	4.582	2.968
3.865	2.592	3.861	2.561	3.865	2.420
3.147	2.222	3.144	2.098	3.147	2.043
2.429	1.667	2.426	1.636	2.429	1.654
1.711	1.296	1.708	1.117	1.711	1.098
0.990	0.710	0.990	0.636	0.990	0.623
HSCM	Size Fraction 5	HSCM	Size Fraction 6	HSCM	Size Fraction 7
6.012	3.632	6.010	3.432	6.001	3.241
4.577	2.654	4.571	2.525	4.565	2.438
3.859	2.296	3.853	2.154	3.847	2.099
3.141	1.907	3.135	1.778	3.129	1.703
2.423	1.457	2.417	1.370	2.412	1.346
1.705	1.043	1.699	0.975	1.694	0.926
0.987	0.586	0.982	0.549	0.976	0.518

Table 3.36 Wall friction for HSC Milled Liquorice

Normal stress σ kPa	Shear stress τ kPa	Normal stress σ kPa	Shear stress τ kPa	Normal stress σ kPa	Shear stress τ kPa
BMa	Size Fraction 2	BMa	Size Fraction 3	BMa	Size Fraction 4
7.465	4.651	6.024	3.366	7.456	3.940
6.030	3.747	4.588	2.636	6.021	3.150
4.594	2.842	3.870	2.261	4.585	2.420
3.876	2.390	3.152	1.796	3.867	1.938
3.158	2.00	2.435	1.453	3.149	1.582
2.440	1.550	1.717	1.033	2.432	1.292
1.722	1.111	0.999	0.600	1.714	0.924
1.004	0.516			0.996	0.594
BMa	Size Fraction 5	BMa	Size Fraction 6		
7.456	3.799	6.015	2.984		
6.021	3.094	4.580	2.326		
4.585	2.384	3.862	2.009		
3.867	2.054	3.144	1.608		
3.149	1.673	2.426	1.234		
2.432	1.330	1.708	0.904		
1.714	0.962	1.708	0.510		
0.996	0.549				

Table 3.37 Wall friction for Ball Milled Liquorice

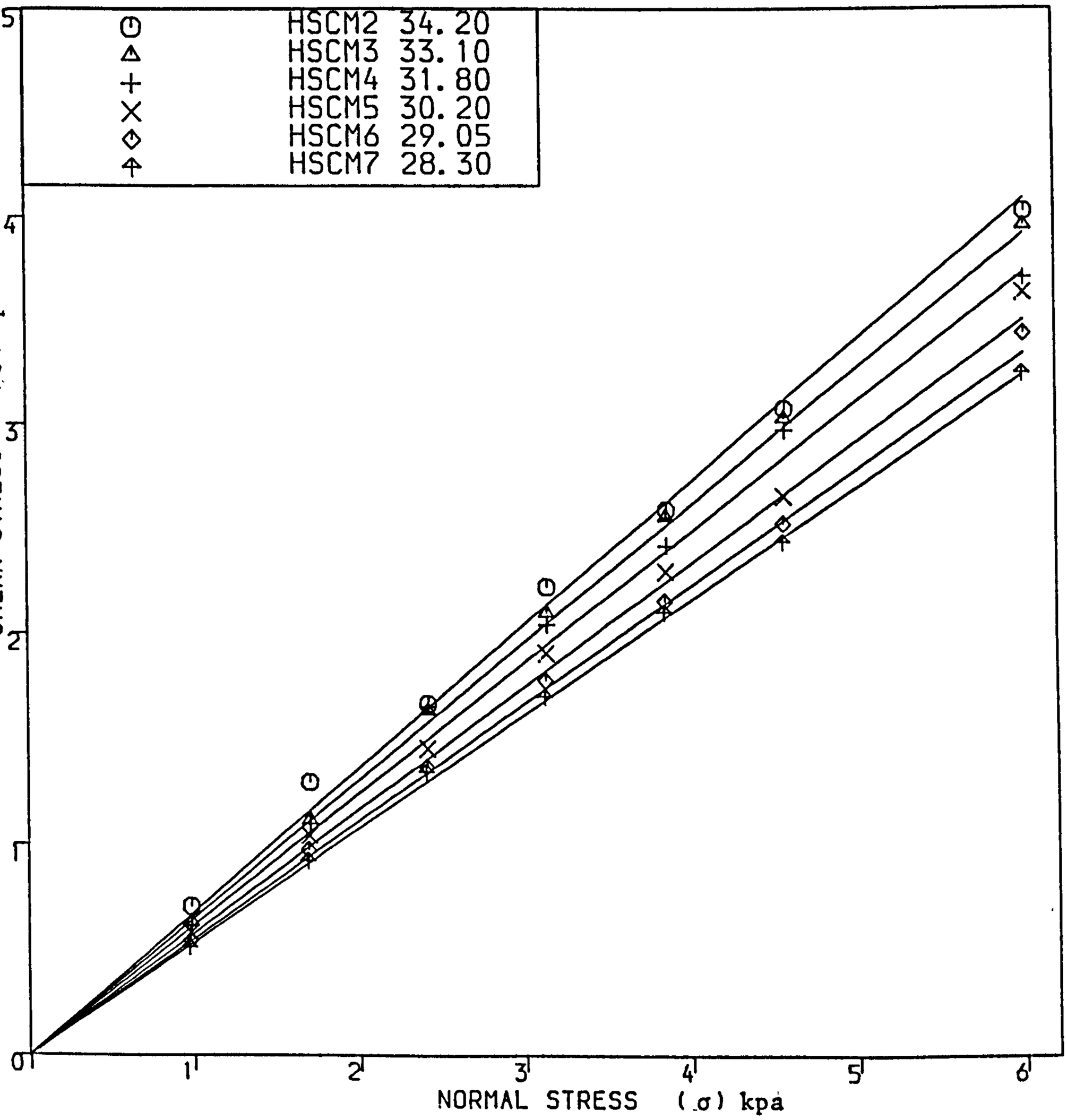

FIGURE (3.25)
WALL FRICTION ON MILD STEEL PLATE
FOR H.S.C.M. FRACTIONS

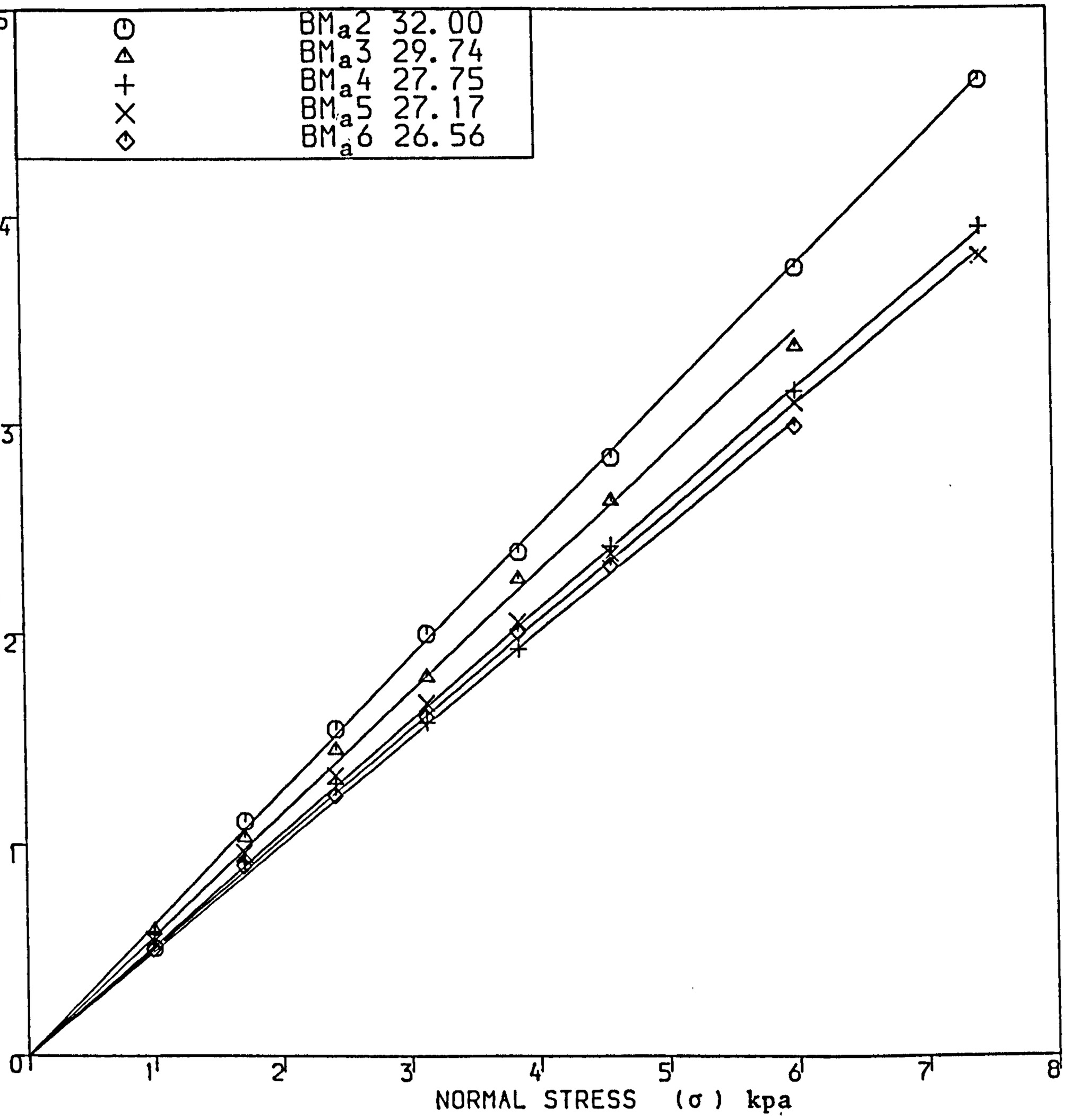

FIGURE (3.26)
WALL FRICTION ON MILD STEEL PLATE
FOR B.M. . FRACTIONS

Size Fraction	Slope (Figs. 3.25 & 3.26)	Angle of wall friction degree ϕ_w
HSCM2	0.681	34.20
HSCM3	0.653	33.17
HSCM4	0.620	31.80
HSCM5	0.583	30.25
HSCM6	0.555	29.05
HSCM7	0.538	28.30
BMa2	0.625	32.0
BMa3	0.571	29.74
BMa4	0.526	27.75
BMa5	0.513	27.17
BMa6	0.500	26.56

Table 3.38 Angle of Wall frction for HSCM and BMa fractions

3.3 Bulk density and rate of packing

Tables 3.39-a and 3.39-b show the initial bulk density, packed density and the rate of packing of 8 liquorice fractions over a period of time obtained from an automatic bulk tester (Section 2.5.5).

Figures 3.27 (a and b) show the packed densities and rate of packing via different tapping time intervals for two factions (2 and 6) of HSCM and BMa products.

Time of packing	Initial bulk and packing densities (kg m^{-3})							
sec.	HSCM2	HSCM3	HSCM5	HSCM6	BMa2	BMa3	BMa5	BMa6
0	409.8	390.1	400.2	365.9	473.3	446.7	456.6	460.2
6	474.5	456.3	431.9	393.2	527.4	522.0	493.6	481.9
12	511.9	485.1	440.4		566.4	543.3	504.8	
18	531.2	498.5	449.8	403.7	600.7	552.5	512.1	494.6
24	544.7	-	-	-	629.1	-	-	-
30		513.8	455.2	409.4		563.4	519.1	502.2
36	566.8	-	-	-	666.8	-	-	-
42	-	521.5	459.6	-	-	569.9	527.4	502.5
48	580.9	-	-	413.5	696.9	-	-	-
54	-	526	460.8	420.8	709	573.2	529.9	
60	588.6				720.4			
72	597.8				731.6			

Table 3.39a Bulk density of various shaped and sized fractions from HSCM and BMa

Time of packing	Rate of packing ($g\ s^{-1}$)							
sec.	HSCM2	HSCM3	HSCM5	HSCM6	BMa2	BMa3	BMa5	BMa6
6	1.08	1.11	0.53	0.45	0.91	1.26	0.62	0.36
12	0.86	0.80	0.34	-	0.78	0.81	0.40	-
18	0.68	0.60	0.27	0.21	0.71	0.59	0.31	0.19
24	0.56	-	-	-	0.65	-	-	-
30	-	0.42	0.18	0.15	-	0.39	0.21	0.13
36	0.44	-	-	-	0.53	-	-	-
42	-	0.31	0.14	-	-	0.29	0.11	0.10
48	0.34	-	-	0.12	0.47	-	-	-
54	-	0.25	0.12	-	-	0.24	0.11	-
60	0.30				0.42			
72	0.26				0.36			

Table 3.39b Rate of packing of various shaped and sized fractions from HSCM and BMa

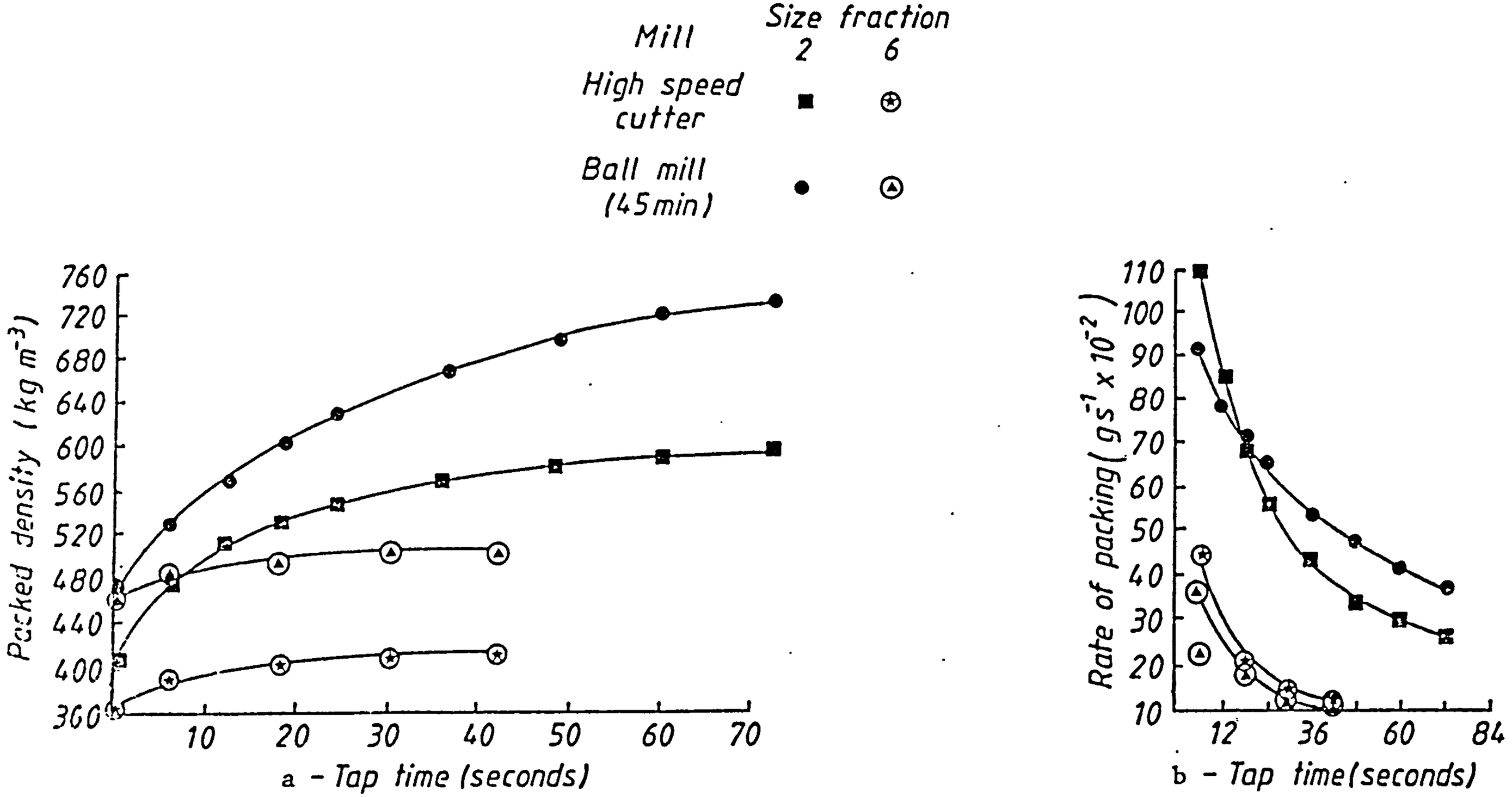

Figure 3.27 (a, b) *The effect of shape on the packing density and rate of packing of milled liquorice*

3.4.1 Shape Analysis

The size fractionated powders used for the measurement of flow rate, flow uniformity and shear properties were used for the measurement of shape. The procedure for preparation of the microscope slides, microphotographs and transparencies have already been described in Section 2.2.4 and 2.3.

The Quantimet 720 Image Analyser was used for the all shape analysis of the 17 size fractions obtained from the comminuted liquorice.

Tables 3.40 to 3.57 show the evaluation of three different shape factors (sphericity, roughness and irregularity, and elongation respectively, Section 1.4.2 and 2.3.5) where the term FEATURE (F) refers to the particle image. These Tables represent the shape factors obtained from individual particles of the HSCM, BM (a and b) and ERM (a and b) comminuted products.

Table 3.58 summarises the mean results from Tables 3.40 to 3.59 and also the elongation factors obtained from the F_V/F_H ratio for all 17 size fractions of the fibrous material. In Table 3.58 the code for the mean particle size within each size fraction obtained from the High Speed Cutter Mill (HSCM), the Ball Mill for 45 minutes (BMa) and 75 minutes (BMb) and the End Runner Mill for 10 minutes (ERMa) and 20 minutes (ERMb) are also tabulated. The subscripts refer to the size fractions of each milled product.

Figures 3.29 and 3.30 show the relationships between the evaluated shape factors and the mean sizes of the HSCM and BMa respectively, while Figure 3.31 shows the relationships between the different shape factors obtained from the 3 mills for fractions 3 and 5 having a mean size value of 76 and 152 μm respectively.

F. PERIMETER ** 2 / FEATURE AREA * 12.57	PROJ.HEIGHT * PROJ.W / FEATURE AREA	FEATURE LENGTH / FEATURE BREADTH
1.22478	1.60561	
1.10061	1.42044	1.55422
1.45883	1.72481	1.33684
1.28894	1.45161	1.85714
1.29588	1.74699	1.95
1.2409	1.50696	1.50617
1.08896	1.31749	1.97059
1.73008	2.19972	1.39024
1.71291	1.98579	1.05333
1.52897	1.81034	1.9359
1.34956	1.6767	1.34862
1.49319	1.93766	1.29293
1.43845	1.82211	
2.10794	1.97349	2.46667
1.96538	1.51903	1.17021
2.09176	2.07852	1.89474
2.10382	1.48491	1.35616
2.37769	2.31133	3.86667
1.58513	1.68844	1.25641
2.2655	2.84866	2.37879
3.98544	1.6922	1.84375
2.95946	2.16774	2.54545
1.66602	2.6045	1.80488
3.65315	2.33201	2.0625
1.91698	2.45565	1.97015
1.16585	2.47479	3.19608
1.55508	1.88353	1.28986
1.29404	2.66312	2.06122
2.4793	4.43275	1.8
1.40086	3.87692	1.96078
2.56866	1.92418	1.5
1.32306	4.32639	2.41667
1.19884	1.47445	1.17241
1.52894	1.67342	1.87097
1.53029	1.74098	1.80328
1.33436	1.54103	2
1.62856	1.76449	2.45833
4.67304	3.21598	7.69565
1.24035	1.3888	1.53704
1.25521	1.47142	1.04444
1.3874	1.69072	1.28814
1.34952	1.67861	1.20988
1.33029	1.50097	2.02083
1.52108	1.97096	1.58427
1.51618	1.87669	1.90698
1.43303	1.35088	2.2
1.45329	1.71842	1.33333
1.2642	1.56356	1.55
1.21168	1.71329	1.09302
1.43289	1.73316	1.76119

Table 3.40 Shape characterisation of individual particles

(HSCM Size Fraction 2)

F. PERIMETER ** 2 / FEATURE AREA*12.57	PROJ.HEIGHT* PROJ.W / FEATURE AREA	FEATURE LENGTH / FEATURE BREADTH
1.54906	1.83165	1.42735
1.9113	1.96324	2.98851
2.95114	2.86907	3.70149
2.81835	2.88321	3.64583
1.84334	1.85333	2.36769
3.25454	1.47429	4.30832
2.81772	2.08046	3.43572
2.08422	2.45324	2.55232
2.04987	1.97222	2.68887
2.34051	1.54918	3.03023
1.58206	1.27481	2.05427
1.20845	1.12658	1.65715
1.56479	2.01686	1
1.97182	2.69109	1.94318
2.62863	3.57784	1.44693
2.75091	3.69236	1.75
3.52113	4.34433	3.83721
1.79064	2.21865	1.51786
1.88318	2.36429	2.34667
1.77771	1.95431	1.93507
2.66725	3.91738	2.22619
2.84156	3.54864	1.49724
2.06121	2.21502	2.56934
2.13028	2.7054	1.61983
1.78753	2.475	2.1
1.08081	1.59721	1.13253
1.53936	1.90584	1.408
3.89349	2.1875	1.4058
1.94541	2.05894	1.02649
2.1251	2.15991	1.99213
2.37956	1.88635	3.19048
1.49891	1.93607	1.22901
3.64571	2.09602	4
2.06167	2.82324	1.83333

Table 3.41 Shape characterisation of individual particles
(HSCM Size Fraction 3)

F. PERIMETER ** 2 / FEATURE AREA*12.57	PROJ.HEIGHT* PROJ.W / FEATURE AREA	FEATURE LENGTH / FEATURE BREADTH
1.43487	1.94996	1.27536
2.37411	3.04898	1.5122
2.52229	2.96313	2.08861
1.98193	2.18346	2
2.50225	2.50728	3.80488
1.33954	1.87089	1.04819
1.70292	2.10329	1.19277
1.52465	1.85457	1.56977
2.26413	2.67712	3.42187
3.02308	3.32324	4.27273
3.25381	4.2534	1.84848
1.37462	1.64632	1.75
1.5428	2.12758	1.14851
2.05308	2.65495	2.02667
2.1301	2.71344	2.24468
3.18192	3.82433	4.04839
1.51577	1.74432	1
1.61586	1.95051	1.95122
1.31413	1.62905	1.02105
2.21427	2.57854	3.11765
1.82335	2.375	2.28169
2.58653	3.10297	2.86111
1.56928	1.94611	1.54321
1.24177	1.45516	1.36667
1.50052	1.87491	1.89189
1.7254	1.9034	1.97403
2.86335	3.49308	2.01538
1.39106	1.55076	1.43038
1.55778	1.95946	1.51899
1.17719	1.5883	1.05479
1.82865	2.15336	1.97368
1.76646	2.11253	1.35514
1.42376	1.95845	1.30208
1.29066	1.5569	1.04598
2.28596	3.48059	1.35052
2.57304	2.30937	2.31343
1.73742	2.32929	1.52308
1.92124	6.13114	1.67105
4.88024	5.56338	1.77019
6.96795	6.5837	10.7727
5.80954		6.93671

Table 3.42 Shape characterisation of individual particles
(HSCM Size Fraction 4)

F. PERIMETER ** 2 / FEATURE AREA*12.57	PROJ.HEIGHT* PROJ.W / FEATURE AREA	FEATURE LENGTH / FEATURE BREADTH
1.54424	1.64764	1.88298
2.82763	3.45475	1.41429
2.7437	3.10618	3.96552
2.20314	2.0108	1.01325
2.80861	2.94768	3.40323
7.60666	7.77086	8.15517
1.40209	1.80773	1.42857
1.84571	2.38704	2.15789
5.39176	7.39948	1.28415
2.35491	3.03591	2.272
3.05372	3.35075	3.93103
1.63775	2.22496	1.09524
1.96528	2.49846	1.57377
2.15995	2.84852	1.82178
2.2088	2.92496	1.30573
2.36033	2.90004	1.72727
1.98576	2.29804	2.75904
3.12403	3.03962	4.48718
2.39867	2.50026	3.61905
1.73828	2.25279	1.03509
2.24818	2.77074	1.81905
2.14195	2.62493	2.82558
4.55656	4.9202	4.84459
2.42765	3.02958	2.2
2.88626	3.59407	2.04444
1.70073	2.02309	1.53719
3.49952	3.14522	5.51923
2.50845	3.13433	1.61905
1.40637	1.80666	1.40945
1.9556	2.37802	2.22078
4.47079	5.86992	1.68794
2.45609	3.20245	2.24409
3.00933	3.53465	3.88636
1.82015	2.15269	1.07619
2.06237	2.60377	1.56098
2.02491	2.72134	1.83333

Table 3.43 Shape characterisation of individual particles
(HSCM Size Fraction 5)

F. PERIMETER ** 2 / FEATURE AREA*12.57	PROJ.HEIGHT* PROJ.W / FEATURE AREA	FEATURE LENGTH / FEATURE BREADTH
1.49796	1.62162	2.11538
2.07882	2.26817	2.92308
1.97328	2.11829	2.58621
2.36776	2.18984	3.79167
2.54055	2.26911	3.75
1.67904	1.89457	1.22222
1.6206	2.05987	1.66667
3.19924	3.48716	3.2
3.02193	3.30886	3.95455
2.25646	2.09334	3.5
1.73226	1.93763	2.13889
1.30301	1.76299	1.15909
1.36064	1.49143	1.87097
1.50056	1.70847	1.60526
1.28546	1.43952	1.10256
1.5125	1.8602	1.5
1.6197	1.7914	2.06818
1.50255	1.62471	1.78378
1.5288	1.92876	1.05405
1.39091	1.71544	1.65185
2.14461	2.26952	2.59375
1.68915	1.84286	2.71429
2.12381	2.21293	1.65517
2.80451	3.95426	3.66667
2.39887	2.55829	3.44444
2.74756	3.20355	2.25
2.22113	2.40142	4.70833
4.28654	3.91489	1.97674
1.555	1.69344	2.75862
2.07266	2.53553	3.38462
2.40083	2.83756	2.81081
2.45308	2.6704	1.67347
1.46965	1.7909	1.12766
1.72637	2.06009	1.10256
1.37867	1.70447	2.7
2.05601	2.30207	2.28125
1.64176	2.05414	14.3636
8.76025	6.76213	

Table 3.45 Shape characterisation of individual particles
(HSCM Size Fraction 6)

F. PERIMETER ** 2 / FEATURE AREA*12.57	PROJ.HEIGHT* PROJ.W / FEATURE AREA	FEATURE LENGTH / FEATURE BREADTH
1.83209	1.09995	1.19355
2.13283	1.36712	1.7551
1.99648	1.55591	2.64
2.22346	1.59929	3.39535
2.15446	1.74434	3.02
1.926	1.96622	1.86667
2.51071	1.68183	3.15909
2.07922	2.01487	2.5098
2.04974	1.97952	2.27907
2.51619	2.57659	2.39216
1.51143	1.89242	1.16949
2.09702	1.66098	2.82222
2.00758	1.48905	1.51613
1.59547	2.02575	2.09302
2.45212	1.70788	2.26316
1.49679	1.92809	1.64706
2.19158	3.02609	1.8
1.58629	1.89987	1.64516
3.57437	21.4987	2.73438
2.02625	2.85714	1.1017
1.78171	1.86344	2.44231
1.71541	1.87513	1.94872
9.28444	6.94145	5.67308
1.92848	2.33428	1.56
1.45348	1.9016	1.32143
2.57688	2.77097	2.75
1.85125	2.62689	2.72222
3.29717	3.91802	5.16071
1.92722	2.48278	1.75862
1.31224	1.58763	1.19403
1.77605	2.11427	1.66667
1.80621	1.96812	2.4386
1.94508	2.00952	2.80357
2.01538	2.0753	3.55556
1.77571	2.0557	1.8125
1.88421	1.88376	3
1.80353	2.10853	2.23913
1.8957	2.11162	2.23333
2.17993	2.48346	2.24561
1.90908	1.87945	2.78723
1.37271	1.6433	1.12308
1.27324	1.48403	1.49231
1.90299	2.25507	2.11905
1.46019	1.66658	2.06383

Table 3.46 Shape characterisation of individual particles

(HSCM Size Fraction 7)

F. PERIMETER ** 2 / FEATURE AREA*12.57	PROJ.HEIGHT* PROJ.W / FEATURE AREA	FEATURE LENGTH / FEATURE BREADTH
1.19585	1.61028	1.27907
1.28865	1.61043	1.14545
1.76991	2.1236	1.53488
1.42424	1.83674	1.06452
1.52116	1.96562	1.59702
1.22114	1.60218	1.32432
1.29559	1.73172	1.36
1.52797	1.72447	1.14925
1.99731	2.21004	2.58537
2.30708	2.43167	2.775
1.26458	1.55571	1.58824
1.36509	1.72655	1.81818
1.62319	1.73529	1.86
1.56111	1.86613	1.15873
1.63646	2.09424	1.67347
1.52589	2.02964	1.40625
1.73757	1.9625	1.19048
1.38591	1.5044	1.40741
1.60368	2.13066	1.20225
1.28229	1.70066	1.07143
1.69734	1.93197	1.75
1.63605	1.92332	2.18182
1.39995	1.69471	1.95833
1.75436	1.95689	2.4386
3.31269	2.63921	4.53333
1.41931	1.675	1.4375
1.25533	1.55801	1.38095
1.26882	1.4927	1.5
1.94745	2.49884	2.43243
2.17122	2.53518	1.73239
1.47577	1.78125	1.64444
1.97725	2.45276	1.61538
1.18156	1.53105	1.06349
1.77475	2.0127	2.54839
1.33603	1.50225	1.48889
1.74179	1.90014	2.15909
1.12522	1.41429	1.41379
1.33345	1.77031	1.28571

Table 3.47 Shape characterisation of individual particles
(BMa Size Fraction 2)

F. PERIMETER ** 2 / FEATURE AREA *12.57	PROJ.HEIGHT* PROJ.W / FEATURE AREA	FEATURE LENGTH / FEATURE BREADTH
2.09972	2.91154	1.16456
1.30077	1.65498	1.55738
1.52701	1.83357	1.86364
1.2686	1.6809	1.34286
1.20428	1.65328	1.16552
1.51133	1.76283	1.52439
1.40614	1.74652	1.048
2.65328	3.44764	2.14286
1.54411	2.01275	1.26761
1.96438	2.53621	1.91057
1.39671	1.77552	1.45714
2.44119	2.93623	1.66667
1.70626	2.10375	1.07519
1.4779	1.74908	1.57143
1.38407	1.84532	1.2268
1.76178	2.41646	1.64179
1.53949	1.90058	1.62295
1.28876	1.68094	1.05
1.33474	1.5481	1.07407
1.50652	1.85733	1.45545
1.96411	1.98262	2.32143
2.87385	3.37496	3.11429
1.45482	1.74845	1.53947
1.36834	1.71235	1.23762
1.44983	1.88238	1.58915
1.64004	2.14356	1.60993
1.79624	1.70016	1.04724
1.79875	1.57741	1.01361
1.95122	2.72271	2.18478
1.39931	1.84564	1.43925
2.05864	2.47716	2.98684
1.24868	1.74119	1.15116
1.73433	2.41959	1.52713
1.54314	2.57333	1.82014
1.22929	1.78507	1.30973
1.22023	1.63341	1.06707
1.89525	2.17738	1.51136
1.33596	1.67618	1.06107

Table 3.48 Shape characterisation of individual particles

(BMa Size Fraction 3)

F. PERIMETER ** 2 / FEATURE AREA/ 12.57	PROJ.HEIGHT* PROJ.W / FEATURE AREA	FEATURE LENGTH / FEATURE BREADTH
1.38244	1.89899	1.26866
1.42491	1.72187	1.16
1.55508	1.83977	2.05797
1.98806	2.26016	2.33333
1.44593	1.78668	1.64634
1.40852	1.6844	1.39506
1.84749	2.29441	2.07895
1.35825	1.81114	1.37209
1.16027	1.48861	1.21333
1.91115	2.18536	2.4
3.35547	2.85345	5.12727
1.53734	2.12946	1.52
3.20075	3.7235	3.14773
1.52981	1.74413	1.27397
1.32252	1.44114	1.06612
1.5232	1.90751	1.10084
3.21018	4.09708	1.73864
1.53598	1.95383	1.64384
1.27313	1.46334	1.45614
1.35048	1.51532	1.57746
1.53538	1.74799	1.7037
1.20598	1.59535	1.16438
1.53676	2.13857	1.4878
1.6725	1.91597	1.64211

Table 3.49 Shape characterisation of individual particles

(BM_a Size Fraction 4)

F. PERIMETER ** 2 / FEATURE AREA * 12.57	PROJ. HEIGHT * PROJ. W / FEATURE AREA	FEATURE LENGTH / FEATURE BREADTH
1.41869	1.78888	1.49107
1.59551	2.24427	1.69307
2.15871	2.87156	2.74713
1.80137	2.33928	2.39286
1.94193	2.32336	2.37903
1.39349	1.65448	1.08163
2.16834	2.48469	2.475
1.37835	1.80627	1.12174
1.60632	2.0655	1.15596
1.56035	2.04676	1.1626
1.53273	1.84594	1.75532
1.429	1.88636	1.31387
1.81418	2.34149	1.02162
2.71111	3.19527	3.15789
3.0724	3.33043	3.45
1.43605	1.67655	1.12739
1.9259	2.54332	1.04969
3.37898	4.08663	1.57143
1.63837	2.23358	1.40196
2.62414	2.05559	1
1.47131	1.90261	1.10811
2.05706	2.71224	1.46721
1.78558	2.29435	1.07186
1.35651	2.42261	1.13665
1.50796	2.00348	1.08466
2.56759	2.87938	3.36792
1.37542	1.79396	1.33333
2.09567	1.7339	1.71569
2.52253	2.90729	3.03883
1.35645	1.69676	1.432
1.58358	1.8328	1.66364
2.65794	2.88942	2.57576
1.68094	2.49128	2.25
2.03262	2.01159	2.26277
1.67522	2.50563	1.07362
2.14322	1.99282	2.40909
1.22259	1.58388	1.11024
1.44112	1.79261	1.13934
1.32506	1.71003	1.16296
2.01199	3.03447	1.30303

Table 3.50 Shape characterisation of individual particles
(BMa Size Fraction 5)

F. PERIMETER ** 2 / FEATURE AREA*12.57	PROJ.HEIGHT* PROJ.W / FEATURE AREA	FEATURE LENGTH / FEATURE BREADTH
1.99731	2.58386	1.12335
3.05193	3.97491	1.98477
3.0683	3.39279	3.80952
2.91827	3.32238	4.62105
4.10364	4.97911	2.73504
2.36423	3.33119	1.56425
2.20654	2.61849	2
5.49759	8.79592	2.12299
1.97769	2.59877	1.10442
1.61162	1.94488	1.16749
1.47128	1.80322	1.54088
1.56818	1.82505	1.71724
1.70421	2.05546	1.49215
3.24937	3.84245	3.02469
1.76863	2.1318	1.17436
1.37001	1.7737	1.35542
1.68523	2.37336	1.03653
1.54924	2.02724	1.54018
1.34629	1.78254	1.09434
4.12488	4.9592	3.47468

Table 3.51 Shape characterisation of individual particles (BMa Size Fraction 6)

F. PERIMETER ** 2 / FEATURE AREA*12.57	PROJ.HEIGHT* PROJ.W / FEATURE AREA	FEATURE LENGTH / FEATURE BREADTH
1.61718		
1.29834	2.13254	1.16
1.58807	1.61404	1.40952
1.26979	2.06251	1.1761
1.38848	1.38916	1.07767
1.89479	1.7477	1.0813
1.24576	2.31734	1.8
1.63084	1.63835	1.25714
1.62063	2.18908	1.16842
1.48281	2.15737	1.76471
1.786	1.87733	1.73267
1.45654	2.07956	2.10227
1.22464	1.71617	1.36709
1.38566	1.64152	1.3125
1.23513	1.67944	1.63158
1.42806	1.65399	1.13178
1.25095	1.78774	1.59406
1.54778	1.72559	1.30303
1.61199	1.95178	1.27723
1.64897	2.14728	1.30337
1.73702	1.96807	1.71429
1.46617	2.8256	2.04301
1.40183	1.87476	1.69811
1.21082	1.8227	1.31765
1.36655	1.63089	1.30952
2.15341	1.67697	1.59259
1.33948	1.72198	1.57547
1.19739	1.71646	1.10219
1.83157	1.66523	1.32692
1.31423	1.95255	1.22018
1.30821	1.88546	1.14458
1.30833	1.59855	1.12844
1.75761	1.62832	1.04444
2.9793	2.67145	1.70492
1.57382	4.51267	1.38182
1.42882	3.00066	1.17778
1.61846	1.65128	1.39474
	1.98872	1.19883

Table 3.52 Shape characterisation of individual particles
(BMb Size Fraction 3)

F. PERIMETER ** 2 / FEATURE AREA *12.57	PROJ.HEIGHT* PROJ.W / FEATURE AREA	FEATURE LENGTH / FEATURE BREADTH
1.61492	2.36677	1.05303
1.50236	2.40448	1.05161
2.09951	2.27493	1.31788
1.63338	2.19257	1.84298
1.59908	2.24791	1.24306
1.56364	1.93536	1.56818
2.17399	2.61408	1.01942
1.59828	2.35547	1.80189
2.01685	2.05867	1.975
1.31064	1.64258	1.20168
1.39385	1.98273	1.02976
3.34278	2.75424	2.32
1.67378	1.99403	1.82482
1.70587	2.74572	1
3.61095	2.76404	4.53333
1.87983	2.78128	2.11607
1.63473	1.51428	1.49231
1.40281	1.94276	1.37662
1.33553	1.60118	1.45985
1.87238	2.41872	1.59055
1.53168	2.06165	1.0603
1.23616	1.57359	1.33566
1.32214	1.69826	1.14925
1.50804	1.6006	2.01942
1.46547	1.82514	1.81818
1.33672	1.53737	1.11511
1.39993	1.73868	1.4878
6.26169	7.07156	1.29703
2.32837	2.13775	1.36364
1.39938	2.45483	1.6281
1.83164	1.69532	1.8
1.73401	1.81341	1.23179
1.51874	2.15221	1.90533
1.38933	1.92272	1.03636
1.55849	2.59983	1.07914
1.54679	2.04813	1.83465
1.38739	1.9814	1.30675
1.33251	1.60618	1.10582
1.77361	2.38657	1.50714
2.17945	2.76711	1.06699
1.22698	1.55323	1.31169
1.97668	3.16671	1.6055
1.33033	2.45245	1.13699
1.49969	2.21002	1.8547
1.38717	1.65933	1.12081
1.49536	2.14219	1.80672
2.15527	1.82007	1.42697
2.23593	2.86896	1.20513

Table 3.53 Shape characterisation of individual particles

F. PERIMETER ** 2 / FEATURE AREA*12.57	PROJ.HEIGHT* PROJ.W / FEATURE AREA	FEATURE LENGTH / FEATURE BREADTH
1.36325	1.90763	1.06897
1.25883	2.37425	1.02941
1.47731	1.72239	1.47107
2.4062	2.75656	2.52174
1.49564	1.76734	1.54717
1.48206	2.77368	1.04487
2.55817	3.41181	1.83333
1.77607	2.18851	1.71015
1.99308	2.34704	1.77551
1.44527	1.75023	1.15459
1.49859	1.89926	1.35484
1.72286	2.12542	1.12183
3.21634	5.25097	2.33607
3.28581	2.91978	1.4058
1.69069	2.2837	1.35772
2.18527	1.73452	1.82171
1.33183	1.72567	1.05031
1.62494	1.93597	1.62308
1.99218	2.47504	2.37755
2.41694	2.91596	1.94776
1.83356	1.77026	1.9127
1.87105	2.37455	1.86228
1.51087	1.9551	1.33036
1.66881	2.24329	1.04734
2.00496	2.42421	1.7
1.29909	1.57405	1.14778
2.47716	3.28856	1.86364
1.70537	1.98487	1.72593
1.47202	1.78333	1.05229
2.44225	2.74395	2.67692
1.22445	1.66579	1.05224
1.4722	1.66425	1.57595
1.42432	1.92248	1.07895
1.50874	1.92295	1.52101

Table 3.54 Shape characterisation of individual particles
(ERMa Size Fraction 3)

F. PERIMETER ** 2 / FEATURE AREA*12.57	PROJ.HEIGHT* PROJ.W / FEATURE AREA	FEATURE LENGTH / FEATURE BREADTH
1.67062	2.04981	1.76923
2.10841	2.22459	3.07792
1.74272	2.19042	1.7
2.01934	2.41778	2.0625
2.59774	3.03772	2.63636
2.10363	2.73215	2.26263
1.80857	2.17286	1.38889
1.6225	2.09693	1.50345
1.50776	1.83124	1.13659
1.91999	2.32738	2.05941
1.52966	1.95129	1.84397
2.16709	2.52622	3.09091
2.93037	3.4128	2.03704
1.38265	1.72793	1.51765
1.44817	1.9252	1.53125
1.43224	1.85141	1.84444
5.74914	5.67527	5.87805
4.68904	4.49537	5.30393
3.33016	2.97494	3.63903
1.7059	2.11828	1.78295
1.84581	1.875	1.7027
2.16241	3.34177	3
2.04872	2.06923	2.07042
2.64505	1.55	2.53509
2.07604	1.64655	2.24
1.73723	2.29075	1.37037
1.53729	2.34177	1.1592
1.60734	2.60428	1.51389

Table 3.55 Shape characterisation of individual particles
(ERMa Size Fraction 5)

F. PERIMETER ** 2 / FEATURE AREA * 12.57	PROJ.HEIGHT* PROJ.W / FEATURE AREA	FEATURE LENGTH / FEATURE BREADTH
2.61904	3.4489	1.31206
2.3012	2.93173	1.15544
3.24303	3.76199	1.71756
1.67681	2.29531	1.49673
1.77802	2.1458	1.07519
1.72656	2.40431	1.504
1.81991	2.26599	2.09412
1.92251	2.44505	1.87037
1.64139	2.57115	1.22124
1.84299	2.6446	1.37302
1.97604	2.66187	1.31757
2.39165	3.26755	2.58025
1.49587	1.85657	1.2459
2.25238	2.91851	2.17568
1.71775	2.35827	1.35443
1.73845	2.35988	1.50968
1.34394	1.97424	1.22018
2.05359	2.62046	1.20541
1.81698	2.55546	1.34641
1.44985	2.0643	1.128
1.87205	2.50839	1.37302
1.78996	2.42877	1.09945
1.49551	1.98472	1.47368
1.83079	2.09435	1.76389
1.32489	1.80312	1.26549
1.70444	2.1364	1.36424
1.42992	1.81884	1.60563
1.53817	1.97807	1.23214
1.77814	2.26277	1.39669
2.53761	3.10987	2.6625
1.76919	2.26544	1.34722

Table 3.56 Shape characterisation of individual particles

(ERMb Size Fraction 3)

F. PERIMETER ** 2 / FEATURE AREA*12.57	PROJ.HEIGHT* PROJ.W / FEATURE AREA	FEATURE LENGTH / FEATURE BREADTH
1.92188	2.62998	1.44355
1.34304	1.7885	1.18261
1.31729	1.80744	1.15569
1.50176	1.94085	1.12605
2.36249	2.66598	2.63478
1.4996	2.1071	1.31008
1.70065	2.24278	1.34444
2.2392	3.04971	1.54622
3.23003	4.45148	1.05021
3.04079	3.75919	2.44828
1.58456	2.23022	1.1017
1.38874	1.78202	1.0603
2.48367	3.11197	1.53763
1.78694	2.1101	2.4322
4.85994	5.16438	3.74419
1.9757	2.46856	1.61151
1.37736	1.61092	1.05096
2.14873	2.89857	1.80488
1.49185	2.10979	1.31183
1.97223	2.66649	1.49587
1.38308	1.90432	1.32031
3.04024	4.06165	1.0332
1.46118	2.04251	1.10656
1.25615	1.73854	1.21239
1.92296	2.15435	2.55462
1.33035	1.86406	1.1747
2.03408	2.68701	1.42857
2.86936	4.21536	1.34711
1.39091	1.98194	1.11976
2.04966	2.409	1.95699
2.97291	3.82264	1.18265
1.95597	2.24192	1.03101
2.57065	2.68354	1.55556
1.84541	2.59329	1.30714
1.91751	2.40614	1.25503
	3.69164	2.19048
	2.33307	1.1165

Table 3.57 Shape characterisation of individual particles
(ERMb Size Fraction 5)

Specimen Code (see text)	Mean Sieve Size m	Shape Factors			
		$\frac{P^2}{A4\pi}$	$\frac{P_V \times P_H}{A}$	L/B	F_V/F_H
HSCM2	50	1.755	2.000	1.907	1.760
HSCM3	75	2.233	2.343	2.260	2.073
HSCM4	106	2.293	2.766	2.305	2.178
HSCM5	152	2.625	3.113	2.444	2.420
HSCM6	215	2.690	2.744	2.755	2.650
HSCM7	282	2.035	2.125	2.216	2.525
BMa2	50	1.587	1.879	1.703	1.460
BMa3	76	1.638	2.058	1.545	1.512
BMa4	106	1.719	2.033	1.740	1.683
BMa5	152	1.860	2.274	1.706	1.770
BMa6	215	2.444	3.101	1.980	1.862
BMb3	76	1.493	1.988	1.343	1.390
BMb5	152	1.790	2.152	1.508	1.554
ERMa3	76	1.888	2.325	1.550	1.655
ERMa5	152	2.411	2.705	2.260	2.212
ERMb3	76	1.915	2.430	1.455	1.573
ERMb5	152	2.020	2.595	1.956	1.910

Table 3.58 Summary of mean shape factors from the data of individual particles (Table 3.40 and 3.57)

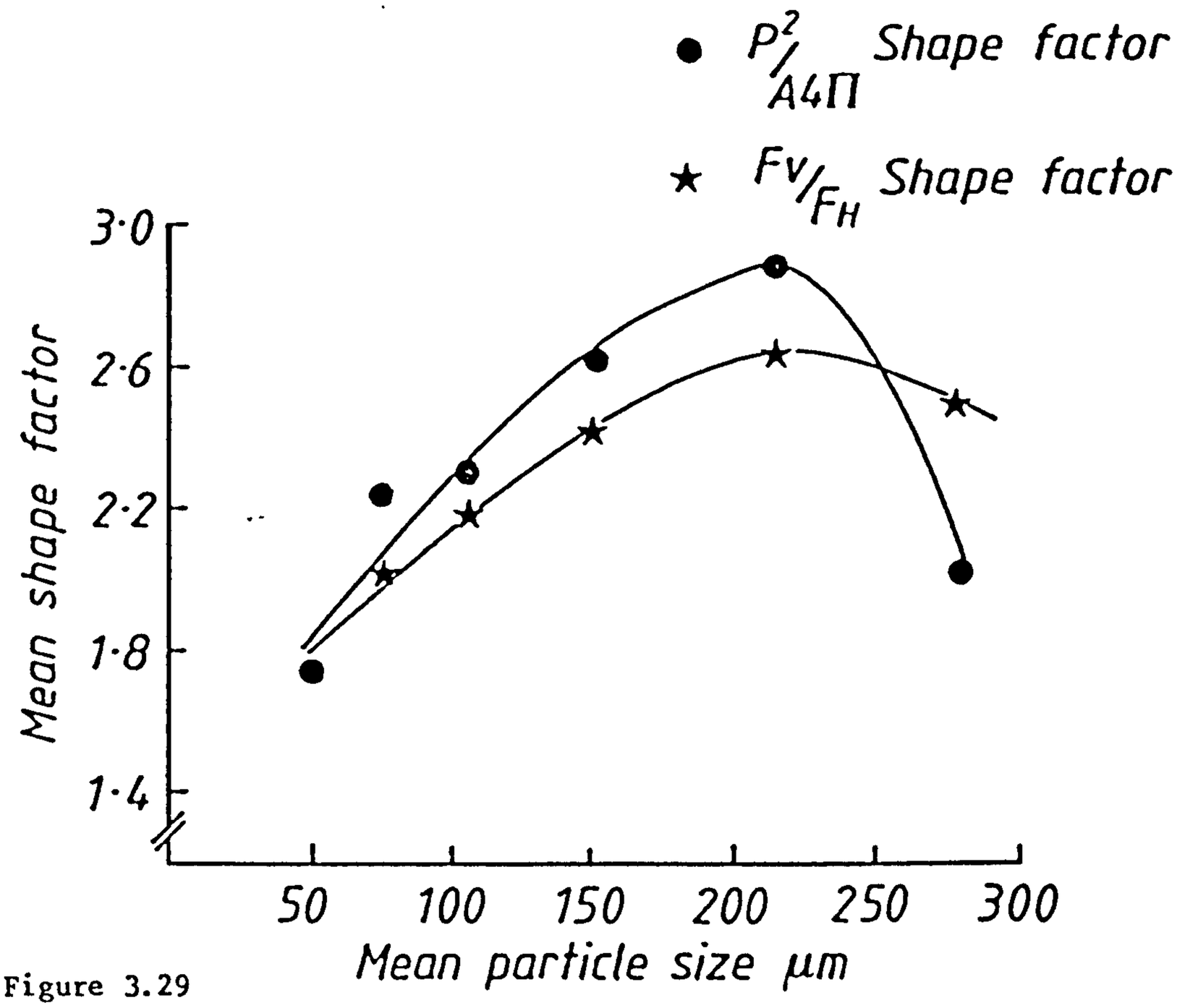

Figure 3.29

Mean shape -factors versus mean particle sieve sizes from a high speed cutter mill

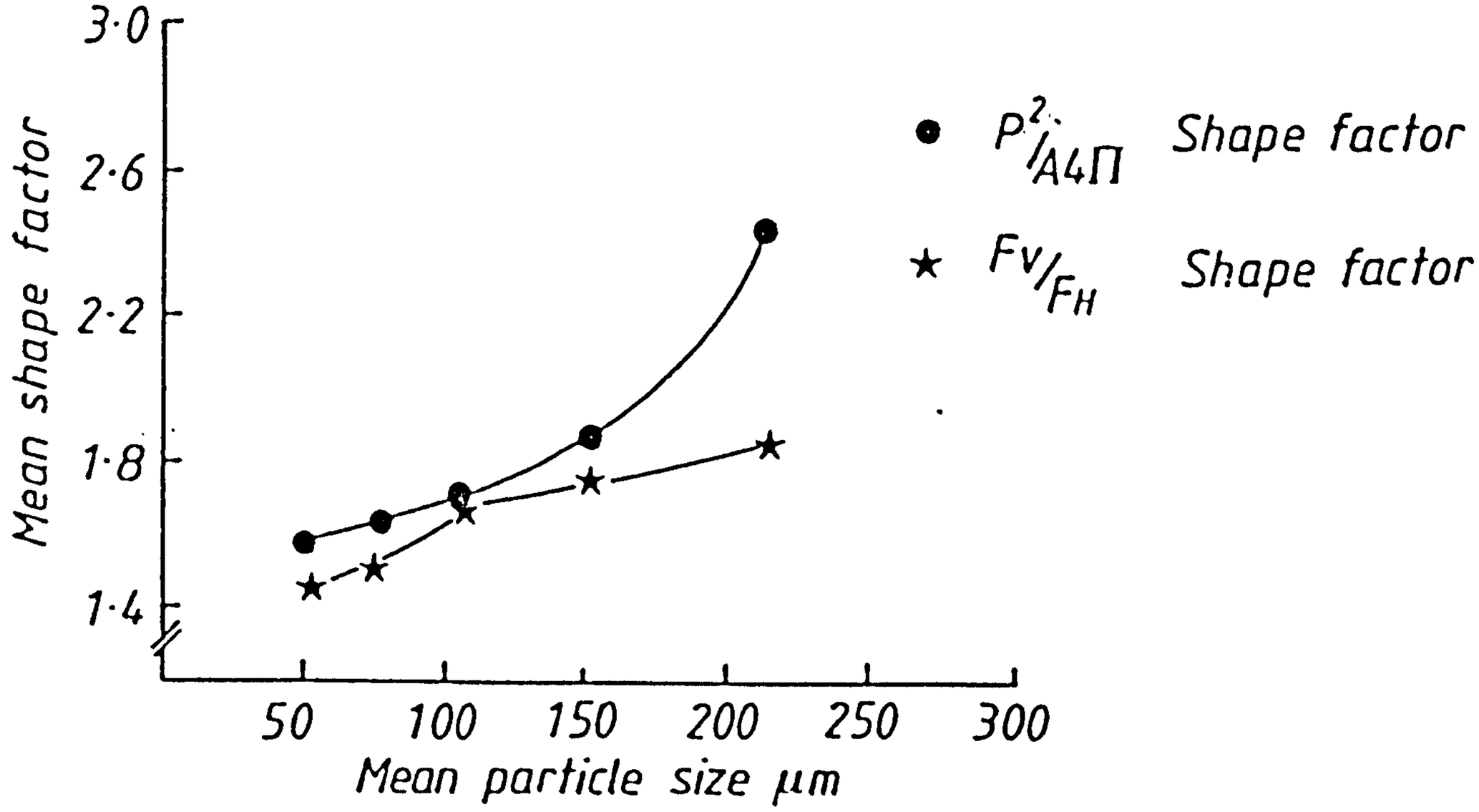

Figure 3.30

Mean shape factors versus mean particle sieve sizes from a ball mill

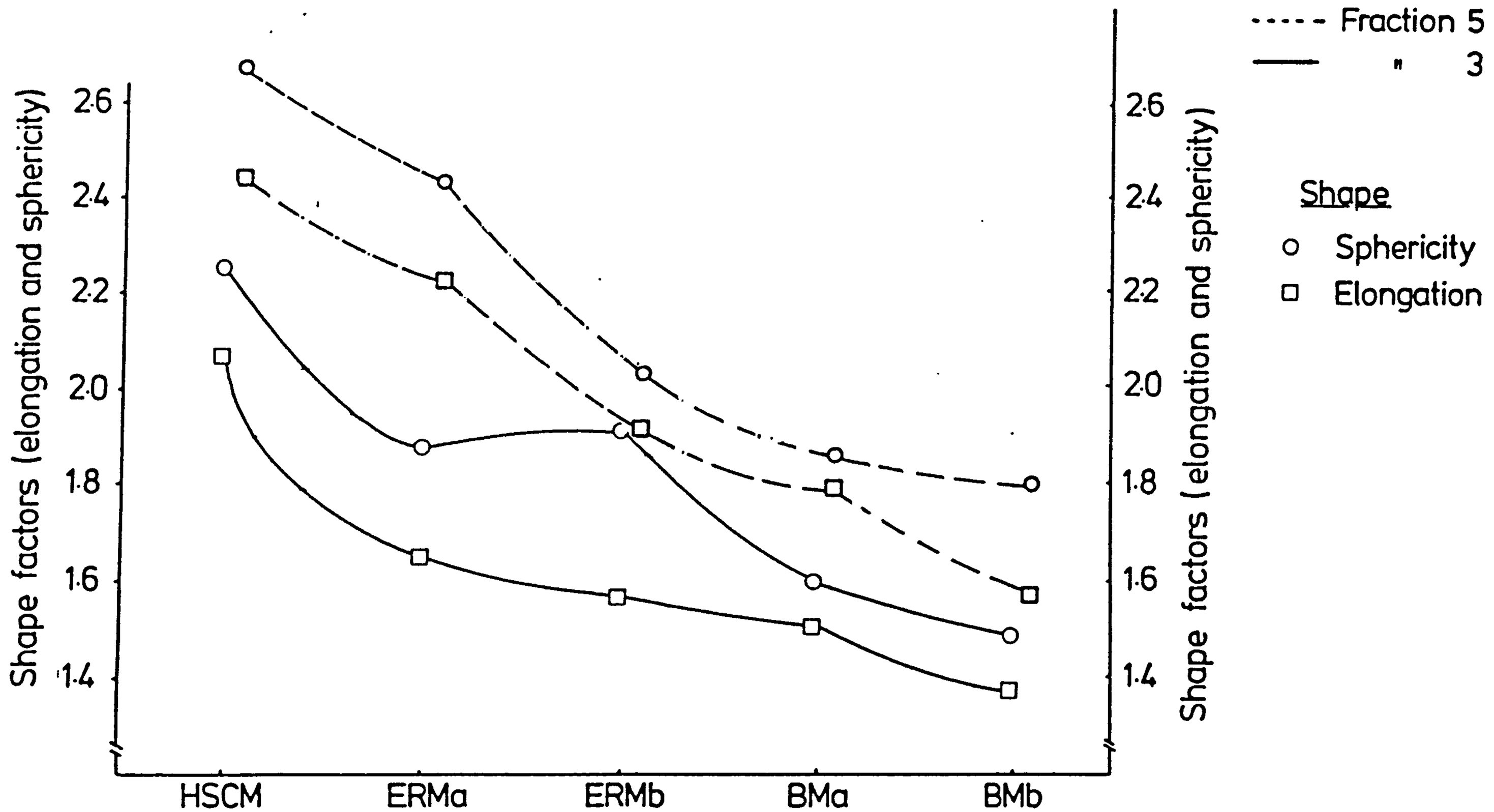

Figure 3.31 Variation of shapes (Fraction 5) & (Fraction 3) from different milled products

3.4.2 Shape factor distribution

Eight shape factors obtained from the fractions HSCM3, HSCM5, BMa3 and BMa5 (Tables 3.41, 3.43, 3.48 and 3.50) were analysed in terms of the shape distribution and cumulative proportions. The two shape descriptors selected to explain the shape distributions for all the four fractions were elongation (L/B) and sphericity ($P^2/A4\pi$).

Table 3.59 and 3.60 show the sphericity and elongation frequency and cumulative proportion (cumul. prop.) values together with the median, mode and mean of each distribution for HSCM3 and HSCM5 fractions, while Tables 3.61 and 3.62 gives the same informations for BMa3 and BMa5. Figures 3.32, 3.33, 3.34, and 3.35 show the histograms of shape factor distributions along with their cumulative proportion for the HSCM3, HSCM5, BMa3 and BMa5 products.

SPHERICITY				ELONGATION			
Shape intervals	Frequency F	Rela-tive F	Cumul. prop. over size	Shape intervals	Frequency F	Rela-tive F	Cumul. prop. over size
1.00-1.30	2	0.06	1	1.00-1.30	3	0.09	1
1.30-1.60	5	0.15	0.94	1.30-1.60	11	0.32	0.91
1.60-1.90	5	0.15	0.79	1.60-1.90	4	0.12	0.59
1.90-2.20	9	0.26	0.64	1.90-2.20	6	0.18	0.47
2.20-2.50	2	0.06	0.38	2.20-2.50	3	0.09	0.29
2.50-2.80	3	0.08	0.32	2.50-2.80	1	0.03	0.21
2.80-3.10	4	0.12	0.24	2.80-3.10	1	0.03	0.18
3.10-3.40	2	0.06	0.12	3.10-3.40	1	0.03	0.15
3.40-3.70	1	0.03	0.06	3.40-3.70	1	0.03	0.12
3.70-4.00	1	0.03	0.03	3.70-4.00	3	0.09	0.09
TOTAL	34			34			
Median	2.08	slight positive		Median	1.80	positive	
Mode	2.05	skewed		Mode	1.45	skewed	
Mean	2.09			Mean	1.91		

Table 3.59 Shape distribution and cumulative proportion (Milled Product : HSCM3)

SPHERICITY				ELONGATION			
Shape intervals	Frequency F	Rela-tive F	Cumul. prop. over size	Shape intervals	Frequency F	Rela-tive F	Cumul. prop. over size
1.40-170	4	0.11	1	1.00-140	6	0.16	1
1.70-2.00	7	0.19	0.89	1.40-1.80	9	0.25	0.84
2.00-2.30	7	0.19	0.70	1.80-2.20	6	0.16	0.59
2.30-2.60	6	0.17	0.51	2.20-2.60	4	0.11	0.43
2.60-3.20	4	0.11	0.34	2.60-3.00	2	0.06	0.32
2.90-3.20	3	0.08	0.23	3.00-3.40	—	—	—
3.20-3.50	1	0.03	0.15	3.40-3.80	2	0.06	0.26
3.50-3.80	—	—	—	3.80-4.20	3	0.08	0.20
3.80-4.10	—	—	—	4.20-4.60	1	0.03	0.12
4.10-4.40	—	—	—	4.60-5.00	1	0.03	0.09
4.40-4.70	2	0.06	0.12	5.00-5.40	—	—	—
4.70-5.00	—	—	—	5.40-5.80	1	0.03	0.06
5.00-5.30	2	0.06	0.06	5.80-6.20	1	0.03	0.03
TOTAL	36				36		
Median	2.31	positive		Median	2.00	positive	
Mode	2.00	skewed		Mode	1.60	skewed	
Mean	2.97			Mean	2.13		

Table 3.60 Shape Distribution and cumulative proportion (Milled Product : HSCM5)

SPHERICITY			
Shape intervals	Frequency F	Relative F	Cumul. prop. over size
1.20-1.35	8	0.21	1
1.35-1.50	9	0.23	0.79
1.50-1.65	7	0.18	0.56
1.65-1.80	5	0.13	0.38
1.80-1.95	2	0.05	0.25
1.95-2.10	4	0.10	0.20
2.10-2.25	—	—	—
2.25-2.40	—	—	—
2.40-2.55	1	0.03	0.10
2.55-2.70	1	0.03	0.07
2.70-2.05	1	0.03	0.04
TOTAL	38		
Median	1.540	positive	
Mode	1.425	skewed	
Mean	1.578		

ELONGATION			
Shape intervals	Frequency F	Relative F	Cumul. prop. over size
1.00-1.15	8	0.21	1
1.15-1.30	3	0.08	0.79
1.30-1.45	5	0.13	0.71
1.45-1.60	9	0.23	0.58
1.60-1.75	5	0.13	0.35
1.75-1.90	2	0.05	0.22
1.90-2.05	1	0.03	0.17
2.05-2.20	2	0.05	0.14
2.20-2.35	1	0.03	0.09
2.35-2.50	—	—	—
2.65-2.80	—	—	—
2.80-2.95	1	0.03	0.06
2.95-3.10	1	0.03	0.03
38			
Median	1.50	negative	
Mode	1.525	skewed	
Mean	1.49		

Table 3.61 Shape distribution and cumulative proportion (Milled Product : BMa3)

SPHERICITY				ELONGATION			
Shape intervals	Frequency F	Rela-tive F	Cumul. prop, over size	Shape intervals	Frequency F	Rela-tive F	Cumul. prop. over size
1.20-1.40	7	0.17	1	1.00-1.20	16	0.40	1
1.40-1.60	10	0.25	0.83	1.20-1.40	3	0.08	0.60
1.60-1.80	5	0.13	0.58	1.40-1.60	5	0.12	0.52
1.80-2.00	4	0.10	0.45	1.60-1.80	4	0.10	0.40
2.00-2.20	7	0.17	0.35	1.80-2.00	—	—	—
2.20-2.40	—	—	—	2.00-2.20	—	—	—
2.40-2.60	2	0.05	0.18	2.20-2.40	4	0.10	0.30
2.60-2.80	3	0.08	0.13	2.40-2.60	3	0.08	0.20
2.80-3.00	—	—	—	2.60-2.80	1	0.02	0.12
				2.80-3.00	-	-	-
3.00-3.2	1	0.02	0.05	3.00-3.20	2	0.05	0.10
3.2-3.4	1	0.02	0.03	3.20-3.40	2	0.05	0.05
TOTAL	40			40			
Median	1.70	positive		Median	1.42	negative	
Mode	1.50	skewed		Mode	1.10	skewed	
Mean	1.76			Mean	1.78		

Table 3.62 Shape distribution and cumulative proportion (Milled Product : BMa5)

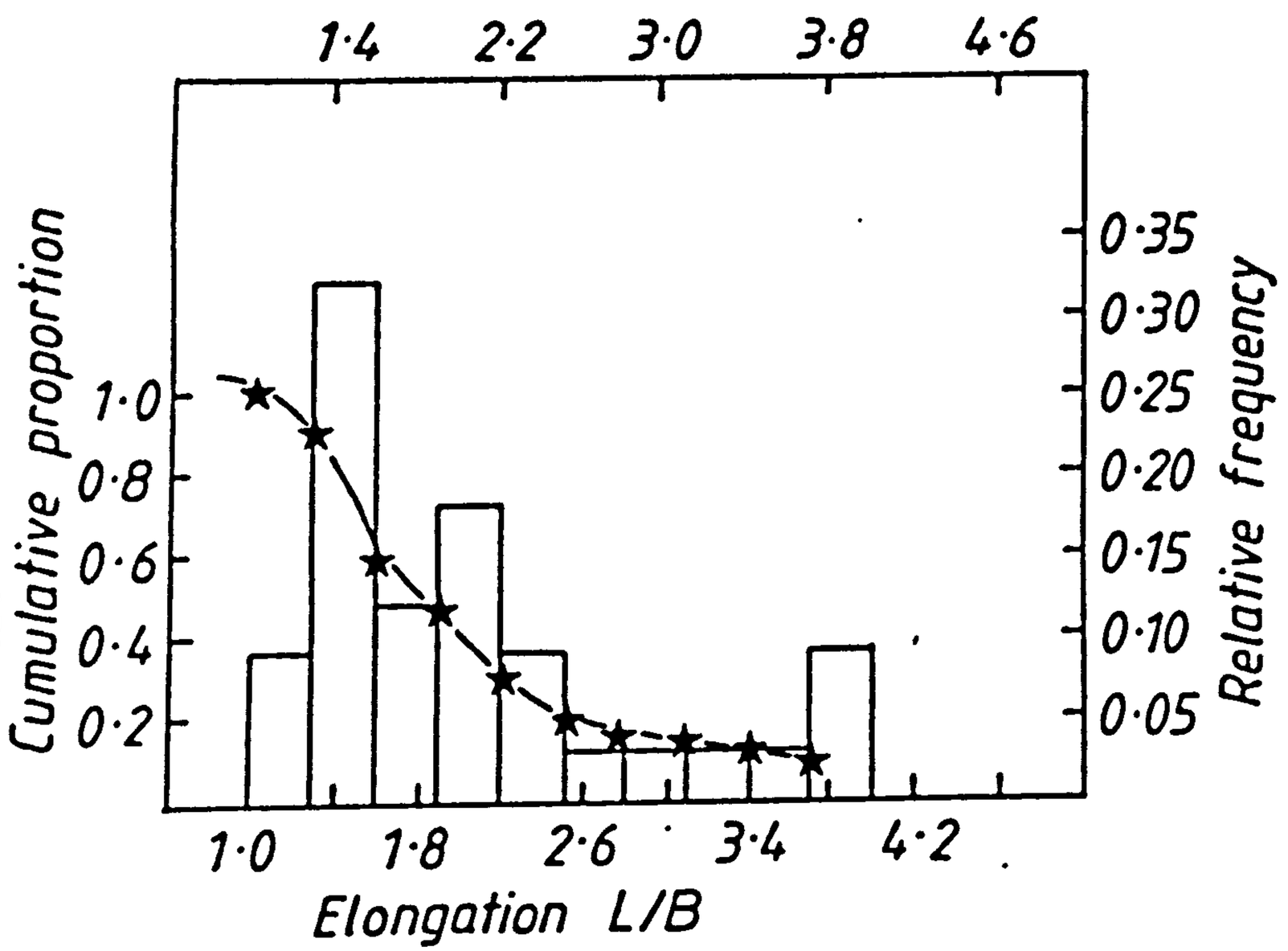

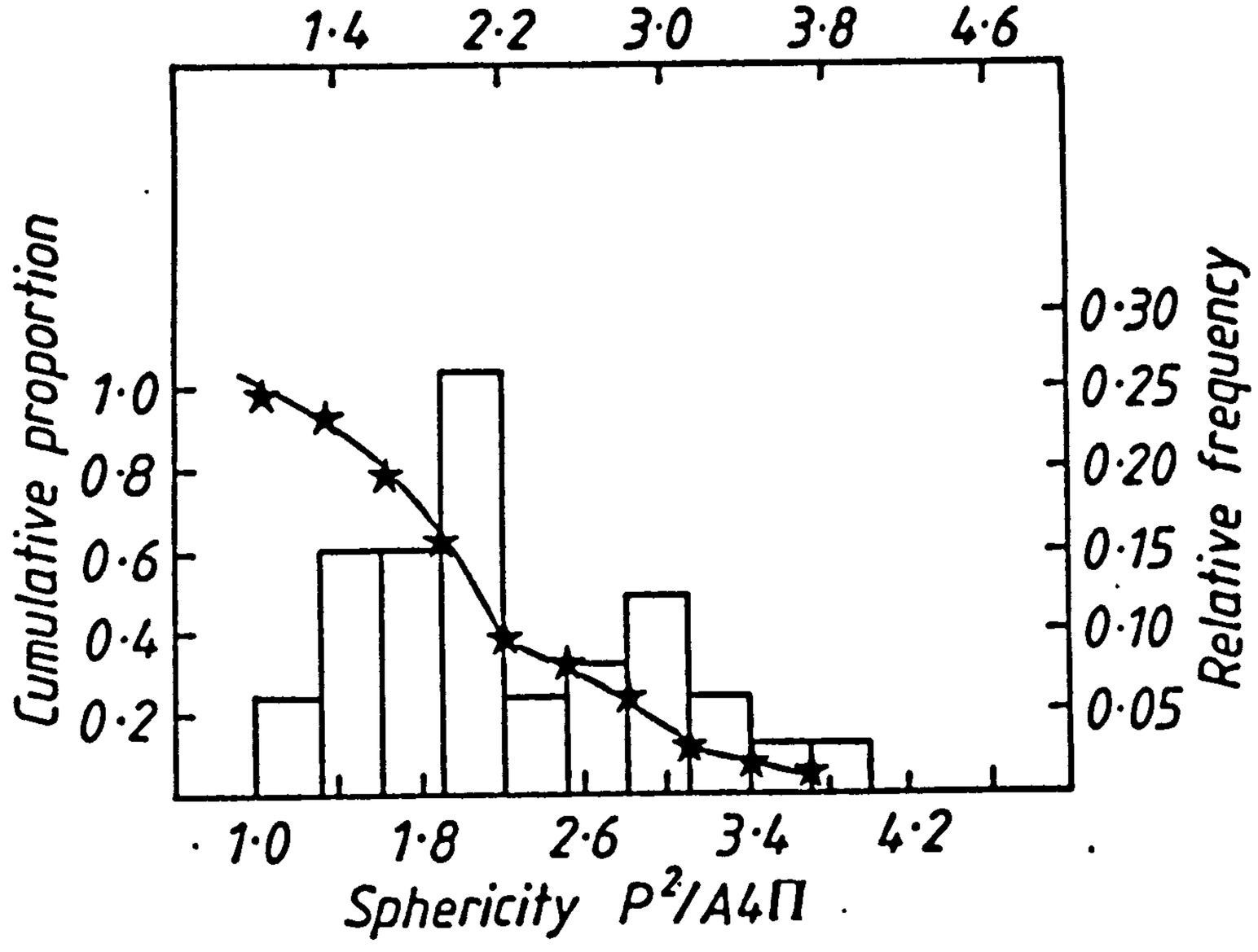

Figure 3.32 *Cumulative and Frequency Distribution of shapes from high speed cutter mill (HSC3)*

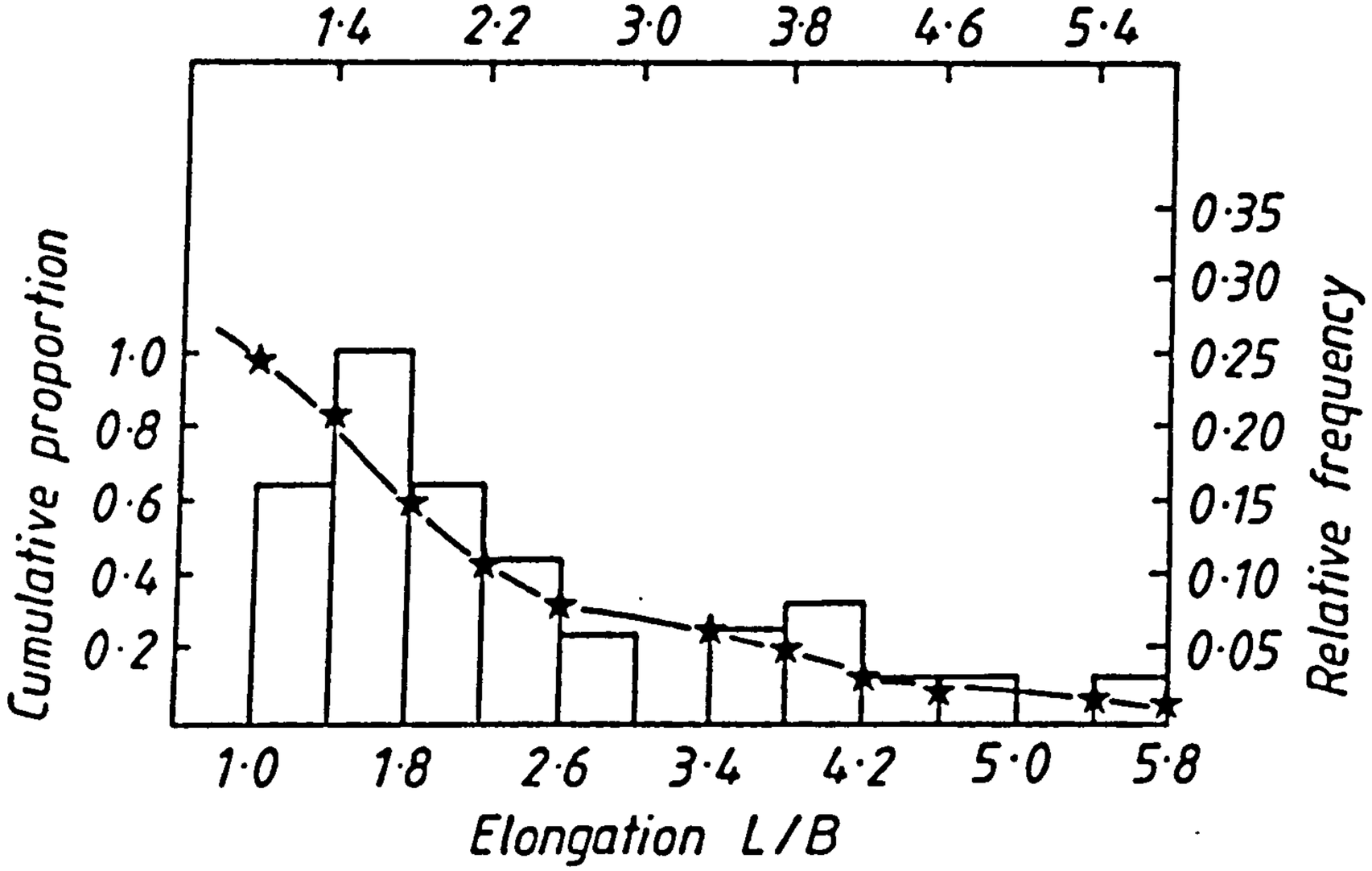

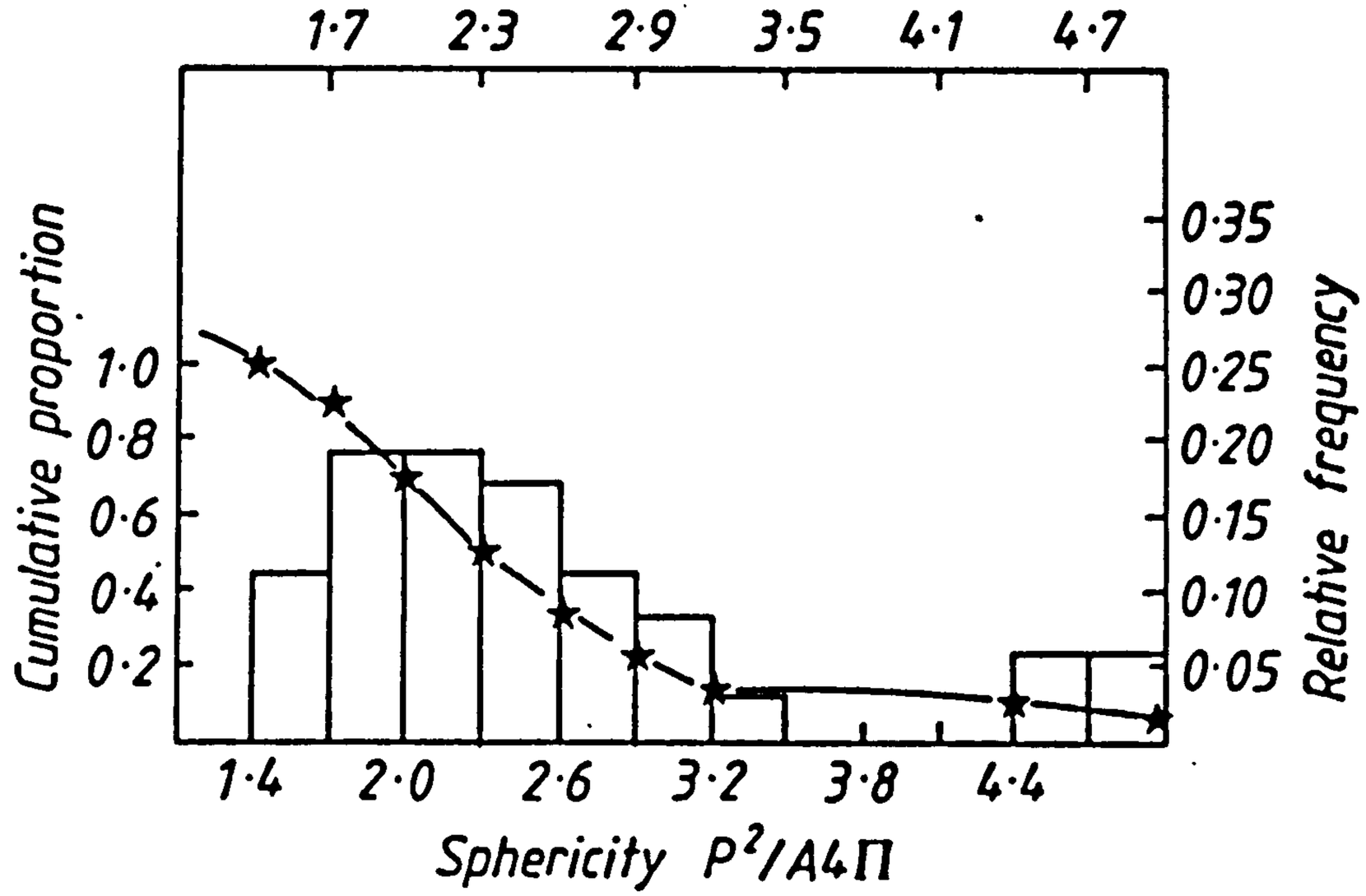

Figure 3.33 *Cumulative and Frequency Distribution of shapes from high speed cutter mill (HSC5)*

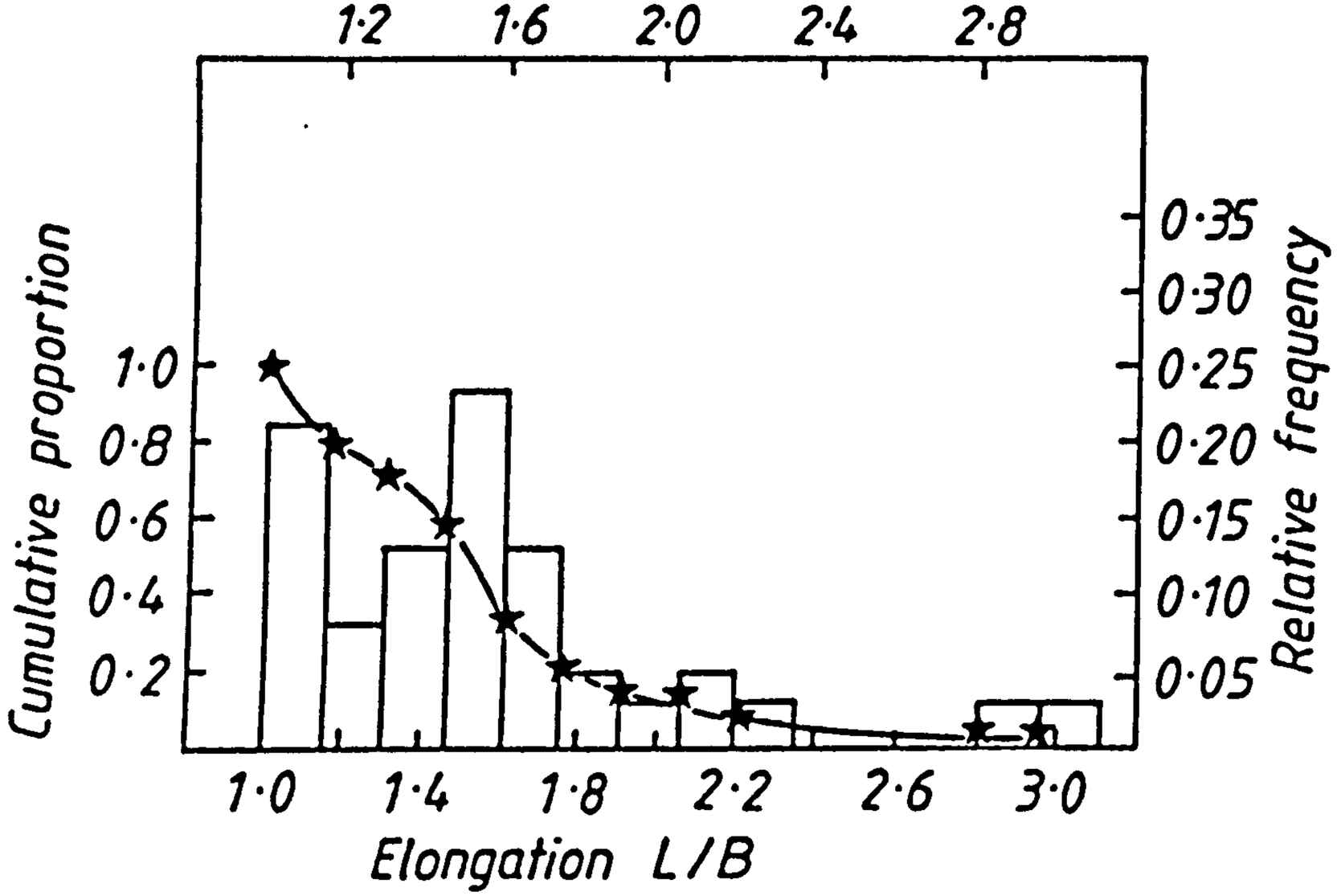

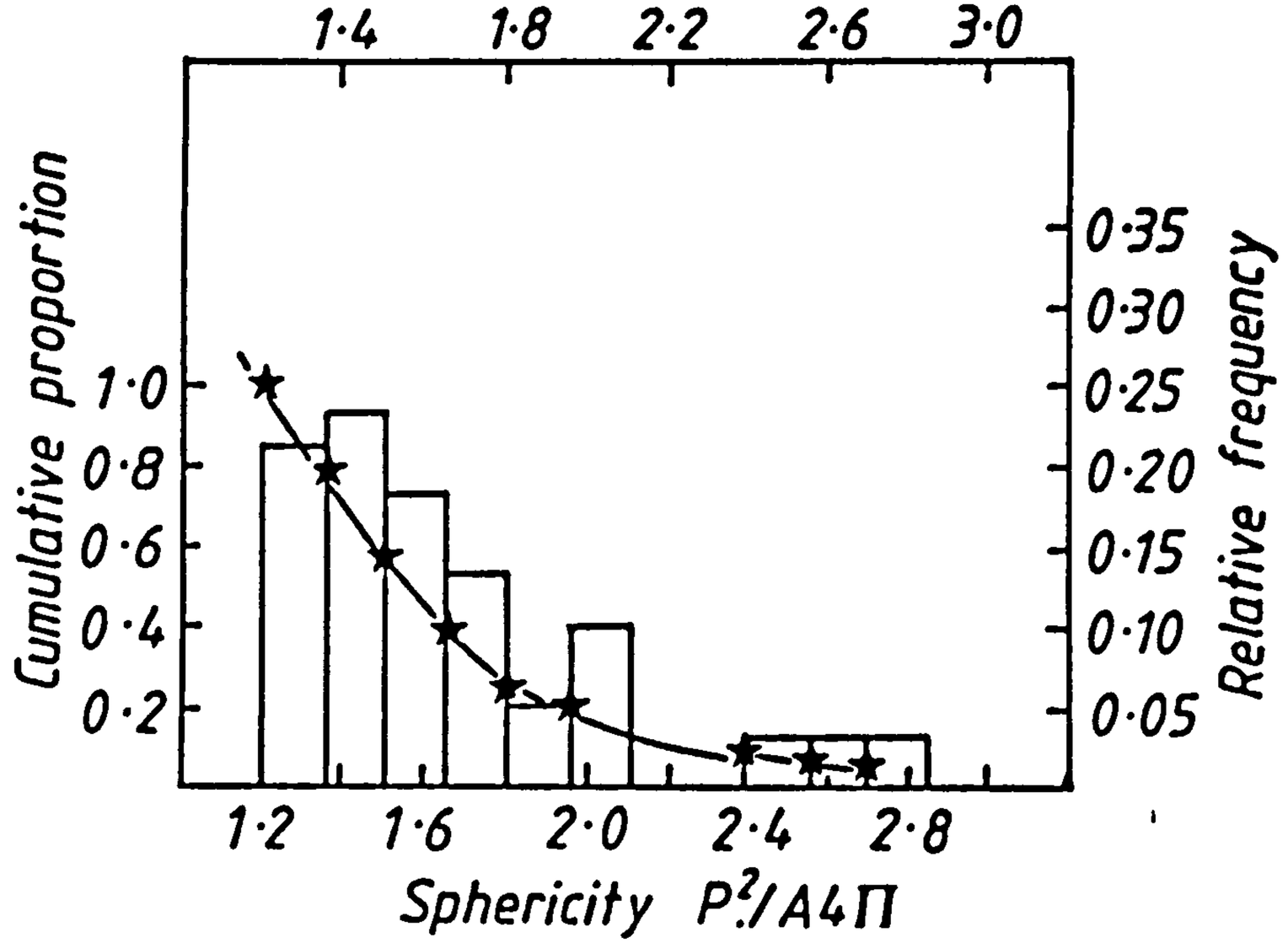

Figure 3.34 *Cumulative and Frequency Distribution of shapes from ball mill (BMa3)*

3.4.3 Fractal measurement

The Quantimet 720 with a software program designed for fractal measurement was used to evaluate the fractal behaviour of two samples of fibrous material (HSCM3 and BMa3) which had already had their shape factors measured (Section 3.4.1).

Tables 3.63 (HSCM3) and 3.64 (BMa3) tabulate the data-printout from this fractal analysis and show a representative format for the other measurements in the present work.

Tables 3.65 (a and b) give summary of data for all the fractal measurements and the regression analysis of the different stride lengths used for the fractal determination of shape of HSCM3 and BMa3 size fractions.

STEP NUMBER	EQUIVALENT STEP SIZE WRT MAX FD	MICRONS	PERIMETER ESTIMATE WRT MAX FD	MICRONS
1	.0111681	1.36809	2.61679	320.557
2	.0196105	2.40228	2.57838	315.852
3	.0281057	3.44294	2.55189	312.606
4	.0366169	4.48557	2.5446	311.714
5	.0451352	5.52906	2.53533	310.578
6	.0536571	6.57299	2.51149	307.657
7	.0621811	7.61719	2.5088	307.328
8	.0707065	8.66155	2.49401	305.516
9	.0792329	9.70603	2.47743	303.485
10	.0877599	10.7506	2.45977	301.322

REGRESSION OF LOG(Y) ON LOG(X)

STEP RANGE	AV. STRIDE LENGTH (MICRONS)	CORRELATION COEFFICIENT	ESTIMATED FRACTAL DIMENSION
1 TO 2	START AT NUMBER:-?1		
STEP SIZE:-?1			
STEP RANGE:-?3			
	1.36809	-1	1.02627
2 TO 3	2.40228	-1	1.02871
3 TO 4	3.44294	-1	1.01074
4 TO 5	4.48557	-1	1.01753
5 TO 6	5.52906	-1	1.05484
6 TO 7	6.57299	-1	1.00719
7 TO 8	7.61719	-1	1.04598
8 TO 9	8.66155	-1	1.05827
9 TO 10	9.70603	-1	1.06937

Table 3.63 Printout for Fractal Dimension and Regression Analysis for HSCM3 Fraction of an individual particle (y = total length (L), X = stride length (η))

STEP NUMBER	EQUIVALENT STEP SIZE WRT MAX FD	MICRONS	PERIMETER ESTIMATE WRT MAX FD	MICRONS
1	.0139601	1.36809	4.20295	411.889
2	.0245131	2.40228	3.79743	372.148
3	.0351321	3.44294	3.60593	353.381
4	.0457712	4.48557	3.53466	346.397
5	.056419	5.52906	3.46397	339.469
6	.0670713	6.57299	3.42614	335.762
7	.0777264	7.61719	3.40939	334.121
8	.0883832	8.66155	3.40586	333.774
9	.0990411	9.70603	3.40639	333.826
10	.1097	10.7506	3.41586	334.754

REGRESSION OF LOG(Y) ON LOG(X)

STEP RANGE AV. STRIDE LENGTH CORRELATION COEFFICIENT ESTIMATED FRSTART AT NUMBER:-?1

STEP SIZE:-?1

STEP RANGE:-?2

STEP RANGE	AV. STRIDE LENGTH (MICRONS)	CORRELATION COEFFICIENT	ESTIMATED FRACTAL DIMENSION
1 TO 2	1.36809	-1	1.18023
2 TO 3	2.40228	-1	1.1438
3 TO 4	3.44294	-1	1.07544
4 TO 5	4.48557	-1	1.09672
5 TO 6	5.52906	-1	1.06364
6 TO 7	6.57299	-1	1.03317
7 TO 8	7.61719	-1	1.00786
8 TO 9	8.66155	.999995	.998823
9 TO 10	9.70603	1	.972983

Table 3.64 Printout for Fractal Dimension and Regression Analysis for BMa3 Fraction of an individual particle (y = total length (L), X = stride length (η))

Estimated Fractal Dimension for Seven Individual Particles at different stride length (HSCM3)

Av. Stride Length µm	1	2	3	4	5	6	7	Row Av. of 7 particles
1.368	1.026	1.034	1.040	1.051	1.172	1.162	1.035	1.074
2.402	1.028	1.024	1.038	1.046	1.136	1.119	1.042	1.061
3.442	1.010	1.034	1.035	1.046	1.099	1.110	1.085	1.059
4.485	1.017	1.015	1.029	1.030	1.101	1.088	1.046	1.046
5.529	1.054	1.015	1.086	1.019	1.114	1.063	1.010	1.051
6.572	1.007	1.029	1.025	1.217	1.128	1.065	1.004	1.067
7.617	1.045	-	-	-	1.153	1.073	-	1.090
8.661	1.058	-	-	-	1.172	1.071	-	1.100
9.706	1.069	-	-	-	-	-	-	1.069
Overall Fractal average for 7 particles								1.068

Estimated Fractal Dimension for Seven Individual Particles at different stride length (BMa3)

Av. Stride Length µm	1	2	3	4	5	6	7	Row Av. of 7 particles
1.368	1.180	1.019	1.210	1.176	1.160	1.031	1.026	1.101
2.402	1.143	1.020	1.098	1.146	1.146	1.049	1.055	1.094
3.442	1.075	1.014	1.097	1.114	1.078	1.026	1.017	1.060
4.485	1.096	1.020	1.171	1.079	1.066	1.037	1.028	1.071
5.529	1.063	1.042	1.120	1.095	1.148	1.040	1.022	1.075
6.572	1.033	1.042	1.098	1.097	1.098	-	1.063	1.071
7.617	1.007	1.079	1.097	1.070	-	-	1.001	1.050
8.661	-	-	-	-	-	-	1.067	1.067
9.706	-	-	-	-	-	-	-	
Overall Fractal average for 7 particles								1.073

Table 3.65 Regression analysis of the Fractal Dimenaion HSCM3

CHAPTER 4

DISCUSSION

4. DISCUSSION

4.1 Morphology

In this thesis considerable attempt has been made to obtain both a comprehensive and a precise description of the particle shape from the liquorice powder under investigation, and to relate a numercial particle shape value to the bulk properties of the powder.

To achieve correct morphological information the data obtained should permit:

I) Production of an approximate sketch of the particle profile.

II) The prediction of the behaviour of a particle in a multi-particulate system.

These criteria can not be achieved by the measurement of a single shape factor. It is thus desirable and beneficial to have more information and more than one shape factor to describe the different morphological aspects of a particle. In the present work four different shape descriptors, which have been recommended and used by many workers (24, 77, 78, 81, 99, 124, 125, 134, 172) were obtained for seventeen milled and classified fractions (Table 3.58). The surface descriptor shape factors ($P^2/A4\pi$ and $(P_V \times P_V)/A$) showed roughly similar values, while the form descriptor shape factors (F_V/F_H and L/B), although similar in terms of an elongation value, are different from the surface shape factors. These two different shape descriptors thus enabled a more efficient distinction to be made between various shaped particles.

The relationship between particle shape and size is shown in Figures 3.29 and 3.30. For both sphericity and elongation shape factors there is a non-linear relationship between shape and size. With milled liquorice from the HSCM as the mean size increased from 50 μm to about 220 μm both the surface and form shape factors

also increased but eventually showed a tendency to decline, but never any independency. However the behaviour of the size and shape relationship for particles in the same particle size range (Figure 3.30) obtained with different equipment (Ball Mill) is quite different. At a particle size of approximately 220 μm there is no sign of any shape factor decrease as particle size increases. The effect that different comminuting equipment has on the size-shape interrelationships may explain the variation seen in the size-shape behaviour reported by different workers, (15, 57, 158, 190, 204, 212). The variation in particle shapes obtained from three different mills with different grinding times revealed that comminution equipment affects the shape of final product of natural fibrous material (Figure 3.31, Figure 4.1) for all size fractions. This is in agreement with work on non-fibrous materials (29, 61, 158, 190). The duration of milling also altered the shape of particles towards a smaller shape factor value (Figure 4.1). This effect on the powder is more prevalent with the Ball Mill products which are generally known to produce more regular shaped particles (88).

Fractal dimensional analysis of both the products of HSCM and BMa size fractions 3 (Table 3.65) showed no noticeable difference for differently shaped (surface and form) particles. The overall fractal dimensions averaged between particles from both HSCM3 and BMa3 milling systems which had different mean shape (surface and form) factors showed no significant difference in fractal dimensions. Beddow (11) indicated that there is a fundamental difference between the structural configuration of a particle and the particle texture. Observation and measurement of the surface and form descriptors of the different particles together with the fractal behaviour indicates an independency between the surface/form factors and the fractal values

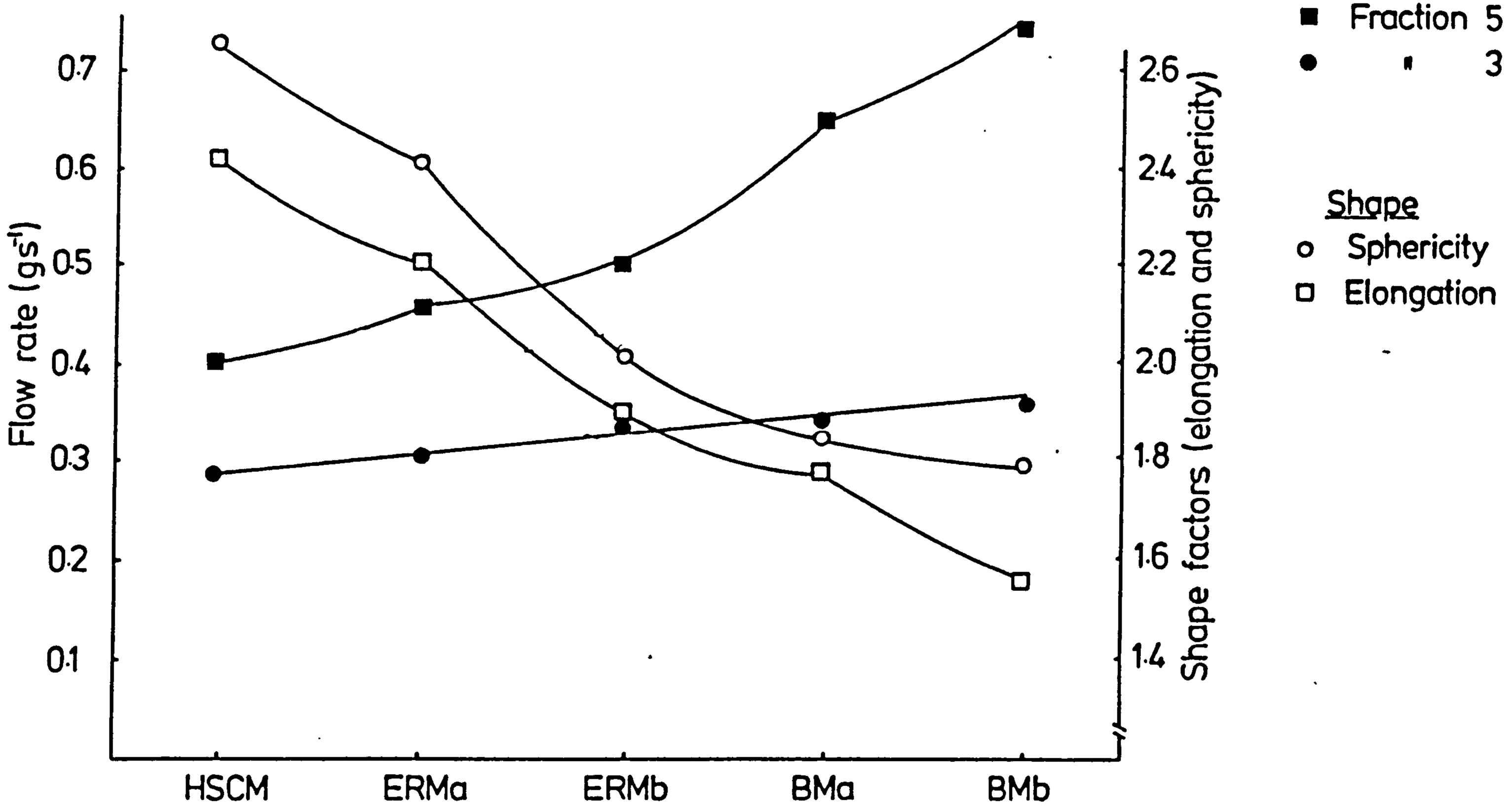

Fig 4.1 Variation of flow rates and shapes (Fraction 5) from different milled products

obtained from the natural fibrous material used in this investigation. This thus supports the original statement that for some materials the determination of shape factors in terms of structural surface and form factor analysis produce more information than fractal dimensions to describe a particle shape characteristic. Although the texture of the mother material may remain the same the particle shape can vary.

4.2 Shape Distribution

The behaviour of bulk powders is the aggregate behaviour of many particles not simply the summation of the behaviour of a number of single particles, thus analogous to particle size and particle size distribution there must be in real systems both particle shape and particle shape distribution.

A particle shape distribution can be expressed either by frequency distribution or a cumulative distribution curve in which the area under the curve is a measure of the total range from minimum to maximum shape factor (Figures 3.32 to 3.35). Shape versus mean size can then show a range of minimum-maximum shape value (Figure 4.2). Information from a shape distribution gives the opportunity to identify with a great degree of certainty the quality of powder and equipment from which particles were processed. Comparison of the HSCM and BMa products in terms of their shape distributions (Figures 3.32 to 3.35) shows that the mechanism of comminution not only affecting the particle shape but also the shape distribution. The difference in shape distribution caused by various equipment is more apparent with large particle size. Size itself has an affect on the shape distribution, as is clearly illustrated in Figure 4.3, shape distribution difference between two types of mills can be observed by comparing the 50 percentile and other percentile values. Generally in shape characterisation a mean shape value is measured, but for greater

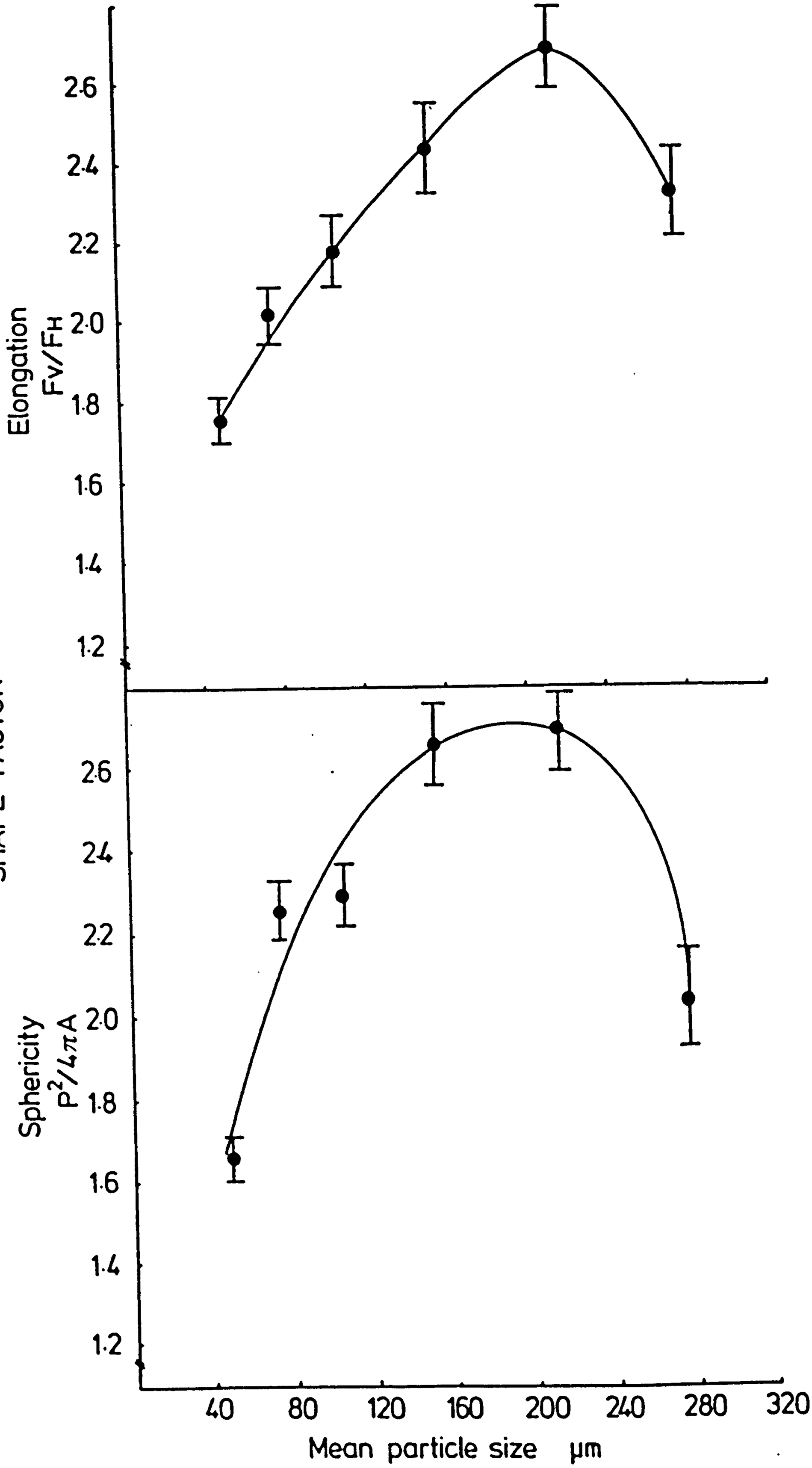

Fig. 4.2 Variation of particle shape with size from high speed cutter mill

Figure 4.3 Cumulative distribution (percentile) defined by elongation for HSCM and BMa, fractions 3(a) and 5(b)

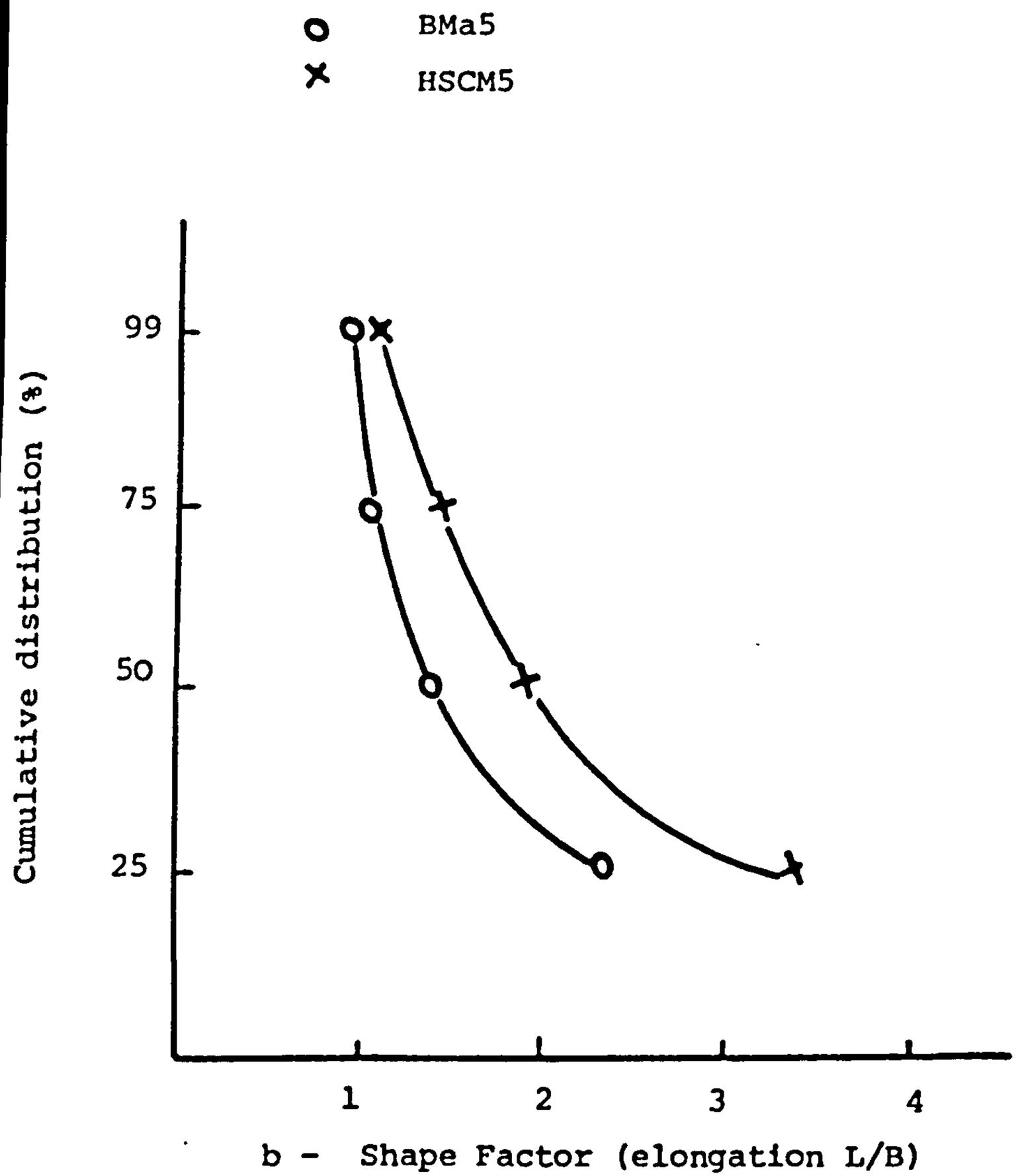

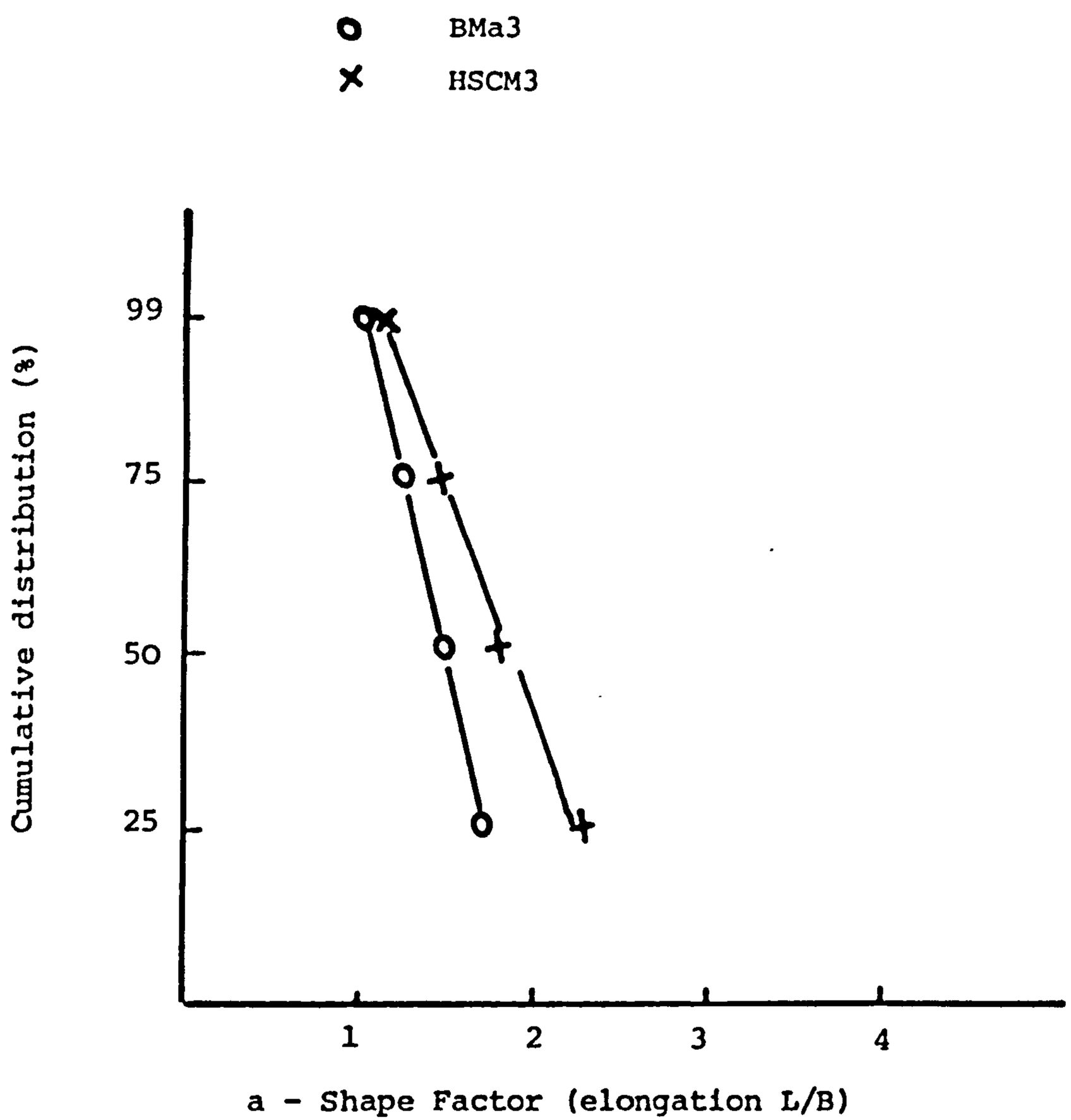

precision other factors also should be measured to allow the statistical analysis to be more effective. In the case of normal distribution of variables (Figure 4.4) a log probability graph shows that the sphericity shape factor for both HSCM and BMa products tend to have a normal distribution with the following 50 percentile values:

HSCM3	=	1.96
HSCM5	=	2.33
BMa3	=	1.53
BMa5	=	1.69

While the overall average values of the same fractions give the following sphericity values (TAble 3.58):

HSCM3	=	2.23
HSCM5	=	2.62
BMa3	=	1.63
BMa5	=	1.86

This indicates that the mean shape factors obtained in the present work are in a great degree of agreement and therefore representative of actual mean values obtained from a normalised distribution, because the deviation between the two values is around or less than 10%. In terms of the shape homogeneity of a system (Figure 4.4 (a-b)) the smaller mean size of the two products have nearly the same slope value (BMa3 = 1.35, HSCM3 = 1.47) and thus no apparent difference can be seen between the two distributions. For size fraction 5 however there is a significant difference between the two distributons (HSCM5 = 4.7, BMa5 = 2.9). These numerical values indicate that the extremes of shape are more abundant for HSCM5 than for BMa5 which has a more homogeneous shape spectrum.

Figure 4.4 (a-b) Log-normal distribution of shape factor defined by $P^2/4A\pi$

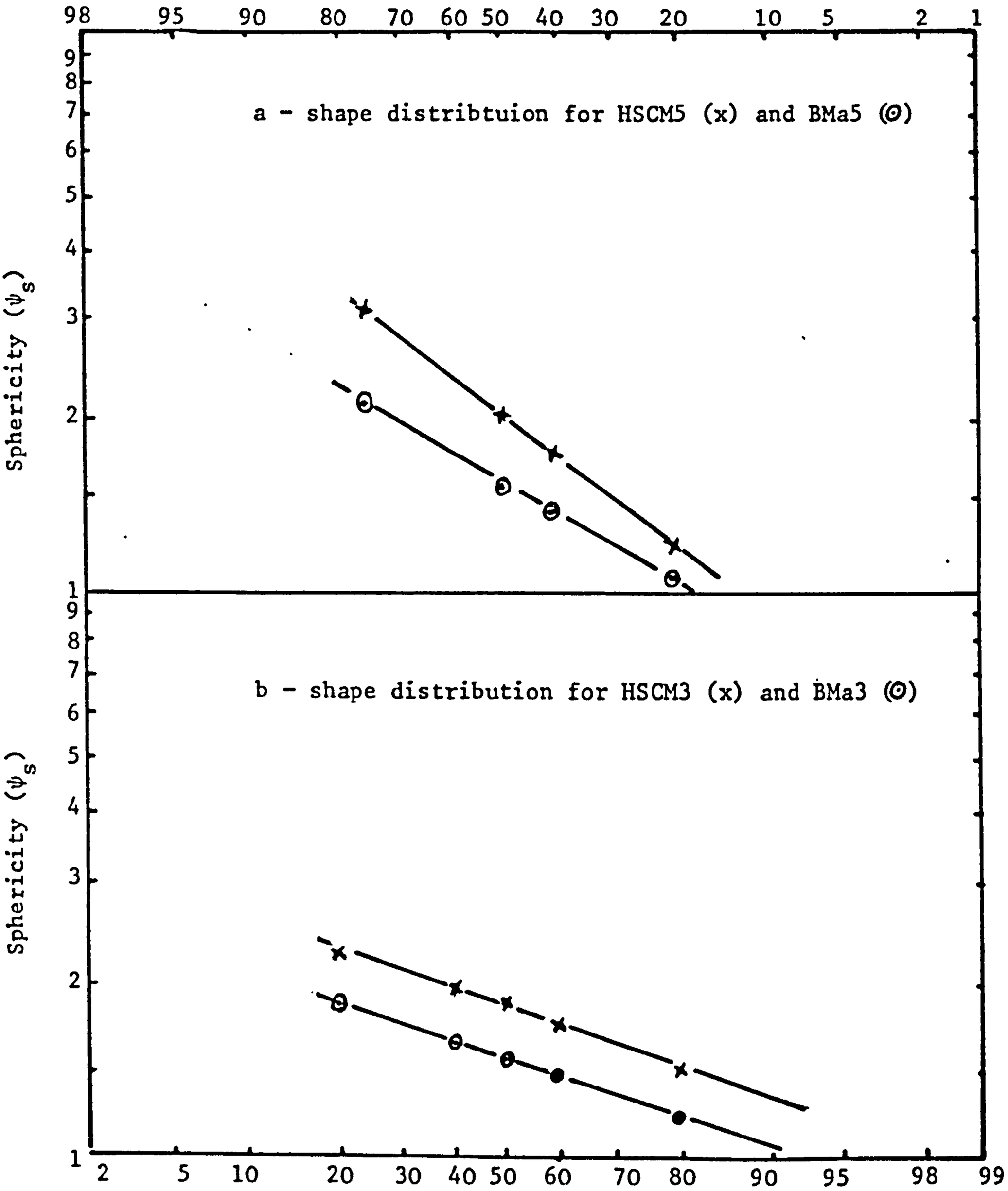

For a pharmaceutical active ingredient where there are minimum and maximum effective levels of drug in blood, it is vitally important to achieve a narrow size and shape distribution, because of the need for absorbtion uniformity.

4.3 Bulk density and rate of packing

The study of bulk and tapped density can provide important information in terms of the storage efficiency of solids. It is desirable therefore to predict the extent of densification without particles deformation or flow obstruction. In tableting and other compacting processes the knowledge of initial packing density and rate of packing is desirable because a higher initial bulk density can transmit the compression forces to deeper layers, and produce a more uniform product better than a product which has a low initial bulk density. It has been shown (120, 130) that the bulk density and rate of packing for hard crystalline and granular material increases as the irregularity of the particles decreases. Table 3.39-a shows that this phenomenon is also applicable for natural fibrous particles. Comparison of the various size fractions from BMa which have small shape factors with the size fractions from HSCM which have a more irregular shaped particle, indicates that any assembly of particles with small shape factors have a greater possibility of achieving a high initial bulk density. The property of bulk density is more sensitive and affected to a large degree by small shape factors (Figure 4.5). When a particulate system consists of a narrow shape distribution with more spherical particles less difficulty is found in the achievement of a closer packing.

The rate of packing is prominently affected when the particle shape factor is less than 1.6 (Figure 4.5-b). The re-orientation of particles with small shape factors is facilitated by tapping and only

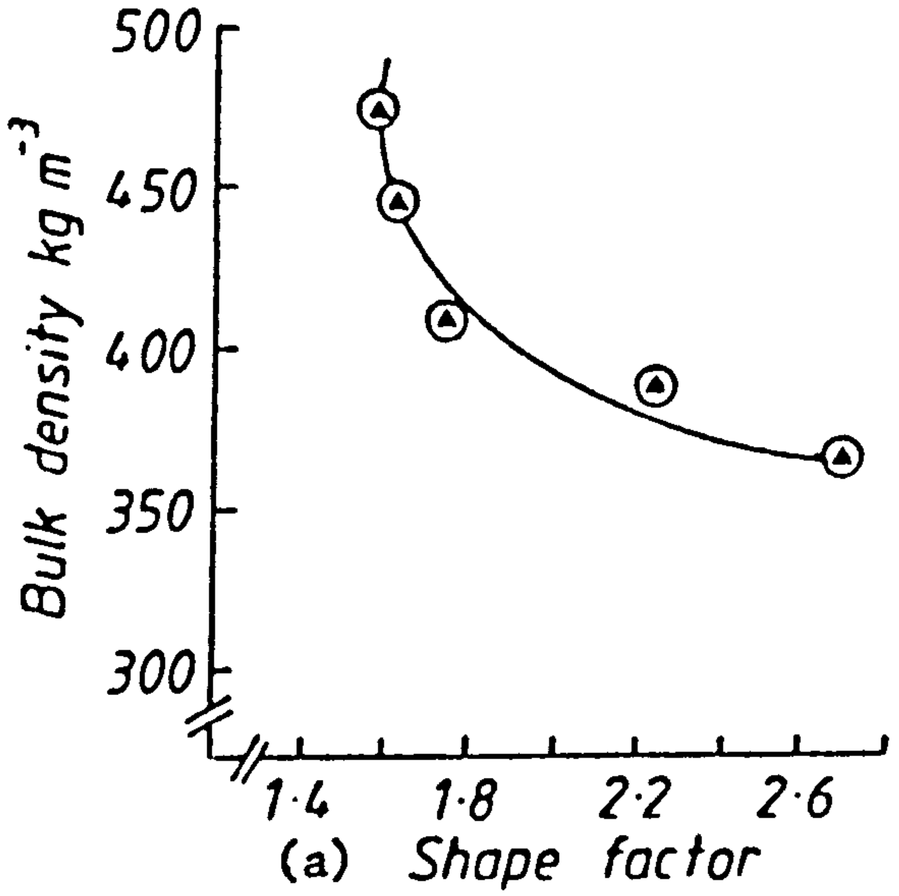

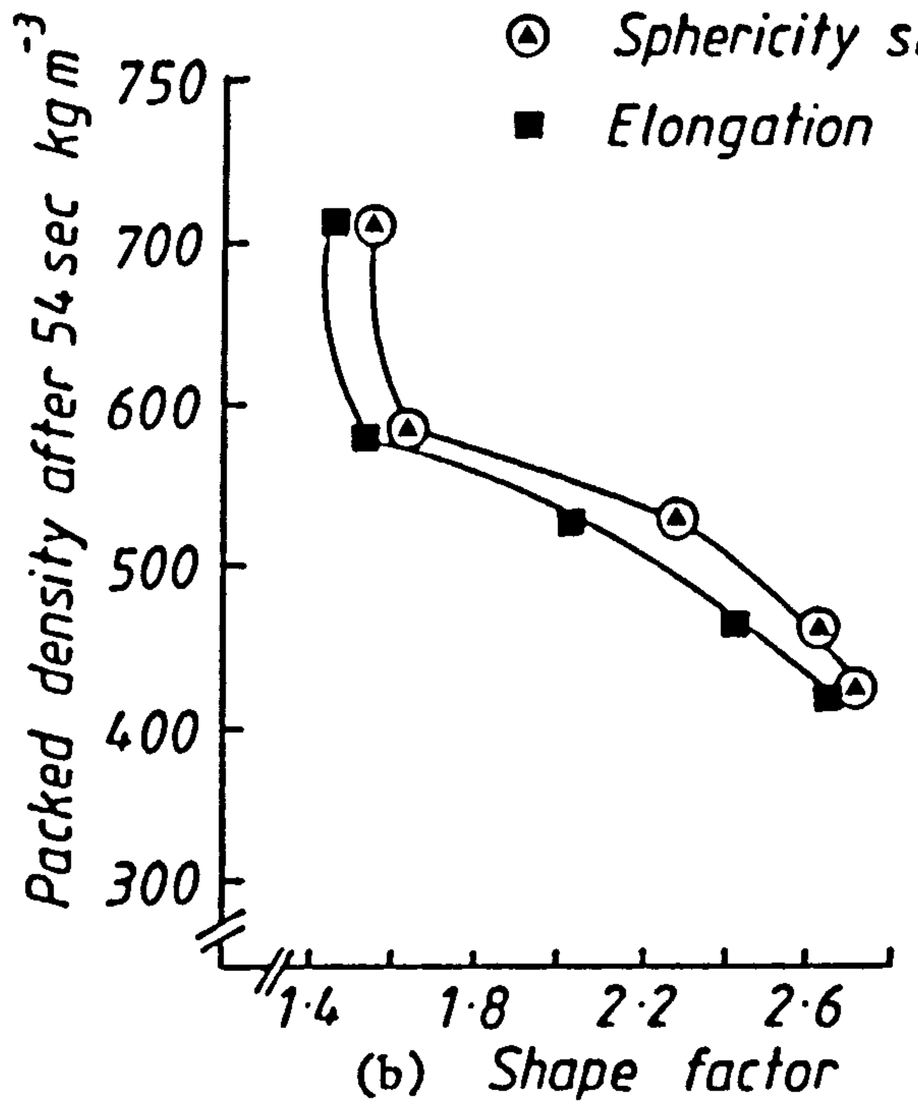

4.5 (a-b) *Variation of bulk and packed densities with shape*

occasionally formation of arches is easily eliminated. With very irregularly and more heterogeneous system when the shape factor is above 1.8 the rate of particle rearrangement becomes difficult and the bed voidage remains high. This can also be seen with large particle sizes (Figure 3.27 b).

Thus both size and shape show an appreciable effect on the rate of packing or tapping time. With a small particle size and shape factor (Fraction 2) the rate of packing at any tap time interval is well over three times that observed with the larger size (fraction 6, Figure 3.27).

For size fraction 2 the higher bulk density can be attributed to the presence of cohesive forces which are lacking in size fraction 6.

Other fractions, from both milled products, showed that as size increased the bulk density also increased except for highly irregular shaped particles (HSCM6). Thus, with a fibrous material the effect of size within a size range normally attributed to the free flow range has a greater dominance than shape. This is in agreement with the work of Gray (67) who used free flowing sands and that of Geotzel (66) who investigated the packing rate of uniformly sized spheres.

4.4 Flow Rate

Because powders are multiparticulate systems the rheological properties of powders are influenced by the factors of size, shape, particle density and the distribution of size and shape. In powders there is an absence of the continuity generally found in liquids. It is not possible therefore with any certainty to predict the flow properties of powders from the physico-mechanical characteristics of a static powder. The relationship found between the mass flow rate and particle size seen with High Speed Cutter ground liquorice product (Figure 3.1) is however characteristic of virtually all material,

although the position and height of the maximum seen in this mass flow-size relationship and the onset where orifice blockage occurs can vary from material to material. The flow behaviour of differently size fractions and various materials may be affected by variation in the physical and or chemical forces acting between particles. The mass flow is less for a product having a more irregular shape of particles (HSCM) than for a product with a more regularly shaped particle (ERM and BM, Figure 3.1).

Some workers observed a correlation between bulk density and flow rate (54, 157). In Section 4.3 it was proposed that the smaller the shape values the greater the rate of packing, therefore the movement of particles down the flow meter should achieve a greater bulk mass with near spherically shaped particles. The mass flow rate for liquorice with a mean shape factor of 1.45 (Figure 4.6) in the free flow size range has a mass flow rate twice that of particles of the same size range but with a mean shape factor of 2.25. The mass-flow rate down an inclined rotating tube in terms of shape is thus similar to that observed with bulk and packed densities.

Therefore, the flowability of milled liquorice in different forms of flow, changes more dramatically with particles having low shape factors (Figure 4.6, 4.5-a, 4.5-b). For particles under a 75 μm mean diameter where particles are in closer contact the possibility of a strong surface force activity may cause particle shape influence on flow to be less dominant (Figure 3.1).

4.5 Flow uniformity

Irregularly shaped particles flow less freely and at the same time do not readily undergo rearrangement into a continous and uniform manner (100). In an analysis of die filling of differently sized (200 - 800 μm) and shaped sands (6) it was found that the coefficient of

Figure 4.6 Variation of flow with shape (sphericity and elongation)

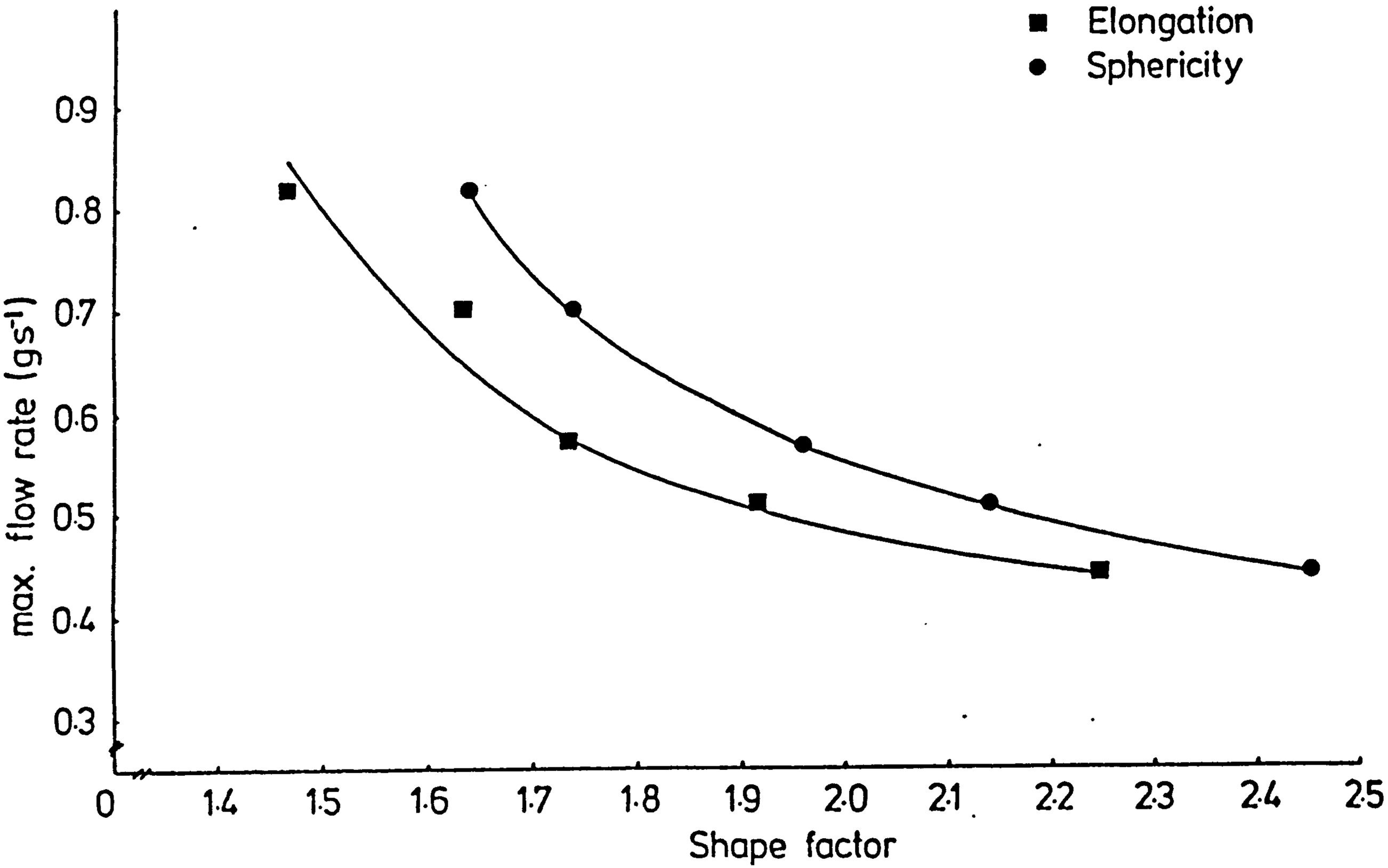

variation of a die fill increased as particle size increased.

The variation of weight for all the liquorice milled products, in terms of the standard deviation around a mean weight (Figure 3.2) collected by the flow meter indicated less weight variation for a certain particle size range and also for more spherically shaped fractions. Increasing the particle size diameter up to certain limit caused a reduction in the failure strength (Figure 4.13) and higher degree of flowability and flow uniformity of the powder. A similar behaviour in the coefficient of flow variation was observed (Tables 3.25, 3.26, 3.27). In the lower size range (50μm) with HSCM (Figure 4.7) a highly non-uniform flow was followed by a constant region of uniformity in the size range 75 - 150 μm until the particle size became large enough to increase the chance of mechanical interlocking and then the coefficient of flow variation sharply increased. Particle sizes <50 μm which have a closer particle-particle contact show a tendency to slip-stick flow behaviour due to surface forces.

Sized fractions from the Ball and End-Runner mills which have low shape factors have a uniformity of flow over a wide size range (75 μm - 225 μm).

It can thus be concluded that there are two distinct phenomena affecting the weight variation and flow uniformity of fibrous material:

I) There is a greater chance of interlocking and mechanical friction between particulate solids in a system which is in the upper size range and have highly irregular shaped particles.

II) Cohesion occurs with small sized particles because of particle-particle surface interaction.

The desirable size range for a homogeneous and uniform flow therefore exists between these two extremes.

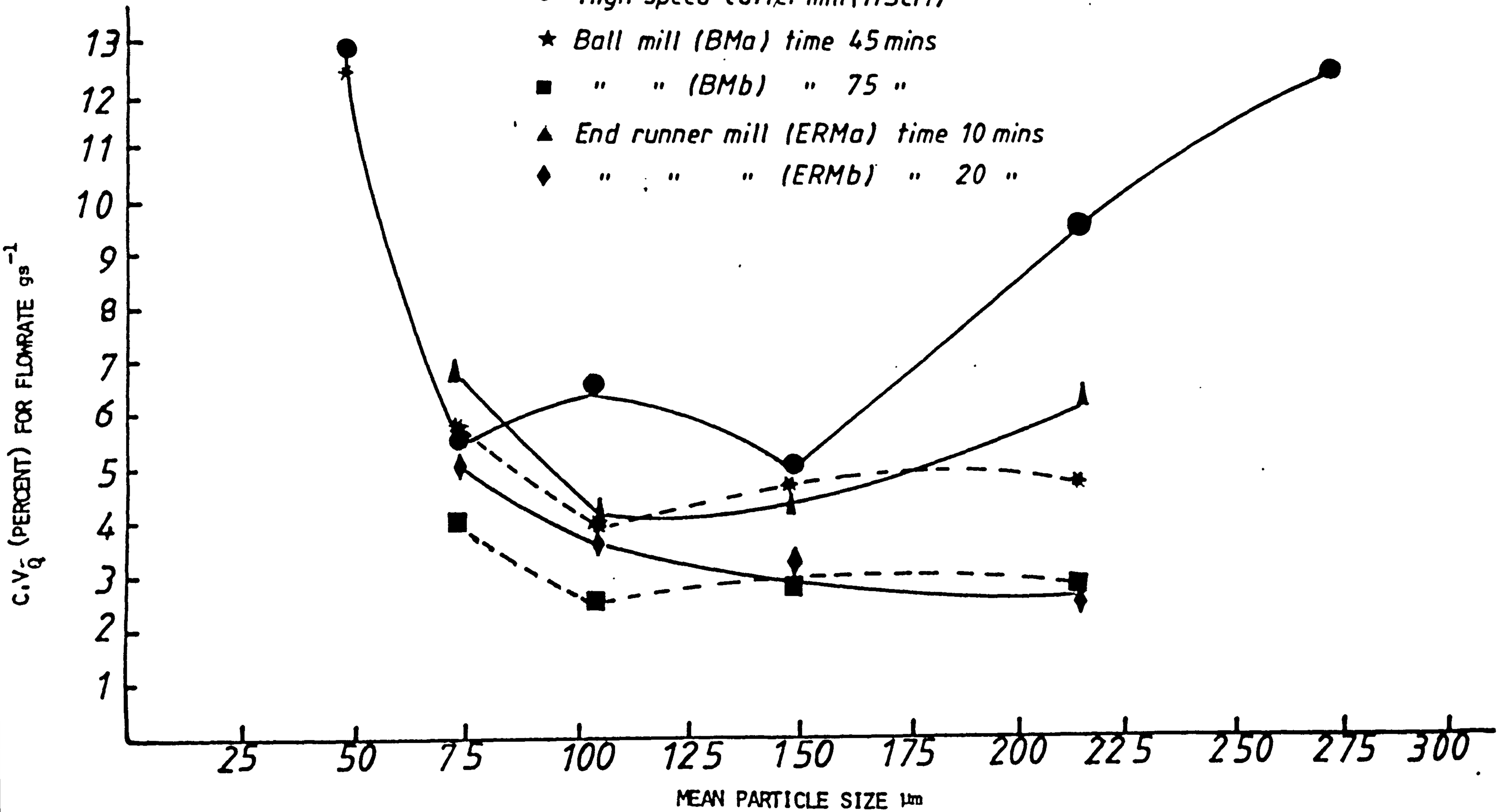

Fig. 4.7 COEFFICIENT OF VARIATION OF FLOW RATE VERSUS MEAN PARTICLE SIZE FROM DIFFERENT MILLS AND MILLING TIMES

4.6 Yield Locus and Failure Properties

It is recommended that many external factors such as moisture, temperature, degradation, consolidation, time and intrinsic phenomena . such as density, particle size and shape affect the flow properties of a powder. The process industries, prefer a simple measurement to characterise the bulk properties of the powder for process control.

To characterise powders, in terms of flow and failure two methods, both based on shear cell experimentation have been suggested:-

I) The method of Jenike et al (94):

failure function (F.F.).

II) The method of Ashton et al (7):

the shear index (n).

In the present work the mechanical and failure behaviour of natural fibrous liquorice powder was measured using the Jenike method to study the parameters of:

I) The internal angle of Friction (δ_E)

II) The unconfined yield stress (f_c)

III) The major consolidation stress (σ_1)

and finally

IV) The failure function (F.F.).

4.6.1 Yield loci for HSCM Fraction 2

An unconsolidated powder has no yield strength. On consolidation air (gas/liquid) is forced out of the assembly of particles and the particle assembly begins to gain strength. Three yield loci at different compaction loads (Table 3.28) were constructed (Figures 3.4 to 3.6) to measure the effective angle of internal friction (δ), f_c and σ_1(Table 3.35). To find also the angle of internal friction (δ_E) the critical state line, obtained from the endpoints of the family of

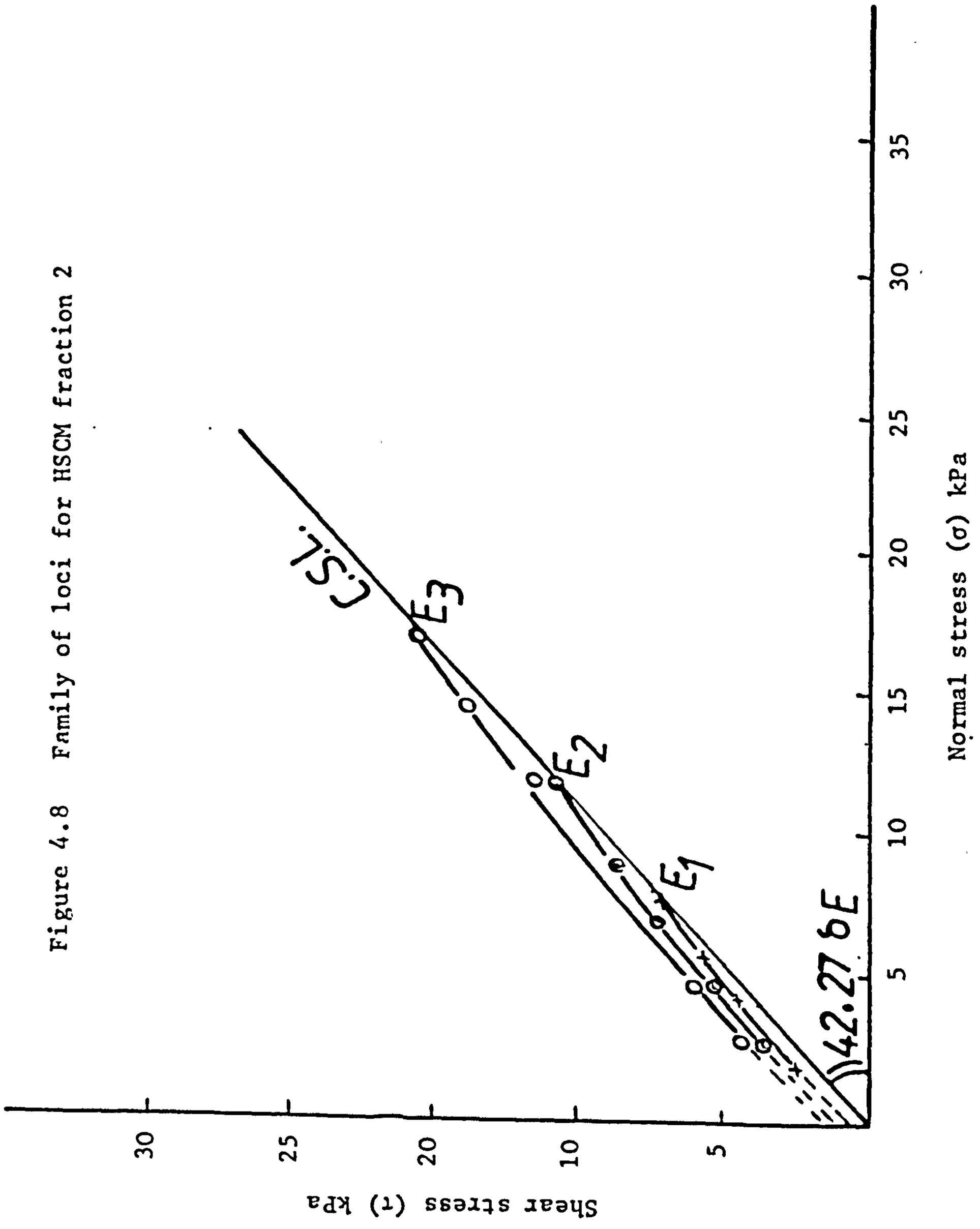

Figure 4.8 Family of loci for HSCM fraction 2

loci, was also drawn (Figure 4.8). δ_E shows nearly the same values as average of three effective angle of internal friction (δ).

The general shape of the natural fibrous liquorice root yield loci show a geometrical configuration similar to that seen with many organic or mineral material previously reported (7, 76, 101, 177, 192, 208), and the failure function behaviour obtained for liquorice categorises it as a simple powder. The HSCM2 family of loci showed some degree of curvature (Figure 4.8) which indicates a mildy cohesive behaviour which will be described in more detail in Section 4.6.6.

4.6.2 Yield loci for Ball Milled size fraction 2 (BMa2)

Using the same compaction loads and experimental conditions as for the HSCM2 sample, three yield loci were obtained for BMa2 (Figure 4.9). Similar parameters as measured for the HSCM2 fraction were evaluated, and the general shape of the yield loci is similar to that observed from the High Speed Cutter milled products. The striking difference between these two size fractions is the variation of the angle of internal friction which for HSCM2 was 42.27^{o} while for the BMa2 was 41.5^{o}. This difference of similar sized fractions must be attributed to the different shape factors (Table 3.58) and its influence on δ_E. The BMa2 sample with less irregular shaped particles will produce less friction during the shear test unlike the more irregular shaped particles of the HSCM2 fraction. The difference observed between the values of δ_E are not however of a great magnitude because:

I) The differences between the particle shape factors are small (e.g. HSCM2 = 1.755, BMa2 = 1.587 by sphericity, and HSCM2 = 1.907, BMa2 = 1.703 by elongation).

II) The particle size fractions are in a relatively small

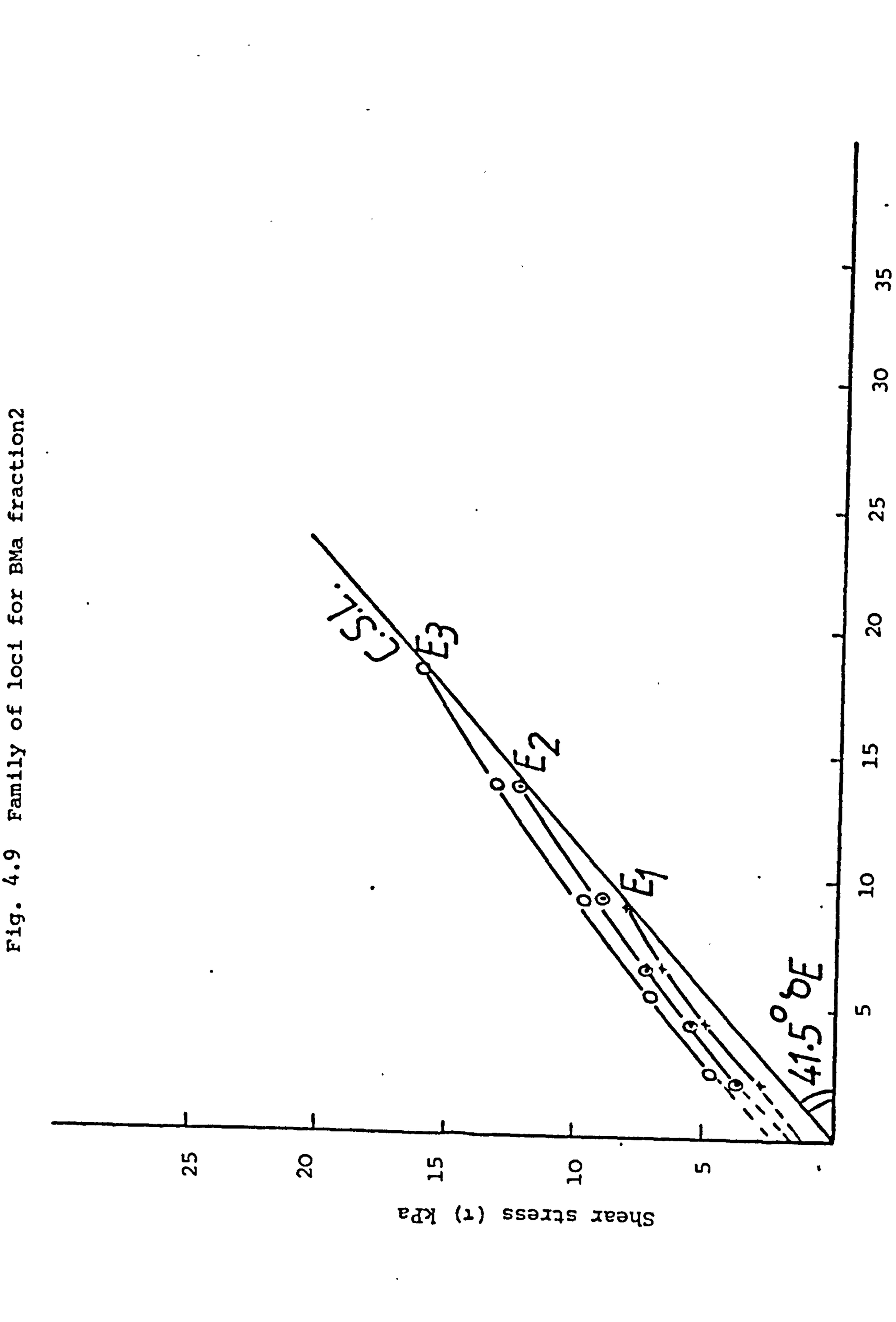

Fig. 4.9 Family of loci for BMa fraction2

particle size range and the high surface forces involved may be more predominant than the effect of shape.

4.6.3 The yield loci for HSCM3 and HSCM5 size fractions

From the Tables 3.29 and 3.30 the yield loci at different compaction loads were constructed (Figure 4.10 -a, b).

From these families of yield loci the yield lociwere seen to be nearly linear, particularly for fraction five (HSCM5). This indicates a high degree of free flowing behavour. As the particle size increases the compressibility of the material decreases, because of the absence of measureable cohesive forces between these sized particles. The angle of internal friction (δ_E) also showed a significant increase as size increased. Kocova and Pilpel suggested that the angle of internal friction is probably the most important and useful parameter to evaluate and characterise an assembly of particles. The angle of internal friction is dependented upon both the size and shape of particle in the assembly.

The angle of internal friction also measures the difficulty of maintaining steady state or constant volume flow. This can be monitored by comparing δ_E from different HSCM size fractions. A higher work and energy content needed to reach the equilibrium endpoint for a higher δ_E. Thus the coarser the material, the more difficult it becomes to maintain a steady state of flow without volume change.

In terms of shape, the sample HSCM5 (Table 3.58) has the higher shape factor and thus is more irregular as well as being of a large particle size. The variation of δ_E from these two samples (HSCM3 and HSCM5) must not therefore be due only to the particle size, but must also include the factor of shape. Individual particles do not move in straight lines within a shear cell but tend to move up and down the

Fig. 4.10 Family of loci for HSC3(a) and HSCM5(b) fractions

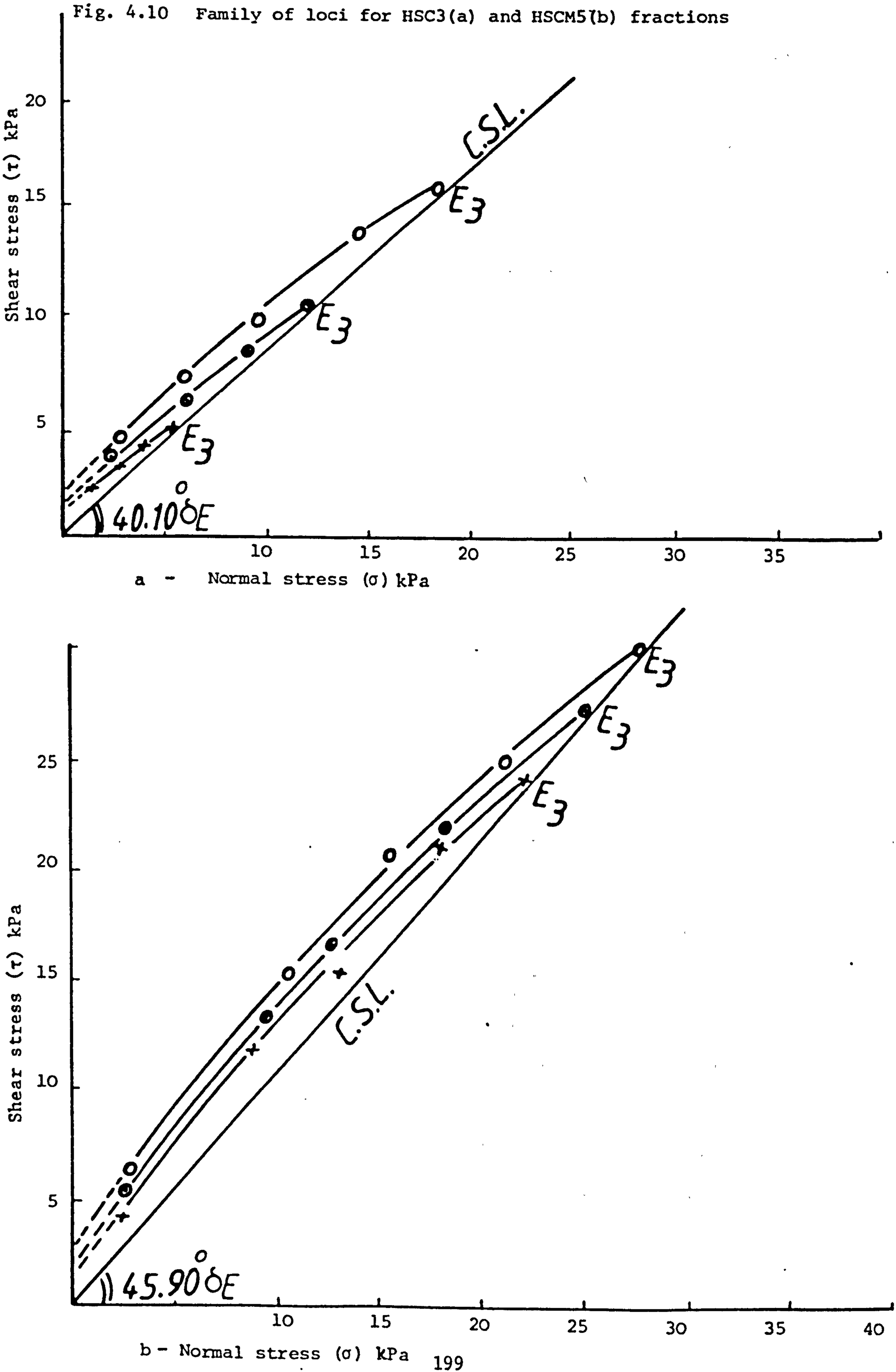

cell as particles pass over each other. Work done by the shear force is dependent upon the length of particle travel and particle surface irregularities. This may explain why the angle of internal friction increases with increase both in size and shape. To support the statement that "the shape effect is even more significant than size" similarly sized fractions with different shape factors should be compared. This will be discussed in Section 4.6.4.

4.6.4 Yield loci for BMa3 and BMa5 Fractions

From Tables 3.33 and 3.34, families of yield loci were constructed (Figure 4.11 -a,b). Similar to the HSCM samples, the BMa products also showed that as particle size increased the angle of internal friction increased.

Because the BM particles have smaller shape factors compared to the HSCM fractions (Table 3.58) the difference between the δ_E values of BMa products were also smaller.

Comparison of Figures 4.10 (a,b) and 4.11 (a,b) show that as the shape factor of the similar sized fractions increased the angle of internal friction also increased. In the free flowing size region the effect of shape on the internal angle of friction is more predominant than size because when two identically sized powders are taken (HSCM5 and BMa5) the shape factor difference (ψ_s (HSCM5) - ψ_s (BMa5)) was 0.72 and caused an increase in the internal angle of friction of 4.35 degrees. When however the mean size (BMa3 and BMa5) having a shape difference of 0.122 changed from 76 μm to 152μm, or infact doubled, the internal angle of friction increased only by 3.10 degrees. With HSCM3 and HSCM5 fraction the shape difference was 0.392 which gave an increase in internal angle of friction of 5.80. Thus this substantiates the statement that the affect of shape is more significant than size on the internal angle of friction measurements.

Figure 4.11 Family of loci for BMa3 (a) and BMa5 (b) fractions

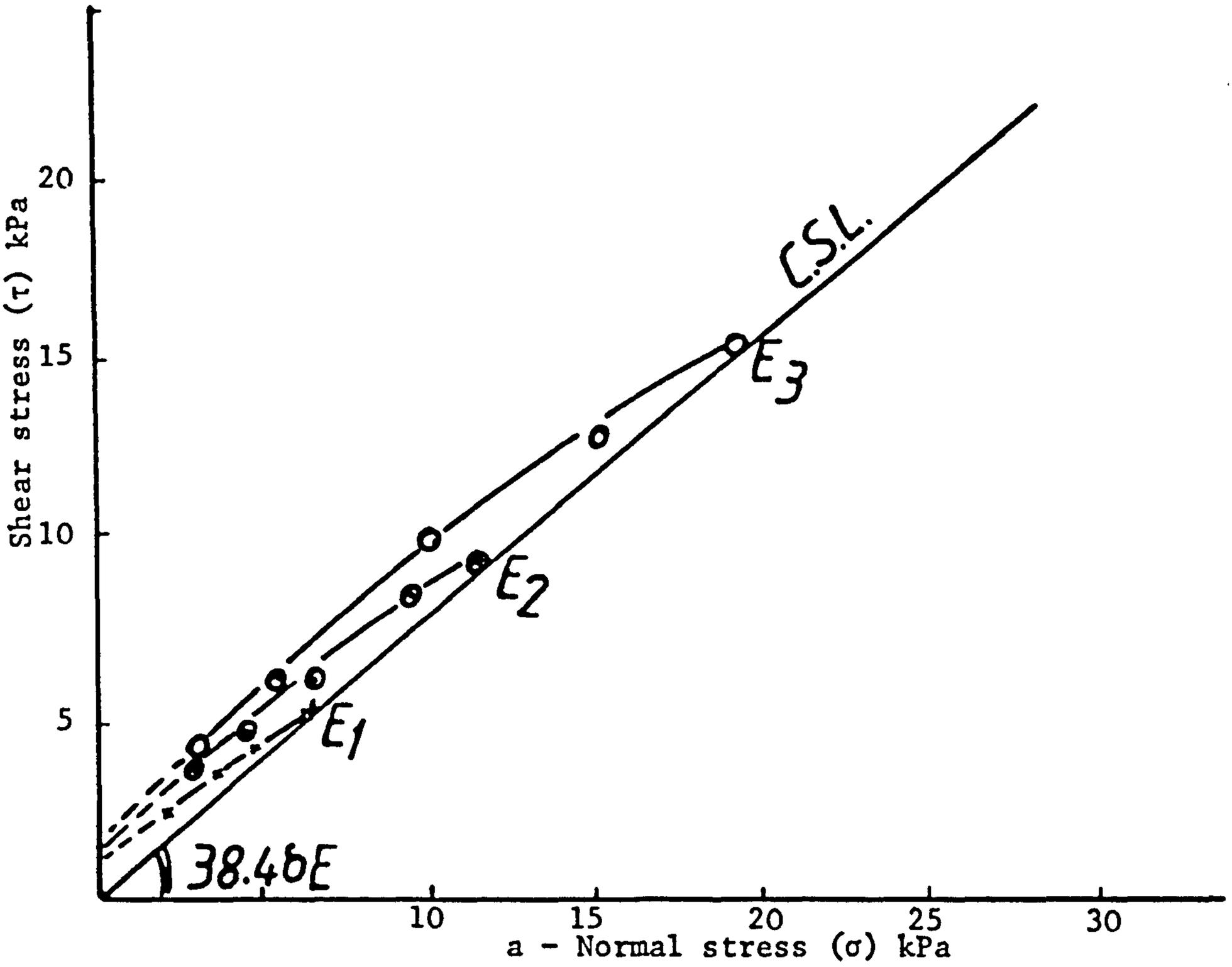

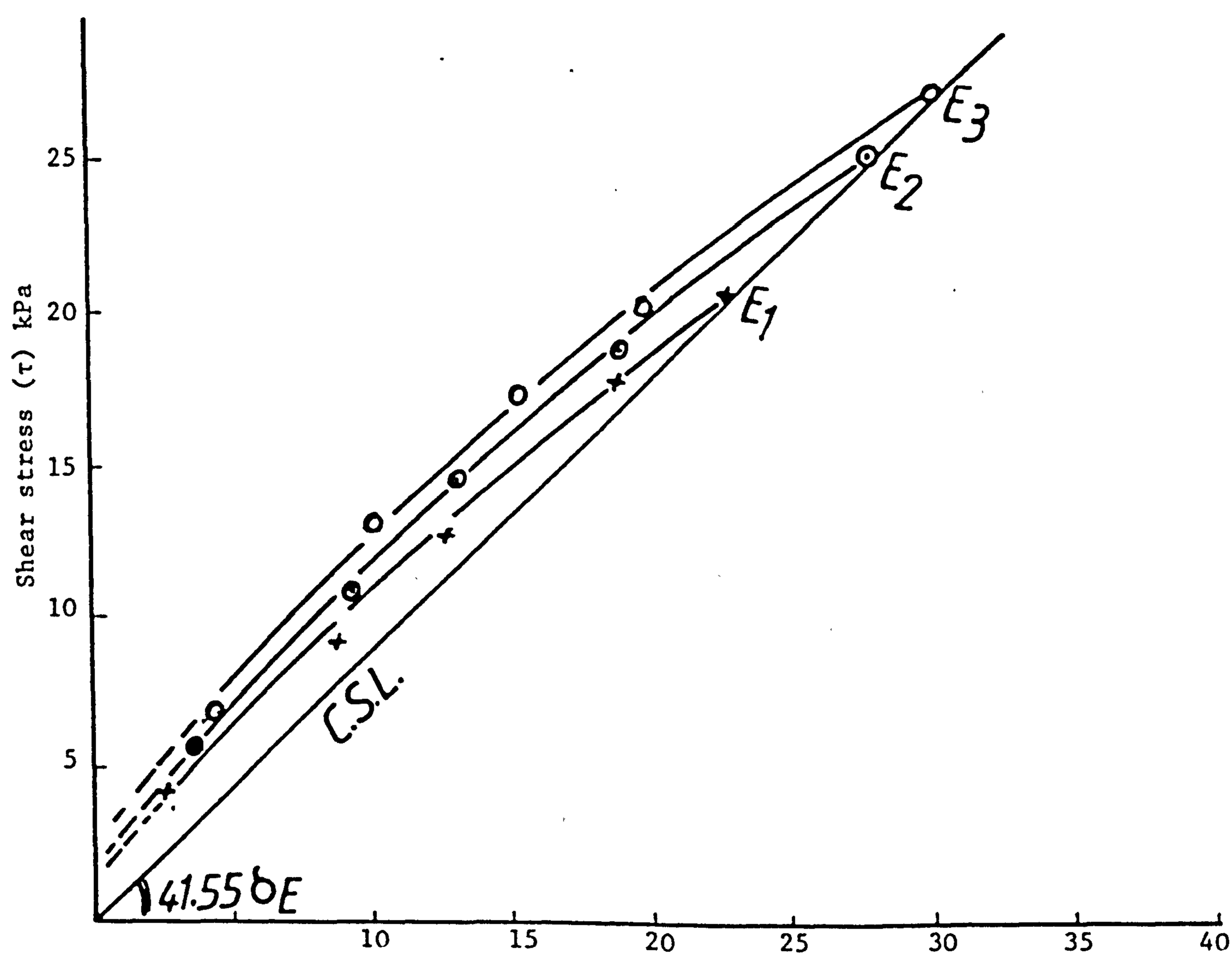

In this study forparticles having a mean diameter over 75 μm the fibrous material behaved as a free flowing material (Section 4.6.6), where C, in the Coulomb equation (1.7), is small. The angle of internal friction thus becomes an important failure factor and tends to modify the Coulomb friction equation to become $\tau = \sigma \text{Tan}\, \delta$.

The above fact can also explain why the more spherical particles from the BMa5 fraction has a much higher flow rate, measured by flow meter (Section 4.4), and also higher rate of packing (Section 4.3), compared with the HSCM5 fraction.

Pilpel and Walton (141) indicated that an increase in the particle shape coefficient decreases the range of forces of attraction between the particles which decrease the power of cohesion. In section 4.6.6 it will be shown that size fraction 2 with a smaller shape factor showed a higher cohesive property.

4.6.5 Yield loci for a HSCM-mix

The powder sample HSCM-mix is a combination of four size fractions from the size fractionated HSC milled products (Section 3.2). The shear and normal stresses for three yield loci of this mixture are given in Table 3.31. The angle of internal friction for the HSCM-mix (figure 4.12) is relatively high (43.76°) but this is not unexpected because about 90% of the powder mixture is in the middle to upper size limits which have also high shape factors. On visual examiantion of the yield loci and comparison with the individual size fractions yield loci from the mono-sized systems, it can be seen that the HSCM-mix yield loci become less linear and with larger distance between each yield locus. These observations for HSCM-mix indicate a less free flowing and a more compressible powder. During application of a compaction load smaller particles within the HSCM-mix can move through the interparticle space produced by the large particles in the

Figure 4.12 Family of loci for HSCM-mix

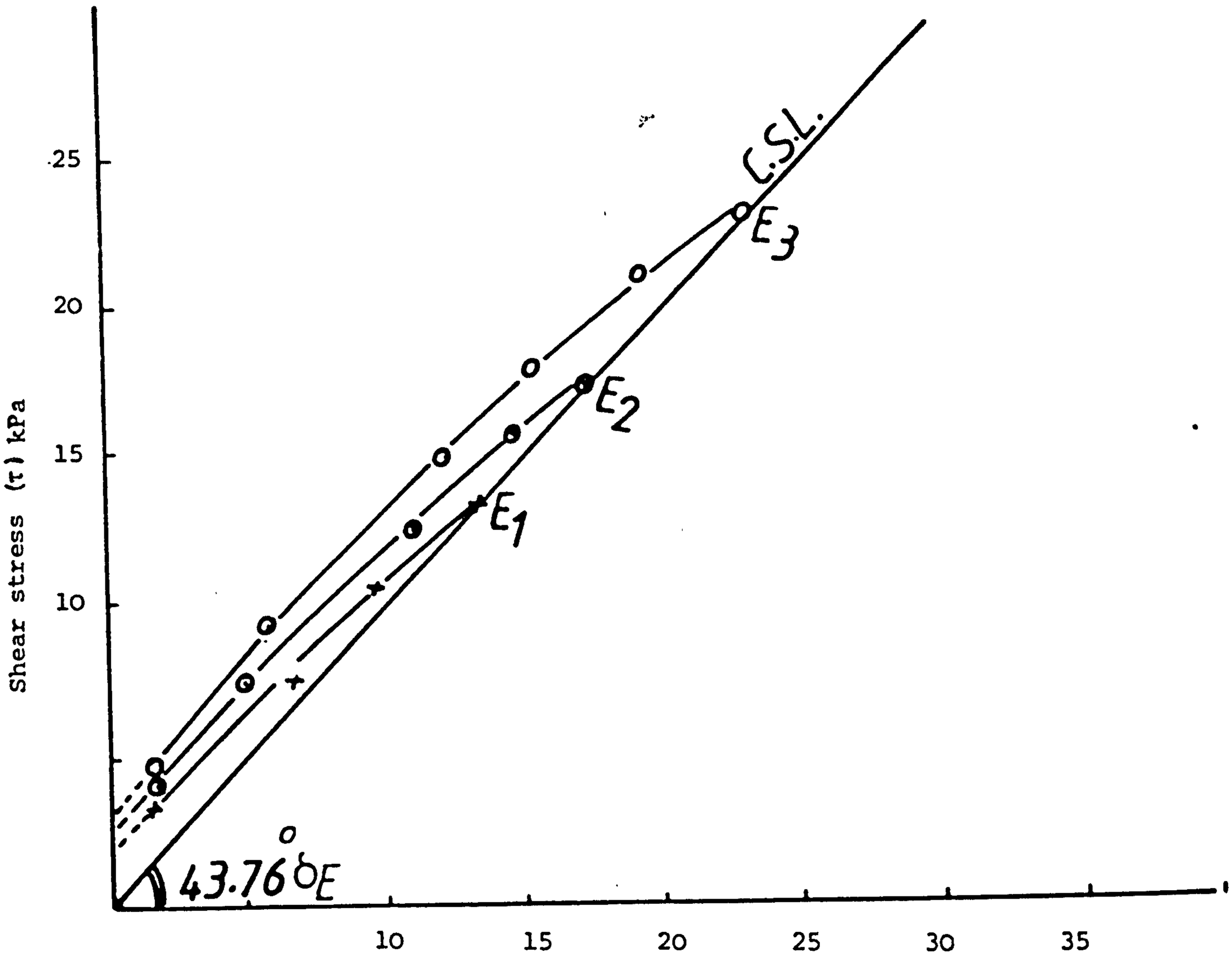

mixture. As compaction increases more volume change is thus possible to give a better compaction with multisized systems than with monosized systems. This assumption together with the possibility of the coating of larger particles with fine particles, which could act as binding agents, may explain why the addition of a small portion of a mildly cohesive body can change radically the flow characteristics of a multiparticulate system. In an investigation of limestone failure (109) it was shown that the most influential factor on failure was the proportion of fine particles in the system.

4.6.6 Failure Functions (FF)

The failure functions of seven size fractions (Table 4.1) of milled liquorice powder (HSCM and BMa) were obtained from the unconfined failure (yield) strength (f_c) and the major consolidation stress (σ_1) (Figures, 3.4 to 3.24 and Table 3.35). According to Jenike (Section 1.3.4) powder failure functions are the most important and acceptable parameters for the analysis of powder cohesion and flowability.

I) <u>The failure functions of HSCM2, HSCM3 and HSCM5.</u>

A linear relationship exists between f_c and σ_1 passing through origin for all size fractions (Figure 4.13). The failure behaviour of this fibrous powder is similar to many organic and inorganic powders (Section 4.6.1) and milled liquorice can be termed a "simple" or "regular" powder.

For many powder mixtures (Stainforth, Kocova and Pilpel) the instantaneous failure functions of a material do not pass through the origin. Small particle sizes when mixed with soft and large particles (i.e. filler or polymer), can under stress create and increase the number of physical bonds between particles, which in turn can affect the shape of the yield loci and subsequently the

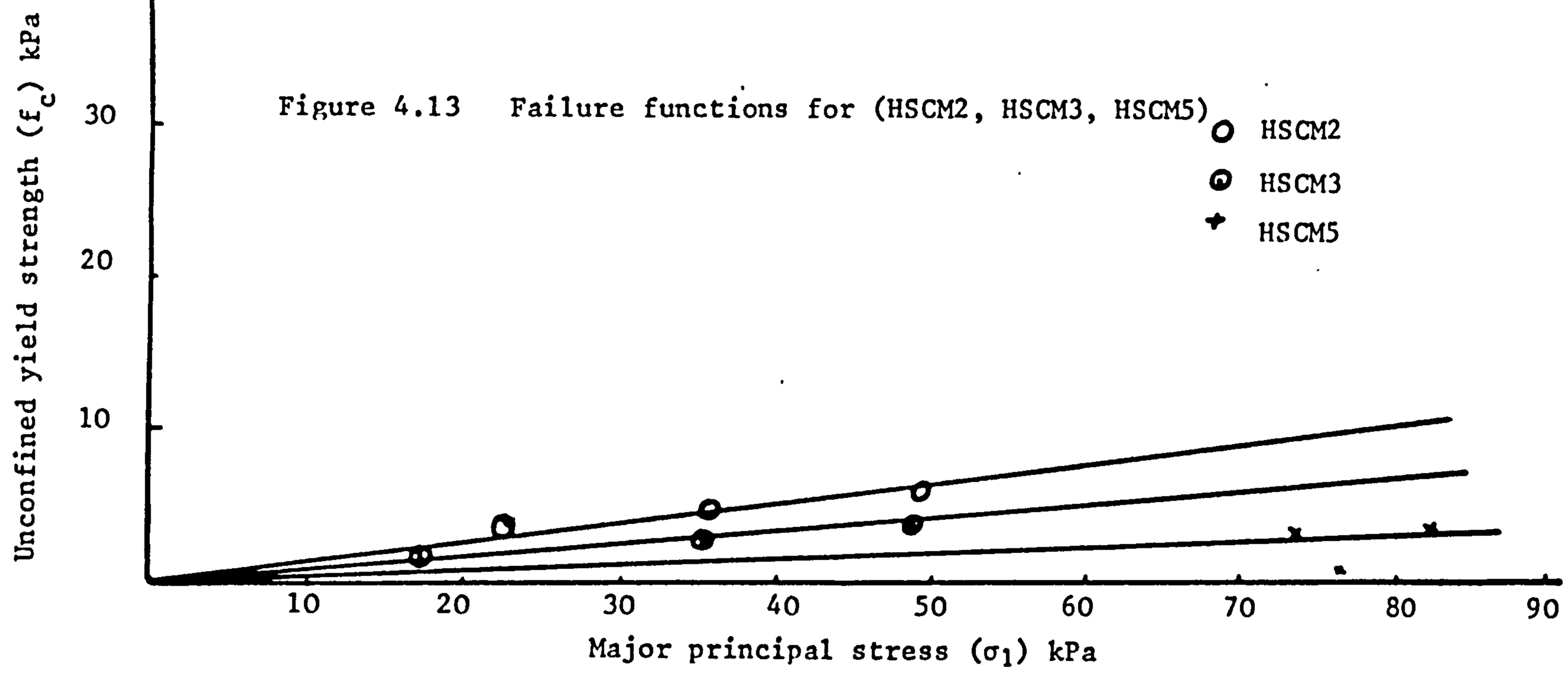

Figure 4.13 Failure functions for (HSCM2, HSCM3, HSCM5)

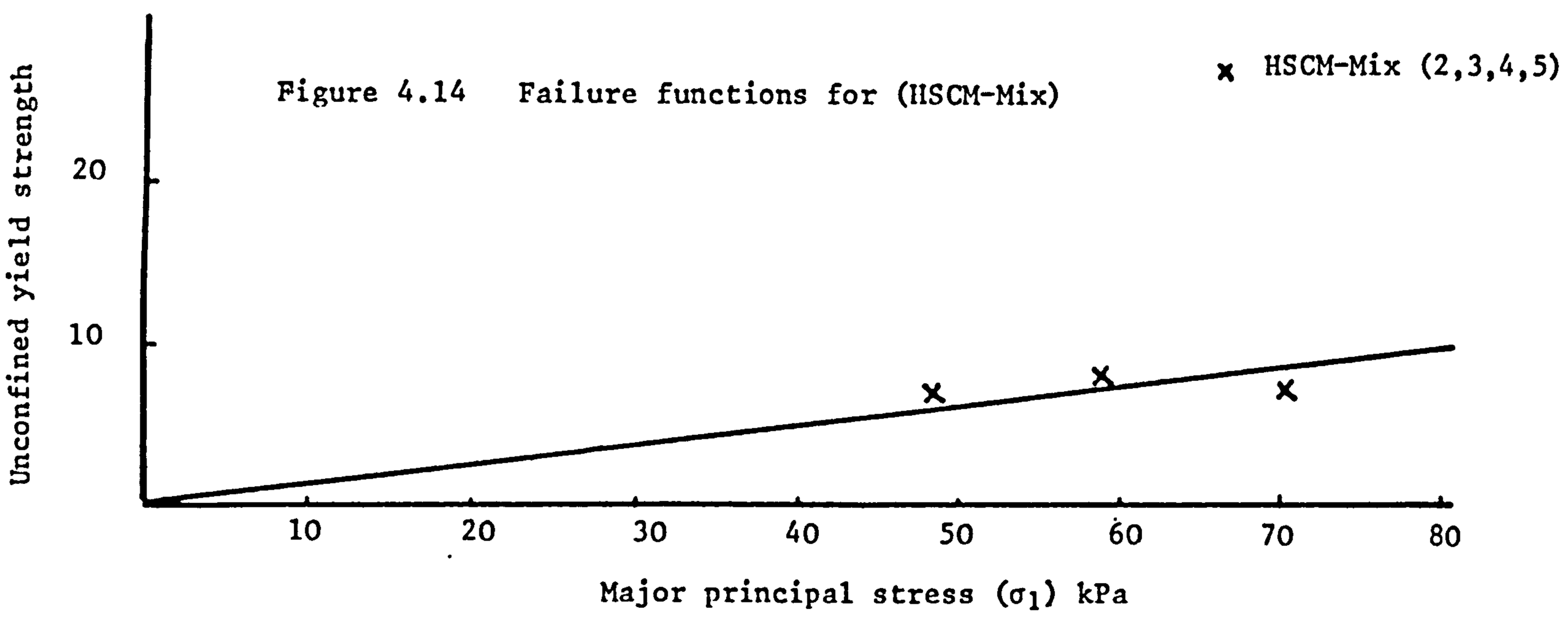

Figure 4.14 Failure functions for (HSCM-Mix)

failure function. This type of material is generally termed a complex or irregular powder.

According to Jenike's classification, Figure 4.13 indicates that the flowability of the liquorice powder increased as particle size increased. The basis of the Jenike failure function (F.F.) is that the unconfined yield strength (f_c) of a powder is a function of the consolidating stress (σ_1) applied during the sample preparation. Small value of, f_c, in relation to the value of, σ_1, will indicate a non-compressible free flowing powder. As the ratio of σ_1/f_c becomes larger, which is the case for the samples, HSCM5> HSCM3> HSM2 in the present work, flowability increases. For the large size fractions compared with small sizes the material is less compressible and does not consolidate to gain strength. Figure 4.13 and the failure functions values (Table 4.1) show that HSCM2 behaves as a mildly cohesive powder while HSCM3 and HSCM5 are free flowing powders.

II) <u>The failure function for the HSCM-mix.</u>

In Section 4.6.5 it was postulated that the introduction of small portions of fines to an assembly of individually free flowing particles can initiate a considerable change to the failure property and flowability of the resultant mixture. This postulate can be supported by observation of the failure function and the value obtained from HSCM-mix (Figure 4.14) which falls into a mildly cohesive classification.

III) <u>The failure function of BMa2, BMa3 and BMa5.</u>

Figure 4.15 shows the failure functions obtained from the different size fractions of the Ball milled product. In terms of different sizes the flowability behaviour is similar to that seen with the High Speed Cutter milled product of the same size

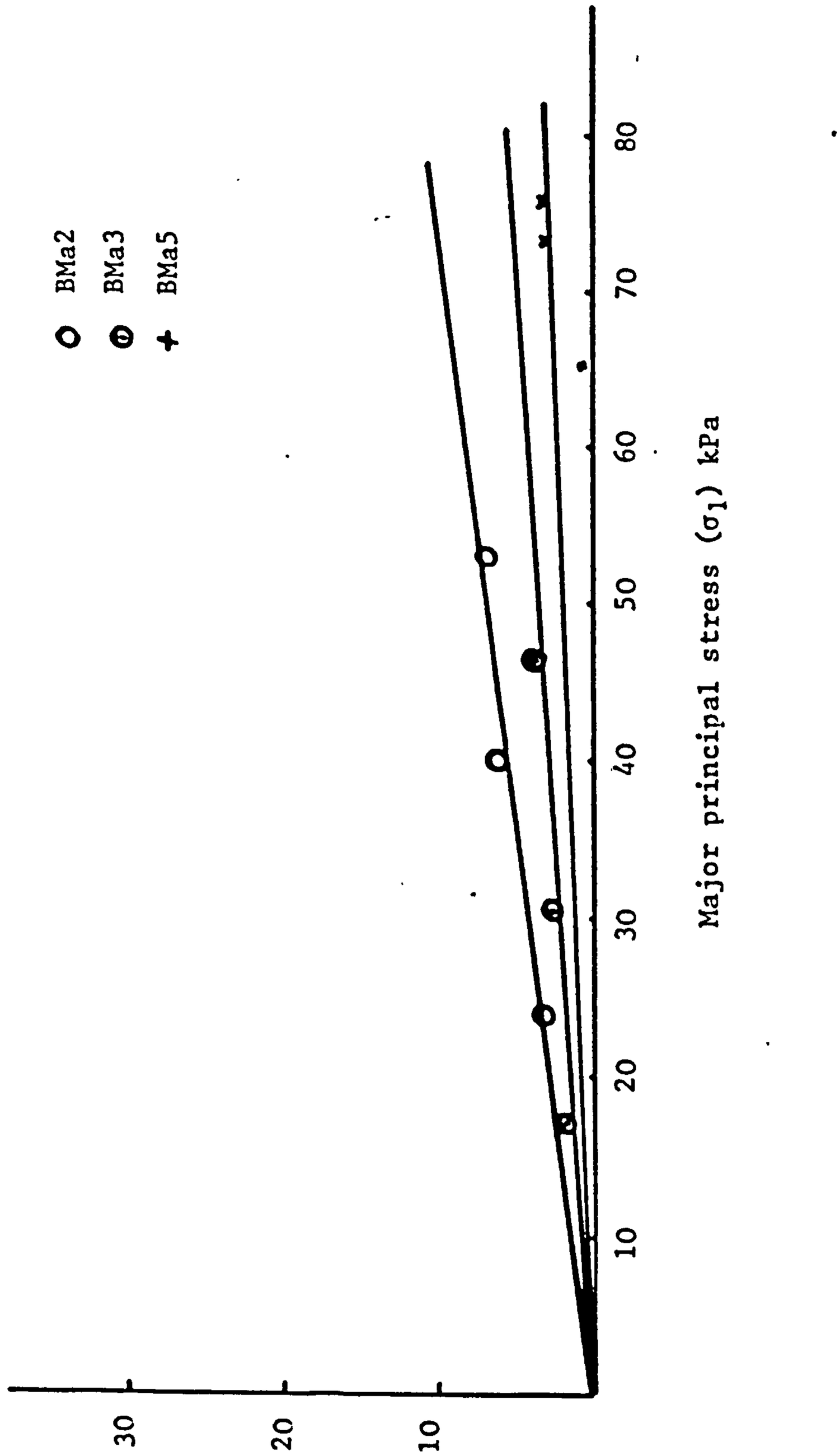

Figure 4.15 Failure Envelope Functions for (BMa2, BMa3, BMa5)

fraction.

The effect of particle shape on the failure function can be studied by comparing the products for these two mills. For the size fractions 2 of both products in the cohesion region the influence of shape on flowability is not appreciable possibly because of the effect of surface forces. The more spherical BMa2 fraction, compared to the HSCM2 fraction showed a slightly smaller failure function value (BMa2 = 7.21 and HSCM2 = 7.77) or more cohesion. A less flowability behaviour was also observed for more spherical particles in lower size range with the flow from flowmeter (BMa2 = 0.15 gs^{-1}, HSCM2 = 0.17 gs^{-1}).

This follows the work of others (141) where the effect of shape has an affect on the force of attraction in the cohesive region. However in the free flowing range the failure function values increase as the shape factors decreased.

Table 4.1 shows that the failure function is highly correlated with the flow rate of a fibrous powder down the designed inclined flowmeter.

Size Fraction	Mean Size μ m	Angle of internal friction degree	Failure Function FF	Flowrate g/s (Q_r)	Shape factor ψ_s (sphericity)
HSCM2	50	42.27	7.77	0.174	1.755
HSCM3	76	40.10	11.50	0.290	2.233
HSCM5	152	45.90	21.80	0.400	2.625
BMa2	50	41.50	7.21	0.155	1.587
BMa3	76	38.40	14.28	0.330	1.638
BMa5	152	41.55	22.72	0.650	1.860
HSCM-mix	mixture	43.76	8.128	0.309	2.49(app)

Table 4.1 Comparison of bulk and particle characteristics between HSCM and BMa fractions

CURFIT GRAPH OF USER FUNCTION

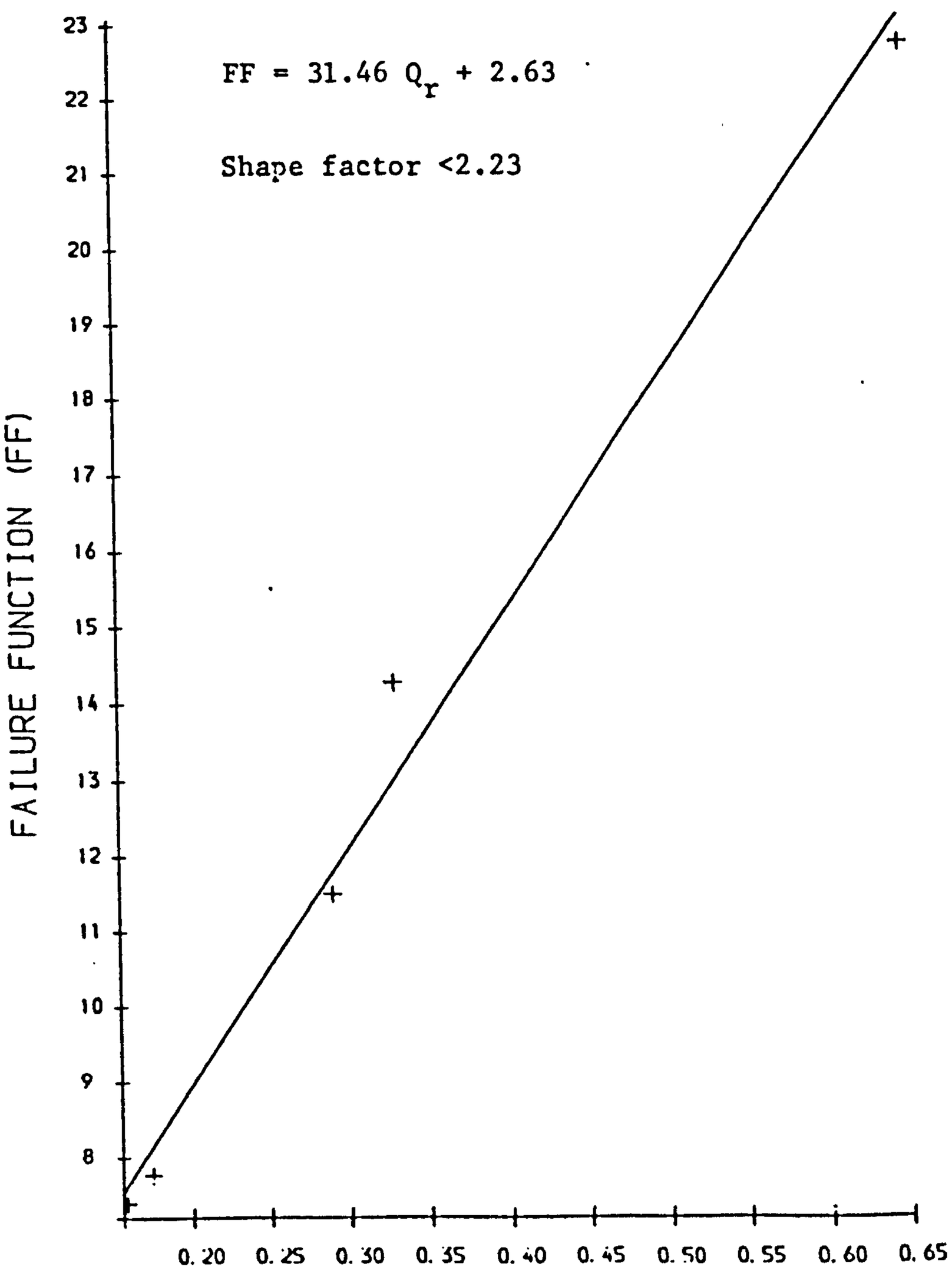

Fig. 4.16 CORRELATION BETWEEN FAILURE FUNCTION AND FLOW RATE

USER FUNCTION MINIMISED ON ABSOLUTE SUM OF SQUARES
PARAMETER VALUES
AFTER FIT 31.46 2.636

The correlation between failure function and flow rate has been plotted with a best curve fit computer program (Appendix 2-2) which shows a linear relationship (Figure 4.16), and gives experimental constants. The following empirical equation mathematically describes the relationship between FF and Q_r:

$$FF = 31.4Q_r + 2.63 \qquad (4.1)$$

From equation 4.1 it should then be possible to predict the failure function and cohesiveness of the material within acceptable approximations without the use of a Jenike shear cell.

4.7 Wall Friction

The angle of wall friction (ϕ_w) is an important parameter used in the evaluation of the frictional property of lubricants and in the design of solids handling and processing equipment.

Values of the angle of friction (ϕ_w) measured for the 11 size fractions of HSCM and BMa in contact with a surface of mild steel plate are shown in Table 3.38. All the wall loci for HSCM and BMa drawn by curve fit computer program (Figure 3.25 and 3.26) are passed linearly through the origin.

I) **The effect of size on the angle of wall friction.**

Present work shows that with an increase in particle size the angle of wall friction for both High Speed Cutter and Ball Milled products decrease. This is opposite to that seen with angle of internal friction. A similar behaviour has also been seen for free flowing materials such as sand and crushed polystyrene material. This behaviour can be reversed if the powder is coated with finer particles (161). The difference in behaviour of ϕ_w and δ_E may be due to the different deformation patterns occuring when a fibrous liquorice powder is in contact with another fibre or in contact with an unyielding metal

surface. Particles in contact with a solid wall tend to move in straight lines, thus the main factor affecting the angles of wall friction is the area of contact between particles and wall. Maximum friction occurs when there is particle-particle contact and the particle slides over itself. Strijbos (185) distinguished two frictional situations according to whether the particle diameter in contact with a wall was:

a) Larger or smaller than the dimension of the wall roughness.

b) The particle hardness was greater or smaller than the wall hardness.

When particle diameters are smaller than the wall roughness a layer of powder may stick at the wall surface, the wall friction can then become similar to a particle-particle interaction and independent of the particle/steel hardness. This is thus related to the plastic deformation or attrition between the yielding solid particulates resulting in a higher dynamic wall friction for smaller particles. It is logical to relate these observations to the different liquorice powder size fractions. As particle size increases from fraction 2 to the higher size fractions, the particle diameter over wall roughness ratio gradually increases and less material sticks to the wall. Thus a transition from particle-particle friction to a particle-wall friction takes palce. The number of contact points between particle and wall will accordingly decrease. In case of a mixture of differently sized particles, small particles tend to concentrate closer to the plate and the fines produced can migrate to the plate (8, 53).

II) **The effect of shape on angle of wall friction.**

The variation of, ϕ_w , (Figures 3.25 and 3.26) for the

different size fractions of HSCM and BMa is not solely caused by variation in particle size. It can be observed that on comparison of the entire size range of the BMa material which also has small shape factors (Table 3.58), with the HSCM material with similar and analogous size fractions, smaller values of the angle of wall friction are obtained. The inter-relationship between size, shape and wall friction can be shown by a three dimensional representation (Figure 4.17). With particles in the lower size range there is a degree of cohesivity with a high angle of wall friction. Then as the particle size increases, the wall friction tends to decrease rapidly until the particles became highly coarse and irregular, then wall friction tends to become constant and reaches a uniform value.

	Mean size μm	Shape factor (ψ_s)	Angle of wall Friction ϕ_w
1	50	1.587	32.00
2	76	2.233	33.10
3	106	2.293	31.80
4	152	2.625	30.20
5	215	2.444	26.56
6	282	2.035	28.30

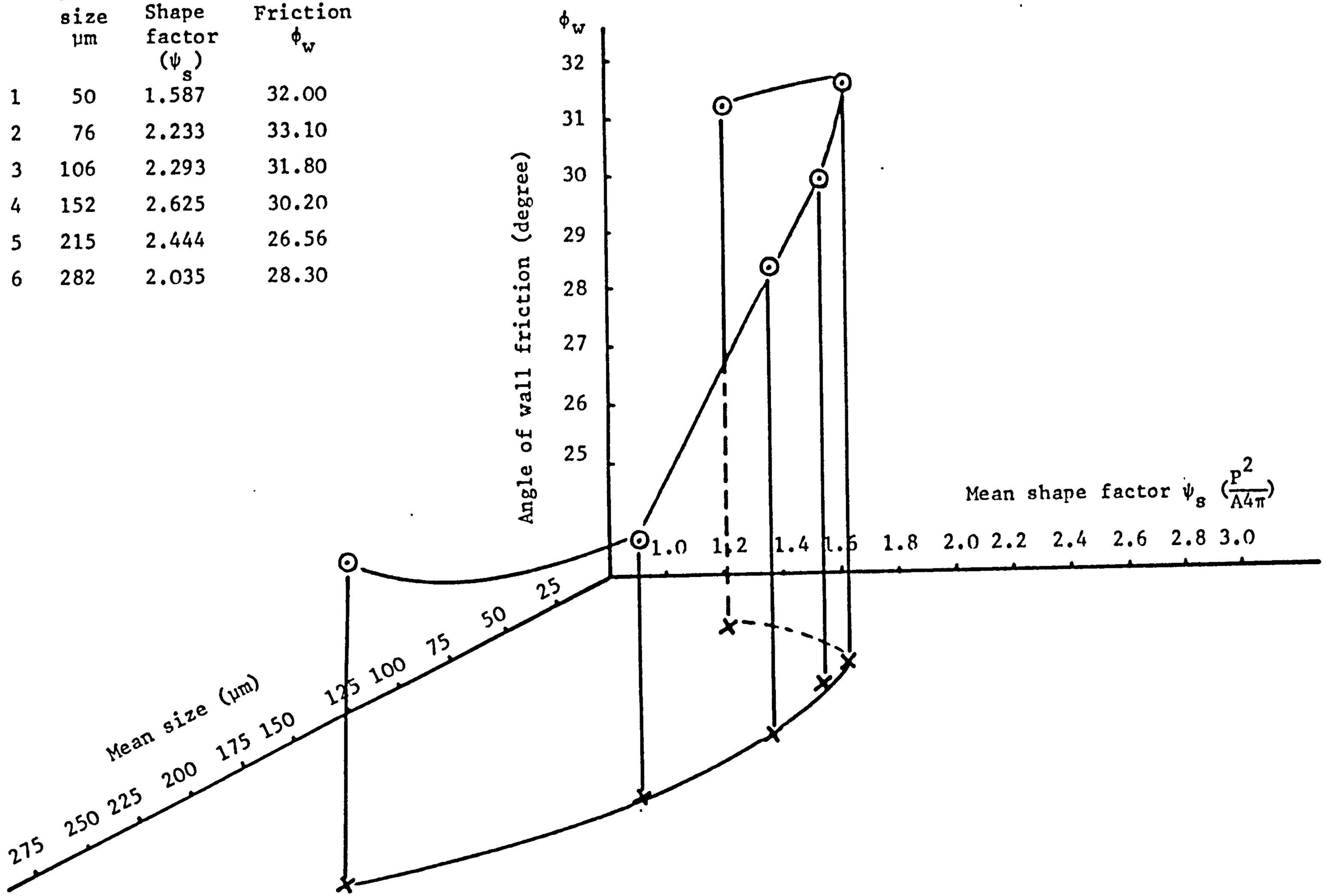

Figure 4.17 Three dimensional relationship representation of size shape, and wall friction.

C H A P T E R 5

CONCLUSIONS

5. CONCLUSIONS

5.1 Particle and Bulk characteristics

A - **Shape characterisation** by image analysis produced information in terms of the structural surface and particle configuration. The shape of particles can readily be distinguished by four shape factors, two of which are surface factors ($P^2/A4\pi$ and $P_V \times P_H/A$) and the other two elongation factors (F_V/F_H and L/B).

In most size fractions examined the larger the particle, the more irregular the shape.

The particle morphology changes with milling technique and milling time. The present work can help to distinguish between shape and shape distribution of comminuted product in terms of equipment and size fraction, as milling not only changes particle shape, but also the distribution of the shape.

Fractal measurement showed no significant change with differently shaped particles.

B - **The Bulk density, packed density and rate of packing** of the fibrous natural powder is a function of both particle size and shape. For size fraction in cohesive range (< 75 μm) the bulk density increased as size decreased. With particles in free flowing range (> 75 μm) as size increased the bulk density also increased. For all fractions with any degree of cohesivity, packed density decreased as size increased. This is similar to the rate of packing behaviour seen with respect to size.

For all size fractions examined, the system with smaller shape factors has apparently .. higher bulk and packed densities and similarly a higher rate of packing. The following equations were found to define the relationships between the bulk and packed densities and shape factor (Appendix 3 - 4 and 5).

Bulk density as a function of sphericity:

$$\rho_B = \frac{372.1}{(\psi_s - 1.5)^{0.01}}$$

Packed density as a function of sphericity:

$$d_p = \frac{462.4}{(\psi_s - 1.5)^{0.154}}$$

C - The flow rate and flow uniformity of bulk solids through a circular orifice is a function of both size and shape of particles. Comparison of flow rates of the same size fraction obtained from different milling systems showed that for the fractions with higher shape factors (more irregular), the mass flow rate was lower. In free flowing size range (over 100 μm) when the shape factor was halved the mass flow rate of liquorice powder nearly doubled. The relationship between flow rate and shape factor is of power magnitude. The following equation obtained mathematically describes the relationship between the flow rate and shape factor defined by both sphericity and elongation (Appendix 3 - 2 and 3).

Flow rate as a function of sphericity:

$$Q_r = \frac{0.447}{(\psi_s - 1.6)^{0.21}}$$

Flow rate as a function of elongation:

$$Q_r = \frac{0.45}{(\psi_e - 1.4)^{0.207}}$$

Flow uniformity for the lower and upper size range investigated showed a non-uniform flow characteristic. There is however a constant flow region between the two extremes which also showed shape factor dependency.

The laboratory flowmeter designed in the present work mimics conveying and flow systems used on industrial scales.

D - **Powder failure by Jenike shear cell**

All size fractions of the powdered liquorice when critically consolidated behaved as a "simple" powder.

For the size fractions investigated two distinct groups in terms of flow behaviour were observed. For size fractions over a mean size of 76 μm (size fraction 3) the powders had a free flowing character while for the fractions below a mean size of 50 μm the powder showed a cohesive character.

Angle of internal friction increased as size increased. From the two comminuted products (HSCM and BMa) at a similar mean size, the angle of friction increased as the shape of particle became more irregular. The effect of shape on angle of internal friction showed to be more dominant than size.

The angle of internal friction is not therefore only a function of the normal compressive force but also of size, shape and surface properties of the particulate system.

The mixture of High Speed Cutter milled fractions showed that a small proportion of fine particles can radically affect the failure property of the particulate system.

From the correlation found between the failure function and flow rate, the following empirical equation was derived.

$$FF = 31.4\ Q_r + 2.63$$

E - **The angle of wall friction** for liquorice powder on a mild steel plate has an inverse correlation with particle size. This behaviour is opposite to that seen with the free flowingpowders for δ_E in the same size range. The different behaviour between ϕ_w and δ_E can be related to whether particles slide over a particle or solid metal surface.

The effect of particle shape on wall friction is also

significant. More spherically shaped particles showed smaller values of wall friction for all size fractions of liquorice examined.

5.2 The industrial significance of the flow and failure properties

The flow properties of pharmaceutical powders and formulations are extremely important to the industrial pharmacist. Increasingly complicated manufacturing techniques and modern dosage forms and transportation systems require a deeper understanding of the science and technology of particles and bulk powders. Different methods of studying the flow properties of solid particulates are based on the concepts of powder mechanics. An essential question is therefore which is the best and most acceptable method for achieving better control of powder flowability characterisation in industrial processes.

Because powder flowability depends, in a complex way, on several particle properties, it cannot be satisfactorily characterised by a single measurement. The time for a measurement must be within reasonable limits, but at the same time precise and based on sound physical principles. Selection of an appropriate flowability measurement depends also on material characteristics such as "cohesion" and on particle characteristics, such as "size" and "size distribution". Three methods of flowability:

I) **Rate of packing**

II) **Flow from inclined tube flowmeter**

III) **Shear test**

were used in the present work to study the effect of particle size and in more extent particle shape. It was found that each method had some limitations.

The measurement of rate of packing to reach a constant bulk

volume although relatively gave fast results, for larger size and very irregularly shaped particles were not reproducible and consistent. Also the information obtained was of a qualitative nature and only useful when the aim was to monitor changes in the flowability of products or to compare the bulk behaviour of different powders.

Industry in general needs to know the time required to fill or discharge a container, while in pharmaceutical industries this is of greater importance in the control in filling and handling unit doses of particulate materials. Measurement of the flow rate and flow uniformity can be achieved by using an inclined tube flowmeter.

The flowmeter although providing this information cannot produce information about the mechanical strength of a material or the conditions which cause flow stoppage. A flowmeter also does not have great application with small particle sizes which may be cohesive.

In the case of cohesive materials it is possible to change the powder properties by incorporation of a flow aid or even an auger inside a hopper. Such methodologies can change both shear and compressive stress, which affect the material strength, agglomeration, and packing density, which can cause fluctuations in the rate of powder flow.

The shear test method can give information about:

I) the angle of internal friction

II) the effect of time consolidation and,

III) mechanical properties derived from the yield loci.

The requirements that flow from a container, once started, will continue without interruption can be established by using a shear cell. This is therefore the only technique which can be used to design handling and processing equipment.

However, it can not be used to control the timed delivery and flow uniformity of materials. Thus for a comprehensive flowability study no single method can be used but a combination of flowmeter and a shear test can possibly solve most problems encountered.

The following comparison of two sized fractions but of different shape can be used to support the above statement.

The inclined tube flowmeter showed that the size fraction BMa5 with the same mean size as HSCM5 particles but with smaller shape factors (i.e. more nearly spherical) had a higher flow rate (Q_r= 0.65 gs^{-1}) than the HSCM5 fraction (Q_r= 0.40 gs^{-1}). The shear tests on the same two fractions, show that the angle of internal friction for BMa5 was $\delta_E = 41.55^{o}$ which is smaller than the HSCM5 fraction (δ_E = 45.9^{o}). This means that BMa5 particles can slide easily over each other and therefore the chance of arch formation is less. At the same time, however, the ratio of the values of major consolidation stress (σ_1 = 65.15) to unconfined yield stress (f_c = 0.79) derived from the first yield locus for BMa5 is higher than the ratio for HSCM5 values (σ_1 = 73.71, f_c = 3.26). This variation in flow factor (ff = $\frac{\sigma_1}{f_c}$) thus predicts a higher flowability for BMa5. The study of the unconfined yield strength and the flow factor thus becomes more important for smaller size fractions where change of flow obstruction is high.

Further the angle of wall friction for BMa5 (ϕ_w = 27.17^{o}) is also smaller than for HSCM5 (ϕ_w = 30.20^{o}). This indicates that the particles of BMa5 fraction also slide more easily over the wall, as well as over particles, thus it contributed less stress transmission into the powder body to form a dome. At the same time the possibility of the volume change and therefore vacuum to affect the flow for BMa5 decreased.

Because of the high cost of shear cell tests, it is essential that only during the development stage of a new product, that a shear cell be used to understand the flow mechanics of the powders. While in production, application of an inclined tube flowmeter may be sufficient, because the results of this thesis have shown that a flowmeter can trace not only a change in flowability and flow uniformity of the powders but also identify any particle size and shape alteration caused by powder/particle generating equipment or change in the physical composition of powder mixtures.

REFERENCES

1. Ahmad, M., Pilpel, N., Rheological Acta, **8**, (1969) 448.

2. Ahmad, M., Pilpel, N., Ibid, **9**, (1970) 585.

3. Allen, T., Particle Size Measurement, 3rd ed., Chapman Hall, London, (1981).

4. Alling, H.L., J. Sedimentary Petrology, **14**, 3, (1944) 103.

5. Aravamudhan, N., et al, Powder Technology, **39**, (1984) 93.

6. Arnold, P.C., McLean, A.G., Roberts, A.W., Bulk Solids Storage, Flow and Handling., The University of New Castle Research Ass. (TUNRA) Ltd., 2nd ed. (1980).

7. Ashton, M.D., Cheng, D.H., Farley, R., Valintin, N., Rheol. Acta, **4**, (1965) 206.

8. Austin, L.G., Shoji, K., Hogg, R., Carlson, J., Powder Technology, **20**, (1978) 219.

9. Avnir, D., Farin, D., Pfeifer, P.J., Colloid interface Sci., **103**, 1, (1985) 112.

10. Beddow, J.K., et al, Powder Metallurgy international, **8**, 2, (1976) 69.

11. Beddow, J.K., Philip, G.C., Vetter, A.F., Powder Technology, **18**, (1977) 19.

12. Beddow, J.K., Particulate Science and Technology, Chemical Publishing Co., New York (1980).

13. Bickle, W., Crushing and Grinding; H.M.S.O., London (1958).

14. Bingham, E.C., Wikoff, R.W., J. Rheology, **2**, (1960) 60.

15. Bond, F.C., Chem. Eng., **61**, (1954) 195.

16. Bosley, J., Schofield, C., Shook, C.A., Trans. Instn. Chem. Engrs., **47**, (1969) 147T

17. Brain, B.H., Kaye, J.E., Leblanc, J.E., Abbot, P., Particle Charact., **2**, (1985) 56.

18. Bridgewater, J., Cooke, M.H., Scott, A.H., Trans. Inst. Chem. Eng., **56**, (1978) 157.

19. British Standard 2955, Glossary of Terms Related to Powder, B.S., London, (1958).

20. Brown, R.L., Hawksley, P.G.W., Fuel, Lond. **26**, (1947) 159.

21. Brown, R.L., Richards, J.C., Trans. Instn. Chem. Eng., **37**, (1959) 108.

22. Brown, R.L., Nature, London, **191**, (1961) 458.

23. Brown, R.L., Richards, J.C., Principles of Powder Mechanics, Pergamon Press, London, (1970)

24. Butters, G., Particle sise Analysis Conference, The University of Bradford, Wiley, England, (1985).

25. Butters, G., Wheatley, A.L., Particle Size Analysis, 1981, Stanley-Wood, N.G., Allen, T., (eds), Witey-Heydon Ltd., (1982).

26. Burak, N., Chemistry and Industry, 1, (1966) 844.

27. Campbell, C.S., Brennen, C.E., Saberskey, R.H., Powder Technology, 41, (1985) 77.

28. Carr, J.F., Walker, D.M., Powder Technology, 1, (1967/68) 369.

29. Charles, R.J., Min. Eng., (1956) 1028.

30. Cheng, D.C.H., Farley, R., Valentin, F.H., Inst. Chem. Engrs., Symposium Series 29, (1968) 14.

31. Cheng, D.C.H., Chem. Engng. Sci., 23, (1968) 1405.

Cheng, D.C.H., J. Adhesion, 2, (1970) 82.

32. Cheng, D.C.H., Sutton, H.N., Nature, London, 232, (1971) 192.

33. Clark, N.N., et al, Powder and bulk solids Tech., 8, 3, (1984) 21.

34. Clark, N.N., Powder Technology, 46, (1986) 45.

35. Cole, M., American Laboratory, (1971) 19.

36. Danish, F.Q., Parrott, E.L., J. Pharm. Sci., 60, 4 (1971) 548.

37. Davidson, J.F., Nedderman, R.M., Trans. Inst. Chem. Engrs., 51 (1973) 29.

38. Davies, C.N., Air Filtration Academic Press, New York (1973).

39. Davies, R., Powder Technology, 12, (1957) 111.

40. Beck, M.S., Wainwright, N., Powder Technology, 2, (1968/69) 189.

41. Deming, W.E., Mehring, A.L., Industr. Engng. Chem., 29, (1929) 661.

42. Delaplaine, J.W., A. E. Chem. Eng. J., 2, (1956) 127.

43. Derjaguin, B.V., powder in Industry, S.C.I. Monograph, 14, (1961) 102.

44. Dwyder, J.L., et al, Proc. Particle Size Analysis, published by, The Society for Analytical Chemistry, London, (1970) 114.

45. Edmundson, I.C., Advances in Pharmaceutical Science, Academic Press, 2, (1967).

46. Egon, S., Drug Analysis by Chromatography and Microscopy, Ann ARbor Science Publishers, Michigan, U.S.A. (1973).

47. Ensor, D.S., Mullins, M.E., Part. Charact., 2, (1985) 77.

48. Farley, R., Valentin, F.H., Powder Technology, 1, (1967/68) 344.

49. Fisher, C., Bond, C.P., Microscope, 20, (1972) 203.

50. Fisher, R.A., J. Agric. Sci., 16, (1926) 492.

51. Flook, A.G., Powder Technology, 21, (1978) 295.

52. Fong, S.T., Beddow, J.K., Proc. Powder and Bulk Solids, Rosement, Chicago, (1978).

53. Foo, W.S., Powder Technology, 36, (1983) 271.

54. Fowler, R.T., Chodziesner, Chem. Engn. Sci., 10, 157, (1959) 162.

55. Franklin, F.C., Jahason, L.N., Chemical Engineering Sci., (1955) 119.

56. Fu, K.S., Synthetic Methods in Pattern Recognition, Academic Press, New York, (1974).

57. Gaudin, A.M., Trans. AIME., 73, (1926) 253.

58. Gerritsen, A.H., Dekker, R., Powder Technology, 34, (1983) 203.

59. Gibbard, D.W., et al, Microscope, 20, (1972) 37.

60. Gibbons, J., et al, Microscope, 20, (1972) 1.

61. Giles, A.W., Jour. Geol., XL (1932) 97.

62. Gold, G., Duvall, R.N., Palermo, B.J., Slater, C., J. Pharm., 55, (1966) 1291.

63. Gold, G., et al, Ibid., 55, (1966) 1133.

64. Golder, H.Q., Engineering, 5, (1942) 501.

65. Gosh, B.N., Gacanja, N., J. Agri. Eng. Res., 15, 2, (1970) 91.

66. Goetzel, C.G., Treatise on Powder Metallurgy, New York, London, Interscience, 1, (1949) 102.

67. Gray, W.A., The packing of solid particles, Chapman & Hall, London, 2, (1968) 102.

68. Greenwood, J.A., Tripp, J.H., J. Appl. Mechanics, 34, (1967) 153.

69. Gregg, S.J., The surface chemistry of solids, Chapman & Hall, London, 2nd Ed., (1961).

70. Groves, M.J., Wyatt-Sargent, J.L., Proc. particle size analysis conference, published by The Society for analytical chemistry, London (1970) 3.

71. Guo, A., Beddow, J.K., Vetter, A.F., Powder Technology, 43, (1985) 279.

72. Harmes, A., Chemical Eng. Sci., 18, (1963) 297.

73. Harkins, W.D., Physical Chemistry of Surface Films, Reinhold Publishing Corp., New York, London (1952) 192.

74. Harwood, C.F., Pilpel, N., Chem. Process Engn., 49, (1968) 92.

75. Harwood, C.F., Ph.D. Thesis, University of London, (1969).

76. Harwood, C.F., J. Pharc. Sci., 60, (1971) 161.

77. Hausner, H.H., Planseeberichte fur Pulver Metallurgie, 14, 2, (1966) 75.

78. Hausner, H.H., Proc. Symp. Particle size analysi., Loughborough (1967) 20.

79. Heiss, J.K., Coll.J. Chem. Eng. Prog., 48, (1952) 133.

80. Hersey, J., J. Powder Technolgoy, 11, (1975) 41.

81. Hess, W.M., et al, Rubber Chemistry and Tech., 46, 1, (1973) 204.

82. Heywood, H., Proceeding Inst. Mech. Engs., 125, (1933) 383.

83. Heywood, H., Trans. Inst. Chem. Engr., (P.S.A.), 22, (1947) 14.

84. Heywood, H., Imp. Coll. che. Engng. Soc., 8, (1954) 25.

85. Heywood, H., Powder in Industry Symposium, Soc. Chem. Ind., (1961) 25.

86. Heywood, H., J. Pharm. Pharmc. 15, (1963) 56T.

87. Hibbott, H.W., Powder in the cosmetics industry, Soc. Chem. Ind. Monograph, 14.

88. Holt, C.B., Powder Technology, 28, (1981) 59.

89. Horne, M., Proc. Roy. Soc., Series a, 62, (1969) 286.

90. Hvorselv, M.J. Uber die Festigkeits eigens chaften gestarter Bindiger Boden, Ingenior Videnskab, Skrifter A, 45, (1937) 143.

91. Hvorselv, M.J., Proc. Am. Sco. Testing Mater, 39, (1939) 999.

92. Hvorselv, M.J. Waterways Exp. Stat., U.S. Army, Vicksburg Bull., 38 (1952) 48.

93. Jenike, A.W., Sheild, R.T., J. Appl. Mechanics, 26, (1959) 599.

94. Jenike, A.W., Elsey, P.J., Woolly, R.H., Proc. Am. Soc. Testing Mater, 60, (1960) 1168.

95. Jenike, A.W., Bulletin Utah Eng. Exp. Station, University of Utah, 108, (1961).

96. Jenike, A.W., Ibid, 123, (1964).

97. Jenike, A.W., Trans. Inst. Chem. Engs, London, 40, (1962) 264.

98. Johanson, J.F., J. of appl. Mech., Series E, 86, (1964) 68.

99. Johanson, J. F., Rosen, L.J., Powder Technology, 14, (1976) 195.

100. Jolliffe, I.G., Newton, J.M., Walters, J.K., Powder Technology, 27, (1980) 189.

101. Jones, T.M., Manufacturing Chemist and aerosal News, March (1968) 38.

102. Jones, T.M., Pilpel, N., J. Pharm. Pharmcol., 18, (1966) 81.

103. Jones, T.M., J. Soc. Cosmet. Chem., 21, (1970) 483.

104. Kaye, B.H., Powder Technolgoy, 21, (1978) 1.

105. Kaye, B.H., Symp. on fine particle Sci., California, Am. Chem. Soc., March, (1978).

106. Kaye, B.H., Direct charact. of fine particles., Wily, New York, (1981).

107. Keikshi, G., Powder Technolgoy, 23, (1979) 131.

108. Ketchem, M.S., The Design of walls, bins and grain elevators, New York, McGraw Hill, (1929).

109. Korz, H.P., Munz, G.P., Powder Technology, 11, (1975) 37.

Kocova, S., Pilpel, N., Powder Technolgoy, 8, (1973) 33.

110. Kostelnick, M., Beddow, J.K., Advances in powder Metallurgy processes, Hausner, H.H. (ed.) Plenum, New York (1971) 29.

111. Krinstensen, H.G., Dansk Tidskr Farm., 45, (1972) 64.

112. Krumbein, W.C., J. Sedimentary Petrology, 11, (1941) 64.

113. Krupp, H., Adv. Colloid Interf. Sc., 1, (1967) 111.

114. Kuga, K., et al, Powder Technolgogy, 44, (1985) 281.

115. Laird, W.E., Particle Technology Proc., Seminar, Indian, Inst. Tech., Madras (1971) 67.

116. Langmaid, R.N., Rose, H.E., J. Inst. Fuel, 30, (1957) 166.

117. Lees, G.S., Sedimentology, 3, (1964) 2.

118. Lees, G.S., J. British Granite and Whistone Fed., 4, (1964) 2.

119. Leschonski, K., Rumpf. H., Powder Technology, 2 (1968/69) 175.

120. MaGrae, J.C., Gray, W.A., Britt. J. Appl. Physics., 12, (1960) 164.

121. Mandelbrot, B.B., Fractals; Form, chance and dimension, W.H. Freeman, San Francisco, (1977).

122. Matchett, M.J., Smith, G.R., Powder Technology, 41, (1985) 11.

123. McDougull, R.R., Evans, A.E., Rheol., Acta, 4, (1962) 218.

124. Medalia, A.I., J. Colloid Interface Sci., 24 (1967) 393.

125. Medalia, A.I., Powder Technology, 4, (1970/71) 117.

126. Meloy, T.P., J. Powder and bulk solids Tech., 2, 2, (1978) 13.

127. Meloy, T. P., et al, Particulate science and tech., 2, (1984) 259.

128. Meltzer, N.H., Searl, E., Brown, R., Nature, London, 216, (1967) 32.

129. Morgan, B.B., Nature, 205, (1965) 36.

130. Neumann, B.S., Advances in pharmaceutical Sci., Academic Press, London, (1967) 181.

131. Newitt, D.M., Conway-Jones, J.M., Trans. Inst. Chem. Engnrs., 36, (1958) 422.

132. Newton, R.H., Dunham, G.S., Simpsonit, P.J., Ame. Inst. Chem. Engs, 41, (1945) 219.

133. Nikolakakis, I, Pilpel, N., Powder Technology, 42, (1985) 279.

134. Novak, J. W., Thampson, J.R., Powder Technolgoy, 45, (1986) 159.

135. Novosad, J., Surapat, K., Powder Technology, 2 (1968/69) 86.

136. Orford, J.D., Whalley, W.B., Sedimentology, 30, (1983) 655.

137. Pickness, R.G., J. Colloid and interf. Sci., 27, (1969) 173.

138. Pilpel, N. Paint manufacture, July, (1969) 23.

139. Pilpel, N., Mfg. Chem., 41, 4, (1970) 19.

140. Pilpel, N., Advanced Pharmaceutical Sci., William Clowes & Sons, London, 3, (1971) 173.

141. Pilpel, N., Walton, C.A., J. Pharm., Pharmac., 26, (1974) 1S.

142. Poley, M., Normand, M.D., Powder Technology, 43, (1985) 187.

143. Princen, J., J. Colloid and Interf. Sci., 26, (1968) 249.

144. Princen, J., Kwolek, W.F., Rev. Sci. Instrument, 36, (1965) 646.

145. Rausch, J.M., Gravity Flow of Solid beds in vertical towers, Ph.D., Thesis, Princeton University, (1949).

146. Rees, J.E., Stainforth, J.N., Powder Technolgoy, 23 (1979) 135.

147. Reiner, M., Deformation and Flow, H.K. Lewis, London, (1949).

148. Reiner, M., Rheology, Eirich, F.R., (ed.), Academic Press, New York, (1962).

149. Ridgway, K., Tarbuck, K.J. J. Pharm. Pharmac., 18, (1966) 1685.

150. Ridgway, K., Rupp, R., Ibid, 21, (1969) 30S.

151. Ridgway, K., Scotton, J.B., Ibid, 22, (1970) 24S.

152. Ridgway, K., Scotton, J.B., Chem. and process eng., 51, (1970) 82.

153. Ridgway, K., Scotton, J.B., Powder Technology, 4, (1971) 195.

154. Rittenhouse, G., J. Sed. Pet., 13, 2, (1943) 79.

155. Roscoe, K.H., Schofield, A.N., Worth, C.P., Geotechnique, 8, (1958) 22.

156. Roscoe, K.H., Poorooshasb, H.B. Ibid, 13, (1963) 12.

157. Rose, H.E., Tanaka, T., The Engineer, 208, (1959) 465.

158. Rose, H.E., Powders in Industry, Soc. Chem. Ind., (1961) 130.

159. Rosselein, D., Quarry Managers J., 30, 4, (1946) 30.

160. Rowe, P.W., Proc. Roy. Soc., Series-a, 62, (1969) 269.

161. Rowshanfekr-Fallah, M., M.Phil. Thesis, University of Bradford, (1981).

162. Rumpf, H., Chemie-Ing. Techn., 30, 144, (1958) 329.

163. Sarrafi, M., M. Phil. Thesis, University of Bradford (1986).

164. Savage, S.B., Int. J. Mech. Sci., 9, (1967) 651.

165. Scarlett, B., Todd, A.C., Trans. Am. Sco. Mech. Engrs., Series b, 91 (1968).

166. Scarlett, B., Proc. particle size analysis, published by The Society for analytical chemistry, London, (1970) 101.

167. Schramli, W., Powder Technology, 1, (1967) 221.

168. Schwarcz, H.P., Shane, K.C., Sedimentology, 13, (1969) 213.

169. Schwarz, H.P., Ekner, H.E., Powder Technology, 27, (1980) 207.

170. Scott, J.R., Soil Mechanics and Foundation, 3rd ed. Applied Science Publishers Ltd., London (1980).

171. Scott, J.R., Proc. particle size analysis, published by The Soc. for analytical chemistry, London, (1970) 101.

172. Scott, W.J., Ph.D Thesis, Leeds University, (1984).

173. Shatton, E., Obiorah, B.A., J. Pharm. Sci., 25, (1973) 37S.

174. Shergold, F.A., Magazine of concrete Research, 5, 13, (1953) 3.

175. Smalley, V., Smalley, I.J., Nature, 202, (1964) 168.

176. Sneed, E.D., Folk, R.L., J. Geol., 66, (1958) 114.

177. Stainforth, P.T., Berry, R.E.R., Powder Technology, 8, (1973) 243.

178. Stein, F., Corn, F., Powder Technology, 13, (1976) 133.

179. Stanley-Wood, N.G., Englargement and Consolidation of Particulate Solids, Butterworths & Co. Ltd., (1983).

180. Stanley-Wood, N.G., Zolfaghari, M.E., Particle size analysis conf., Wiley, England, (1985).

181. Stanley-Wood, N.G., Abd lkarim, A.M., Powder Technology, 35 (1983) 185.

182. Stanley-Wood, N.G., Shubair, M.S., Ibid, 25, (1979) 25.

183. Stanley-Wood, N.G., Johanson, M.E., 1st international conf. of pharmac. technolgoy, Paris, (1977).

184. Stanley-Wood, N.G., Zolfaghari, M.E., 3rd symposium on particle size, Analysis and Powder Technology, Balatonfured, Hungary, Sep. 16, (1986).

185. Strijobos,S.J. Powder Bulk Solids Technol., 1, (1977) 83.

186. Tou, J.T., Gonzales, R.C., Pattern-Recognition Principles, published by Addisowesely, (1974).

187. Treasure, C.R.G., The storage and recovery of particulate solids, Inst. Chem. Engnrs, London, (1966) 28.

188. Tsubak, J., Jimbo, G., Powder Technology, 22, (1979) 171.

189. Turba, E., Rumpf, H., Chem. Ing. Technology, 36, (1964) 230.

190. Twenhofel, W.H., Tyler, S.A., Methods of study of sediments, McGraw Hill, New York, (1941) 138.

191. United Nation, I.D.O., Report in conference of the technical consultation on production of drugs from medicinal plants, Lucknow, India, March, (1978).

192. Van den Bergh, Wim. J.B., Dalen, A.G., Scarlett, B., Part. Charact., 2, (1985) 71.

193. Van Denborg, J.F., Bauer, W.C., Chem, Engr., 71, 28 (1964) 135.

194. Viswanathan, K., et al, Powder Technology, 39, (1984) 83.

195. Wadell, H., J. of Geology, 40, (1932) 443.

196. Wadell, H., Ibid, 43, (1935) 250.

197. Wadlow, D.E., et al, Microscope, 20, (1972) 37.

198. Wales, M., Wilson, J.N., Rev. Sci. Instrument, 33, (1962) 575.

199. Waltan, C.A., Pilpel, N., J. Pharm. Pharmc., 24, (1972) 10.

200. Walton, C.A., Pilpel, N., Ibid, 26, (1974) 1.

201. Wason, D.T., proc. The workshop on particle tech., ASTM, Philadelphia, Aug., (1975) 21.

202. White, E.T., Batsone, R.J., Powder-Technology, 5, (1971/72) 127.

203. White, E.T., et al, Ibid, 5, 2, (1972) 27.

204. Whittemore, O.J., Varela, J.A., Ceramica, Nov., (1979) 66.

205. Williams, J.C., Khan, M.I., The Chemical Engineers, 71, 28, (1964) 135.

206. Williams, J.C., Chemical engineering Sci., 32, (1977) 247.

207. Williams, J.C., Birks, A.H., Rheological Acta, 4, 3, (1965) 170.

208. Williams, J.C., Birks, A.H., Powder Technology, 1, (1967) 199.

209. Williams, J.C. Birks, A.H., Bhattacharya, D., Powder Technology, 4, (1970/71) 328.

210. Williams, J.C. private communication, University of Bradford (1986).

211. Worth, C.P., Bassett, R.H., Geotechnique, 15, (1965) 32.

212. Yigit, E., Johnston, N.A., Marovdas, N.G., Quarr Managers J., 12, (1967) 467.

213. Young, J.F., J. Appl. Chem., 17, (1967) 241.

214. Zahn, C.T., Roskies, R.Z., I.E.E.E. Trans. on Computer C-31, (1972) 269.

CHAPTER SIX

APPENDICES

APPENDIX 1

List of Symbols

LIST OF SYMBOLS

A	Particle projected area
B	Particle projected breadth
BMa	Ball Mill (milling time 45 minutes)
BMb	Ball Mill (milling time 75 minutes)
C	Cohesion force between assembly of particles
CL	Compaction load
CSL	Critical state line
D	Fractal dimension
d_p	Packed density
E	Endpoint
ERM_a	End Runner Mill (milling time 10 minutes)
ERM_b	End Runner Mill (milling time 20 minutes)
EYL	Effective yield locus
F_H	Horizontal Feret
F_V	Vertical Feret
FF	Failure function
f	Surface coefficient in particle surface area = fda^2
f_c	Unconfirmed yield strength
ff	Flow factor
HSCM	High Speed Cutter Mill
JYL	Jenike yield locus
K	Volume coefficient in particle volume = kda^3
kPa	Kilo-Pascal
L	Particle projected length
n	Shear index
N	Normal force
NL	Normal load
P	Particle primeter
P_H	Horizontal projection

P_V	Vertical projection
Q_r	Flow rate (average of all rows values)
S	Shear force
T	Tensile strength
W	Flow rate (average of column values)
YL	Yield locus
Z	Shape factor (Heywood)
δ	effective (Jenike) angle of internal friction
δ_E	angle of internal friction (slope of CSL)
Δ	true angle of internal friction (free flowing material)
Δ_c	angle of internal friction from τ vs $T+\sigma$
β	angle of shear plane to horizontal (constant for particulate material)
μ	inter particle coefficient of friction (constant for particulate material)
λ	angle of shear plane to incline plane (constant for particulate material)
ρ_B	Bulk density
ρ_p	Particle density
ε_B	Bed porosity
σ	Normal stress
σ_1	Major principal stress
σ_E	Normal stress at equilibrium (Endpoint)
$\sigma + T$	Compound stress
τ	Shear stress at failure
τ_E	Shear stress at end point
τ_f	Critical failure at critical consolidation
τ_r	Residual shear strength
ϕ_w	Angle of wall friction between wall and plate
ψ_s	Shape factor (sphericity)
ψ_e	Shape factor (elongation)

APPENDIX 2

Computer Programs

The University of Bradford Cyber computers were used for all curve fit programs and calculations of required constants.

In Appendix A2-2 the equation is expressed as:

FNDEFN = P(1)*X + P(2)

which is the best fit to linear regression between failure function (FF) and flow rate (Q_r).

Programs in Appendix A2-3 to 5 which are expressed as:

FNDEFN = (P(1)/(X-const.)**P(2))

are the best fit to parabolic regression between variables (flow rate, bulk density, packed density) as a function of shape factor.

The parameter P(1) and P(2) are the required constant values which are printed both in output informations and on the relevant computer graphs in Appendix 3.

A2.1 PROGRAM ESMAIL USED TO PLOT GRAPHS OF WALL FRICTION

```
      PROGRAM ESMAIL
C
      DIMENSION AY(2),AX(2),X(99),Y(99),CX(2),CY(2),SX(2),SY(2)
      CHARACTER*80 XTIT,YTIT1,YTIT2,T1,T2,TEX(5),TIT(3)
      READ *,XPACK,YPACK
      READ *,NGRA1
      READ *,AY(1),AY(2)
      READ *,AX(1),AX(2)
      READ *,XLEN,YLEN
      READ(*,'(A)')XTIT,YTIT1
      READ(*,'(A)')(TEX(I),I=1,5)
      READ(*,'(A)')(TIT(I),I=1,3)
      CALL PAGE(21.0,29.7)
      CALL PACKIN(XPACK,YPACK)
C
C     <><><> PLOT FF & FC VS. X <><><><>
C
      CALL GRIDLN(0)
      CALL GRIDS(0)
      CALL SETPNS(1,1,1,1)
      CALL JBAXES(AX,+2,XLEN,XTIT,40,AY,+2,YLEN,YTIT1,40)
      CALL JOINPT(AX(1),AY(2))
      CALL JOINPT(AX(2),AY(2))
      CALL JOINPT(AX(2),AY(1))
      CALL BREAK
      DO 100 J=1,NGRA1
         READ *,GTYPE,NPTS
         IF (GTYPE.EQ.1) THEN
            DO 200 I=1,NPTS
               READ *,X(I),Y(I)
200            CALL MARKPT(X(I),Y(I),J)
         ELSE
            READ *,(X(I),Y(I),I=1,NPTS)
            CALL DRAWCV(X,Y,NPTS)
         END IF
100   CONTINUE .
      CALL SETKY('T','L',5,15)
      DO 300 I=1,5
300      CALL MARKKY(I,TEX(I),15)
      DO 400 I=1,3
400      CALL TITLE('L','L',TIT(I),60)
      CALL END PLT
      STOP
      END
```

A2-2 CURVE FIT VERSION OF LINEAR EQUATION

```
**********************************************

      FUNCTION FNDEFN(X,P,N)
      DIMENSION P(N)
      FNDEFN=P(1)*X+P(2)
      END

**********************************************
```

A2-2-1 OUTPUT DATA OF CURVE FIT TO LINEAR EQUATION

```
   CORRELATION BETWEEN FAILURE FUNCTION AND FLOW RATE

   NUMBER OF PARAMETERS                    2

   NUMBER OF DATA POINTS                   5

   ABSOLUTE OPTION USED FOR SUM OF SQUARES

************ COMMENCEMENT OF MINIMISATION ************
```

	XEXPT	YEXPT	YEVAL	YEXPT-YEVAL	PERCENT
1	0.155	7.210	7.51193	-.3019345	-4.187718
2	0.174	7.770	8.10961	-.3396120	-4.370810
3	0.290	11.50	11.75859	-.2585901	-2.248610
4	0.330	14.28	13.01686	1.2631420	8.845529
5	0.650	22.72	23.08301	-.3630050	-1.597733

```
  FINAL PARAMETER VALUES
  ----------------------

  ALL THE PARAMETERS ARE BOUNDED AS NON NEGATIVE
```

	LOWER PARAMETER BOUNDS	PARAMETER VALUES	UPPER PARAMETER BOUNDS
1	0.	31.456708	1000000.0
2	0.	2.6361447	1000000.0

```
FINAL SUM OF SQUARES OF ABSOLUTE DIFFERENCES =2.0006689
                                  (RMS VALUE =0.63256128)

   ************************************************
   * THE MODEL HAS BEEN SUCCESSFULLY FITTED TO THE DATA *
   ************************************************
```

A2-3 CURVE FIT VERSION OF QUADRATIC EQUATION

```
**************************************************

      FUNCTION FNDEFN(X,P,N)
      DIMENSION P(N)
      FNDEFN=(P(1)/(X-1.6)**P(2))
      END

**************************************************
```

A2-3-1 OUTPUT DATA OF CURVE FIT TO QUADRATIC EQUATION

FLOW RATE VS SHAPE FACTOR (SPHERICITY)

NUMBER OF PARAMETERS 2

NUMBER OF DATA POINTS 5

ABSOLUTE OPTION USED FOR SUM OF SQUARES

********** COMMENCEMENT OF MINIMISATION **********

	XEXPT	YEXPT	YEVAL	YEXPT-YEVAL	PERCENT
1	2.690	0.440	0.4387983	.1201695E-02	.273112
2	2.410	0.460	0.4669662	-.6966166E-02	-1.514384
3	2.020	0.500	0.5358686	-.3586859E-01	-7.173718
4	1.790	0.690	0.6327752	.5722477E-01	8.293444
5	1.650	0.820	0.8370409	-.1704087E-01	-2.078154

FINAL PARAMETER VALUES

ALL THE PARAMETERS ARE BOUNDED AS NON NEGATIVE

	LOWER PARAMETER BOUNDS	PARAMETER VALUES	UPPER PARAMETER BOUNDS
1	0.	.44679458	1000000.0
2	0.	.20955610	1000000.0

FINAL SUM OF SQUARES OF ABSOLUTE DIFFERENCES =0.49015921E-02
(RMS VALUE =0.31310037E-01)

```
**************************************************
* THE MODEL HAS BEEN SUCCESSFULLY FITTED TO THE DATA *
**************************************************
```

A2-3-2 CURVE FIT VERSION OF QUADRATIC EQUATION

```
**************************************************

      FUNCTION FNDEFN(X,P,N)
      DIMENSION P(N)
      FNDEFN=(P(1)/(X-1.4)**P(2))
      END
**************************************************
```

A2-3-3 OUTPUT DATA OF CURVE FIT TO QUADRATIC EQUATION

FLOW RATE VS SHAPE FACTOR (ELONGATION)

NUMBER OF PARAMETERS 2

NUMBER OF DATA POINTS 5

ABSOLUTE OPTION USED FOR SUM OF SQUARE

********** COMMENCEMENT OF MINIMISATION **********

	XEXPT	YEXPT	YEVAL	YEXPT-YEVAL	PERCENT
1	2.750	0.440	0.4225495	.1745054E-01	3.966031
2	2.260	0.460	0.4638280	-.3828005E-02	-.832175
3	1.950	0.500	0.5087273	-.8727343E-02	-1.745469
4	1.510	0.690	0.7095175	-.1951746E-01	-2.828617
5	1.460	0.820	0.8042210	.1577896E-01	1.924263

FINAL PARAMETER VALUES

ALL THE PARAMETERS ARE BOUNDED AS NON NEGATIVE

	LOWER PARAMETER BOUNDS	PARAMETER VALUES	UPPER PARAMETER BOUNDS
1	0.	.44959111	1000000.0
2	0.	.20670129	1000000.0

FINAL SUM OF SQUARES OF ABSOLUTE DIFFERENCES =0.10252481E-02
(RMS VALUE =0.14319554E-01)

```
**************************************************
* THE MODEL HAS BEEN SUCCESSFULLY FITTED TO THE DATA *
**************************************************
```

A2-4 CURVE FIT VERSION OF QUADRATIC EQUATION

```
**************************************************

      FUNCTION FNDEFN(X,P,N)
      DIMENSION P(N)
      FNDEFN=(P(1)/(X-1.5)**P(2))
      END

**************************************************
```

A2-4-1 OUTPUT DATA OF CURVE FIT TO QUADRATIC EQUATION

BULK DENSITY VS SHAPE FACTOR (SPHERICITY)

NUMBER OF PARAMETERS 2

NUMBER OF DATA POINTS 5

ABSOLUTE OPTION USED FOR SUM OF SQUARES

********** COMMENCEMENT OF MINIMISATION **********

	XEXPT	YEXPT	YEVAL	YEXPT-YEVAL	PERCENT
1	2.690	365.9	366.0664	-.16641	-.4548171E-01
2	2.233	390.1	383.0817	7.01827	1.799095
3	1.775	409.0	419.9645	-10.96452	-2.680811
4	1.638	446.7	448.0123	-1.31232	-.2937817
5	1.587	473.3	467.8171	5.48289	1.158440

FINAL PARAMETER VALUES

ALL THE PARAMETERS ARE BOUNDED AS NON NEGATIVE

	LOWER PARAMETER BOUNDS	PARAMETER VALUES	UPPER PARAMETER BOUNDS
1	0.	372.08599	1000000.0
2	0.	.93761978E-01	1000000.0

FINAL SUM OF SQUARES OF ABSOLUTE DIFFERENCES =201.28879
(RMS VALUE =6.3449001)

```
**************************************************
* THE MODEL HAS BEEN SUCCESSFULLY FITTED TO THE DATA *
**************************************************
```

A2-5 CURVE FIT VERSION OF QUADRATIC EQUATION

```
**************************************************

      FUNCTION FNDEFN(X,P,N)
      DIMENSION P(N)
      FNDEFN=(P(1)/(X-1.5)**P(2))
      END
```

```
**************************************************
```

A2-5-1 OUTPUT DATA OF CURVE FIT TO QUADRATIC EQUATION

```
   PACKED DENSITY VS SHAPE FACTOR (SPHERICITY)

   NUMBER OF PARAMETERS                    2

   NUMBER OF DATA POINTS                   5

   ABSOLUTE OPTION USED FOR SUM OF SQUARES

************ COMMENCEMENT OF MINIMISATION ************
```

	XEXPT	YEXPT	YEVAL	YEXPT-YEVAL	PERCENT
1	2.690	420.8	450.1713	-29.37135	-6.979883
2	2.625	460.8	454.0785	6.72146	1.458651
3	2.233	526.0	485.0146	40.98538	7.791896
4	1.638	573.2	627.0928	-53.89281	-9.402094
5	1.587	709.0	673.2207	35.77925	5.046439

```
   FINAL PARAMETER VALUES
   ----------------------

   ALL THE PARAMETERS ARE BOUNDED AS NON NEGATIVE
```

	LOWER PARAMETER BOUNDS	PARAMETER VALUES	UPPER PARAMETER BOUNDS
1	0.	462.38195	1000000.0
2	0.	.15385157	1000000.0

```
FINAL SUM OF SQUARES OF ABSOLUTE DIFFERENCES =6772.2446
                                    (RMS VALUE =36.802838)

**************************************************
* THE MODEL HAS BEEN SUCCESSFULLY FITTED TO THE DATA *
**************************************************
```

APPENDIX 3

Graphs to fit equations

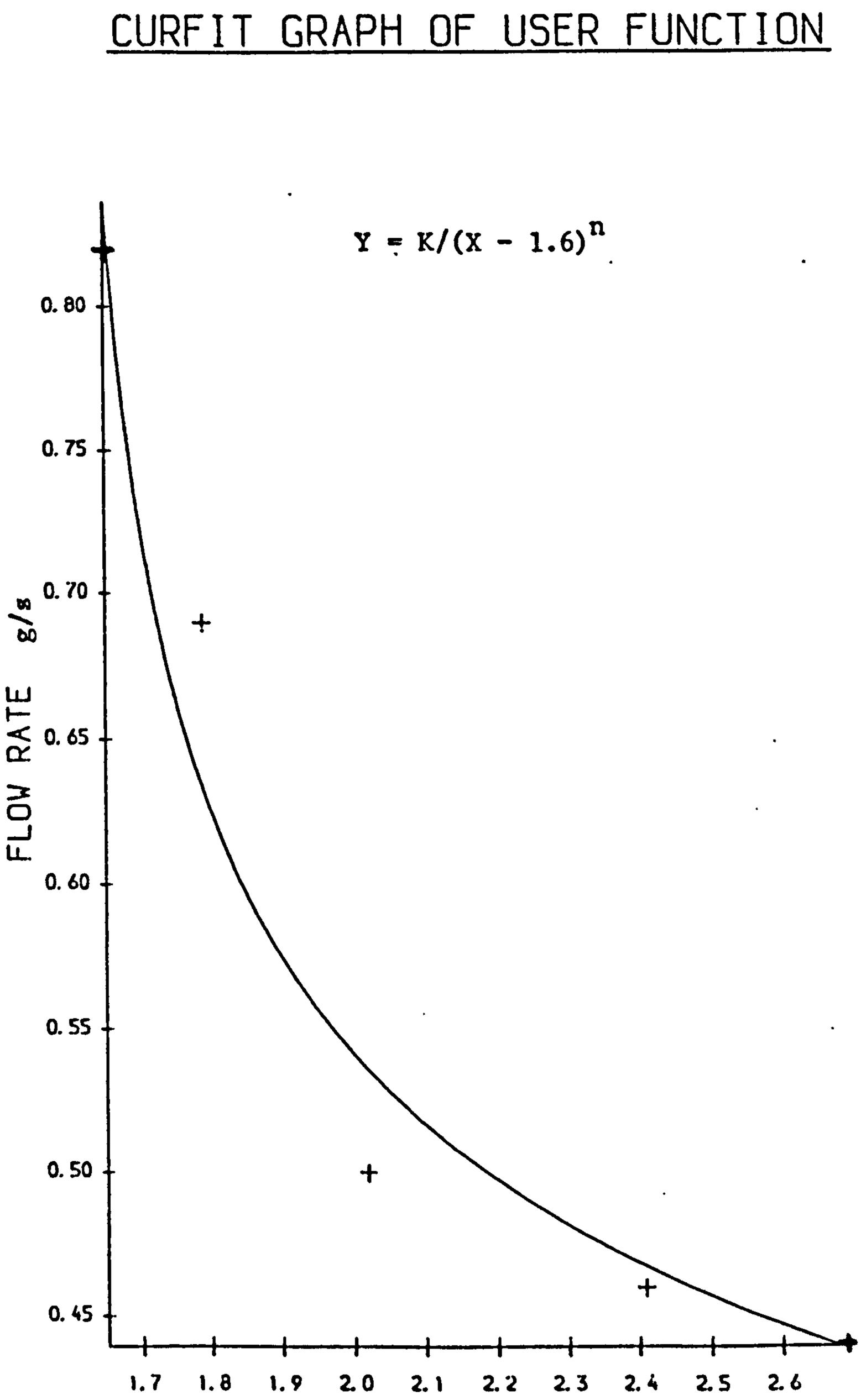

Figure A 3-2 FLOW RATE VS SHAPE FACTOR (SPHERICITY)

CURFIT GRAPH OF USER FUNCTION

$$Y = K/(X - 1.4)^n$$

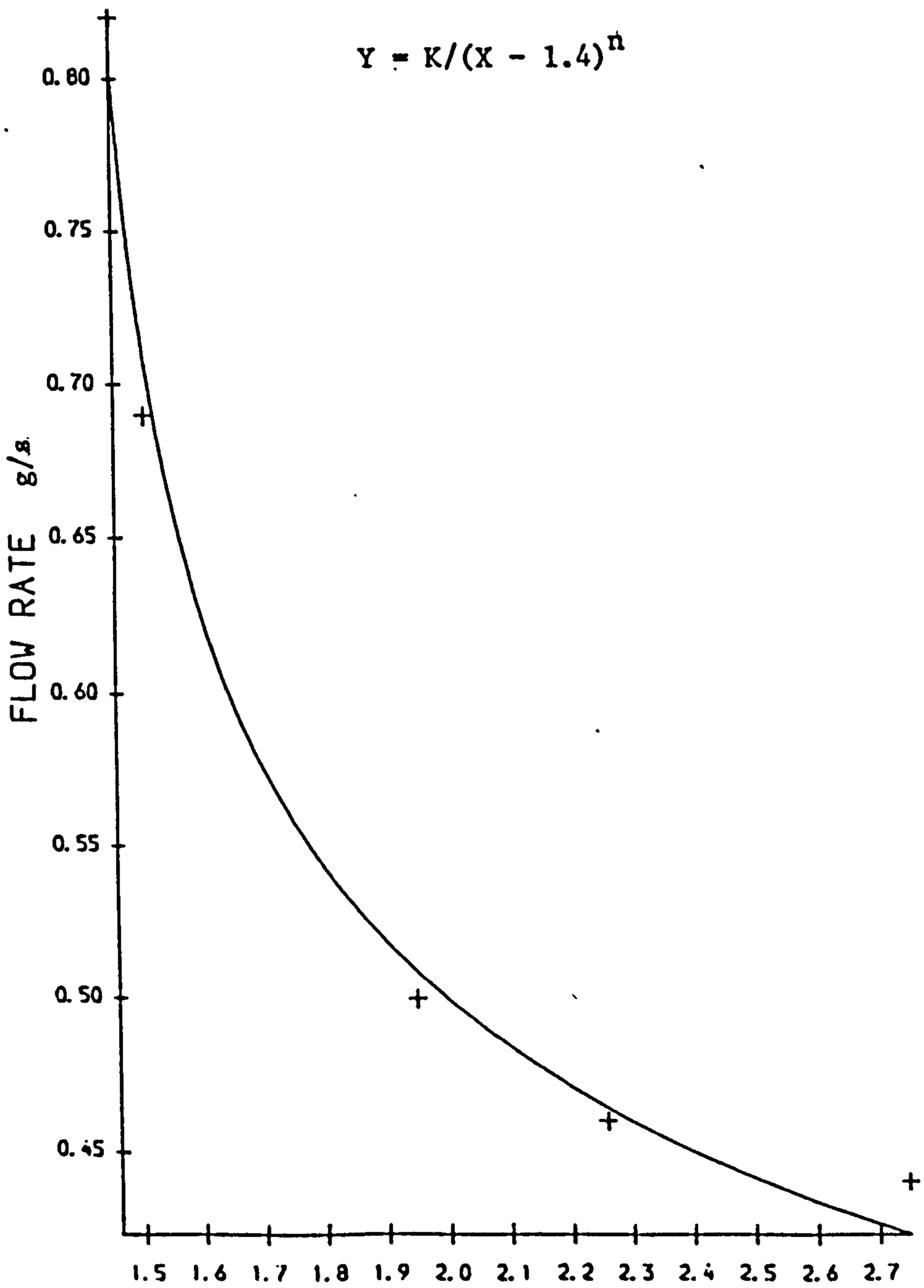

Figure A 3-3 FLOW RATE VS SHAPE FACTOR (ELONGATION)

USER FUNCTION MINIMISED ON ABSOLUTE SUM OF SQUARES
PARAMETER VALUES
—— AFTER FIT 0.4496 0.2067

CURFIT GRAPH OF USER FUNCTION

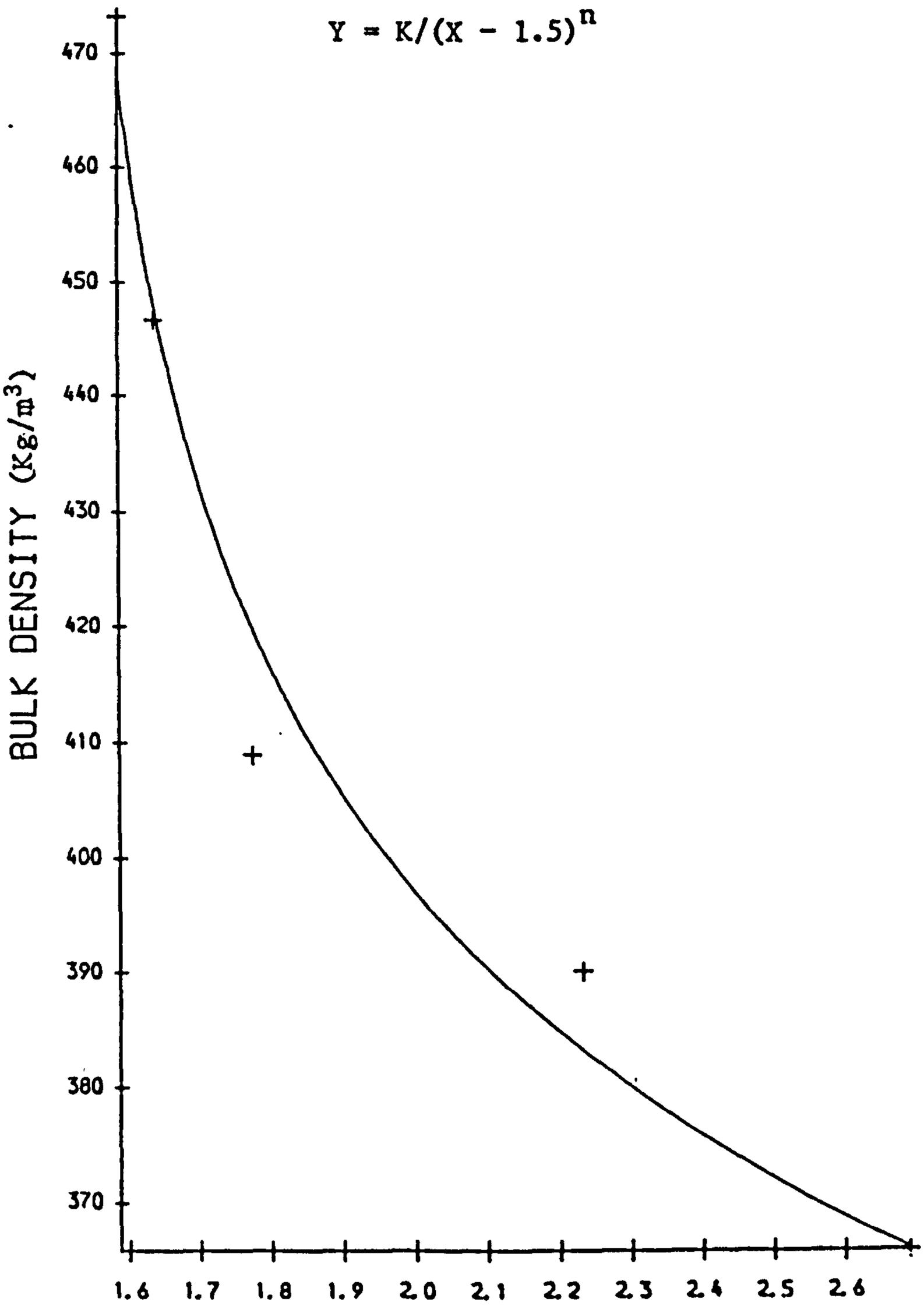

Figure A 3-4 BULK DENSITY VS SHAPE FACTOR (SPHERICITY)

USER FUNCTION MINIMISED ON ABSOLUTE SUM OF SQUARES
PARAMETER VALUES
——— AFTER FIT 372.1 9.3762E-02

CURFIT GRAPH OF USER FUNCTION

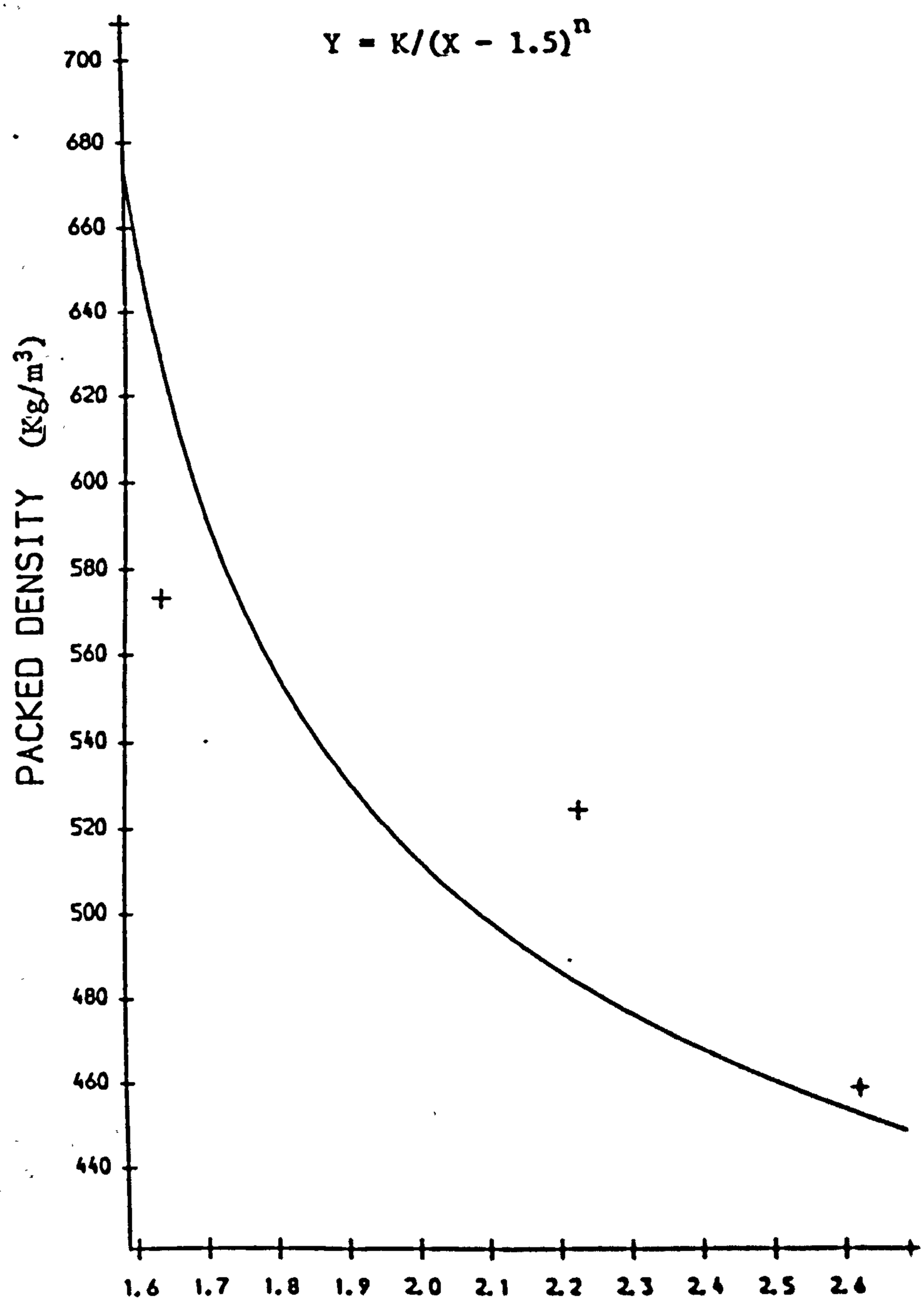

Figure A 3-5 PACKED DENSITY VS SHAPE FACTOR (SPHERICITY)

USER FUNCTION MINIMISED ON ABSOLUTE SUM OF SQUARES

PARAMETER VALUES		
AFTER FIT	462.4	0.1539

CONFERENCE PREPRINTS

PSA 85

Preprints of papers to be presented at the
Fifth Particle Size Analysis Conference,
University of Bradford, Yorkshire, UK,
16–19th September 1985

Organised by the Analytical Division of
The Royal Society of Chemistry

CONFERENCE
PREPRINTS ONLY
THE FULL CONFERENCE
PROCEEDINGS WILL BE PUBLISHED BY

JOHN WILEY & SONS
Chichester · New York · Brisbane · Toronto · Singapore
A Wiley–Interscience Publication

THE MEASUREMENT OF FLOW UNIFORMITY OF VARIOUS SHAPED AND SIZED FIBROUS PARTICLES

N.G. Stanley-Wood and M.E. Zolfaghari

Postgraduate School of Powder Technology
University of Bradford, Bradford, BD7 1DP,
West Yorkshire, U.K.

ABSTRACT

The consistency of powder flow to achieve product uniformity and quality assurance is paramount in many industries.
With the technological development in biologically orientated industries more and more fibrous matter is being handled than powdered or granulated material.
A fibrous root material was milled in three types of equipment (High speed cutter, ball and end-runner mill) and the comminuted product characterised in terms of size and shape over the size range 38-300 micrometres.
To measure the uniformity of flow the milled fibrous product was conveyed from a hopper along an inclined revolving tube to discharge into a series of collection chambers. The mean flowrate and standard deviation when correlated with the different milled products showed a relationship with shape and size fraction.

INTRODUCTION

The consistency of powder flow to achieve product uniformity when packing, filling or dispensing powders is essential in numerous industries which quantify powders either by weight or volume. Information on the flowability in terms of particle size, particle shape and powder cohesiveness, together with measurement of the uniformity of flow rate is advantageous to ensure quality assurance in production. In the design of hoppers to deliver mass flow the shear between the particle-particle surfaces is measured by shear test equipment to evaluate the internal angle of friction, the flow factors and unconfined yield stresses of powdered or granulated material. The angle of repose now being regarded as an unreliable technique because of the gross variation in measurement and lack of mathematical information for design (1,2).
When the particle size is large (>200 μm) there is relatively little difficulty in choosing conditions for a multi-phasic system to flow. The factors of 'head' of material; ratio of particle diameter to hopper orifice diameter; wall effects and bulk densities or voidage (3,4,5 and 6) required to achieve particle/powder flow are well understood. The materials which present difficulties are, however, generally less than 100 micrometre in size and are influenced by

electrostatic, frictional and surface forces (12,13). These are regarded as mildly or truely cohesive powders. The smaller the particle size then the greater the tendence for surface forces to cause cohesiveness. The smaller the size, however, the greater the tendence for the particle to be regular or spherical in shape and thus be free- flowing (11).

The industrial solution to the measurement of the mass flow rate of powdered or granular material transported from one location to another, and not necessarily out of hoppers, can be accomplished by weighing a conveyor belt; optical or electronic measurement or reflected radiation; the torque on a submerged impeller; the force on an inclined plate or volumetrically (20). All these techniques have limitations due to the low mechanical strength, lack of radiation attenuation or reflection of or from the flowing material and the ability to become cohesive and non-free flowing.

There is a remarkable lack of simple equipment and measurement protocol to measure the flowability of cohesive powders except for the highly specialised technique of measurement of the failure functions of a material by a Jenike Shear Test (5,14), the qualitative ultrasimple test of the rate of passage of particles through a sieve or the mobility test (7).

In the measurement of flowability of both free flowing and cohesive materials, the emphasis has been largely on the size of the material (10). Free flowing materials tend to be greater than 200 μm in size, but this is dependent upon the type of material, and some 50 μm size material can be free flowing. It is generally accepted that the problems of cohesiveness in materials occurs when the median particle size of a distribution is in the range 50 - 100 μm. The lower size (20-50 μm) being for inorganic slightly irregularly shaped particles and the upper size range (100-200 μm) for highly irregularly shaped material of an organic nature (8).

The material chosen for this investigation was in the size range 38-300 μm which covers the general range of cohesive and free flowing powders from a size criteria. The shape of the material on the flowability and uniformity on this mildly cohesive material has been investigated by a rotating inclined tube, rather than investigating the effect of shape on shear tests (8,9).

EXPERIMENTAL

Powder The powder chosen for this investigation was the milled product of the fibrous root of liquorice. The liquorice rhizome was milled in three different types of equipment:

1. High Speed Cutter Mill (HSCM)
   This mill was the Exteck model manufactured by Loher Gmbh West Germany. The product was milled for 20 minutes.
2. Ball Mill (BM)
   This was a 22 cm dia. porcelain drum ball mill of length 25 cms. containing a load of mild steel balls of 25 mm and 9 mm diameter, manufactured by Pascall Engineering Comp. Ltd. The drum was rotated at a speed of 35 rpm for either 45 minutes (BMa) or 75 minutes (BMb) to give two ball milled products.

3. End Runner Mill (ERM)
The mill consisted of a 25 cm. dia. mild steel bowl with an 11 cm dia. runner, manufactured by Crofts (Engineers) Ltd. The time of milling was either 10 minutes (ERMa) or 20 minutes (ERMb).

The milled products were then sieved with Endecott Test Sieves to the British Standard BS410 specification into eight size fractions. Tables 1 and 2 show the range of sieve sizes of the milled liquorice product. Each size sample was stored in air tight glass jars and the moisture of all samples determined before flow and uniformity measurements. The amount of moisture present, after 16 hours drying time at 80°C, for all samples was 6.5% ± 0.2%.

Inclined roller tube flow meter The equipment designed to measure the flow uniformity and flow rate over a wide range of size fractions (40-300 μm) for mildly cohesive to free-flowing, low density, natural fibrous material is shown in figures 1 and 2. The equipment basically consists of a 66° conically shaped mild steel hopper of 15 cm diameter and 15 cm height with a 2 cm. diameter circular orifice above a vibrating feeder (Sinex Minor Feeder). The vibrating feeder feed the milled material into a 40 mm diameter perspex tube of length 500 mm supported on mild steel rollers of approximately 6 cm diameter driven by a ¼ H.P. electric motor with variable speed control. (Rotary Regavolt, British Electric Resistance Co. Ltd.). The degree of inclination of the revolving perspex tube was adjusted by two screws under the main mild steel baseplate. When dry powder flows from the hopper onto the vibrating feeder - the clearance from the hopper to the feeder being adjustable - and then into the revolving perspex tube, the sized natural product material moves along the cylinder until discharged onto a horizontal revolving collection table containing eight sample containers. The collection speed of the sample collecter varies from one revolution of the eight sample containers per minute to one revolution every 120 minutes. This variation in collection speed and time enables very poorly flowing materials to be distributed evenly between the eight collection containers.
The inclination of the tube was found, by trial and error, to be best at 10° to the horizontal to ensure a reasonable time interval for collection. Mass transport along an inclined tube has already been physically and mathematically described (15,16,). The flow inside the tube is a function of the cumulative frictional hold up of particles between the discharge and head of the material.

Uniformity of flow and flowability measurement The hopper was filled with approximately 200 g of a known sized fraction. The adjustable parameters, to ensure flow, remained constant throughout the measurement of the differently milled products and sized fractions. The hopper clearance was 6 mm, the perspex tube revolved at 12 rpm and the angle of inclination was 10°. The samples were collected at one revolution every 448 seconds except for the first section which had double the collection time per compartment but whose contents were recycled to eliminate any possible effect of material head on the flow rate from the hopper. From the weight collected in each container the average flow rate and flow uniformity

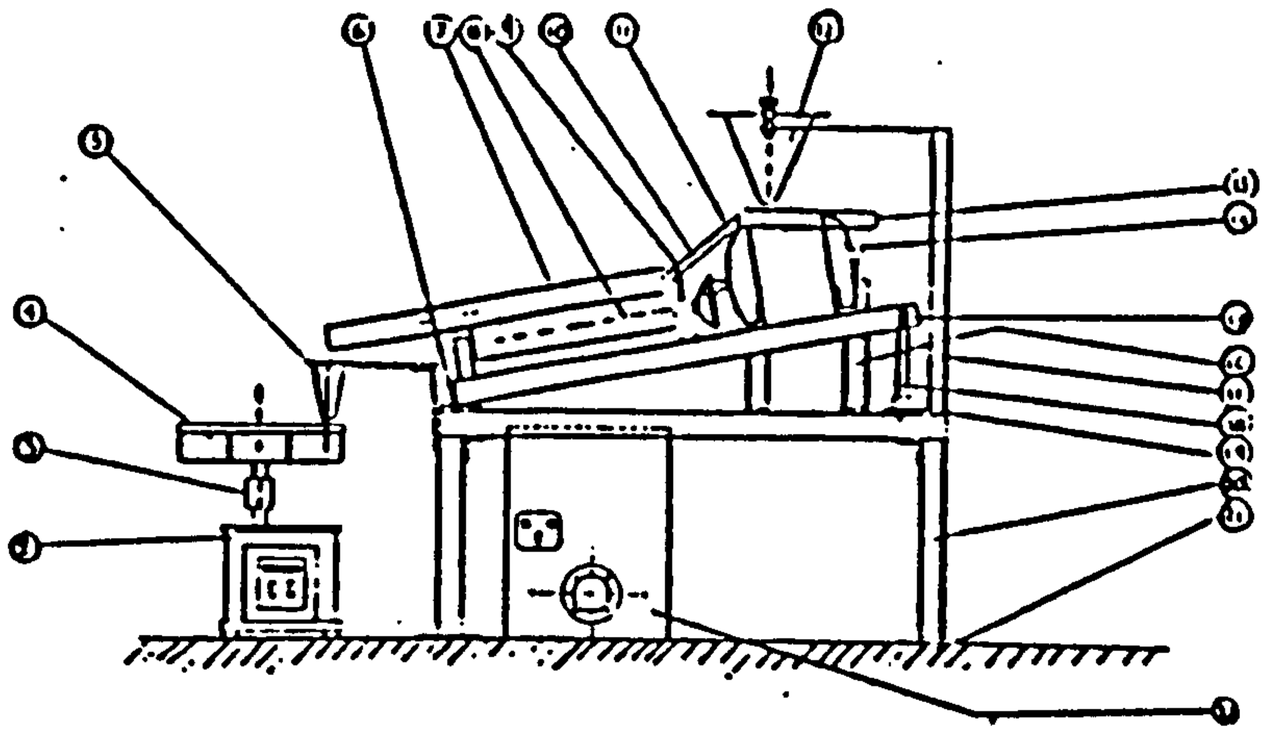

1 - sample container
2 - speed controller
3 - coupling
4 - collecting tray
5 - conical shute
6 - stops
7 - revolving tube
8 - rollers
9 - pillar blocks
10 - pulleys & belt
11 - adjustable feeder
12 - storage hopper
13 - vibrating feeder
14 - motor ½ HP
15 - base plate
16 - feeder platform
17 - hopper framework
18 - adjustable screw
19 - horizontal plate
20 - main framework
21 - feet
22 - tube speed controller

Fig. 1 Inclined Rotating Tube Flow Meter

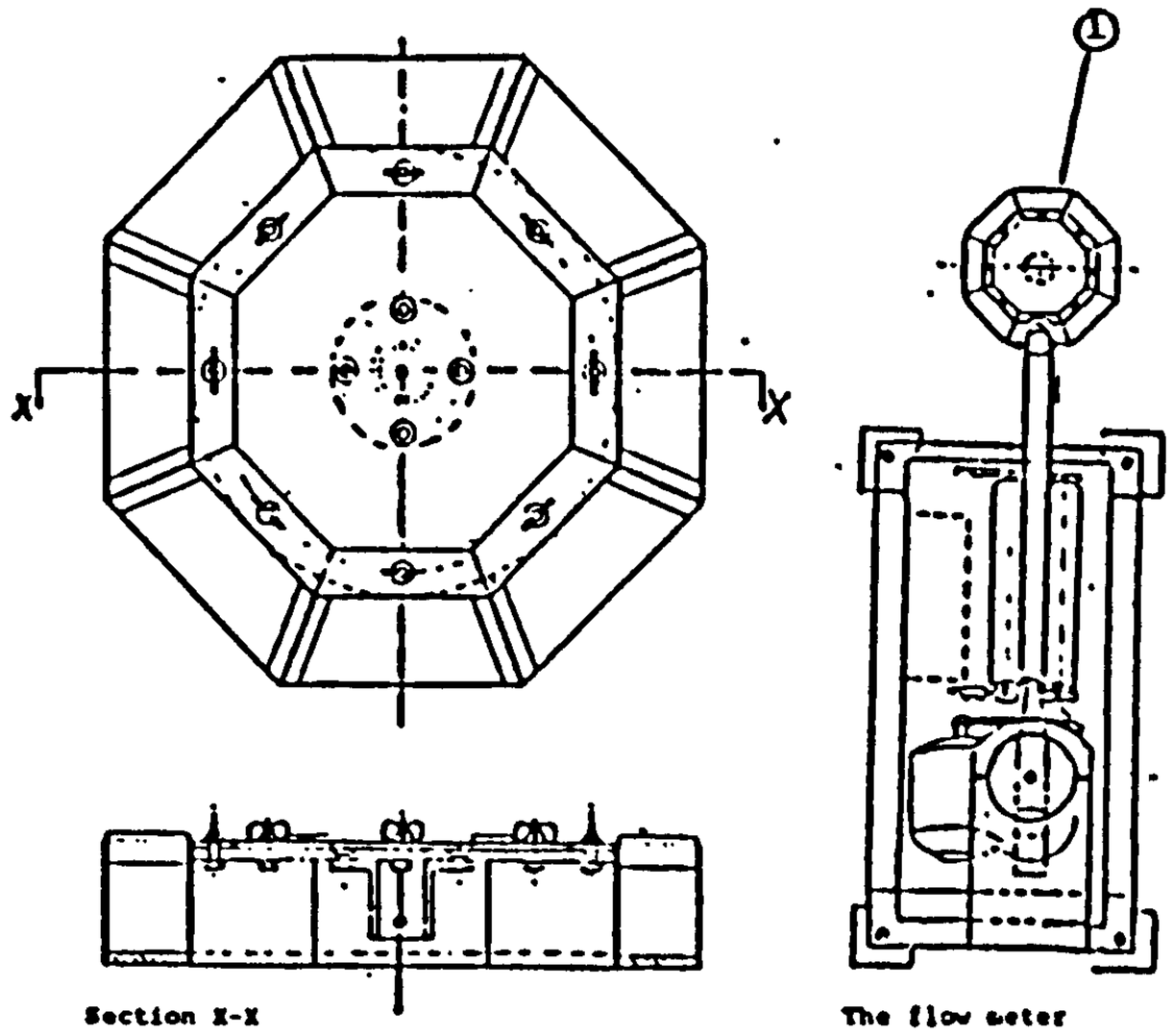

Section X-X

The flow meter top view

Fig. 2 Collection Unit

was calculated. The measurement of the flow rate was repeated twice to give the overall mean flow rate. From the weights collected in each container over three experiments, the standard deviation of the weight was calculated to give an indication of the uniformity of flow. The mean flow rate and standard deviation of uniformity of these various sized and shaped fractions obtained from the mills are shown in Tables 1 and 2.

Measurement of Shape The milled products when sieved into different sized fractions were then photographed using an optical microscope (Olympus, Model BHB, Olympus Optical Co. Ltd., Tokyo, Japan) and the optical image shape analysed using a Quantimet 720. (Cambridge Instruments Ltd., Cambridge). Figure 3 shows the images of particles in the size fractions 3 and 5 (63 - 90 μm and 125 - 180 μm: Table 1) obtained from the High Speed Cutter mill, the Ball Mill at grinding times of 40 minutes (a) and 75 minutes (b), and the End Runner Mill at 10 minutes (a) and 20 minutes (b). The shape factor determined was the elongation shape factor which is defined as the ratio of the Feret diameter in the vertical direction (d_F) vert. to the Feret diameter in the horizontal direction (d_F) horz. For a sphere the ratio of (d_F) vert./(d_F) horz is equivalent to unity while for a rectangle of dimensions length 10 unit to breadth 1 unit the elongation shape factor is 10. The elongation shape factors for the different sized and shaped milled liquorice are shown in Table 3.

TABLE 1. Measurement of flow rate and flow uniformity for High Speed Cutter Mill

Fraction Number	Size Range (μm)	Mean Flowrate ($g\ s^{-1}$)	Flow Uniformity Standard Deviation of Mean weight in container (g)
1	<38	-	-
2	38 - 63	0.174	2.71
3	63 - 90	0.290	1.03
4	90 -125	0.350	1.06
5	125 -180	0.400	1.30
6	180 -250	0.440	2.75
7	250 -300	0.370	3.10

TABLE 2. Measurement of flow rate and flow uniformity

Mill	SIZE RANGE	TIME OF MILLING			
		45 mins		75 mins	
		MEAN FLOW RATE	FLOW UNIFORMITY Stan.Dev.in container	MEAN FLOW RATE	FLOW UNIFORMITY Stan.Dev.in container
	(μm)	(g s^{-1})	(g)	(g s^{-1})	(g)
Ball Mill	63 - 90	0.33	1.27	0.35	1.05
	90 - 125	0.58	0.90	0.53	0.74
	125 - 180	0.65	1.18	0.69	1.05
	180 - 250	0.70	1.12	0.82	0.92
End Runner Mill		10 mins		20 mins	
	63 - 90	0.31	1.27	0.33	1.24
	90 - 125	0.35	1.16	0.40	1.12
	125 - 180	0.46	1.50	0.50	1.04
	180 - 250	0.52	1.87	0.57	1.46

Fig. 3 Irregular shaped particles from mills

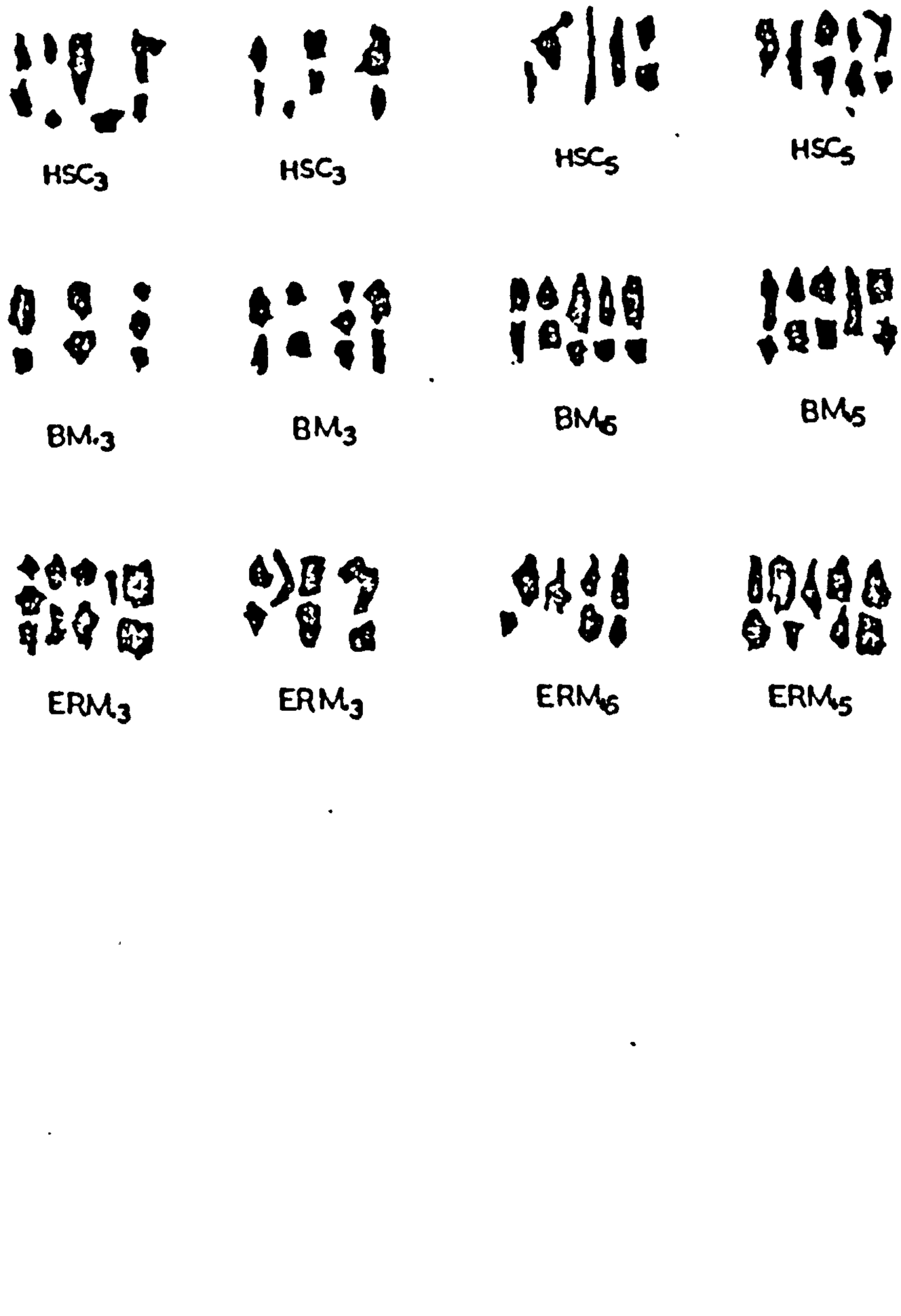

TABLE 3. Elongation Shape Factor for products milled by various Mills

MILL	SHAPE FACTOR * SIZE FRACTION No.3 (63 - 90 μm)	SIZE FRACTION No. 5 (125 - 180 μm)
High Speed Cutter (HSC_3 & HSC_5)	2.07	2.42
Ball Mill Time 45 min (BMa3 & BMa5)	1.51	1.77
Time 75 min (BMb3 & BMb5)	1.39	1.55
End Runner Mill Time 10 min (ERMa3 & ERMa5)	1.68	2.40
Time 20 min (ERMb3 & ERMb5)	1.58	2.03

*Elongation Shape Factor is the ratio of Feret diameter in the vertical to that in the horizontal direction.

RESULTS AND DISCUSSION

Tables 1 and 2 Figure 4 show the mean mass flowrate of various sized fractions of milled liquorice passing down an inclined (10° to the horizontal) revolving perspex tube. Since powders consist of discrete particles there is an absence of the continuity found in liquids and the factors of size, shape and distribution influence the rheological properties of the flowing powder. It is not feasible with any great certainty to predict the flow properties of powders from the characters of the static powder. The relationship between mass flowrate and particle size seen with the milled product from the High Speed Cutter Mill is however characteristic of virtually all materials. The position and height of the maximum and onset of blocking vary from material to material. Comparison of the shape of particles obtained from the various mills, (Figure 3) with the position and height of the maximum flowrates seen in Figure 4 shows that for elongated particles the mass flowrate is less than for the more regularly shaped particles. It is however, difficult to visually distinguish between the shapes at different size fractions produced by the same mills as well as the different shapes produced by different mills. Measurement of an arbitary shape factor - the elongation shape factor - in this investigation aids the powder technologist to distinguish between the shapes of

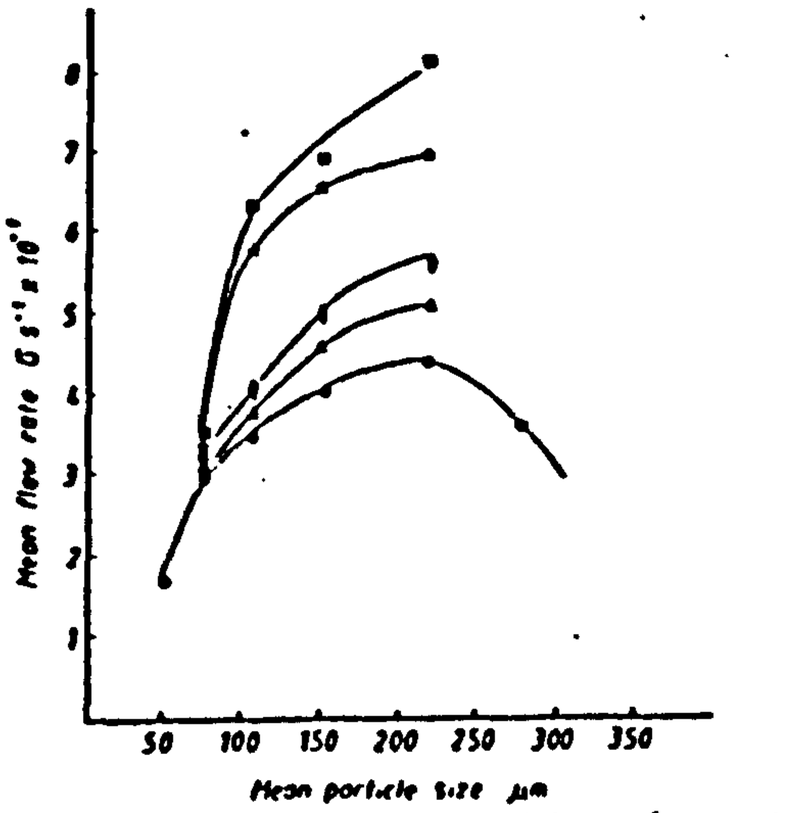

Fig 4 Mean rate of flow versus mean particle size for various milled products

- High speed cutter mill (HSCM)
- Ball mill (BMa) time 45 mins
- " " (BMb) " 75 "
- End runner mill (ERMa) time 10mins
- " " " (ERMb) " 20 "

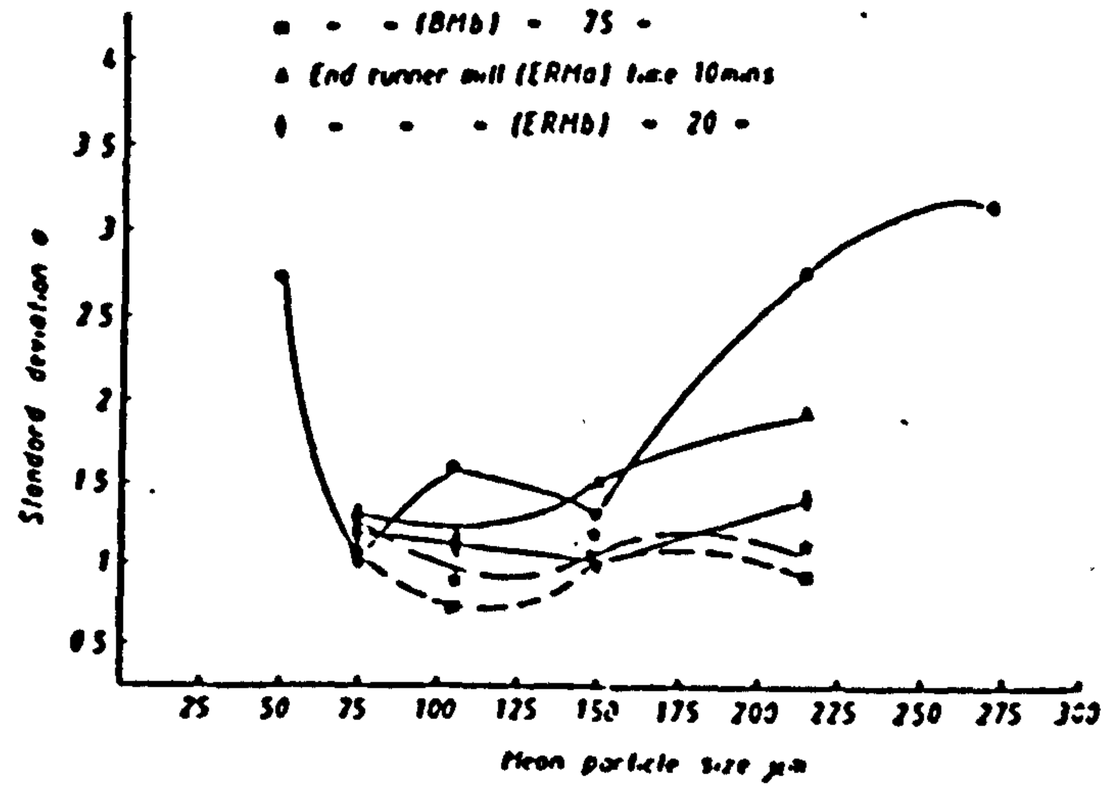

Fig 5 Standard deviation of collected weight versus mean particle size by different mills and times

milled products in terms of equipment and size fractions. The shape of the milled product at different sized fractions is remarkably dissimilar (Table 3). It has been shown (17) that the packing of particles increases as the irregularity of the particles decrease. Movement down an inclined tube should therefore achieve a greater bulk density with regularly shaped particles and thus an increase in mass flowrate. Comparison of the flowrates of known shape factors from the HSC mill with the Ball mill flowrates shows that this deduction is confirmed with more regularly shaped particles.

An analysis of die filling with differently sized and shaped sands found that the coefficient of variation of the diefill increased as particle size increased (18). The sand sizes being in the range 200 - 800 micrometre. The shape of the sand particles were characterised by the Heywood shape factors of elongation - L/B - and flatness - B/T - where the three dimensions of the particle are length L, breadth B and thickness T (19). Irregular particles flowed less freely and were less ready to rearrange themselves and thus gave less mean weight in the die. Figure 5 shows the variation in the weight collected in eight sample containers as material is discharged from the inclined rotating tube, expressed as the standard deviation or spread of the weights collected in each individual container from the mean collected weight from all containers. In the case of the elongated particles from the High Speed Cutter Mill a similar decrease in weight variation was seen with particle size decrease. This was followed by a fairly constant region of uniformity of flow between the size 150 - 75 µm and then with the smaller size and possible surface force effects the non-uniformity of flow increased... The milled products of the Ball Mill and End-Runner Mill gave a relatively constant uniformity over the size range 225 - 75 micrometres. There is a possibility that the minimum and constant uniformity region seen with cohesive materials (figure 4) with the High Speed Cutter milled product may be a combination of two effects. Cohesiveness decreases with increase in size, thus the uniformity of flow would also improve wih increase in size due to less surface interaction between particles. In opposition to the effect of cohesiveness on flow uniformity is the factor of shape. As particles become smaller they tend to become more regular and spherical in shape. The larger more irregular particles have therefore a greater chance of interlocking and causing non-uniformity of flow than the smaller more regular particles.

CONCLUSION

The inclined rotating tube flowmeter can measure the flowability of cohesive fibrous materials in the size range 40 - 300 µm and show the variation in flow uniformity in terms of size and shape.

REFERENCES

1. Gold, G., and Duvall, R.N., J. Pharm.Sci., 55, 1291 - (1966).
2. Jones, T.M., and Pipel, N., J. Pharm.Pharmacol, 18, 1825 - 1895 (1966).
3. Brown, R.L., and Richards, J.C., Tran. Inst.Chem.Engrs., 37, 105 - 119, (1959).
4. Danish, F.A., and Parrott, E.L., J.Pharm.Sci., 60, 548, (1971).
5. Rose, H.E., and Tanaka, T., Engineer, 208, 48, (1959).
6. McGougull, I.R., and Evans, A.E., Rheol.Acta, 4, 215, (1962).
7. Jones, T.M., Man. Chem. and Aerosol. News March 35 - 40 (1968).
8. Kristensen, H.G., Dansk Tidsskr Farm., 45, 64 - 72.
9. Kocava, S., and Pilpel, N., Powder Technology, 8, 33 - 55, (1973)
10. Stainforth, P.T., and Barry, R.E.R., Powder Technology, 8, 243 - 251, (1973).
11. Smaley and Smaley, Nature, 207, 168, (1964).
12. Krupp, Advances Colloid Interface Sci., 1, 111, (1967).
13. Agglomeration Interscience N. York 1962, Ed. Knepper.
14. Stanley-Wood, N.G., Enlargement and Consolidation of Particulate Solids, Published Butterworths & Co. Ltd., Sevenoaks, 1983.
15. Austin, L.G., Short, K., Hogg, R., and Carlson, J., Powder Tech. 20, 219, (1978).
16. Vahl, L., and Kingma, W.G., Chem. Eng. Sci., 1, 253, (1952).
17. MaCrae, J.C., and Gray, W.A., Brit. J. Appl. Physics, 12, 164, (1960).
18. Ridgway, K., and Tarbuck, K.J., J. Pharm. Pharmacol., 18, 1685 - 1755, (1966).
19. Heywood, H., J. Imp. Coll. Chem. Eng. Soc., 8, 25 - 23, (1954).
20. Beck, M.S., and Wainwright, N., Powder Technol., 2, 189, (1968/9)

PORANAL '86

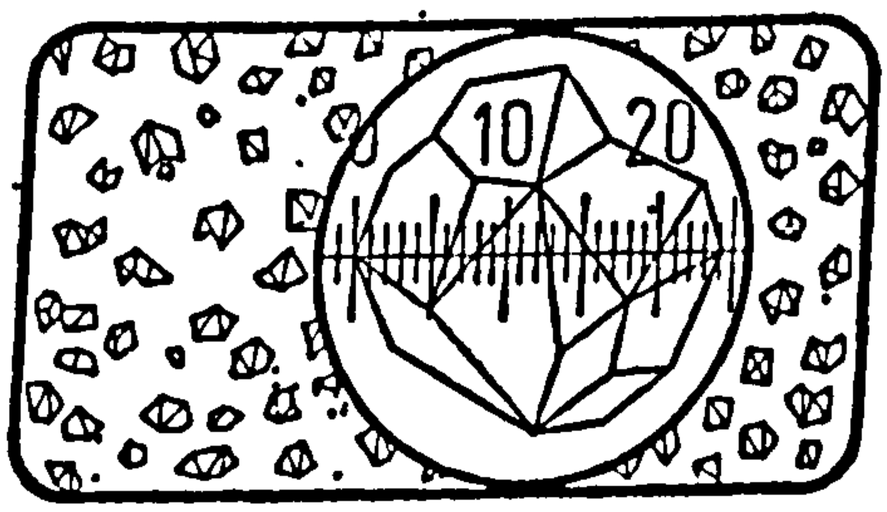

3rd

SYMPOSIUM ON PARTICLE SIZE ANALYSIS AND POWDER TECHNOLOGY with INTERNATIONAL PARTICIPATION

BALATONFURED, HUNGARY

September 16—18, 1986

PORANAL, 86, Hungary, Sep. 16-18, 1986
Symposium on 3rd Particle Size Analysis and Powder Technology
with international participation

MORPHOLOGICAL IMAGE ANALYSIS OF FRACTIONATED FIBROUS PLANT MATERIAL AND ITS CORRELATION WITH BULK POWDER PROPERTIES

Stanley-Wood, N.G., and Zolfaghari, M.E.
University of Bradford
Bradford BD7 1DP
West Yorkshire, United Kingdom

ABSTRACT

Analogous to the measurement of the size of irregularly shaped particles, characterisation of the shape of particles is difficult, at times inaccurate and the metrology is technique dependent. To identify and discriminate between particle shapes it is advisable to measure, from an optical image numerous dimensions and evaluate more than one dimensionless shape factor.

In this paper the characterisation of the morphology of a natural fibrous plant was achieved by the optical measurement, using a Quantimet 720 Image Analyser, of the perimeter, (P), projected area, (A), breadth (B), length (L), horizontal and vertical projected lengths (P_H and P_V) and the horizontal and vertical projected Feret particles diameters (F_H and F_V) of 17 size fractions of milled and separated liquorice. Variation in particle size and shape was generated by milling the material in either a High Speed Cutter, a Ball Mill or an End Runner Mill.

The morphological ratios or dimensionless groups evaluated were the Hausner ratio, ($P^2/4\pi A$), projected length area ratio, ($(P_H \times P_V)/A$), the length-breadth ratio (L/B) or the Feret Ratio (F_V/F_H). The surface texture of the particles were ascertained by fractal analysis.

The fractal dimensions showed little variation with the different surface textures obtained from the various milled products. The four morphological groups when correlated with the bulk and tap densities of the milled powders showed a relationship dependent upon size, shape and particle packing.

1.0 INTRODUCTION

In the production, handling and interaction of particulate materials where particles break, react, flow, agglomerate and mix or in which particle assemblies can be stored, packed, transported, fluidized and suspended the shape of the particle is now recognised as an important parameter in predicting the behaviour of powders.

The investigation of particle morphology in the combined terms of size and shape has in many cases been neglected and the shape variation of comminuted particulate materials with size has received scant attention. Gaudin, (1), Giles (2) Twenhofel and Tyler (3) and Alling (4) measured the shape of various minerals crushed by different grinding equipment and found that the shapes of the powdered products were dependent upon the size of the particles. Giles found that for sandstone the particle angularity showed an increase with increasing fineness while Gaudin observed for quartz that the grinding and crushing action from a jaw crusher, roll mill and a ball mill had basically no effect on the shape of the comminuted particulate product. Other workers (5,6) did not however support this machine independence as it is now generally agreed that ball mills produce more equidimensional rounded particles (7) while the shape of fractured glass particles measured by Charles(8) was dependent upon the rate of applied stress. In contrast, Heywood (9) suggested that the shapes obtained were dependent upon the type of material undergoing comminution but Rose (10) stated that although the properties of the material had some effect it was the type of equipment which predominately effected the shape of the comminuted materials.

In any morphological investigation it is desirable to select a technique which will accurately measure particle shape. Various authors (19, 20, 21, 22, 23) have chosen literal or graphical arbitrary terms to describe particle shape while other workers have tried to estimate the particle shape from particle system behaviour, such as the ability of particles to roll down inclined planes (24,25); the residence time on a sieve cascadograph (26,27), the variation of bulk and tap densities (17) or the ratio of apparent density to tap density (18).

More sophisticated analyses have used either Walsh Functions or Fourier Transformations. Fourier image analysis techniques (28, 29,30) are

only suitable in the shape characterisation of smooth rounded particles (31) because conventional Fourier analysis of very jagged or highly re-entrant silhouettes is only accomplished with some mathematical difficulty (32,33). Fractal analysis, first introduced by Mandelbrot (36) is however more successfull with highly irregularly shaped particles (34,35) but it has limitations due to the type or texture of the material and because fractal shape analysis is image resolution dependent (37,28,39) rugged particulate regions may be erroneously measured (40).

In the last two decades, individual particle shape characterisation in terms of the comparison of the particle diameter with an equivalent sphere or circle has become an acceptable methodology (41, 42, 43, 44, 45). Shape factors derived from the perimeter, the area, or the projected length of particles achieve, at times, a more accurate estimate of shape than other shape metrologies. Hausner (20, 46) was one of the first to describe both the shape factor and the texture of particles. He defined three particle shape characteristics:

Elongation Factor: the ratio of particle length (L) to particle breadth (B)

Bulkiness Factor: the ratio of area (A) to the product of L and B

and the

Surface Factor: the ratio of particle perimeter (P) to the product of Area and 4π

Hess (49) later used the shape factor of $(PH \times Pv)/A$ were P_H and P_V are the horizontal and vertical orientated projection lengths respectively, to measure surface irregularity and particle branching of carbon blacks.

In this present work a natural fibrous material, obtained from liquorice root, was comminuted in three different mills to produce various shaped particles which were then measured and their shape factors related to the bulk properties of the powder.

2. EXPERIMENTAL

2.1 Materials

The material chosen was the milled product of the naturally grown liquorice rhizome or powderd Glycyrrhiza collected from the southern province of Iran.

2.2 Sample Comminution

The rhizome was milled in three different types of equipment:

i) A high speed cutter mill (HSCM). This mill was the continuous EXTECK model manufactured by Loher Gmbh, West Germany.

ii) A ball mill (BM), with a 22 cm diameter Porcelain drum of length 25 cm, manufactured by Pascall Engineering Co. Limited. The drum contained a 50% w/w load of mild steel balls of 25 mm and 9 mm diameter. Rotation of the drum was at 35 rpm for either 45 minutes (BMa) or 75 minutes (BMb).

iii) An end runner mill (ERM). This mill was manufactured by Crofts (Engineers) Limited, and the milling time was either 10 (ERMa) or 20 minutes (ERMb).

From these different mills and different milling times various particle shapes were produced.

The five different products from the three mills were sieved on nest of Endecott test sieves using an automatic "Retsch" vibrator into 6 size fractions. (Fraction 2:38-63 μm, Fraction 3: 63-90 μm, Fraction 4: 90-125 μm, Fraction 5: 125-180 μm, Fraction 6: 180-250 μm, Fraction 7: 250-315 μm). All these fractions were stored in air tight glass jars in a dessicator. The moisture content of all the different sized fractions was 6.5% ± 0.12 w/w.

2.3 Microscope slide preparation

A spinning riffler at 15 rpm was used to accurately sample one gram of comminuted product which was then dispersed in acetone using ultrasonics (50 watts). (Ultrasonic Limited, Shipley, Yorkshire). Approximately one millimetre of dispersed suspension was withdrawn and fixed on a microscope slide with particles in their most stable position. For each size fraction at least four slides were prepared and kept in a vacuumed desicator before microscopical examination.

2.4 Equipment

(a) Microscope

An Olympus photomicrographic system camera (Model PM-10-A) made by Olympus Optical Co Limited, Tokyo, Japan, was used to photograph the particle images. Magnifications from 10 x to 40 x was obtained dependent on the size range of the particles and fractions. To calibrate the Quantimet image analyser a British Standard graticule was photographed at each magnification.

(b) Quantimet "Image Analyser"

A Quantimet Image Analyser 720 Model (Cambridge Scientific Instruments Limited) was used for shape analysis in this work (48). The system consists of an input peripheral, a central processor and an output peripheral, each of which can contain many modules. The resolution and accuracy of the measurements of this system has been enhanced by the adoption of a 720 line slow scanning camera compared with a television camera used in earlier models (49,50,51,52 and 53). The Plumbicon camera gives high resolution, less noise and less shading and has allowed the processing of low-contrast features. Details of the Image Analyser have previously been published (54).

2.5 Functions measured by the Imager Analyser

Several different functions can be measured by the Quantimet 720 (58,49,52). In the present work a range of particle dimensions (Fig. 1) have been used to evaluate subsequently the particle shape factors.

1. Projected Area (A)
2. Perimeter (P)
3. Feret's diameter (Vertical Feret F_V and Horizontal Feter F_H)
4. Projected length (Horizontal Projection P_H and vertical projection P_V)
5. Length (L)
6. Breadth (B)

The Feret diameters and projected lengths are however sensitive to image orientation and therefore prior to any measurement of these two parameters, particles should be arranged with the longest dimension in a preferred direction (Fig. 2). The shape factors calculated from the particle dimensions and used in this work are:

1. $\frac{P^2}{A4_{\pi}}$ surface descriptor (sphericity)
2. $\frac{F_V}{F_H}$ form descriptor (elongation)
3. $\frac{P_H \times P_V}{A}$ surface descriptor (roughness and irregularity)

4. L/B form descriptor (elongation)
5. Fractal dimension

2.6 Bulk Density and Rate of Packing

The uniformity of filling a specific container is important in the measurement of bulk and pack densities because these parameters are dependent upon the feed rate and the impact pressure of powders into a known volume. A "powder characteristic tester" (Hosokawa Iron Works Limited, Osaka, Japan) was used to measure the bulk and rate of packing of the comminuted liquorice powders.

2.7 Compaction and Direct Failure Apparatus

Fig. 3 shows the design of the compaction and direct failure apparatus fabricated to investigate the effect of particle shape on the failure stress of compacted powders under different loads.

The brass divided mould has a height of 50 mm with a 20 mm diameter axial circular bore along the entire length. The mould can be divided vertically into two idential sections to release the compacted powder but when used for uniaxial compaction the two sections were tightly clamped together by four horizontal screws.

The compacted specimen was prepared within the mould in increments at a predetermined load using a Denison mechanical press (Denison and Son Ltd., Hunslet Foundry, Leeds). Further separate layers were added, after the initial load was released and the compaction plunger withdrawn, until the height of compact was 50 mm. The two halves of the mould were removed to give an unsupported cylinder of compacted powdered liquorice. The direct unconfined yield stress of the powder was then measured by the direct application of a vertical stress to the top of the powder column using a calibrated Denison mechanical press.

Table 1 Shape Characterisation of individual particles
(IISCM Size Fraction 2)

F. PERIMETER ** 2 / FEATURE AREA*12.57	PROJ.HEIGHT* PROJ.W / FEATURE AREA	FEATURE LENGTH / FEATURE BREADTH
1.22478	1.60561	
1.10061	1.42044	1.55422
1.45883	1.72481	1.33684
1.28894	1.45161	1.85714
1.29588	1.74699	1.95
1.2409	1.50696	1.50617
1.08896	1.31749	1.97059
1.73008	2.19972	1.39024
1.71291	1.98579	1.05333
1.52897	1.81034	1.9359
1.34956	1.6767	1.34862
1.49319	1.93766	1.29293
1.43845	1.82211	
2.10794	1.97349	2.46667
1.96538	1.51903	1.17021
2.09176	2.07852	1.89474
2.10382	1.48491	1.35616
2.37769	2.31133	3.86667
1.58513	1.68844	1.25641
2.2655	2.84866	2.37879
3.98544	1.6922	1.84375
2.95946	2.16774	2.54545
1.66602	2.6045	1.80488
3.65315	2.33201	2.0625
1.91698	2.45565	1.97015
1.16585	2.47479	3.19608
1.55508	1.88353	1.28986
1.29404	2.66312	2.06122
2.4793	4.43275	1.8
1.40086	3.87692	1.96078
2.56866	1.92418	1.5
1.32306	4.32639	2.41667
1.19884	1.47445	1.17241
1.52894	1.67342	1.87097
1.53029	1.74098	1.80328
1.33436	1.54103	2
1.62856	1.76449	2.45833
4.67304	3.21598	7.69565
1.24035	1.3888	1.53704
1.25521	1.47142	1.04444
1.3874	1.69072	1.28814
1.34952	1.67861	1.20988
1.33029	1.50097	2.02083
1.52108	1.97096	1.58427
1.51618	1.87669	1.90698
1.43303	1.35088	2.2
1.45329	1.71842	1.33333
1.2642	1.56356	1.55
1.21168	1.71329	1.09302
1.43289	1.73316	1.76119

Table 2 Summary of mean Shape Factors for milled fibrous liquorice

Specimen Code (see text)	Mean Sieve Size µm	Shape Factors			
		$\frac{P^2}{A \ 4\pi}$	$\frac{P_V \times P_H}{A}$	$L/_B$	$F_V/_{F_H}$
$HSCM_2$	50	1.755	2.000	1.907	1.760
$HSCM_3$	76	2.233	2.343	2.260	2.073
$HSCM_4$	106	2.293	2.766	2.305	2.178
$HSCM_5$	152	2.625	3.113	2.444	2.420
$HSCM_6$	215	2.690	2.744	2.755	2.650
$HSCM_7$	282	2.035	2.125	2.216	2.525
BMa_2	50	1.587	1.879	1.703	1.460
BMa_3	76	1.638	2.058	1.545	1.512
BMa_4	106	1.719	2.033	1.740	1.683
BMa_5	152	1.860	2.274	1.706	1.770
BMa_6	215	2.444	3.101	1.980	1.862
BMb_3	76	1.493	1.988	1.343	1.390
BMb_5	152	1.790	2.152	1.508	1.554
$ERMa_3$	76	1.888	2.325	1.550	1.655
$ERMa_5$	152	2.411	2.705	2.260	2.212
$ERMb_3$	76	1.915	2.430	1.455	1.573
$ERMb_5$	152	2.020	2.595	1.956	1.910

3.0 RESULTS AND DISCUSSION

3.1 Shape Factors

Table 1 shows the evaluation of three different shape factors (sphericity, roughness and irregularity, and elongation respectively, Section 2.5) where the term FEATURE refers to the particle image.

This table is a representation of the shape factors obtained from individual particles of the sized fraction sampled from the comminuted product obtained from the high speed cutter mill.

Table 2 gives a summary and means of the shape factors of four different ratio (Sec. 2.5) for all 17 size fractions of the fibrous material analysed. In addition the code for the mean particle size within each size fraction obtained from the high speed cutter mill (HSCM), the ball mill for 45 minutes (BMa) and 75 minutes (BMb) and also the end runner mill for 10 minutes (ERM_a) and 20 minutes (ERM_b is also tabulated in Table 2. The subscripts refer to the size fractions of each milled product. To obtain a comprehensive and discriminary viewpoint of particle shape it is beneficial to use more than one shape factor to describe the morphology of a particle. From Table 2 and Figures 4a and 4b the surface shape factors ($P^2/A4\pi$ and $P_V \times P_H/A$) are of similar value while the elongation shape factors (Fv/FH and L/B). although similar in terms of elongation are different to the surface shape factors. This variation is advantageous to enable a distinction to be made between various comminuted products. For the seme particle size range (Figures 4a and b) the shapes obtained from the two mills are quite different, each type of equipment not only giving a size distribution but also a variation in particle shape. The relationship between particle shape and size being non-linear and there being a shape distribution of particles analogous to a particle size distribution.

Figure 5 shows the variation in shapes obtained from different mills when comminuting fibrous liquorice rhizome. The size fraction 3 and 5 having a mean size value of 76 and 152 μm respectively (Table 2). In the case of the fractal dimensional analysis of particles (Table 6) there is no noticeable difference in values with different stride lengths. The overall fractal dimension average between the products from the high

speed cutter and the ball mill also show no significant difference.

Beddow (55) has proposed that there is a fundamental difference between the external shape of a particle and the topographical texture of a particle. The natural fibrous material comminuted, in this investigation, by different mills will give different shapes but will most probably be of the same texture. Fractal dimension will therefore be similar for all samples analysed by this methodology.

3.2 Bulk density and rate of packing

Tables 3 and 4 and Figure 6 show the initial bulk density and the rate of packing over a period of time by tapping and the effect of shape on the bulk properties of powders. The innate cohesive forces seen with smaller sized particles, may be the cause of the high bulk density seen in Figure 6. The phenomena observed is not however only due to size as the initial pack density (Bulk density) varies with shape as seen in Figure 7. With the rate of packing (Figure 6) it appears that the movement of particles within an assembly is due solely to the size of the material. With very irregularly shaped particles, with shape factors in the range 1.6-2.6 (Figure 7) the rate or ease of particle rearrangement becomes however more difficult. This was also seen in a previous paper(56) where the effect of shape on the flow rate and flow uniformity of powdered liquorice was measured.

3.3 Compaction and Direct Failure

Table 5 and Figure 8 show the effect of shape for the size fractions $HSCM_3$ and BMa_3 formed into a column of powder under different compaction stress on the failure of a column of comminuted fibrous liquorice powder. The bulk and packed density results have shown that the more spherical and less elongated particles are the higher the bulk density becomes and the easier it is to achieve particle arrangements. In the determination of the unconfined yield strength to cause a column of powder to fail the more elongated the particle shapes ($HSCM_3$) are the greater the compaction stress required to prevent column breakage by slippage. Likewise with the more spherical particles (BMa_3) a greater direct failure stress is required to fail the column at a specific normal column formation stress.

Table 3 Bulk Density of various shaped and sized fractions from HSCM and BM

Time of packing	Initial bulk and packing densities kg m^{-3}							
	$HSCM_2$	$HSCM_3$	$HSCM_5$	$HSCM_6$	BMa_2	BMa_3	BMa_5	BMa_6
sec.								
0	409.8	390.1	400.2	365.9	473.3	446.7	456.6	460.2
6	474.5	456.3	431.9	393.2	527.4	522.0	493.6	481.9
12	511.9	485.1	440.4		566.4	543.3	504.8	
18	531.2	498.5	449.8	403.7	600.7	552.5	512.1	494.6
24	544.7	-	-	-	629.1	-	-	-
30	-	513.8	455.2	409.4	-	563.4	519.1	502.2
36	566.8	-	-	-	666.8	-	-	-
42	-	521.5	459.6	-		569.9	527.4	502.5
48	580.9	-	-	413.5	696.9	-	-	
54	-	526	460.8		-	573.2	529.9	
60	588.6				720.4			
72	597.8				731.6			

Table 4 Rate of Packing of various shaped and sized fractions from HSCM and BM

Time of Packing Sec.	Rate of Packing g s^{-1}							
	$HSCM_2$	$HSCM_3$	$HSCM_5$	$HSCM_6$	BMa_2	BMa_3	BMa_5	BMa_6
6	1.08	1.11	0.53	0.45	0.91	1.26	0.62	0.36
12	0.86	0.80	0.34	-	0.78	0.81	0.40	-
18	0.68	0.60	0.27	0.21	0.71.	0.59	0.31	0.19
24	0.56	-	-	-	0.65	-	-	-
30	-	0.42	0.18	0.15	-	0.39	0.21	0.13
36	0.44	-	-	-	0.53	-	-	-
42	-	0.31	0.14	-	-	0.29	0.11	0.10
48	0.34	-	-	0.12	0.47	-	-	
54	-	0.25	0.12		-	0.24	0.11	-
60	0.30				0.42			
72	0.26				0.36			

Table 5 Compaction and Direct Failure Stress variation due to Particle Shape

Compact Stress kPa	Failure Stress kPa	
	$HSCM_3$	BMa_3
555.4	11.10	72.19
695.2	68.03	111.4
834.3	107.6	149.9
937.8	162.4	188.8
1112.4	224.9	217.9

Table 6 Regression analysis of the Fractal Dimension $HSCM_3$

(a)

Estimated Fractal Dimensions for Seven Individual Particles at different stride length ($HSCM_3$)

Av. Stride Length µm	1	2	3	4	5	6	7	Row Av. of 7 particles
1.368	1.026	1.034	1.040	1.051	1.172	1.162	1.035	1.074
2.402	1.028	1.024	1.038	1.046	1.136	1.119	1.042	1.061
3.442	1.010	1.034	1.035	1.046	1.099	1.110	1.085	1.059
4.485	1.017	1.015	1.029	1.030	1.101	1.088	1.046	1.046
5.529	1.054	1.015	1.086	1.019	1.114	1.063	1.010	1.051
6.572	1.007	1.029	1.025	1.217	1.128	1.065	1.004	1.067
7.617	1.045	-	-	-	1.153	1.073	-	1.090
8.661	1.058	-	-	-	1.172	1.071	-	1.100
9.706	1.069	-	-	-	-	-	-	1.069
Overall Fractal average for 7 particles								1.068

(b)

Estimated Fractal Dimensions for Seven Individual Particles at different stride length (BMa_3)

Av. Stride Length µm	1	2	3	4	5	6	7	Row Av. of 7 particles
1.368	1.180	1.019	1.120	1.176	1.160	1.031	1.026	1.101
2.402	1.143	1.020	1.098	1.146	1.146	1.049	1.055	1.094
3.442	1.075	1.014	1.097	1.114	1.078	1.026	1.017	1.060
4.485	1.096	1.020	1.171	1.079	1.066	1.037	1.028	1.071
5.529	1.063	1.042	1.120	1.095	1.148	1.040	1.022	1.075
6.572	1.033	1.042	1.098	1.097	1.098	-	1.063	1.071
7.617	1.007	1.079	1.097	1.070	-	-	1.001	1.050
8.661	-	-	-	-	-	-	1.067	1.067
9.706	-	-	-	-	-	-	-	
Overall Fractal average for 7 particles								1.073

CONCLUSION

The shape of particles comminuted by three different mills at different time intervals can be distinguished by four shape factors, two of which are surface factors ($P^2/4A\pi$ and $(P_V \times P_H)/A$ and the other two elongation factors (F_V/F_H and L/B). The particle morphology changes with different milling systems and also with the particle size of the comminuted product. In all size fractions examined the larger particles were more irregular in shape than the smaller particles. The bulk density, for natural fibrous particulate material in the cohesive range of smaller sizes, is greater than for larger sizes and is dependent both on the size and the shape of particles.

The failure and the unconfined direct yield stress of a column of powder is dependent mainly on the shape of the particles because as the column formation stress is increased and particles tend to lose their discrete shapes due to deformation the unconfined yield stress tends to a constant value.

4.0 REFERENCES

1. Gaudin, A.M., Trans. AIME, 73 (1926) 253
2. Giles, A.W., Jour. Geo. Vol. XL (1932) 97
3. Twenhofel, W.H. and Tyler, S.A. "Methods of study of sediments", McGraw Hill, New York (1941) 138
4. Alling, H.L. J. of sedimentary petrology, 14, 3, (1944) 103
5. Yigit, E., Johnston, N.A., Maroudas, N.G. Quarry Managers J. 12 (1967)
6. Whittemore, O.J. and Varela, J.A., 12, (1967), 467, Ceramica Nov. (1979)
7. Holt, C.B. Powder Technol., 28 (1981) 59
8. Charles, R.J. Min. Eng. (1956) 1028
9. Heywood, H. Powders in industry, Soc. Chem. Ind. (1961) 130
10. Rose, H.E. IBID 25
11. Ridgway, K., Rupp, R. Chem. and Process Eng. 51 (1970) 82
12. Ridgway, K., Rupp, R. Powder Technology, 4, (1971) 195
13. Ahmad, M., and Pilpel, N. Rheologica Acta 8, (1969) 448
14. IBID 9, (1970) 585
15. Ridway, K. and scotton, J.B., J. Pharm. Pharmac. 22 (1970) p. 24 S
16. " " Pharm. J. 206 (1971) 432
17. Shotton, E., Obiorah, B.A. J. Pharm. Pharmac. 25, (1973) 375
18. Beddow, J.K. et al., Powder Metallurgy International, 8 2 (1976)
19. Heywood, H, J. Pharm. Pharmac. suppl. 15 (1963) 56T
20. Hausner, H.H., Planseeberichte fur Pulvermetallurgie 14 (2) (1966) 75
21. Rosselein, D., Quarry Managers J. 30, 4 (1946)
22. Sneed, E.D. Folk, R.L. J. Geol. 66 (1958) 114
23. Davies, R. Powder Technology, 12 (1975) 111
24. Viswanathan, K. et al Powder Technology, 39 (1984) 83
25. Aravamudhan, N. et al IBID 93
26. Clark, N.N. et al Powder and Bulk Solids Techn. 8, 3 (1984) 21
27. Meloy, T.P. et al Particulate Sci. and Techn. 2 (1984) 259
28. Meloy, T.P. Eng. Found. Conf. Deerfield (1971)
29. Meltzer, N.H. Searle, E. Brown, R. Nature (London) 216 (1967) 32
30. Schwarcz, H.P. Shane, K.C., Sedimentology, 13 (1969) 213
31. Meloy, T.P. J. Powder and Bulk Solids Techn., 2. no. 2 (1978) 13
32. Meloy, T.P. IBID (1985)
33. John, C.T. and Roskies, R.Z. IEEE Trans. Computers C-31 (1972) 269

34. Flood, A.G. Powder Technology, 21 (1978) 295

35. Kaye, B.H., Direct Characterisation of Fine Particles, Wiley, New York (1981)

36. Mandelbrot, B.B., "Fractals: Forum, Chance and Dimension" W.H. Freeman, San Francisco (1977)

37. Kaye, B.H. Powder Technology, 21 (1978) 1

38. Avnir, D., Farin, D. Pfeifer, P. J. Colloid Interface Sci, 103, 1 (1985) 112

39. Avnir, D., Farin, D. Pfeifer, P.,Nature, 308 (1984) 261

40. Schwarz, H. Ekner, H.E. Powder Technology, 27 (1980) 207

41. Wadell, H., J. of Geology, 40 (1932) 443

42. Wadell, H., IBID 43 (1935) 250

43. Lees, G., Sedimentology, 3 (1964) 2

44. Heywood, H., Imp. Coll., C' em. Engng. Soc. 8, (1954) 25

45. Watson, J.H.L., J. Appl. Phys. 17 (1946) 121

46. Hausner, H.H. Proc. Symp. on PSA, Loughborough, Soc. Anal. Chem. London (1967) 20

47. Hess, W.M., McDonald, G.C. and Urben, E. Rubber Chemistry and Technology 46, (2) (1973) 204

48. Cole, M., American Laboratory (1971) 19

49. Wadlow, D.E. Hophins, B.M. Gardner, G.M. Microscope, 20 (1972) 37

50. Gibbons, J., Soames, M.R. and Knowles, W.R., Microscope, 20 (1972) 1

51. Fisher, C. and Bond, C.P. Microscope 20 (1972) 203

52. Gibbard, D.W., Smith, D.J. and Wells, A. Microscope 20 (1972) 37

53. Dwyer, J.L. Manalan, D.A., and Morton, R.R.A. Proc. PSA by Soc. For Analytical Chemistry (1970) 114

54. Zolfaghari, M.E., "The morphological, flow and failure characteristics of fractionated natural bulk material" University of Bradford, Ph.D. Th (1986)

55. Beddow, J.K. Powder Metallurgy International 8 (3) (1976)

56. Stanley-Wood, N.G. and Zolfaghari, M.E Fifth Particle Size Analysis Conference, University of Bradford, Sept. 1985

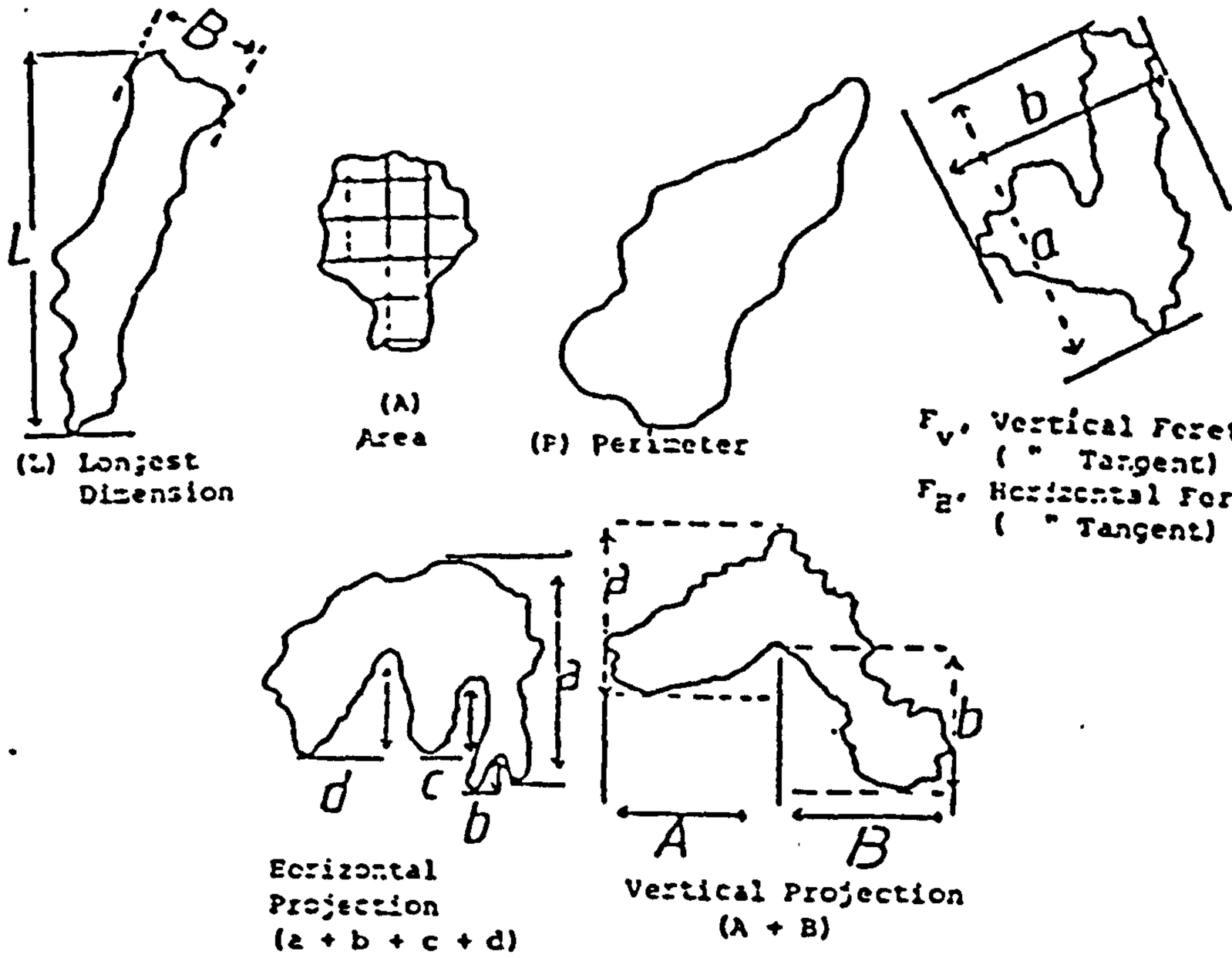

Fig. 1. Particle dimensions measured by an Image Analyser

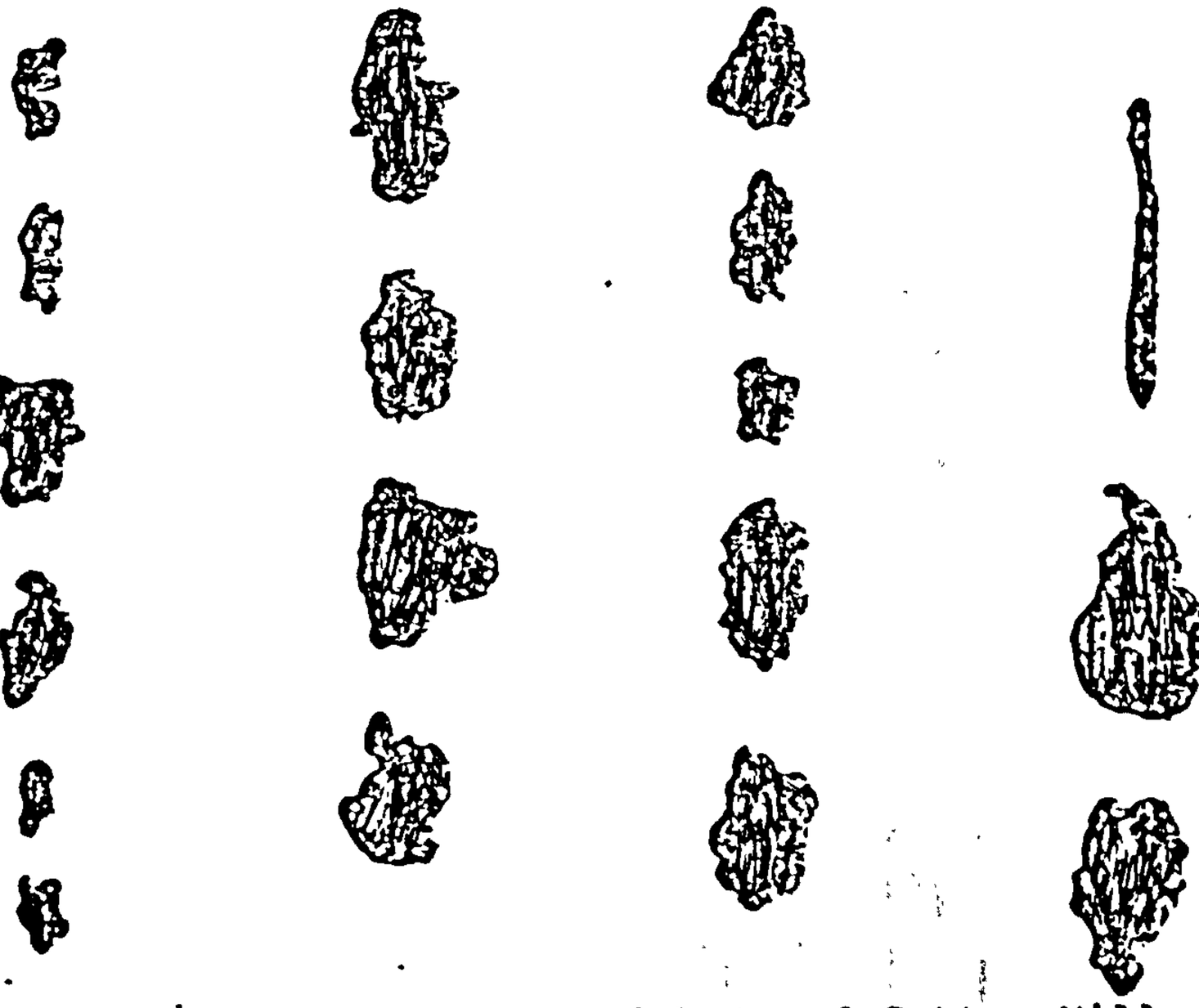

Fig. 2. Orientated Particles from a High Speed Cutter Mill

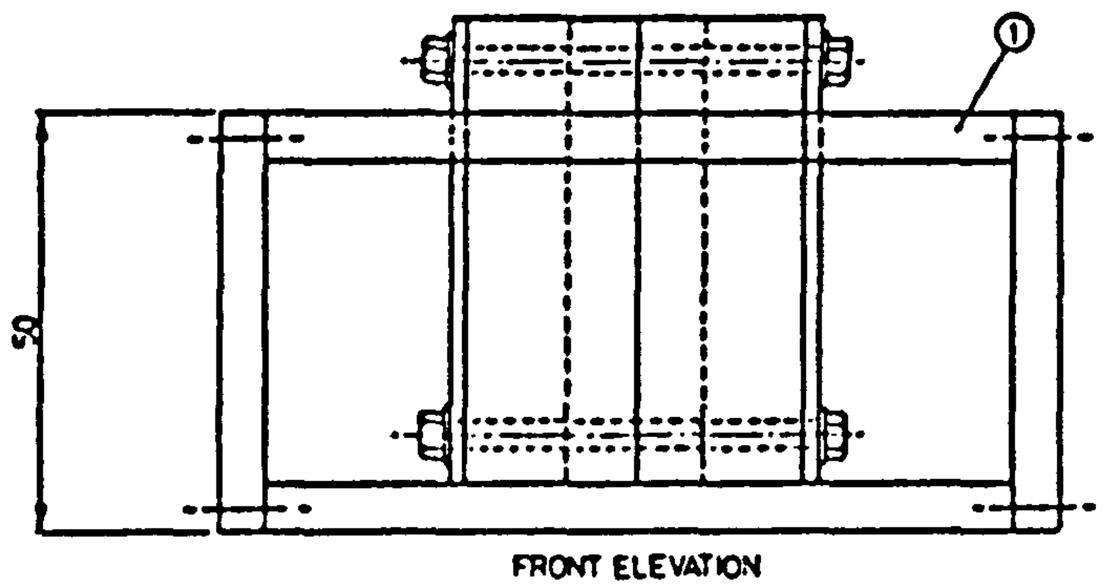

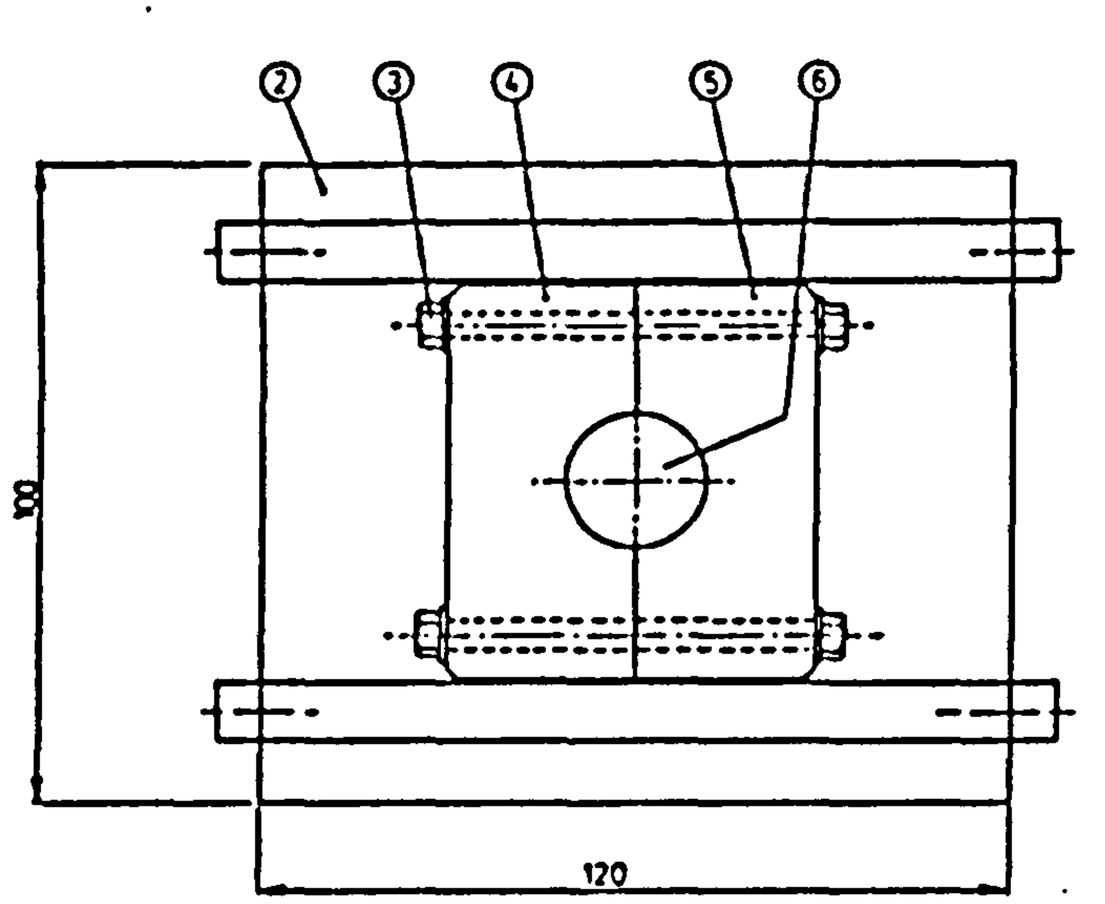

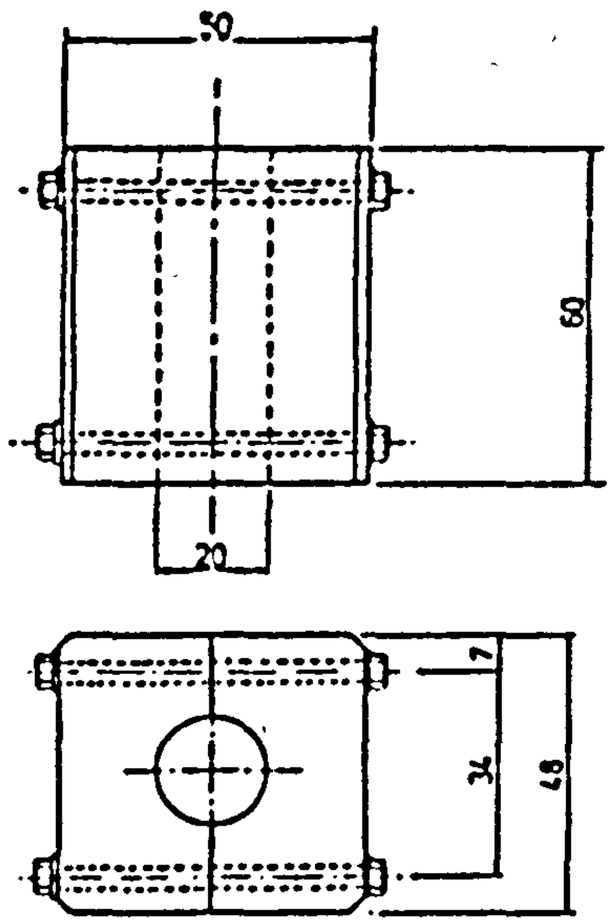

ITEM NO.	DESCRIPTION
1	[illegible] GUIDE
2	BASE PLATE
3	CLAMPING SCREWS
4	LEFT SIDE MOULD
5	RIGHT SIDE MOULD
6	DIE
7	COMPACTING PLUNGER
8	FAILURE PLATE

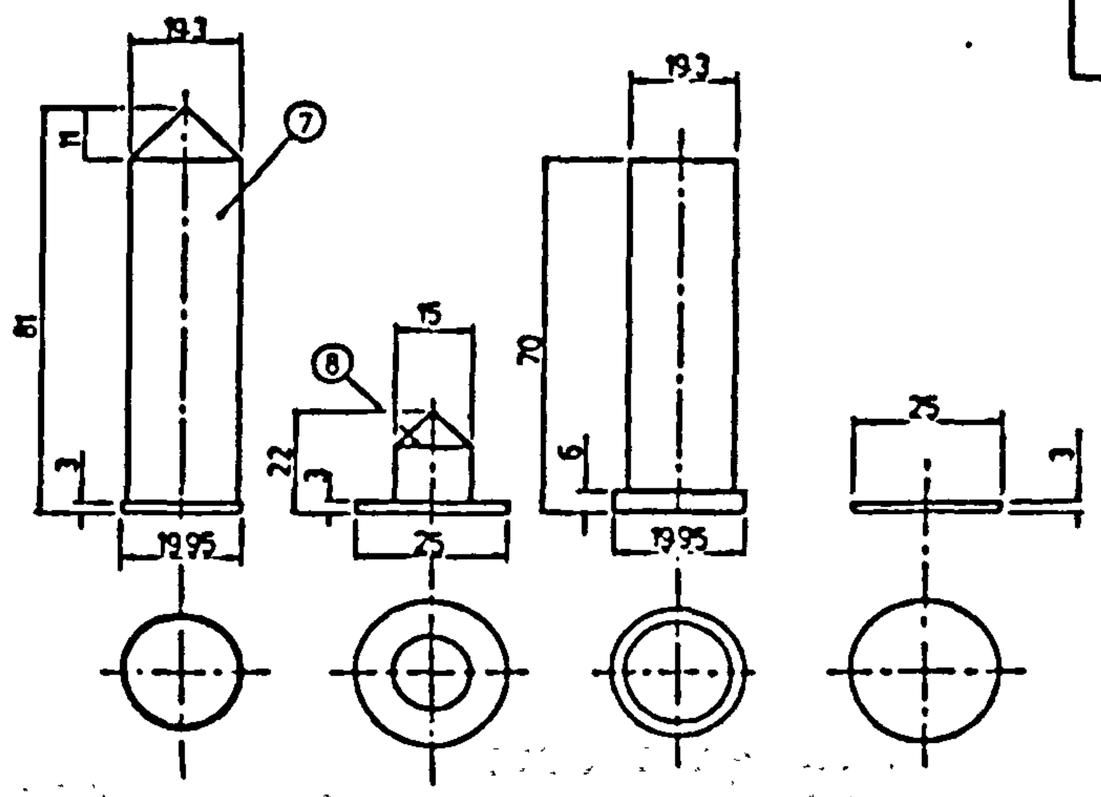

Fig. 3 Compact and Direct Failure Apparatus

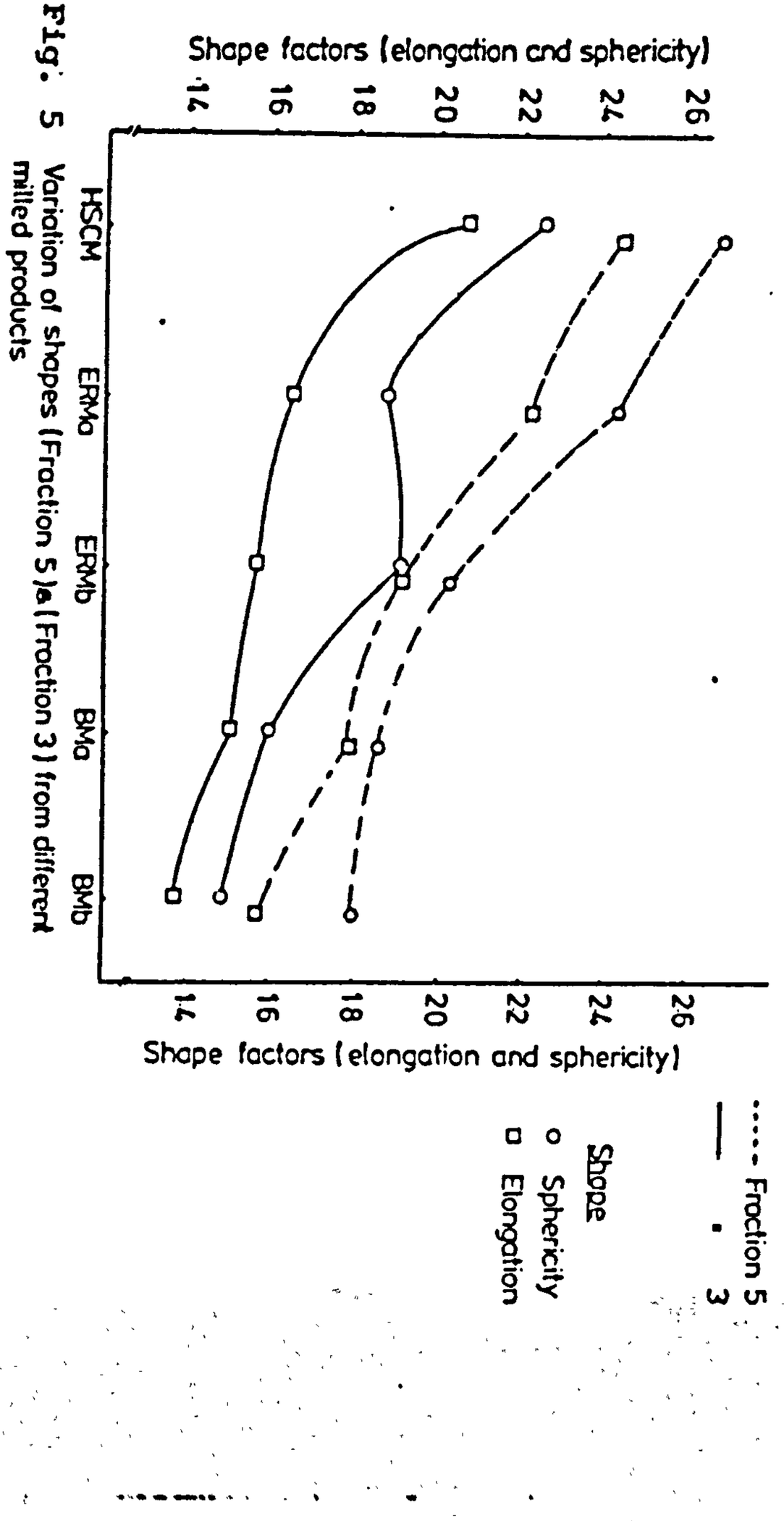

Fig. 5 Variation of shapes (Fraction 5 & Fraction 3) from different milled products

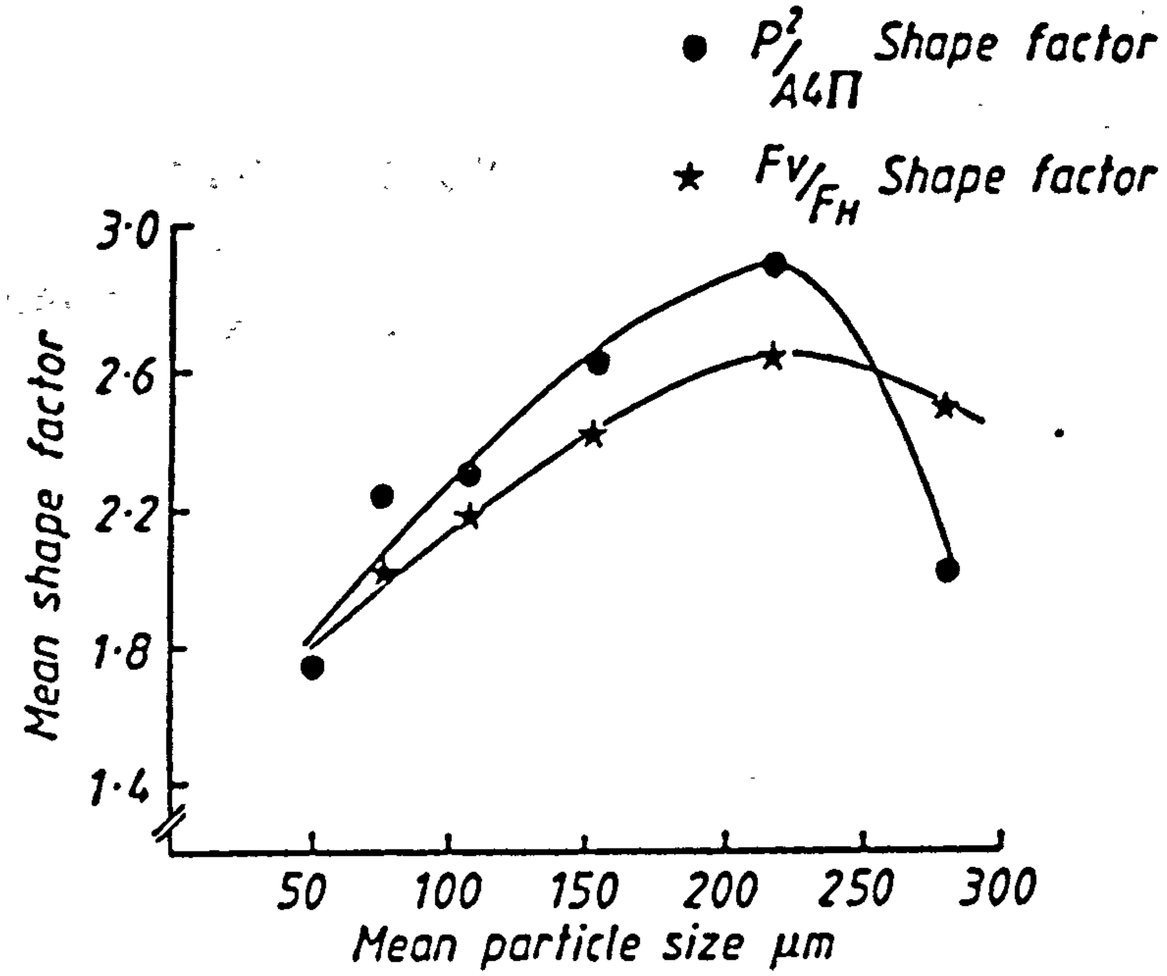

Fig.4a *Mean shape factors versus mean particle sieve sizes from a high speed cutter mill*

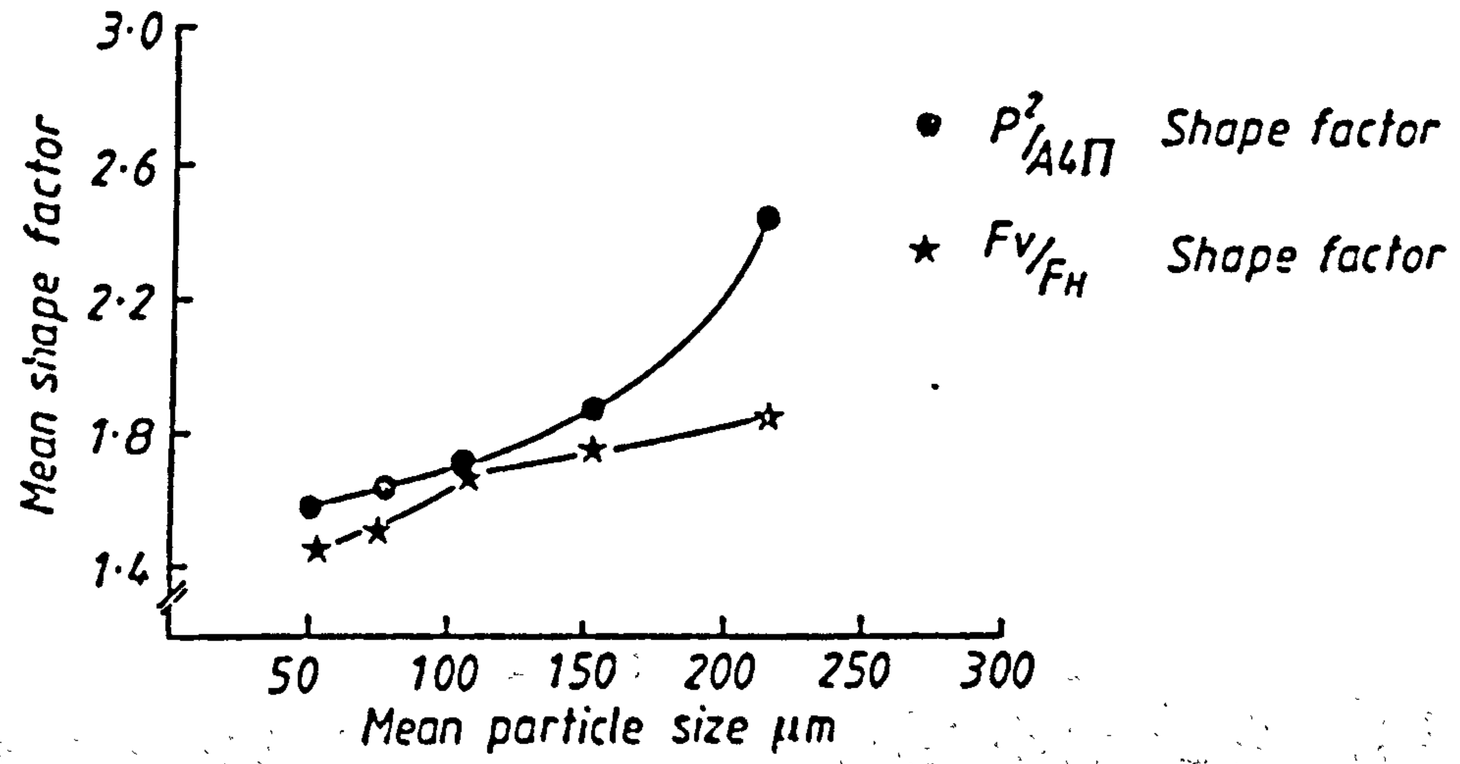

Fig.4b Mean shape factors versus mean particle sieve sizes from a ball mill

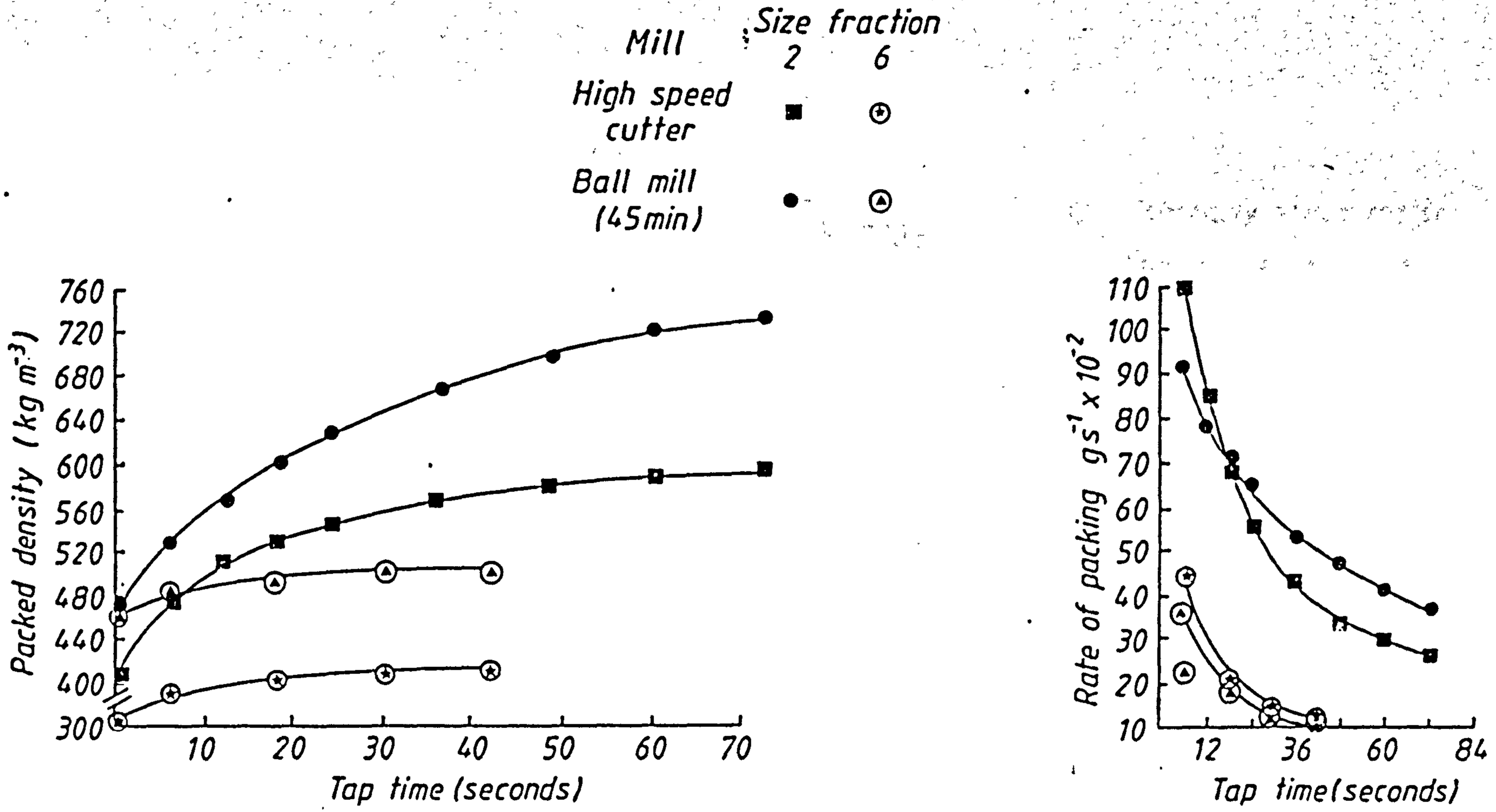

Fig. 6 *The effect of shape on the packing density and rate of packing of milled liquorice*

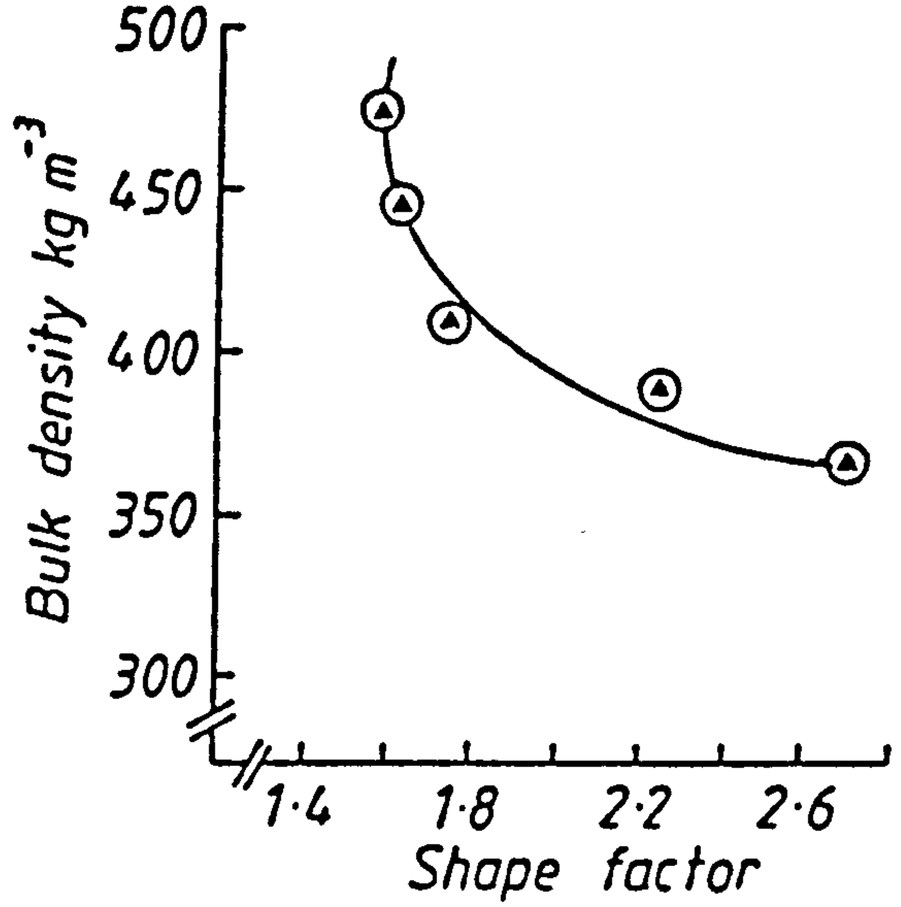

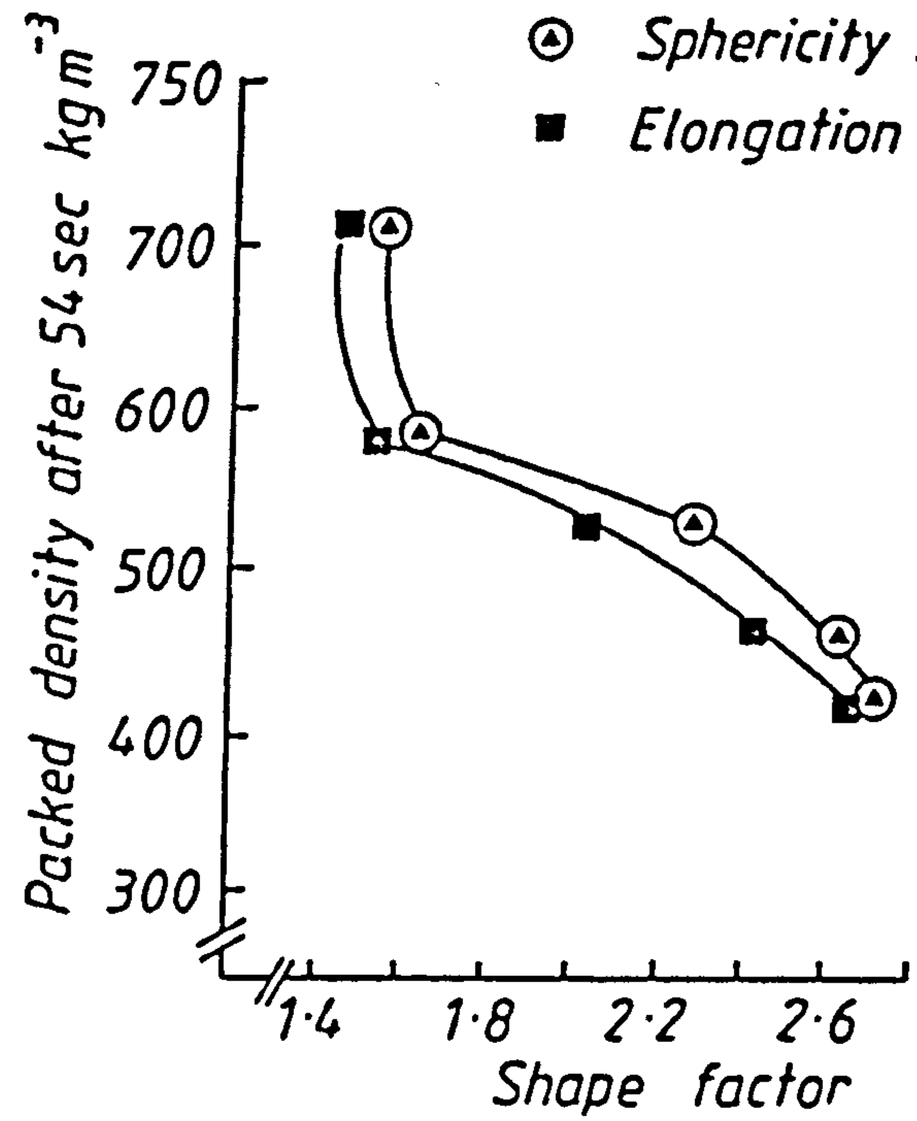

Fig. 7 *Variation of bulk and packed densities with shape*

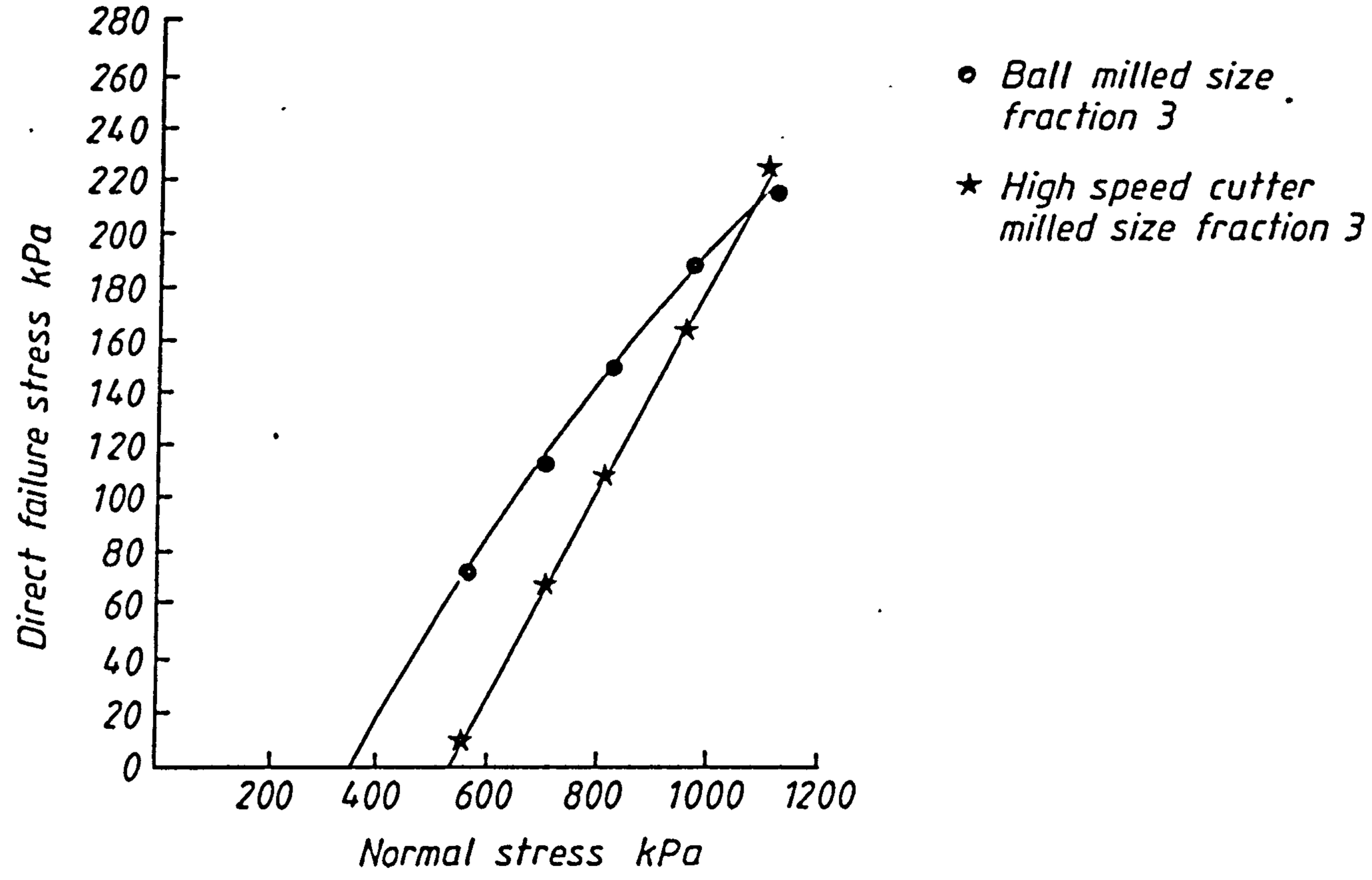

Fig. 8 *Variation of direct failure stress with shape*